Title
Redox Switchable Synthesis and Applications of Biodegradable Lactide Copolymers

Author
Dai, Ruxi

Publication Date
2021

Peer reviewed|Thesis/dissertation

University of California

Los Angeles

Redox Switchable Synthesis and Applications of Biodegradable Lactide Copolymers

A dissertation submitted in partial satisfaction of the

requirements for the degree Doctor of Philosophy

in Chemistry

by

Ruxi Dai

2021

ABSTRACT OF THE DISSERTATION

Redox Switchable Synthesis and Applications of Biodegradable Lactide Copolymers

by

Ruxi Dai

Doctor of Philosophy in Chemistry

University of California, Los Angeles, 2021

Professor Paula Diaconescu, Chair

Lactide copolymers were developed to increase the utility of biodegradable polymers. Using redox switchable ring-opening polymerization, we synthesized a series of zirconium compounds to be used as precatalysts. We studied their geometry change behaviors in polymerization, and one compound, (salfen)Zr(O^iPr)$_2$ (salfen = N,N′-bis(2,4-di-*tert*-butylphenoxy)-1,1′-ferrocenediimine), was selected and then tested as a precatalyst for redox switchable ring-opening polymerization. Copolymers from LA (lactide) and CHO (cyclohexene oxide) were prepared as a proof of concept, and conditions were optimized for the redox switchable copolymerization method. LA-LO (limonene oxide) copolymers were then prepared and their solid state self-assembly properties were studied. Finally, LA-CHDO (cyclohexadiene oxide) copolymers were prepared and post-functionalized to enhance the mechanical properties.

The dissertation of Ruxi Dai is approved.

Ohyun Kwon

Chong Liu

Yves Rubin

Paula Diaconescu, Committee Chair

University of California, Los Angeles

2021

This thesis is dedicated to my families and friends.

TABLE OF CONTENTS

LIST OF FIGURES, SCHEMES, CHARTS AND TABLES

Chapter 1

Chapter 2

Chapter 3

Chapter 4

Chapter 5

ACKNOWLEDGEMENTS

As I write my dissertation, I realize my five years at UCLA are drawing to an end. Although I dreamed of this moment many times when I struggled between failed experiments and reviewer sharp comments, I still feel a bit unprepared and nostalgic now that the time has come. The past five years have witnessed not only my academic progress, but also my receiving of guidance, support, and hope from many people.

First, I would like to thank my parents for their unconditional support. The Pacific Ocean and a 16-hour jet lag separate us, but they are always ready to talk and share my happiness and sorrows. They are not scientists, but they are wise, and they taught me diligence, tolerance, and patience. They are like the Polaris in the sky, watching me and accompanying me throughout my journey.

Second, I would like to thank my PhD advisor, Professor Paula Diaconescu. She is a rigorous scientist, and her tough style and high standards show me what a professional researcher should be. She is not easy-going, as many of my friends put it. However, she gave me full support after I achieved the goals she set. Thanks to her recommendations, I got many awards and scholarships during graduate school, and I was introduced to dinners with other distinguished scholars. When I looked for a job outside the academia, I realized she gave me the tools to do whatever I want. All of those would be impossible if I were not in her group. The five years in her group will bring me five first author papers, but, more importantly, taught me that it takes time to truly know a person, as a warm heart could be buried under a seemingly cold face.

I would like to thank my lab mates without whom my PhD life would have been much more boring. Jonathan Brosmer mentored me when I first came to the lab, and impressed me with his way to tame the glovebox. Amy Lai stepped into the lab the same year as me, and we shared a

lot of experiences. She could always point out the positive side of things. Zach Hern opened the door of bartending to me, and the good taste of Margarita will always remind me of him. Yi Shen and Jenny (Shijie) Deng are like two happy elves, as they work restlessly to do all types of maintenance in the lab. I wish George (Yin Pok) Wong and Hootan Roshandel, the two first year graduate students in the group, to be happy in their life and productive in their research. Also, I wish Shaoran Hu, an undergraduate student I mentored, to be successful in his journey to a PhD degree.

My work in the lab lays solid research progress towards my PhD, while my life outside the lab shows me infinite possibilities in the outer world. Bowei Dong shared much of his graduate school experience with me, and kept updating me about news from China. Shijie Xing and Jinlin Li, two of my friends from the same undergrad cohort at Peking University, showed me the business side of science. Shijie gave me suggestions in a "micro" way, showing me what a venture capital or hedge fund investor looked like, while Jinlin talked in a more "macro" way, enlightening me with his thoughts from the perspective of an economist. My roommates, Peiqi Wang, Chen Lin, and Zhe Wang shared a near 2k square foot house with me, and we lived a happy PhD life together. They are always nice and optimistic, especially when our house suffered from lack of water, power outage, internet disconnection, and an unexpected removal of the ceiling.

I also feel grateful to those who influenced my career choice. Mengfei Zhang knew me since I was an undergrad, and she gave me suggestions from applying to graduate school to becoming a healthcare investor. Ricky Rath mentored me during my internship with UCLA TDG (technology development group); working with a group of scientists, consultants, and lawyers was a great experience. Leili Ran showed me how to thrive in a biotech hedge fund, and mentored me

with great kindness. Although I still have not decided what career path I will take, all their help and training will always be remembered.

In all, I appreciate my life as a PhD student. The stubbornness and aggressiveness of youth faded away, and the academic training shaped me to be calm, patient, and meticulous instead. Those are the personalities I will carry throughout my life. Five years ago, I came to U.S. for graduate school, because as a chemistry student, I did not know what I should do. Now that I see unlimited possibilities lying in front of me, I know what I should do, and it is time for me to return home. I feel honored to make friends with so many fantastic people, and I wish we can always keep in touch and support each other in the future.

VITA

Education

University of California, Los Angeles	Los Angeles, CA
PhD Candidate: Department of Chemistry and Biochemistry	09/2018 – Now
Master's Degree: Chemistry and Biochemistry	09/2016 – 08/2018
Overall GPA 3.95	
Peking University	Beijing, China
Bachelor's Degree: Material Chemistry	09/2012 – 07/2016
GPA ranking top 15%	

Award and Scholarship (since 2016)

UCLA Herbert D. Kaesz Dissertation Award	05/2021
UCLA Dissertation Year Fellowship	07/2020
UCLA George Gregory Excellence in Research Award	05/2020
UCLA Thomas and Ruth Jacobs Fellowship	09/2019
Chinese-American Engineers and Scientists Association Scholarship	03/2019
UCLA Excellence in Second Year Research	07/2018
Peking University Excellent Graduate in Social Activities	07/2016
Peking University Excellent Graduate	07/2016

Conference and Presentations (since 2016)

UCLA Chemistry Student Exit Seminar (Presentation)	05/2021
STUCK Conference (Presentation)	05/2020
American Chemistry Society National Meeting (Presentation)	09/2019
South California Organometallic Meeting (Presentation)	02/2019
South California Organometallic Meeting (Poster)	07/2018
American Chemistry Society National Meeting (Poster)	04/2017

Working Experience

Tech Fellow, Technology Development Group, UCLA 05/2019 – 04/2021

Screened 100+ UCLA-owned technologies and innovations, clarified the unmet needs, and wrote non-confidential disclosure to attract potential commercialization partners

Publications

1. R. Dai, S. Deng, Z. Peng, Q. Pei, P. L. Diaconescu, "Post-functionalization of LA-CHDO copolymers to enhance their mechanical properties" *in preparation*

2. R. Dai, S. Deng, S. Valloppilly, N. D. Alwis, P. Chakma, D. Konkolewicz, P. L. Diaconescu, "Preparation and solid state self-assembly study of LA-LO copolymers" *in preparation*

3. R Dai, J. A. Laureanti, M. Kopelevich, and P. L. Diaconescu, "Developing a Virtual Reality Approach toward a Better Understanding of Coordination Chemistry and Molecular Orbitals" *J. Chem. Educ.*, **2020**, 97, 3647–3651

4. R. Dai, P. L. Diaconescu, "Investigation of a Zirconium Compound for Redox Switchable Ring Opening Polymerization" *Dalton Transactions*, **2019**, 48, 2996-3002

5. R. Dai, A. Lai, A. N. Alexandrova, and P. L. Diaconescu, "Geometry Change in a Series of Zirconium Compounds during Lactide Ring-Opening Polymerization" *Organometallics*, **2018**, 37, 4040-4047

6. R. Dai, S. Zhang, N. Yin, Z. Tan and Q. Shi, "Low-temperature Heat Capacity and Standard Thermodynamic Functions of β-D-(-)-arabinose ($C_5H_{10}O_5$)" *J. Chem. Thermodynamics*, **2016**, 92, 60-65

Chapter 1. Introduction

1.1. Biodegradable polymers

Plastics have been widely used in our everyday life. With a production of around 300 M tons a year, it has certainly become one of the most important materials in the world.[1-5] Consequently, the "white pollution" is growing worse year by year, endangering all the living species on our planet.[6-11] It is estimated that 32 M tons of plastic waste are leaked out to the environment every year, becoming a significant risk to the land and the ocean.[12] Conventional plastics, e.g., polyethylene, polyvinylchloride and nylon, are not biodegradable, and they will stay in nature for hundreds of years polluting the forests and lakes, and killing birds and fish (Figure 1.1).[13-16] One of the potential solutions to this worldwide environmental risk is to develop biodegradable polymers, which can be degraded in nature and minimize the post-usage pollution.[17-20] Many studies have been conducted toward these materials in the last two decades, due to the increasing demand of sustainable alternatives to petroleum-based products.

Figure 1.1. Degradation time of common plastic items. (from THE ECO-STATEMENT webpage)

Lactones and epoxides are two classes of monomers that can be used to construct biodegradable polymers. Common monomers are lactide (LA), ε-caprolactone (CL), valerolactone (VL), and trimethylene carbonate (TMC) as cyclic esters, and cyclohexene oxide (CHO), cyclohexadiene oxide (CHDO), limonene oxide (LO) and propylene oxide (PO) as epoxides. These monomers feature an ester or ether linkage, which is a reaction site for ring-opening polymerization, and also for natural degradation in the future. The most largely produced biodegradable polymer is polylactide (PLA). The production of PLA reached about 190 K tons worldwide, around 10% of all the biodegradable polymers.[21] The most prevalent method to produce PLA in industry is to use $Sn(oct)_2$ (oct = 2-ethylhexanoate) as a catalyst. This method produces PLA with a rather high dispersity, which makes the polymer amorphous and easy to be molded.[22, 23] This method is widely used to produce PLA for everyday use, such as utensils or food boxes. (Figure 1.2a). In order to synthesize PLA for advanced applications, such as 3D printing or tissue scaffolding, relatively complicated metal catalysts are used. For example, aluminum salen (salen = *N*,*N*'-ethylenebis(salicylimine)) compounds can be used to prepare isotactic PLA with low dispersity, which has enhanced mechanical properties and is ready for medical usage (Figure 1.2b).[24, 25]

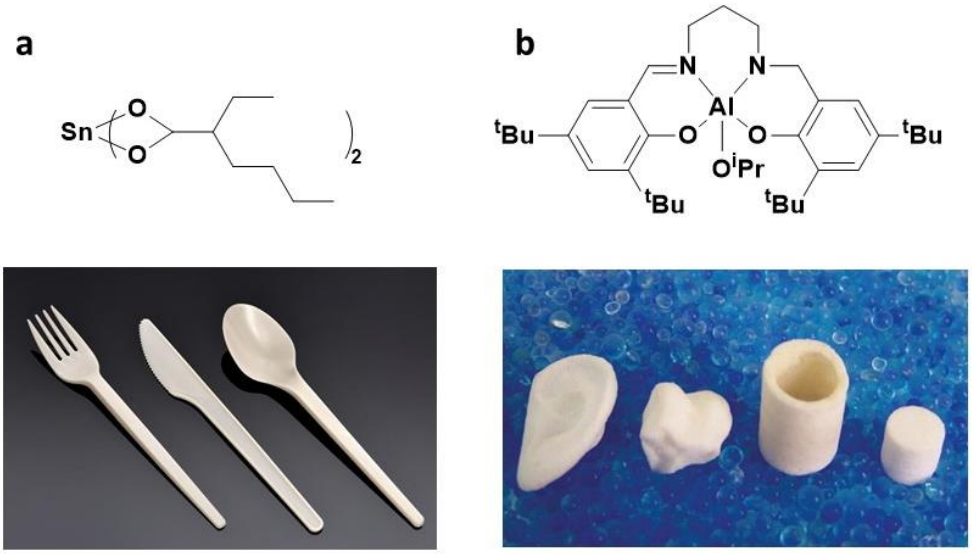

Figure 1.2. (a) $Sn(oct)_2$ catalyst and PLA utensils; (b) Al-salen compound and PLA scaffold.

Despite the advantages and mass production of biodegradable polymers, these new materials still have limitations. For example, PLA is very brittle, and cannot withstand shocks.[26, 27] Besides, PLA has a glass transition temperature of around 65 ^{o}C, above which it will become soft and lose its shape.[28] One way to overcome these limitations is to build block copolymers, to have PLA chemically bound with other polymers. We can tune the mechanical properties by changing the monomers incorporated, by adjusting the chain length of each block, and by adjusting the number of blocks in the copolymer. Once the properties of the material are properly tuned, it will have more applications and become a substituent for the traditional plastics in a much broader scope.

1.2. Redox switchable ring-opening polymerization

Block copolymerization is a method to regulate the properties of polymers through monomer selection, molar mass control, and is considered one of the most feasible approaches

among the large number of methods available.[29-31] Although polymerization methods such as anionic and atom transfer radical polymerization can be used for the synthesis of block copolymers, these methods require additional modification steps, for example, end group modification and bifunctional initiators, especially when different types of monomers, such as LA (lactide) and CHO (cyclohexene oxide), need to be combined.[32-34] Therefore, developing methods to build block copolymers with few or no additional modification steps is necessary.

The concept of redox controlled ring-opening polymerization was first reported in 2006 by White and coworkers, who showed that a titanium Schiff base compound featuring ferrocene groups appended at the periphery of the molecule has a different activity in the polymerization of *rac*-lactide depending on the oxidation state of the ferrocene units.[35] The compound in the reduced state can polymerize LA 30 times faster compared to that in the oxidized state. After the compound is oxidized and reduced back, its original catalytic activity for LA polymerization can be restored (Figure 1.3).

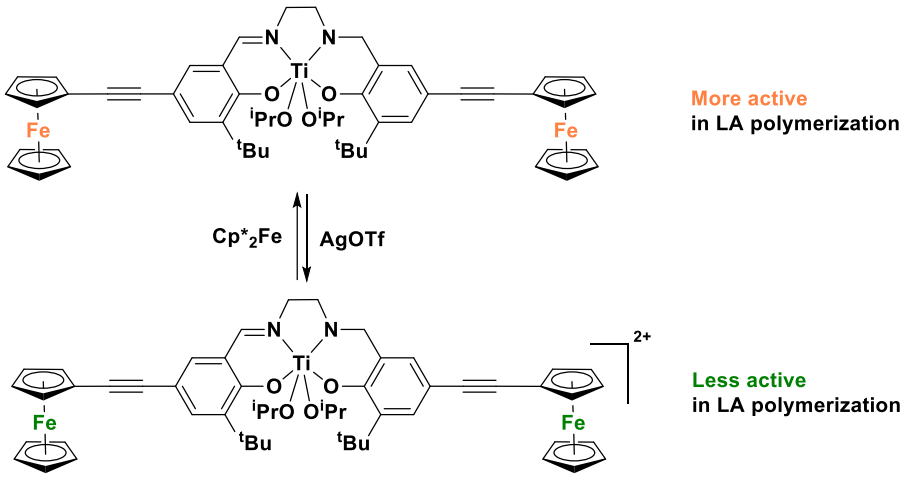

Figure 1.3. Redox switchable polymerization of LA by White and coworkers (AgOTf = silver trifluoromethanesulfonate, Cp^*_2Fe = decamethylferrocene).

Our group has been working in the field of redox switchable polymerization for more than a decade, and reported the first redox switchable polymerization study in 2011. A new ferrocene derived proligand, phosfen (1,1'-di(2-*tert*-butyl-6-diphenylphosphiniminophenoxy)ferrocene), was developed, and two metal compounds, (phosfen)Y(O^{t}Bu) and (phosfen)In(OPh), were synthesized.[36] Both compounds proved redox switchable. (phosfen)Y(O^{t}Bu) can polymerize LA in the reduced state, but not in the oxidized state. When the oxidized compound was reduced back by $CoCp_2$, the activity could be restored. On the other hand, (phosfen)In(OPh) showed no activity in TMC polymerization in the reduced state, but gained activity in the oxidized state (Figure 1.4a). The two compounds were the first reported to show a complementary on/off switch for ring-opening polymerization.

In 2012, Okuda and coworkers reported a cerium compound for redox switchable polymerization.[37] Cerium was supported by two bis(phenolate) ligands (OSSO type) and could be reduced and oxidized *in situ*. The catalytic activity for LA polymerization was faster in the Ce(IV) state, the oxidized state, compared to the Ce(III) reduced state (Figure 1.4b).

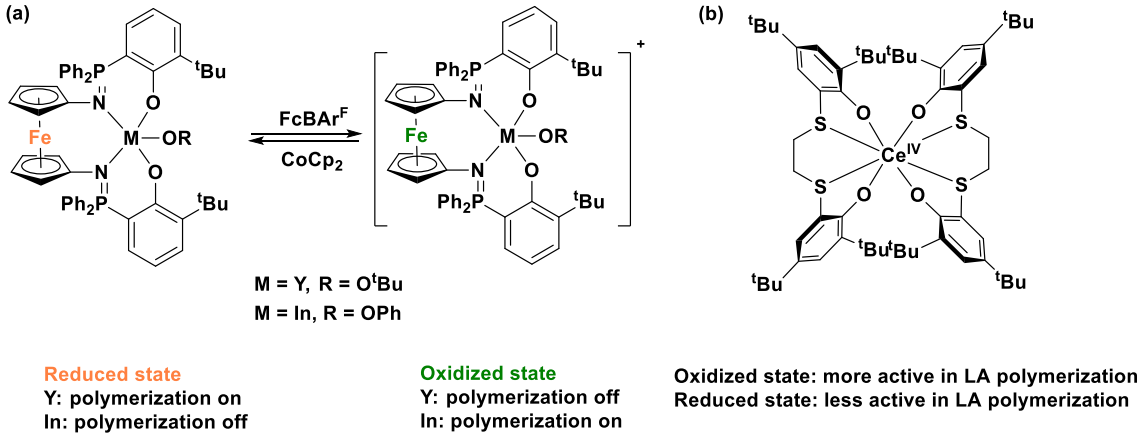

Figure 1.4. (a) Redox switchable compounds (phosfen)Y(O^{t}Bu) and (phosfen)In(OPh); (b) cerium compound developed by Okuda and coworkers.

In 2014, our group reported a new redox switchable titanium compound, (thiolfan*)Ti(O^iPr)$_2$ (thiolfan* = 1,1′-di(2,4-di-*tert*-butyl-6-thiohenol)ferrocene), which could be used to prepare block copolymers based on its redox switchable activity.[38] (thiolfan*)Ti(O^iPr)$_2$ polymerizes LA in the reduced state but not in the oxidized state. However, it can polymerize CL in the oxidized state but not in the reduced state. In the presence of both LA and CL, the compound can prepare a LA-CL copolymer with an *in situ* redox switch (Figure 1.5). This study was the first to move from homopolymerization to copolymerization, showing that more versatile and closer to real world applications polymers may be synthesized by using redox switchable catalysis.

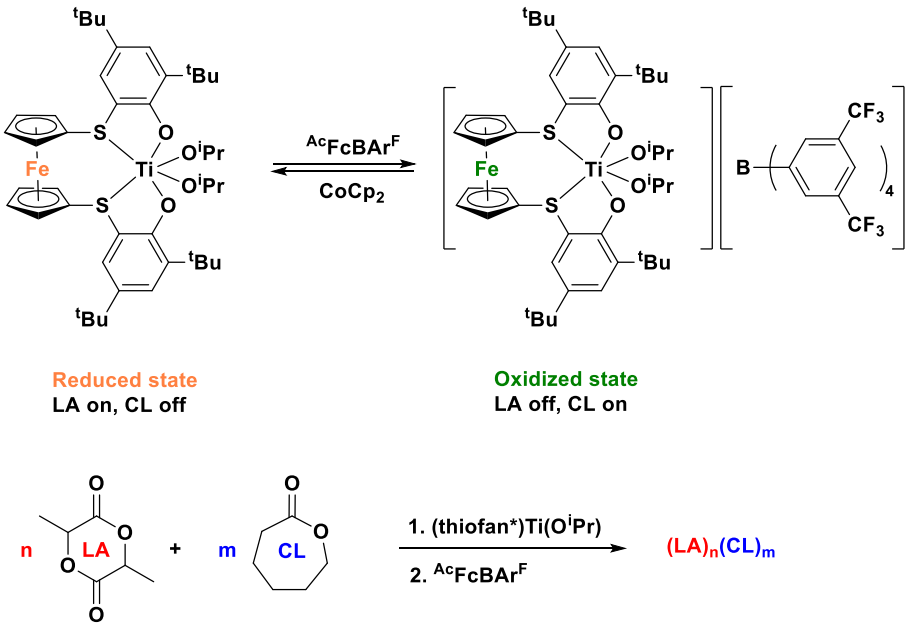

Figure 1.5. Redox switchable copolymerization by (thiolfan*)Ti(O^iPr)$_2$.

In 2017, we reported a zirconium compound that can prepare LA-CHO copolymers by redox switchable copolymerization.[39, 40] (salfan)Zr(O^tBu)$_2$ (salfen = N,N'-bis(2,4-di-*tert*-

butylphenoxy)-1,1'-ferrocenediimine) was synthesized and proved redox switchable with $^{Ac}FcBAr^{F}$ (^{Ac}Fc = acetylferrocenium, BAr^{F} = tetrakis(3,5-bis(trifluoromethyl)-phenyl)borate) as the oxidant and $CoCp_2$ as the reductant. (salfan)Zr(O^tBu)$_2$ can polymerize LA only in the reduced state, and can polymerize CHO only in the oxidized state. Therefore, (salfan)Zr(O^tBu)$_2$ could be used to make PCHO-PLA diblock and PLA-PCHO-PLA triblock copolymers (Figure 1.6). This study laid the foundation of my compound design and some of the polymerization studies, described in Chapter 2 and Chapter 3.

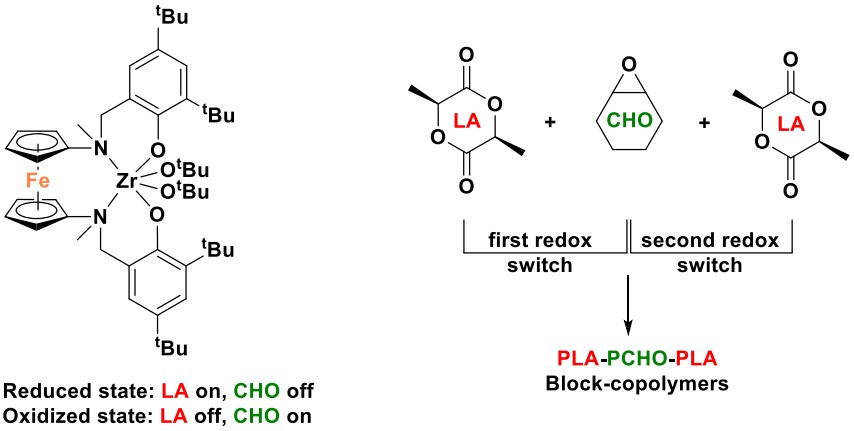

Figure 1.6. (salfan)Zr(O^tBu)$_2$ and the preparation of a PLA-PCHDO-PLA triblock copolymer via the redox switchable method.

In 2013, Byers and coworkers reported an iron compound supported by bis(imino)pyridine ligands.[41] This compound can polymerize LA in the reduced state but showed no activity in the oxidized state (Figure 1.7). Further research showed that the same iron complex can polymerize CHO in the oxidized state but not in the reduced state, opposite to the LA polymerization selectivity.[41, 42] This behavior was then exploited to prepare PLA-PCHO copolymers. Later, Byers and coworkers changed the conventional chemical redox switching method to electrochemical

redox switching, with the purpose of achieving a precise redox control and less waste accumulation from the stoichiometric use of reductant and oxidant.[43] The iron compound was oxidized and reduced on the surface of the electrode, and used for catalysis in solution. A PLA-PCHO diblock copolymer could be prepared by electrochemical redox switchable copolymerization.

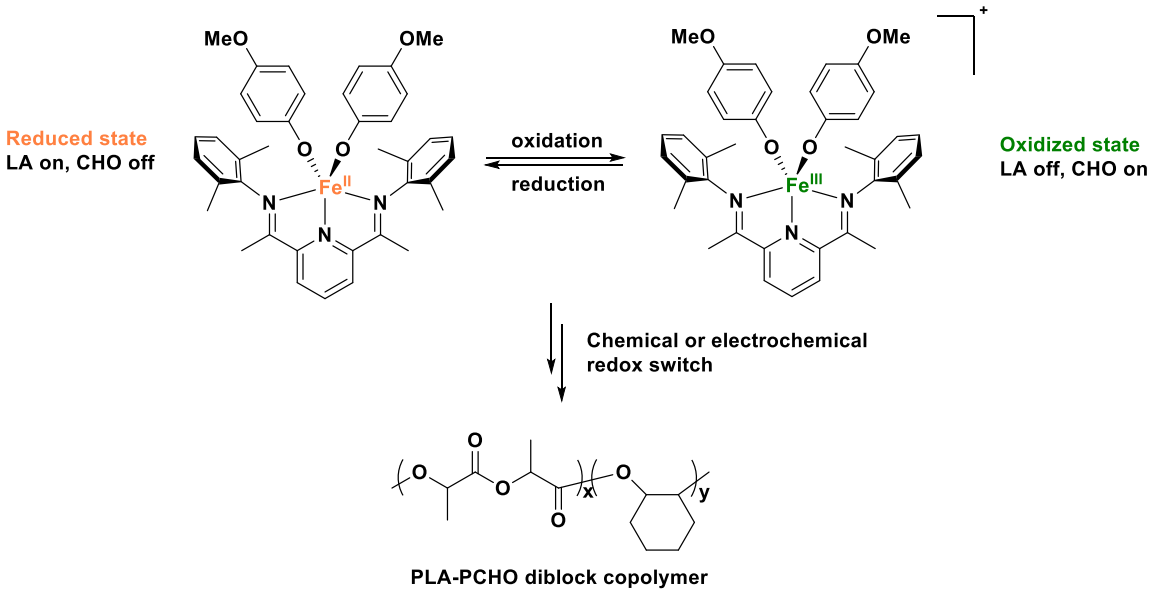

Figure 1.7. Iron compound developed by Byers and coworkers.

Other redox switchable polymerization systems were reported by our group. An aluminum compound, (thiolfan*)Al(O^{t}Bu), was synthesized, and tested for redox switchable polymerization in 2017 (Figure 1.8a).[44] The compound exhibited an orthogonal selectivity for LA and CHO. LA can be polymerized only in the reduced state, and CHO can only be polymerized in the oxidized state. The catalytic behavior in redox switchable polymerizations was studied experimentally and using computationally methods. In 2019, another Al compound was reported (Figure 1.8b).[45] (salfen)Al(O^{i}Pr) (salfen = N,N′-bis(2,4-di-*tert*-butylphenoxy)-1,1′-ferrocenediimine) exhibited an orthogonal selectivity for LA, CHO, and TMC; LA and TMC can be polymerized only in the

reduced state, while CHO can be polymerized only in the oxidized state. Diblock copolymers and a PTMC-PCHO-PLA triblock copolymer were prepared based on the triple orthogonal selectivity via the redox switchable copolymerization method.

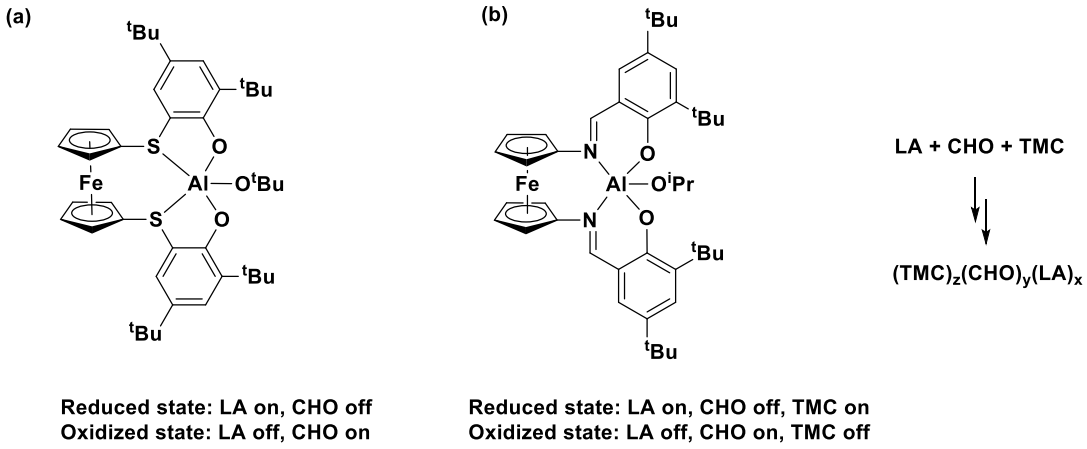

Figure 1.8. Two redox switchable aluminum compounds: (a) (thiolfan*)Al(O^{t}Bu) and (b) (salfen)Al(O^{i}Pr) reported by Diaconescu and coworkers.

Concurrently, dimeric metal compounds were reported by our group and proved redox switchable. In 2018, we reported a dinuclear zinc compound bearing a ferrocene unit at each end (Figure 1.9a).[46] The compound can polymerize LA, CHO, VL (valerolactone), and TMC, but exhibited comparable catalytic activity in the reduced and oxidized state for all monomers. The compound was then used to prepare a series of LA-TMC copolymers, though in a non-redox switchable manner.[47] The reported elasticity measurement inspired my research in Chapter 5.

A bimetallic yttrium compound, [(salfen)Y(OPh)]$_2$, was synthesized with two ferrocene units and reported in 2021 (Figure 1.9b).[48] The compound exhibited a two-step redox behavior, and the catalytic activity of the three oxidation states was tested. The activity toward cyclic esters

(e.g., LA, CL) decreases upon oxidation while the opposite trend was observed in epoxide polymerization (e.g., CHO, propylene oxide).

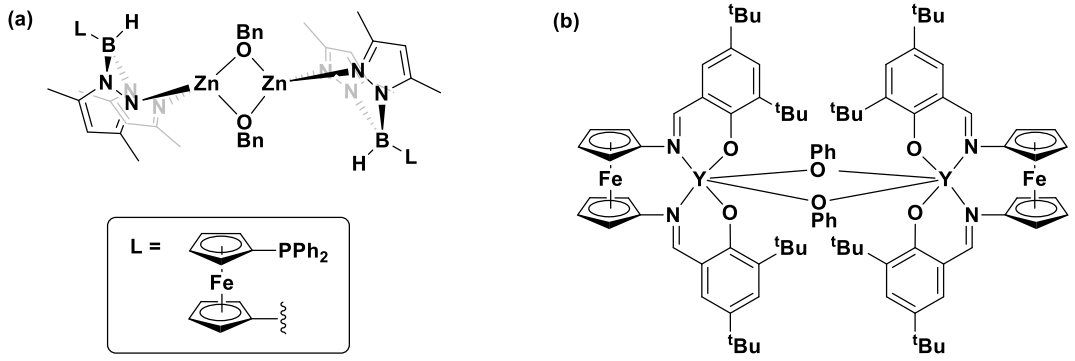

Figure 1.9. (a) Dinuclear zinc and (b) dinuclear yttrium compounds reported by our group.

Although we reached our initial goal of making biodegradable copolymers by developing redox switchable copolymerization catalysts, the resulting copolymers are still far from gaining real world applications. In order to expand the scope of copolymer synthesis, we decided on two approaches: (i) find new applications based on new properties (e.g., light sensitivity, self-assembly) and (ii) functionalize current polymers to address current needs.

For solution (i), new types of copolymers must be prepared. We will need to enlarge the monomer scope, and prepare new copolymers. With new materials, there is a greater possibility to find interesting properties that will lead to new applications. For solution (ii), functionalization methods are needed. Considering that the current LA-CHO copolymers have a saturated structure and are hard to be functionalized, unsaturated polymers need to be prepared to allow further functionalization (Figure 1.10). In this way, the properties of functionalized copolymers, e.g., mechanical properties, could be improved upon from the original plain copolymer, and might meet the requirements of real world applications.

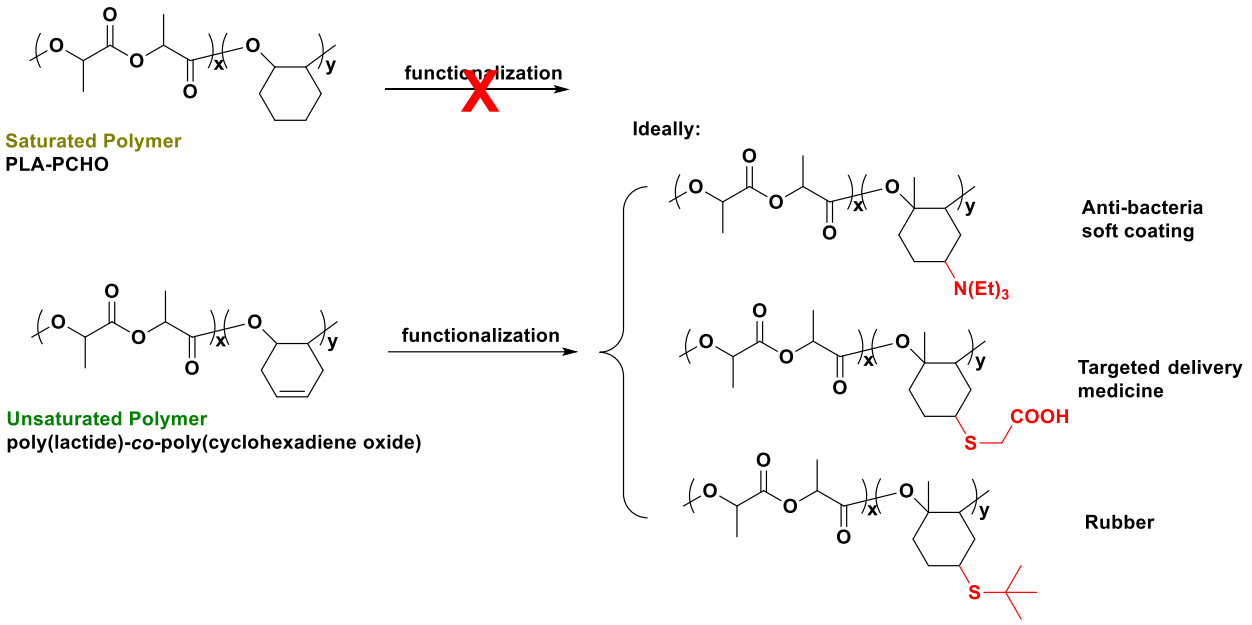

Figure 1.10. Designed unsaturated copolymer and its functionalization methods.

1.3. Thesis summary

My work started with catalyst design, as we wanted a new redox switchable compound that can prepare new copolymers. A series of zirconium compounds was synthesized, and their geometry change behavior during the catalysis was studied. (salfen)Zr(O^iPr)$_2$ was selected to proceed for further studies. Different monomers were screened to understand the activity of (salfen)Zr(O^iPr)$_2$ in the reduced and oxidized state. Redox switchable copolymerization conditions were developed and optimized for LA-CHO block copolymerization and up to triblock copolymers were made. After that, new LA-LO (limonene oxide) copolymers were prepared and its solid state self-assembly properties were studied. A LA-CHDO (cyclohexadiene oxide) copolymer was synthesized as the unsaturated version of the LA-CHO copolymer, and it allowed post-functionalization to enhance the mechanical properties. Both the self-assembly study and post-

functionalization study were attempts to bring biodegradable polymers closer to real world applications. A flow chart that shows the logic of my work is presented in Figure 1.11.

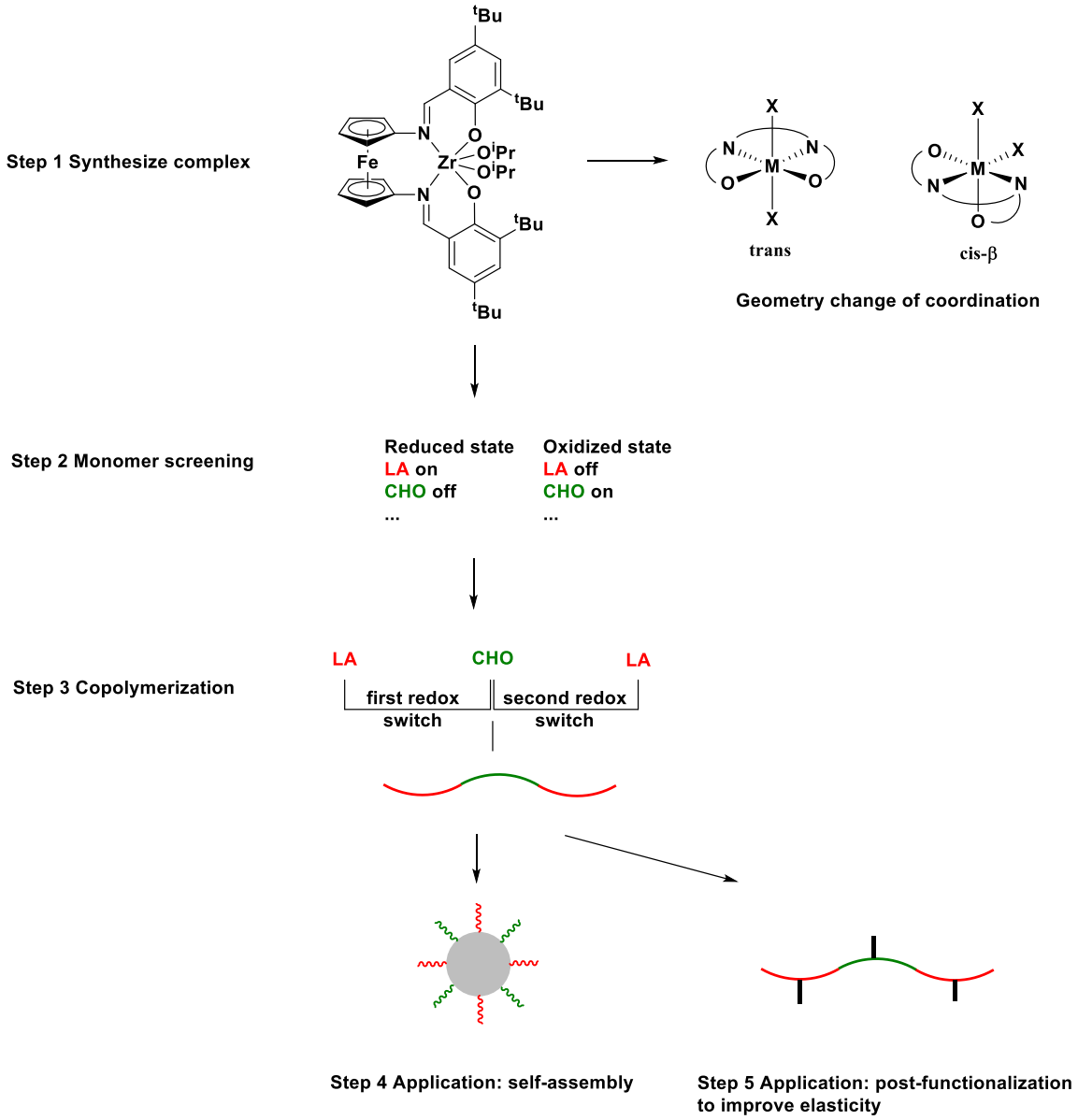

Figure 1.11. Flow chart of the work in this thesis.

Specifically, Chapter 2 is a version of [R. Dai, A. Lai, A. N. Alexandrova, P. L. Diaconescu *Organometallics* **2018**, *37 (21)*, 4040-4047. DOI: 10.1021/acs.organomet.8b00620], Chapter 3 is

a version of [R. Dai, P. L. Diaconescu *Dalton Trans.* **2019**, *48*, 2996-3002. DOI: 10.1039/C9DT00212J], Chapter 4 is a version of a manuscript in the final stage prior to submission [R. Dai, S. Deng, S. Valloppilly, N. D. Alwis, P. Chakma, D. Konkolewicz, P. L. Diaconescu **2021**], and Chapter 5 is a version of a manuscript in the final stage prior to submission [R. Dai, S. Deng, Z. Peng, Q. Pei, P. L. Diaconescu **2021**].

1.4. References

1. Dawson, R.; Cooper, A. I.; Adams, D. J., Nanoporous organic polymer networks. *Progress in Polymer Science* **2012,** *37*, 530-563.

2. Suriano, F.; Coulembier, O.; Hedrick, J. L.; Dubois, P., Functionalized cyclic carbonates: from synthesis and metal-free catalyzed ring-opening polymerization to applications. *Polymer Chemistry* **2011,** *2*, 528-533.

3. Ulery, B. D.; Nair, L. S.; Laurencin, C. T., Biomedical applications of biodegradable polymers. *Journal of Polymer Science Part B: Polymer Physics* **2011,** *49*, 832-864.

4. Vert, M., Aliphatic Polyesters: Great Degradable Polymers That Cannot Do Everything. *Biomacromolecules* **2005,** *6*, 538-546.

5. Ruzette, A.-V.; Leibler, L., Block copolymers in tomorrow's plastics. *Nature Materials* **2005,** *4*, 19-31.

6. Krieger, M. H., What is Wrong with Plastic Trees? *Science* **1973,** *179*, 446.

7. Johnson, W. H., Social Impact of Pollution Control Legislation. *Science* **1976,** *192*, 629.

8. Green, L., Energy Needs versus Environmental Pollution: A Reconciliation? *Science* **1967,** *156*, 1448.

9. Galloway, T. S.; Cole, M.; Lewis, C., Interactions of microplastic debris throughout the marine ecosystem. *Nature Ecology & Evolution* **2017,** *1*, 0116.

10. Romera-Castillo, C.; Pinto, M.; Langer, T. M.; Álvarez-Salgado, X. A.; Herndl, G. J., Dissolved organic carbon leaching from plastics stimulates microbial activity in the ocean. *Nature Communications* **2018,** *9*, 1430.

11. Lebreton, L. C. M.; van der Zwet, J.; Damsteeg, J.-W.; Slat, B.; Andrady, A.; Reisser, J., River plastic emissions to the world's oceans. *Nature Communications* **2017,** *8*, 15611.

12. Geyer, R.; Jambeck, J. R.; Law, K. L., Production, use, and fate of all plastics ever made. *Science Advances* **2017,** *3*, e1700782.

13. Alam, O.; Billah, M.; Yajie, D., Characteristics of plastic bags and their potential environmental hazards. *Resources, Conservation and Recycling* **2018,** *132*, 121-129.

14. Groh, K. J.; Backhaus, T.; Carney-Almroth, B.; Geueke, B.; Inostroza, P. A.; Lennquist, A.; Leslie, H. A.; Maffini, M.; Slunge, D.; Trasande, L.; Warhurst, A. M.; Muncke, J., Overview of known plastic packaging-associated chemicals and their hazards. *Science of The Total Environment* **2019,** *651*, 3253-3268.

15. N V Lakshmi Kavya, A.; Sundarrajan, S.; Ramakrishna, S., Identification and characterization of micro-plastics in the marine environment: A mini review. *Marine Pollution Bulletin* **2020,** *160*, 111704.

16. Baztan, J.; Carrasco, A.; Chouinard, O.; Cleaud, M.; Gabaldon, J. E.; Huck, T.; Jaffrès, L.; Jorgensen, B.; Miguelez, A.; Paillard, C.; Vanderlinden, J.-P., Protected areas in the Atlantic facing the hazards of micro-plastic pollution: First diagnosis of three islands in the Canary Current. *Marine Pollution Bulletin* **2014,** *80*, 302-311.

17. Platel, R. H.; Hodgson, L. M.; Williams, C. K., Biocompatible Initiators for Lactide Polymerization. *Polymer Reviews* **2008,** *48*, 11-63.

18. Nair, L. S.; Laurencin, C. T., Biodegradable polymers as biomaterials. *Progress in Polymer Science* **2007,** *32*, 762-798.

19. Chen, G.-Q.; Patel, M. K., Plastics Derived from Biological Sources: Present and Future: A Technical and Environmental Review. *Chemical Reviews* **2012,** *112*, 2082-2099.

20. Dechy-Cabaret, O.; Martin-Vaca, B.; Bourissou, D., Controlled Ring-Opening Polymerization of Lactide and Glycolide. *Chemical Reviews* **2004,** *104*, 6147-6176.

21. Jem, K. J.; Tan, B., The development and challenges of poly (lactic acid) and poly (glycolic acid). *Advanced Industrial and Engineering Polymer Research* **2020,** *3*, 60-70.

22. Kaplan, D. L., *Biopolymers from Renewable Resources*. Springer-Verlag Berlin Heidelberg: 1998; p 420.

23. Dubois, P.; Coulembier, O.; Raquez, J.-M., *Handbook of Ring-Opening Polymerization*. 2008; p 425.

24. Gao, B.; Li, D.; Li, Y.; Duan, Q.; Duan, R.; Pang, X., Ring-opening polymerization of lactide using chiral salen aluminum complexes as initiators: high productivity and stereoselectivity. *New Journal of Chemistry* **2015,** *39*, 4670-4675.

25. Nomura, N.; Ishii, R.; Yamamoto, Y.; Kondo, T., Stereoselective Ring-Opening Polymerization of a Racemic Lactide by Using Achiral Salen– and Homosalen–Aluminum Complexes. *Chemistry – A European Journal* **2007,** *13*, 4433-4451.

26. Graupner, N.; Ziegmann, G.; Müssig, J., Composite models for compression moulded long regenerated cellulose fibre-reinforced brittle polylactide (PLA). *Composites Science and Technology* **2017,** *149*, 55-63.

27. Becker, J. M.; Pounder, R. J.; Dove, A. P., Synthesis of Poly(lactide)s with Modified Thermal and Mechanical Properties. *Macromolecular Rapid Communications* **2010,** *31*, 1923-1937.

28. Södergård, A.; Stolt, M., Properties of lactic acid based polymers and their correlation with composition. *Progress in Polymer Science* **2002,** *27*, 1123-1163.

29. Guillaume, S. M., Recent advances in ring-opening polymerization strategies toward α,ω-hydroxy telechelic polyesters and resulting copolymers. *European Polymer Journal* **2013,** *49*, 768-779.

30. Wang, Y.; Hillmyer, M. A., Synthesis of Polybutadiene−Polylactide Diblock Copolymers Using Aluminum Alkoxide Macroinitiators. Kinetics and Mechanism. *Macromolecules* **2000,** *33*, 7395-7403.

31. Tamboli, V.; Mishra, G. P.; Mitra, A. K., Novel pentablock copolymer (PLA–PCL–PEG–PCL–PLA)-based nanoparticles for controlled drug delivery: effect of copolymer compositions on the crystallinity of copolymers and in vitro drug release profile from nanoparticles. *Colloid and Polymer Science* **2013,** *291*, 1235-1245.

32. Mecerreyes, D.; Moineau, G.; Dubois, P.; Jérôme, R.; Hedrick, J. L.; Hawker, C. J.; Malmström, E. E.; Trollsas, M., Simultaneous Dual Living Polymerizations: A Novel One-Step Approach to Block and Graft Copolymers. *Angewandte Chemie International Edition* **1998,** *37*, 1274-1276.

33. Jing, R.; Wang, G.; Zhang, Y.; Huang, J., One-Pot Synthesis of PS-b-PEO-b-PtBA Triblock Copolymers via Combination of SET-LRP and "Click" Chemistry Using Copper(0)/PMDETA as Catalyst System. *Macromolecules* **2011,** *44*, 805-810.

34. Chagneux, N.; Camerlynck, S.; Hamilton, E.; Vilela, F. M. L.; Sherrington, D. C., Synthesis of Laterally Linked Poly(tetrahydrofuran)−Poly(methyl methacrylate) Block

Copolymers via Use of a "Jekyll and Hyde" Comonomer. *Macromolecules* **2007,** *40*, 3183-3189.

35. Gregson, C. K. A.; Gibson, V. C.; Long, N. J.; Marshall, E. L.; Oxford, P. J.; White, A. J. P., Redox Control within Single-Site Polymerization Catalysts. *Journal of the American Chemical Society* **2006,** *128*, 7410-7411.

36. Broderick, E. M.; Guo, N.; Vogel, C. S.; Xu, C.; Sutter, J.; Miller, J. T.; Meyer, K.; Mehrkhodavandi, P.; Diaconescu, P. L., Redox Control of a Ring-Opening Polymerization Catalyst. *Journal of the American Chemical Society* **2011,** *133*, 9278-9281.

37. Sauer, A.; Buffet, J.-C.; Spaniol, T. P.; Nagae, H.; Mashima, K.; Okuda, J., Switching the Lactide Polymerization Activity of a Cerium Complex by Redox Reactions. *ChemCatChem* **2013,** *5*, 1088-1091.

38. Wang, X.; Thevenon, A.; Brosmer, J. L.; Yu, I.; Khan, S. I.; Mehrkhodavandi, P.; Diaconescu, P. L., Redox Control of Group 4 Metal Ring-Opening Polymerization Activity toward l-Lactide and ε-Caprolactone. *Journal of the American Chemical Society* **2014,** *136*, 11264-11267.

39. Quan, S. M.; Wei, J.; Diaconescu, P. L., Mechanistic Studies of Redox-Switchable Copolymerization of Lactide and Cyclohexene Oxide by a Zirconium Complex. *Organometallics* **2017,** *36*, 4451-4457.

40. Quan, S. M.; Wang, X.; Zhang, R.; Diaconescu, P. L., Redox Switchable Copolymerization of Cyclic Esters and Epoxides by a Zirconium Complex. *Macromolecules* **2016,** *49*, 6768-6778.

41. Biernesser, A. B.; Li, B.; Byers, J. A., Redox-Controlled Polymerization of Lactide Catalyzed by Bis(imino)pyridine Iron Bis(alkoxide) Complexes. *Journal of the American Chemical Society* **2013,** *135*, 16553-16560.

42. Biernesser, A. B.; Delle Chiaie, K. R.; Curley, J. B.; Byers, J. A., Block Copolymerization of Lactide and an Epoxide Facilitated by a Redox Switchable Iron-Based Catalyst. *Angewandte Chemie International Edition* **2016,** *55*, 5251-5254.

43. Qi, M.; Dong, Q.; Wang, D.; Byers, J. A., Electrochemically Switchable Ring-Opening Polymerization of Lactide and Cyclohexene Oxide. *Journal of the American Chemical Society* **2018,** *140*, 5686-5690.

44. Wei, J.; Riffel, M. N.; Diaconescu, P. L., Redox Control of Aluminum Ring-Opening Polymerization: A Combined Experimental and DFT Investigation. *Macromolecules* **2017,** *50*, 1847-1861.

45. Lai, A.; Hern, Z. C.; Diaconescu, P. L., Switchable Ring-Opening Polymerization by a Ferrocene Supported Aluminum Complex. *ChemCatChem* **2019,** *11*, 4210-4218.

46. Abubekerov, M.; Vlcek, V.; Wei, J.; Miehlich, M. E.; Quan, S. M.; Meyer, K.; Neuhauser, D.; Diaconescu, P. L., Exploring Oxidation State-Dependent Selectivity in Polymerization of Cyclic Esters and Carbonates with Zinc(II) Complexes. *iScience* **2018,** *7*, 120-131.

47. Abubekerov, M.; Wei, J.; Swartz, K. R.; Xie, Z.; Pei, Q.; Diaconescu, P. L., Preparation of multiblock copolymers via step-wise addition of l-lactide and trimethylene carbonate. *Chemical Science* **2018,** *9*, 2168-2178.

48. Deng, S.; Diaconescu, P. L., A switchable dimeric yttrium complex and its three catalytic states in ring opening polymerization. *Inorganic Chemistry Frontiers* **2021,** *8,* 2088-2096.

Chapter 2. Synthesis of a series of zirconium compounds, and their geometry change behavior

2.1. Introduction

Biodegradable polymers, especially polyesters, are promising solutions to the pollution generated by conventional plastics.[1-11] While polyesters can be obtained using enzymatic methods, the ring-opening polymerization of cyclic esters catalyzed by metal compounds[11-13] or small organic molecules[13, 14] is a well-known, controlled process, which allows the synthesis of polymers with specific properties. Zirconium alkoxide compounds have been used as catalysts for the ring opening polymerization of lactide for several decades.[13, 15, 16] Zirconium tetra-alkoxide compounds were the first studied;[17, 18] zirconium tetra-*n*-propoxide, for example, could reach 94% lactide conversion at 90 °C after 24 hours. Recently, in order to achieve controlled polymerization, the synthesis of novel zirconium compounds has been pursued. For example, ONNO-type tetradentate ligands, derived from Schiff bases (Chart 2.1), were successful in supporting zirconium catalysts for the ring opening polymerization of lactones.[15] Compounds featuring both a saturated backbone (Chart 2.1), reported by Kol et al.,[19] and unsaturated C=N backbone (Chart 2.1), reported by Chakraborty et al.,[20] showed a good activity toward the ring opening polymerization of cyclic esters. Zirconium precatalysts bearing other tetradentate ligands, such as the OSSO and OSNO-type, were designed and synthesized later.[21-23]

The structure of the above six-coordinated metal compounds was studied systematically, and it was shown that they can adopt three possible geometries at the metal center: cis-α, cis-β, and trans (Figure 2.1); among these, the cis-β geometry is non-symmetrical,[24] while the other two are symmetrical. For all the group 4 metal precatalysts, it was reported that different geometries

have distinct activities during the lactone ring-opening polymerization: trans and cis-α compounds are usually active, while cis-β compounds show only a low activity.[22-29]

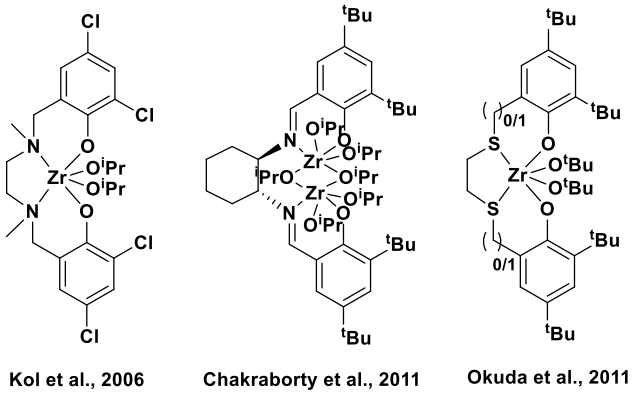

Chart 2.1. Zirconium compounds used as precatalysts for lactone ring opening polymerization.

In 2015, B. Long and co-workers reported a titanium(IV) salfen (salfen = 1,1′- di(2,4-di-*tert*-butyl-6-salicylimine)ferrocene) compound displaying a cis-β geometry (Chart 2.2).[30] By comparison, the geometry of a titanium compound supported by a different ferrocene modified Schiff base, previously reported by N. Long and coworkers, was trans.[31] In B. Long's paper, the ring opening polymerization of L-LA with the reduced state catalyst was significantly slower than that with the oxidized state catalyst, which represented an opposite trend in catalytic activity as compared with most catalysts employed in redox switchable ring opening polymerization.[32-42] However, if the catalyst was oxidized in the presence of L-LA and then reduced back, the reduced species showed a dramatically increased polymerization rate. Once it was oxidized back in situ, the newly formed compound had no activity toward the ring opening polymerization of LA anymore. Although further investigations are needed to explain this phenomenon, based on the *in situ* ^{1}H NMR spectra and the cyclic voltammetry (CV) experiments, the authors proposed that the geometry of the catalyst was changed from its original cis-β conformation to either a cis-α or trans

conformation by using the redox reagents in the presence of LA. In the absence of LA, the geometry of the catalyst remained cis-β after oxidation. Thus, the authors proposed that when the oxidation and reduction reactions were carried out in the presence/absence of monomers, the polymerization activity was completely different.

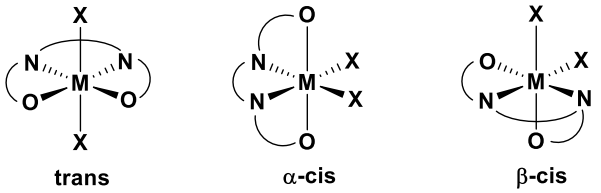

Figure 2.1. Different coordination geometries of group 4 metal compounds supported by tetradentate ligands.

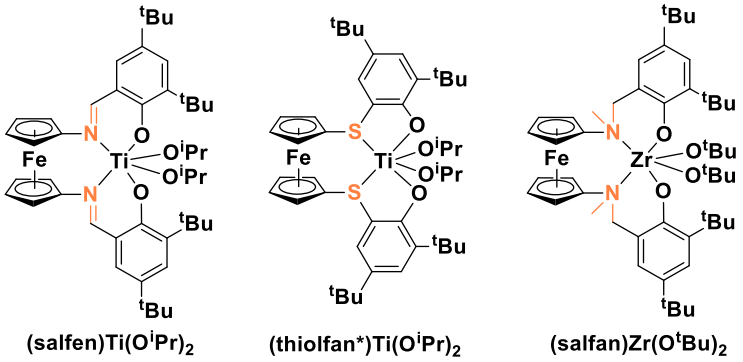

Chart 2.2. Previously reported ferrocene-derived Schiff base group 4 metal compounds.

Our group has been interested in the redox switchable polymerization of lactide and its copolymerization with other monomers.[35-39, 41-50] We were able to show that changing the oxidation state of iron in a ferrocene-based ligand modified the reactivity of a metal compound toward a certain monomer. Various ferrocene ligands were designed in the past few years and their corresponding metal compounds showed orthogonal activity toward cyclic ester polymerization.

For example, (thiolfan*)Ti(O^iPr)$_2$ (Chart 2.2, thiolfan* = 1,1'-di(2,4-di-*tert*-butyl-6-thiophenoxide)ferrocene) can polymerize L-lactide (LA) in the reduced state and ε-caprolactone (CL) in the oxidized state; (salfan)Zr(O^tBu)$_2$ (Chart 2.2, salfan = 1,1′-bis(di-2,4-*tert*-butyl-6-N-methylmethylenephenoxy)ferrocene) can polymerize LA in the reduced state and cyclohexene oxide (CHO) in the oxidized state.[39] We became interested in studying a ferrocene-derived Schiff base zirconium compound in order to simplify the ligand design and to compare its activity with that reported by Long et al. for the corresponding titanium compound. Herein, we discuss our results that indicate that a geometry change is observed for the corresponding zirconium compounds at a temperature above ambient condition. Furthermore, such a geometry change is necessary for these precatalysts to become active in lactide ring opening polymerization.

2.2. Results and discussion

Synthesis and characterization of the zirconium compounds

Three compounds, (salfen)Zr(O^tBu)$_2$, (salfen)Zr(O^iPr)$_2$, and (salfen)Zr(O^nPr)$_2$, were synthesized from the reaction of H_2(salfen) with Zr(O^tBu)$_4$, Zr(O^iPr)$_4$·HO^iPr and Zr(O^nPr)$_4$·HO^nPr (Scheme 2.1).

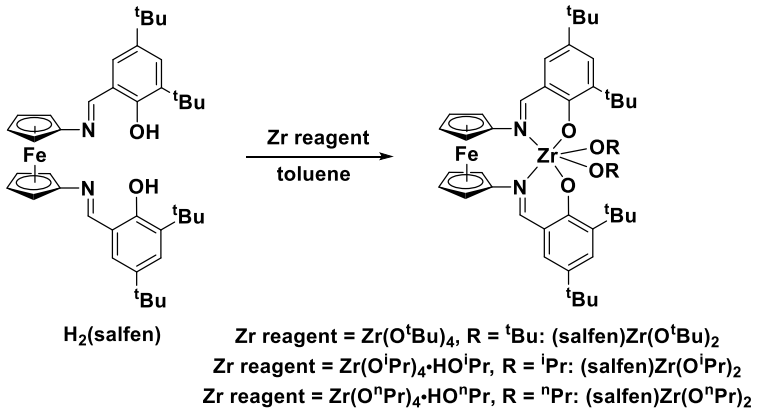

Scheme 2.1. Synthesis of zirconium compounds.

The ^{1}H NMR spectrum (Figure 2.2) of (salfen)Zr(O^{t}Bu)$_2$ indicated a non-symmetrical geometry at zirconium, and was different from the ^{1}H NMR spectrum of the symmetrical compound (salfan)Zr(O^{t}Bu)$_2$ (salfan = 1,1′-bis(di-2,4-*tert*-butyl-6-N-methylmethylenephenoxy)ferrocene), previously reported by our group.[39] This asymmetry made each proton on the aryl, imine, ferrocene, and alkoxide moieties to be magnetically nonequivalent. The solid state molecular structure (Figure 2.3) indicated a cis-β coordination geometry, which explained the asymmetrical peaks observed in the ^{1}H NMR spectrum.[24, 30]

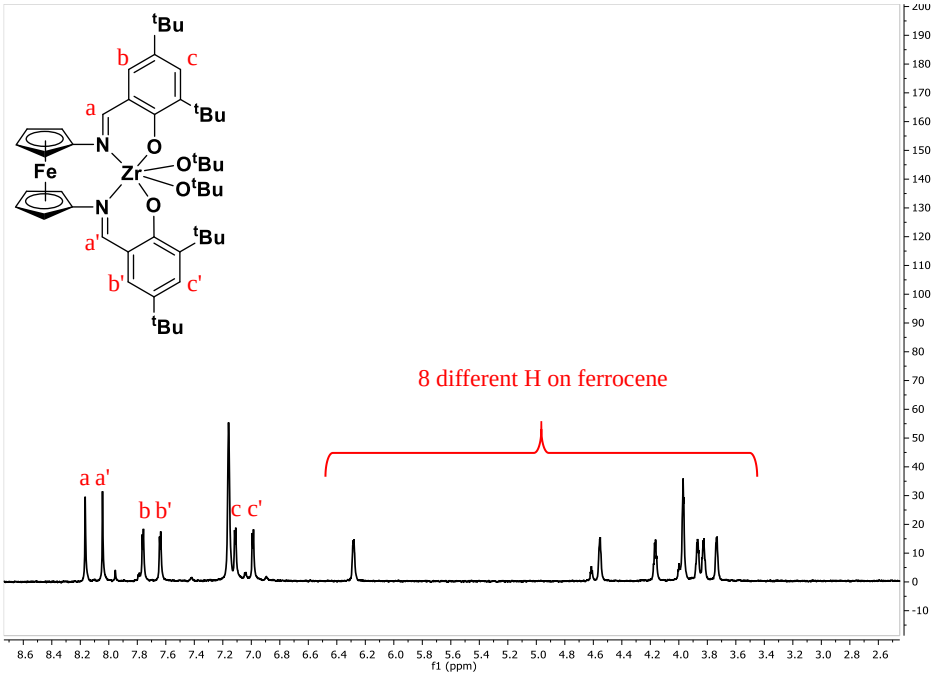

Figure 2.2. ^{1}H NMR spectrum (500 MHz, 25 ^{o}C, C_6D_6) of (salfen)Zr(O^tBu)$_2$.

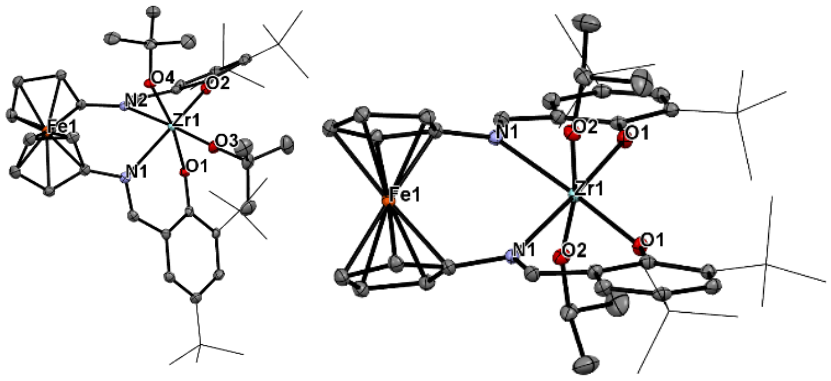

Figure 2.3. Thermal ellipsoid (50% probability) representation of (salfen)Zr(O^tBu)$_2$ (left, cis-β) and (salfen)Zr(O^iPr)$_2$ (right, trans). Hydrogen atoms were removed and aryl *t*-butyl groups are drawn as sticks for clarity.

Similar ^{1}H NMR spectra were obtained for (salfen)Zr($O^{i}Pr$)$_2$ and (salfen)Zr($O^{n}Pr$)$_2$. For both cases, however, there was always a set of small peaks that corresponded to another isomer (Figure 2.4), which could not be separated by purification through filtration or crystallization. The single crystals obtained from these solutions corresponded to these minor isomers, which showed a trans geometry in the solid state structure (Figure 2.3). Therefore, we hypothesized that the two isomers are in equilibrium with each other, with the cis-β geometry as the major isomer in solution at room temperature. This hypothesis was probed by variable temperature ^{1}H NMR spectroscopy (Figure 2.5) performed on (salfen)Zr($O^{n}Pr$)$_2$. At 100 ^{o}C, the peaks coalesced, indicating the existence of a fast equilibrium on the NMR timescale between the two isomers. The ^{1}H NMR spectrum reverted to that of the original sample after cooling to room temperature. The trans and cis-β geometry isomer percent content for all three zirconium compounds is listed in Table 2.1.

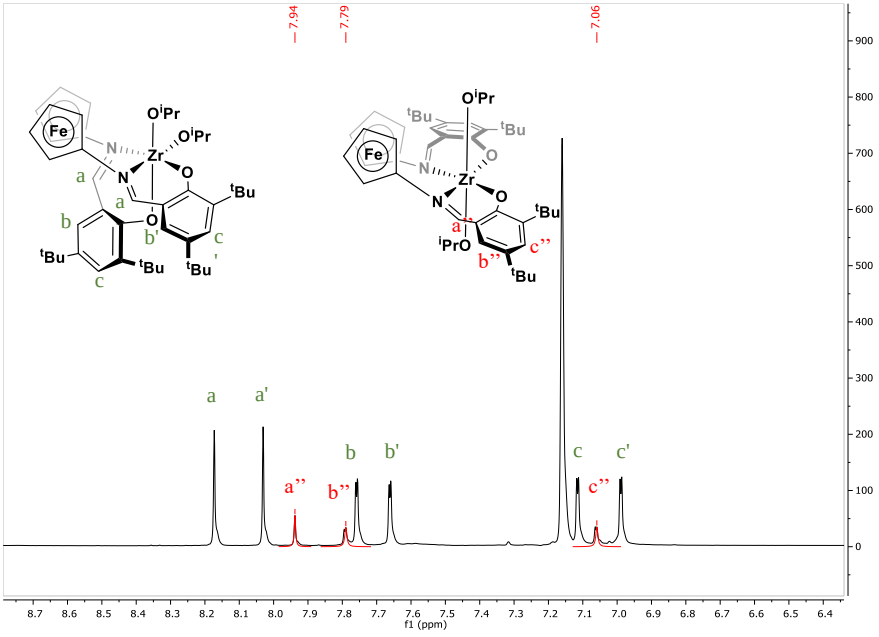

Figure 2.4. ^{1}H NMR spectrum (500 MHz, 25 ^{o}C, C_6D_6) of (salfen)Zr($O^{i}Pr$)$_2$.

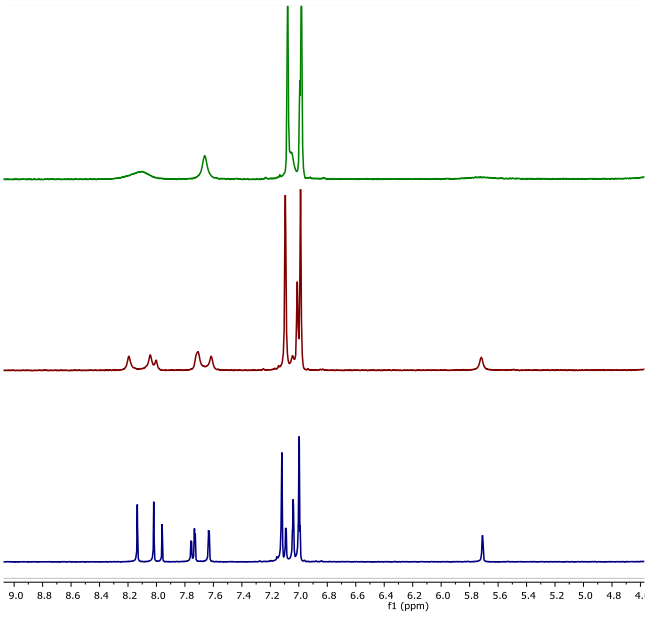

Figure 2.5. ^{1}H NMR spectra (500 MHz, d_8-toluene) of (salfen)Zr(O^{n}Pr)$_2$ at 25 ^{o}C (bottom), 70 ^{o}C (middle), and 100 ^{o}C (top).

Table 2.1. cis-β and trans geometry isomer contribution for each zirconium alkoxide in C_6D_6 solution at room temperature.

Compound	cis-β	trans
(salfen)Zr(O^{t}Bu)$_2$	95%	5%
(salfen)Zr(O^{i}Pr)$_2$	84%	16%
(salfen)Zr(O^{n}Pr)$_2$	71%	29%

DFT calculations were performed to compare the ground state energies of the zirconium compounds in both isomeric forms (Table 2.B3, entries 1-8). For a model compound, in which the ^{t}Bu groups on the phenoxides and the alkoxides (R = ^{t}Bu, ^{i}Pr, and ^{n}Pr) were replaced with H and

methoxides, respectively, the trans isomer was found to be 1.7 kcal/mol higher in energy than the cis-β isomer, in agreement with experimental observations. Calculations on the full molecules also agree with the experimental observations (salfen)Zr(O^tBu)$_2$ and (salfen)Zr(O^iPr)$_2$, for which the cis-β isomer is more stable than the trans isomer by 1.1 and 0.4 kcal/mol, respectively. In the case of (salfen)Zr(O^nPr)$_2$, the trans appeared slightly more favorable by 0.4 kcal/mol than the cis-β isomer. Although the calculations on the full molecules do not reproduce the expected isomer ratio for (salfen)Zr(O^nPr)$_2$, the trend of an increasing amount of trans isomer present at room temperature from (salfen)Zr(O^tBu)$_2$ to (salfen)Zr(O^iPr)$_2$ and to (salfen)Zr(O^nPr)$_2$ is reproduced well.

Polymerization of LA with the three zirconium compounds.

The three compounds were then used as pre-catalysts for LA homopolymerization reactions (Table 2.2). Compound (salfen)Zr(O^tBu)$_2$ did not work (Table 2.2, entry 1), but both (salfen)Zr(O^iPr)$_2$ (entry 2) and (salfen)Zr(O^nPr)$_2$ (entry 3) showed good activity for LA polymerization, with (salfen)Zr(O^iPr)$_2$ giving a slightly better yield: at 100 ^oC in benzene solution, (salfen)Zr(O^iPr)$_2$ reacted with 100 equiv. LA in 24 hours to give a 70% conversion, and (salfen)Zr(O^nPr)$_2$ reacted with 100 equiv. LA in 24 hours to give a 60% conversion.

Table 2.2. Polymerization of LA or ε-caprolactone (CL) with the three zirconium alkoxides.[a]

Entry	precatalyst	Temp. (^oC)	Time (h)	Conv.[b] (%)
1	(salfen)Zr(O^tBu)$_2$	100	24	<3
2	(salfen)Zr(O^iPr)$_2$	100	24	70
3	(salfen)Zr(O^nPr)$_2$	100	24	60

4	(salfen)Zr(O^iPr)$_2$	70	24	<3
5	(salfen)Zr(O^iPr)$_2$	100/70	2/22	21
6	(salfen)Zr(O^iPr)$_2$	100	24	<3
7	(salfen)Zr(O^nPr)$_2$	100	24	<3

[a] All experiments were conducted in 0.8 mL of C_6D_6, with 0.004 mmol zirconium compound and 0.4 mmol LA, except for entries 6 and 7, when CL was used (1:100 equivalents), and hexamethylbenzene as an internal standard; [b] the conversion was calculated from the integration of ^{1}H NMR peaks against those of hexamethylbenzene. Dispersity and molar mass information can be found in Table 2.B1.

^{1}H NMR monitoring experiments showed that (salfen)Zr(O^iPr)$_2$ and (salfen)Zr(O^nPr)$_2$ experienced a geometry change during polymerization after 2 hours at 100 ^{o}C (Figures 2.B15, 2.B16). On the other hand, such a change was not observed for (salfen)Zr(O^tBu)$_2$ at 100 ^{o}C after 24 hours (Figure 2.B17). After the geometry change, (salfen)Zr(O^iPr)$_2$ and (salfen)Zr(O^nPr)$_2$ started catalyzing the polymerization of LA. Such activity was not observed for (salfen)Zr(O^tBu)$_2$, an observation consistent with similar reports indicating no activity for cis-β geometry compounds.[24, 51, 52] The same reaction (Table 2.2, entry 4) was tested at 70 ^{o}C, but less than 5% conversion was observed after 24 hours. A control experiment (Table 2.2, entry 5) was designed as follows: firstly, the sample was heated at 100 ^{o}C for 2 hours, then at 70 ^{o}C for 22 hours. This experiment showed 7% conversion after the first two hours of heating at 100 ^{o}C and then 21% overall conversion, demonstrating that the geometry change from cis-β to trans is necessary for the polymerization to occur.

(salfen)Zr(O^iPr)$_2$ and (salfen)Zr(O^nPr)$_2$ were also tested for CL homopolymerization (Table 2.2, entry 6 and 7) but neither of them showed activity. No polymerization or geometry change of the zirconium compound was observed after heating either zirconium compound at 100 ^oC for 24 hours in the presence of CL. Though it was proved that the zirconium compounds could isomerize to the trans geometry at 100 ^oC by themselves, CL did not allow the geometry change to occur.

Although (salfen)Zr(O^iPr)$_2$ did not react with ε-caprolactone, we reasoned that once the geometry change can be induced, the results would be different. Therefore, an experiment was designed to have (salfen)Zr(O^iPr)$_2$ and 100 equivalents of LA reacting for 24 hours at 100 ^oC first, giving a conversion of 74%, after which, 100 equivalents of CL was added and reacted for another 24 hours at 100 ^oC, giving a CL conversion of 12% and LA conversion of 90%. This result shows that during the second 24 hours, CL did get polymerized. DOSY NMR spectroscopy was used to show that the product is a copolymer (Figure 2.B14).

In order to understand further the relationship between polymerization and geometry change, we decided to isolate the product of a 1:1 molar equivalent reaction between a zirconium alkoxide and LA. (salfen)Zr(O^nPr)$_2$ was chosen since it has the highest trans geometry isomer ratio at 298 K. The (salfen)Zr(O^nPr)$_2$-LA addition compound was successfully synthesized and isolated as a precipitate from *n*-hexane. The corresponding NOESY (Figure 2.B18) spectrum indicated that the structure is consistent with a ring opened lactide product.

Variable temperature ^1H NMR spectroscopic studies with (salfen)Zr(O^nPr)$_2$-LA compound (Figures 2.B10, 2.B20, and 2.B21) indicate that, at room temperature, a mixture of the two isomers, cis-β and trans is present. At -30 ^oC, the trans isomer predominates, indicating that it is the thermodynamically favored isomer, unlike the case of the zirconium bis-alkoxide compounds. As

the temperature was increased, the trans to cis-β interconversion became faster, indicated by the broadening of the NMR peaks.

In order to determine whether the length of the polymer chain has an influence on the cis-β to trans isomerization, we performed another set of variable temperature NMR experiments while the LA polymerization was ongoing (100 equivalents LA added but conversion stopped only at 40%). In this case, there was no difference between the spectra taken at temperatures ranging from 25 ^{o}C to 100 ^{o}C (Figure 2.B23). The spectra are consistent with the presence of the trans isomer.

A comparison of ^{1}H NMR spectra corresponding to (salfen)Zr($O^{n}Pr$)$_2$, (salfen)Zr($O^{n}Pr$)$_2$-LA and (salfen)Zr-polymer (Figures 2.B24 and 2.B25) showed that peaks for cis-β (salfen)Zr($O^{n}Pr$)$_2$ were present alongside the mixture of trans and cis-β isomers of (salfen)Zr($O^{n}Pr$)$_2$-LA. This finding indicates that it is possible that the cis-β isomer reacts with LA to form cis-β (salfen)Zr($O^{n}Pr$)$_2$-LA or that cis-β (salfen)Zr($O^{n}Pr$)$_2$-LA originates only from the trans to cis-β isomerization and the amount of cis-β (salfen)Zr($O^{n}Pr$)$_2$ present at the end of the reaction is unreacted starting material. These possibilities are shown in Scheme 2.2.

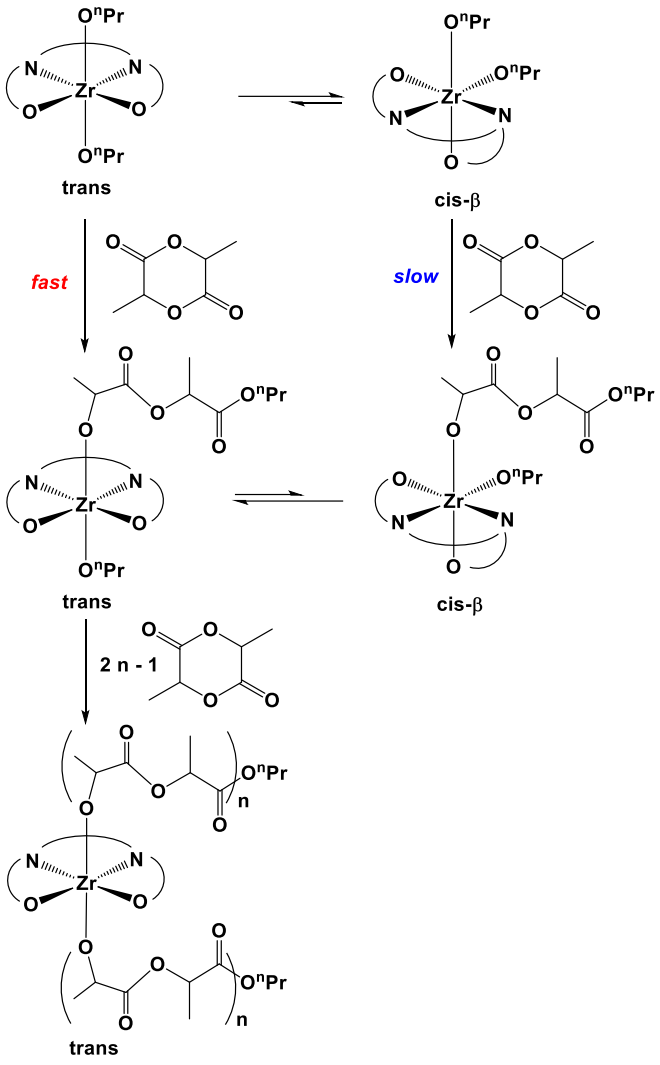

Scheme 2.2. Proposed reactions between (salfen)Zr(O^nPr)$_2$ and LA.

Computational studies also support the fact that the trans isomer of (salfen)Zr(O^nPr)$_2$-LA is more stable than the cis-β form. The products of the ring opening polymerization of one L-lactide by cis-β and trans zirconium modeled compounds (aryl ^{t}Bu groups replaced by hydrogen atoms) were calculated with the full O^tBu, O^iPr, and O^nPr ligands (Table 2.B3, entries 18-23). In all cases, trans (salfen)Zr(OR)$_2$-LA is more favorable than the cis-β isomer by -2.5, -2.1, and -4.4 kcal/mol, respectively.

2.3. Conclusion

We synthesized and characterized a series of zirconium alkoxide compounds bearing a ferrocene unit in the ligand backbone. All three compounds adopted a cis-β coordination geometry as the major isomer in solution in room temperature. The solid state molecular structures showed, however, that although (salfen)Zr(O^tBu)$_2$ crystallized as the cis-β isomer, the trans isomer of (salfen)Zr(O^iPr)$_2$ and (salfen)Zr(O^nPr)$_2$ was characterized by single crystal X-ray diffraction. An equilibrium between the cis-β and trans isomers is established in solution as supported by variable temperature ^{1}H NMR spectroscopy. Compounds (salfen)Zr(O^iPr)$_2$ and (salfen)Zr(O^nPr)$_2$ catalyzed the ring opening polymerization of LA after a geometry change to the trans isomer occurred. The product isolated from a 1:1 LA to (salfen)Zr(O^nPr)$_2$ addition, along with computational studies, also supported the conclusion that a geometry change to the trans isomer is necessary for the reaction with LA to occur.

2.4. Experimental section

General considerations.

All experiments were performed under a dry nitrogen atmosphere using standard Schlenk techniques or an MBraun inert-gas glovebox. Solvents were purified using a two-column solid-state purification system by the method of Grubbs[53] and transferred to the glovebox without exposure to air. NMR solvents were obtained from Cambridge Isotope Laboratories, degassed, and stored over activated molecular sieves prior to use. ^{1}H NMR spectra were recorded on Bruker 300 and Bruker 500 spectrometers at room temperature in C_6D_6 or $CDCl_3$. Chemical shifts are reported

with respect to internal solvent: 7.16 ppm (C_6D_6) and 7.26 ppm ($CDCl_3$) for ^{1}H NMR spectra. Cyclohexene oxide and 1,2-difluorobenzene were distilled over CaH_2 and brought into the glovebox without exposure to air. L-Lactide and hexamethylbenzene were recrystallized from toluene at least twice before use. 2,4-Di-*tert*-butylphenol, *n*-BuLi, cobaltocene, $Zr(O^tBu)_4$, $Zr(O^iPr)_4 \cdot HO^iPr$ and $Zr(O^nPr)_4 \cdot HO^nPr$ were purchased from VWR and used as received. $^{Ac}FcBAr^{F54}$ and H_2(salfen)[39] were synthesized following previously published procedures. Molar masses of the polymers were determined with a GPC-MALS instrument at UCLA. GPC-MALS uses a Shimadzu Prominence-i LC 2030C 3D instrument equipped with an autosampler, two MZ Analysentechnik MZ-Gel SDplus LS 5 μm, 300 × 8 mm linear columns, and Wyatt DAWN HELEOS-II and Wyatt Optilab T-rEX apparatus. The column temperature was set at 40 °C. A flow rate of 0.70 mL/min was used, and samples were dissolved in chloroform or THF. dn/dc values were calculated for PLA and PCHO by making five solutions of increasing concentration (0.1− 1.0 mg/mL), directly injecting them into the RI detector sequentially, and using the batch dn/dc measurement methods in the Astra software. The dn/dc values for PLA and PCHO were calculated to be 0.024 and 0.086 mL/g, respectively, over three trials.

DFT calculations.

Calculations were performed at the density functional theory level in Turbomole.[55, 56] Geometry optimizations and frequency calculations were carried out with the TPSS functional,[57-60] the def2-SVP basis set was used on all non-metal atoms[61, 62] and the def2-TZVPP basis set was used for Fe and Zr.[62] Single point energies were calculated with the TPSSH functional[58-60, 63] and the def2-TZVPP basis set was used on all atoms. DFT-D3 was applied on all calculations to account for dispersion corrections.[64] For solvation effects, COSMO[65, 66] was applied with the dielectric constant corresponding to benzene (ε = 2.27). All structures were confirmed by their

vibrational frequencies; intermediate structures were characterized by zero imaginary frequencies. The Gibbs free energy was calculated as the sum of the *in vacuo* electronic energy, solvation free energy, zero-point energy, and the entropic and thermal corrections obtained from the frequency calculations at 298.15 K and 1 atm.

Synthesis of (salfen)Zr(O^{t}Bu)$_2$.

H_2(salfen) (194.6 mg, 0.3 mmol) and Zr(O^{t}Bu)$_4$ (115.0 mg, 0.3 mmol) were each dissolved in 5 mL toluene. Both solutions were cooled to -78 ^{o}C for 10 min and then combined. The mixture was stirred at -78 ^{o}C for 30 min and warmed to room temperature for 2 h. The volatiles were removed under a reduced pressure and the resulting solids were dissolved into hexanes and filtered through Celite. The hexanes solution was concentrated under vacuum and put into a -30 ^{o}C freezer to give (salfen)Zr(O^{t}Bu)$_2$ as an amorphous precipitate after four days; yield: 134 mg (51%). ^{1}H NMR (300 MHz, C_6D_6, 298 K, δ, ppm): 8.17 (s, 1H, N=C*H*), 8.04 (s, 1H, N=C*H*), 7.76 (d, 1H, *m*-OC$_6$*H*$_2$), 7.64 (d, 1H, *m*-OC$_6$*H*$_2$), 7.11 (d, 1H, *m*-OC$_6$*H*$_2$), 6.99 (d, 1H, *m*-OC$_6$*H*$_2$), 6.27 (s, 1H, C$_5$*H*$_4$), 4.6-3.7 (m, 7H, C$_5$*H*$_4$), 1.78 (s, 9H, OC(C*H*$_3$)$_3$), 1.59 (s, 9H, OC(C*H*$_3$)$_3$), 1.41 (s, 9H, C(C*H*$_3$)$_3$), 1.35 (s, 9H, C(C*H*$_3$)$_3$), 1.33 (s, 9H, C(C*H*$_3$)$_3$), 1.16 (s, 9H, C(C*H*$_3$)$_3$). ^{13}C NMR (500 MHz, C_6D_6, 298 K, δ, ppm): 174.3 (N=*C*), 165.3 (N=*C*), 162.4 (*m*-O*C*$_6$H$_2$), 161.7 (*m*-O*C*$_6$H$_2$), 139.7 (*m*-O*C*$_6$H$_2$), 138.6 (*m*-O*C*$_6$H$_2$), 138.4 (*m*-O*C*$_6$H$_2$), 137.5 (*m*-O*C*$_6$H$_2$), 130.3 (*m*-O*C*$_6$H$_2$), 129.6 (*m*-O*C*$_6$H$_2$), 129.5 (*m*-O*C*$_6$H$_2$), 127.3 (*m*-O*C*$_6$H$_2$), 123.7 (*m*-O*C*$_6$H$_2$), 123.2 (*m*-O*C*$_6$H$_2$), 111.6 (*m*-O*C*$_6$H$_2$), 107.6 (*C*$_5$H$_4$), 76.2 (*C*$_5$H$_4$), 75.4 (*C*$_5$H$_4$), 70.3 (*C*$_5$H$_4$), 69.2 (*C*$_5$H$_4$), 68.1 (*C*$_5$H$_4$), 67.9 (*C*$_5$H$_4$), 66.4 (*C*$_5$H$_4$), 66.3 (*C*$_5$H$_4$), 65.2 (O*C*(CH$_3$)$_3$), 62.6 (O*C*(CH$_3$)$_3$), 35.5 (C(*C*H$_3$)$_3$), 34.9 (C(*C*H$_3$)$_3$), 34.1 (C(*C*H$_3$)$_3$), 33.8 (C(*C*H$_3$)$_3$), 33.1 (C(*C*H$_3$)$_3$), 31.9 (C(*C*H$_3$)$_3$), 31.3 (C(*C*H$_3$)$_3$), 30.4 (C(*C*H$_3$)$_3$), 29.9 (C(*C*H$_3$)$_3$). Anal. Calcd. for (salfen)Zr(O^{t}Bu)$_2$•(C$_6$H$_{14}$)$_{0.5}$ (C$_{51}$H$_{75}$N$_2$O$_4$FeZr): C, 66.06; H, 8.15; N, 3.02; Found: C, 65.63; H, 8.52; N, 2.91.

Synthesis of (salfen)Zr(O^iPr)$_2$.

H_2(salfen) (163.0 mg, 0.25 mmol) was dissolved in toluene (5 mL) and Zr(O^iPr)$_4$•HO^iPr (193.9 mg, 0.5 mmol) was dissolved in toluene (10 mL), respectively. Both solutions were cooled to -78 ^oC for 10 min and combined. The mixture was stirred at -78 ^oC for 30 min and move to room temperature for 2 h. The volatiles were removed under a reduced pressure for 5 h. The solids were dissolved again in toluene, stir for 2 h and the volatiles were removed under a reduced pressure again for 5 h, and repeat this "dissolve-stir-pump" procedure for one more time. The solids were dissolved into hexanes and filtered through Celite. The hexanes solution was concentrated under reduced pressure and put into freezer to give (salfen)Zr(O^iPr)$_2$ as a crystalline precipitate after four days. Yield: 102 mg (47%). ^{1}H NMR (300 MHz, C_6D_6, 298 K, δ, ppm): 8.17 (s, 1H, N=C*H*), 8.03 (s, 1H, N=C*H*), 7.76 (d, 1H, *m*-OC_6H_2), 7.66 (d, 1H, *m*-OC_6H_2), 7.11 (d, 1H, *m*-OC_6H_2), 6.99 (d, 1H, *m*-OC_6H_2), 5.83 (s, 1H, C_5H_4), 4.60 (m, 1H, OC*H*(CH_3)$_2$), 4.30 (m, 1H, OC*H*(CH_3)$_3$), 4.4-3.8 (m, 7H, C_5H_4), 1.78 (s, 6H, OCH(CH_3)$_2$), 1.47 (s, 6H, OCH(CH_3)$_2$), 1.34 (s, 18H, C(CH_3)$_3$), 1.32 (s, 18H, C(CH_3)$_3$). ^{13}C NMR (500 MHz, C_6D_6, 298 K, δ, ppm): 173.3 (N=*C*), 164.8 (N=*C*), 162.5 (*m*-O*C*$_6H_2$), 161.7 (*m*-O*C*$_6H_2$), 139.6 (*m*-O*C*$_6H_2$), 138.7 (*m*-O*C*$_6H_2$), 138.6 (*m*-O*C*$_6H_2$), 137.6 (*m*-O*C*$_6H_2$), 130.0 (*m*-O*C*$_6H_2$), 129.6 (*m*-O*C*$_6H_2$), 129.3 (*m*-O*C*$_6H_2$), 123.5 (*m*-O*C*$_6H_2$), 123.1 (*m*-O*C*$_6H_2$), 111.4, 107.7 (*C*$_5H_4$), 71.7 (*C*$_5H_4$), 70.6 (*C*$_5H_4$), 70.0 (*C*$_5H_4$), 69.7 (*C*$_5H_4$), 68.5 (*C*$_5H_4$), 67.9 (*C*$_5H_4$), 67.3 (*C*$_5H_4$), 66.5, (*C*$_5H_4$), 64.7, 62.3 (O*C*H(CH_3)$_2$), 35.5 (C(*C*H_3)$_3$), 35.1 (C(*C*H_3)$_3$), 34.6 (C(*C*H_3)$_3$), 33.8 (C(*C*H_3)$_3$), 31.3 (C(*C*H_3)$_3$), 30.1 (C(*C*H_3)$_3$), 29.9 (C(*C*H_3)$_3$), 27.3 (C(*C*H_3)$_3$), 26.4 (OCH(*C*H_3)$_2$), 26.3 (OCH(*C*H_3)$_2$). Anal. Calcd. for $C_{46}H_{64}N_2O_4FeZr$: C, 64.54; H, 7.53; N, 3.27. Found: C, 64.42; H, 7.36; N, 3.17.

Synthesis of (salfen)Zr(O^nPr)$_2$.

H_2(salfen) (163.0 mg, 0.25 mmol) was dissolved in toluene (5 mL) and Zr(O^nPr)$_4$•HO^nPr (193.9 mg, 0.5 mmol) was dissolved in toluene (10 mL), respectively. Both solutions were cooled to -78 ^oC for 10 min and combined. The mixture was stirred at -78 ^oC for 30 min and move to room temperature for 2 h. The volatiles were removed under a reduced pressure for 5 h. The solids were dissolved again in toluene, stirred for 2 h and the volatiles were removed under a reduced pressure again for 5 h; this "dissolve-stir-pump" procedure was repeated for one more time. Finally, the solids were dissolved into hexanes and filtered through Celite. The hexane solution was concentrated under reduced pressure and put into freezer to give (salfen)Zr(O^nPr)$_2$ as a crystalline precipitate after four days. Yield: 113 mg (53%). ^{1}H NMR (500 MHz, C_6D_6, 298 K, δ, ppm): 8.17 (s, 1H, N=C*H*), 8.03 (s, 1H, N=C*H*), 7.76 (d, 1H, *m*-OC_6H_2), 7.65 (d, 1H, *m*-OC_6H_2), 7.10 (d, 1H, *m*-OC_6H_2), 6.98 (d, 1H, *m*-OC_6H_2), 5.76 (s, 1H, C_5H_4), 4.38 (m, 2H, $OCH_2CH_2CH_3$), 4.28 (m, 2H, $OCH_2CH_2CH_3$), 4.5-3.8 (m, 7H, C_5H_4), 1.88 (m, 4H, $OCH_2CH_2CH_3$), 1.78 (m, 6H, $OCH_2CH_2CH_3$), 1.47 (s, 18H, $C(CH_3)_3$), 1.33 (s, 18H, $C(CH_3)_3$). ^{13}C NMR (500 MHz, C_6D_6, 298 K, δ, ppm): 174.2 (N=*C*), 169.7 (N=*C*), 163.4 (*m*-OC_6H_2), 162.5 (*m*-OC_6H_2), 140.6 (*m*-OC_6H_2), 138.7 (*m*-OC_6H_2), 138.6 (*m*-OC_6H_2), 137.6 (*m*-OC_6H_2), 129.9 (*m*-OC_6H_2), 129.6 (*m*-OC_6H_2), 129.4 (*m*-OC_6H_2), 124.1 (*m*-OC_6H_2), 123.9 (*m*-OC_6H_2), 112.0 (C_5H_4), 108.7 (C_5H_4), 73.3 (C_5H_4), 72.8 (C_5H_4), 72.1 (C_5H_4), 71.0 (C_5H_4), 68.5 (C_5H_4), 67.9 (C_5H_4), 67.3 (C_5H_4), 65.8 (C_5H_4), 65.6 ($OCH_2CH_2CH_3$), 63.3 ($OCH_2CH_2CH_3$), 36.8 ($OCH_2CH_2CH_3$), 36.4 ($OCH_2CH_2CH_3$), 34.6 ($OCH_2CH_2CH_3$), 33.8 ($OCH_2CH_2CH_3$), 31.3 ($C(CH_3)_3$), 30.1 ($C(CH_3)_3$), 29.9 ($C(CH_3)_3$), 28.9 ($C(CH_3)_3$), 28.5 ($C(CH_3)_3$), 28.1 ($C(CH_3)_3$). Anal. Calcd. for $C_{46}H_{64}N_2O_4FeZr$: C, 64.54; H, 7.54; N, 3.27. Found: C, 63.97; H, 7.48; N, 3.18.

Synthesis of (salfen)Zr(O^nPr)$_2$-LA.

(salfen)Zr(O^nPr)$_2$ (207.6 mg, 0.24 mmol) and LA (35.7 mg, 0.24 mmol) were added to benzene (4.5 mL). The mixture was sealed in a Schlenk tube, brought out of the glovebox, heated and stirred at 100 ^oC overnight. The Schlenk tube was brought into the glovebox the next day. The volatiles were removed under a reduced pressure and the solids were dissolved in hexanes and filtered through Celite. The hexanes solution was concentrated under reduced pressure and put into a freezer to give the compound as a needle-shape crystalline precipitate after 7 days. Yield: 85 mg (35%). ^{1}H NMR (300 MHz, C_6D_6, 298 K, δ, ppm): 8.11 (s, 2H, N=C*H*), 7.71 (s, 2H, *m*-OC_6H_2), 7.02 (s, 2H, *m*-OC_6H_2), 5.33 (br, 2H, C_5H_4), 4.66 (br, 2H, C_5H_4), 4.16 (br, 2H, C_5H_4), 4.07 (br, 2H, C_5H_4), 4.88 (s, 2H, OC*H*(CH_3)COO), 3.81 (br, 2H, OC*H*$_2$$CH_2CH_3$), 3.79 (br, 2H, OC*H*$_2$$CH_2CH_3$), 1.84 (br, 3H, OCH(C*H*$_3$)COO), 1.59 (br, 3H, OCH(C*H*$_3$)COO), 1.41 (br, 2H, OCH_2C*H*$_2$$CH_3$), 1.23 (br, 2H, OCH_2C*H*$_2$$CH_3$), 1.30 (br, 36H, C(C*H*$_3$)$_3$), 0.89 (br, 6H, OCH_2CH_2C*H*$_3$). ^{13}C NMR (500 MHz, C_6D_6, 298 K, δ, ppm): 176.1 (*C*OO), 171.3 (N=*C*), 162.8 (*m*-O*C*$_6$$H_2$), 139.8 (*m*-O*C*$_6$$H_2$), 139.5 (*m*-O*C*$_6$$H_2$), 130.9 (*m*-O*C*$_6$$H_2$), 128.0 (*m*-O*C*$_6$$H_2$), 124.2 (*m*-O*C*$_6$$H_2$), 108.4 (*C*$_5$$H_4$), 75.0 (O*C*HCOO), 69.8 (*C*$_5$$H_4$), 69.3 (*C*$_5$$H_4$), 68.9 (*C*$_5$$H_4$), 68.7 (*C*$_5$$H_4$), 67.7 (*C*$_5$$H_4$), 66.5 (*C*$_5$$H_4$), 65.9 (*C*$_5$$H_4$), 64.8 (*C*$_5$$H_4$), 34.7 (*C*($CH_3$)$_3$), 32.2 (C(*C*$H_3$)$_3$), 31.0 ($OCH_2$*C*$H_2CH_3$), 22.9 ($OCH_2CH_2$*C*$H_3$). Anal. Calcd. for (salfen)Zr(O^nPr)$_2$-LA•(C_6H_{14})$_{0.5}$ ($C_{55}H_{79}N_2O_8FeZr$): C, 63.32; H, 7.63; N, 2.69. Found: C, 63.27; H, 7.46; N, 2.65.

Polymerization of LA by (salfen)Zr(O^iPr)$_2$.

To a C_6D_6 (0.7 mL) solution of (salfen)Zr(O^iPr)$_2$ (3.4 mg, 4.0 μmol) in a J. Young NMR tube were added a solution of hexamethylbenzene (8.1 mg, 5.0 μmol) in C_6D_6 (0.1 mL) and LA powder (57.6 mg, 0.4 mmol). The reaction mixture was heated to 100 ^oC for 24 hours and monitored by ^{1}H NMR spectroscopy. At the end, the reaction mixture was dissolved in CH_2Cl_2 and poured into cold methanol; a white solid precipitated briefly and was filtered.

Copolymerization of LA and CL by (salfen)Zr(O^iPr)$_2$.

To a C_6D_6 (0.7 mL) solution of (salfen)Zr(O^iPr)$_2$ (3.4 mg, 4.0 μmol) in a J. Young NMR tube were added a solution of hexamethylbenzene (8.1 mg, 5.0 μmol) in C_6D_6 (0.1 mL) and LA powder (57.6 mg, 0.4 mmol). The reaction mixture was heated to 100 ^oC for 24 hours and monitored by ^1H NMR spectroscopy. CL (45.6 mg, 4.0 μmol) was added after, and heated for another 24 hours, monitoring by ^1H NMR spectroscopy. At the end, the reaction mixture was dissolved in CH_2Cl_2 and poured into cold methanol; a white solid precipitated briefly and was filtered.

2.5. Appendix B

NMR Spectra

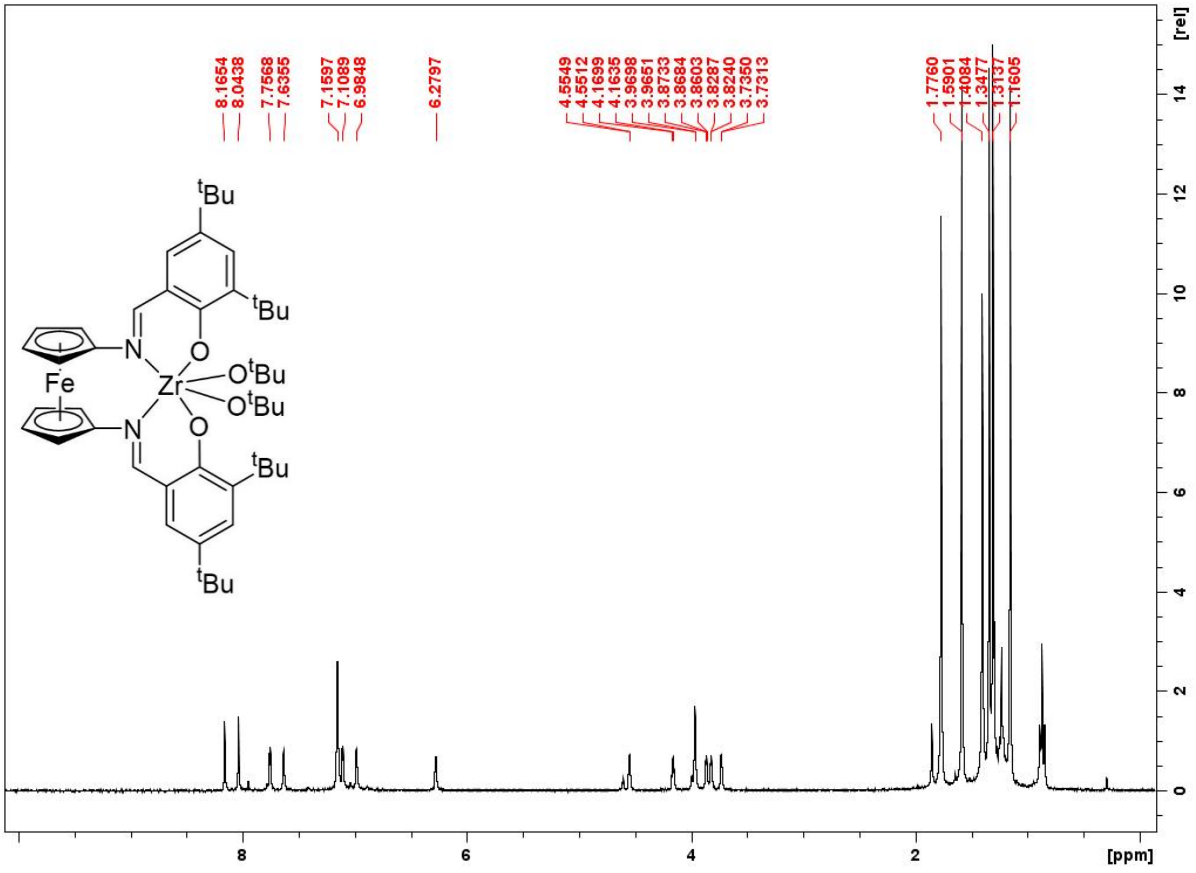

Figure 2.B1. ^{1}H NMR (300 MHz, C_6D_6, 298 K) spectrum of (salfen)Zr(O^{t}Bu)$_2$. δ, ppm: 8.17 (s, 1H, N=C*H*), 8.04 (s, 1H, N=C*H*), 7.76 (d, 1H, *m*-OC$_6$*H*$_2$), 7.64 (d, 1H, *m*-OC$_6$*H*$_2$), 7.11 (d, 1H, *m*-OC$_6$*H*$_2$), 6.99 (d, 1H, *m*-OC$_6$*H*$_2$), 6.27 (s, 1H, C$_5$*H*$_4$), 4.6-3.7 (m, 7H, C$_5$*H*$_4$), 1.78 (s, 9H, OC(C*H*$_3$)$_3$), 1.59 (s, 9H, OC(C*H*$_3$)$_3$), 1.41 (s, 9H, C(C*H*$_3$)$_3$), 1.35 (s, 9H, C(C*H*$_3$)$_3$), 1.33 (s, 9H, C(C*H*$_3$)$_3$), 1.16 (s, 9H, C(C*H*$_3$)$_3$).

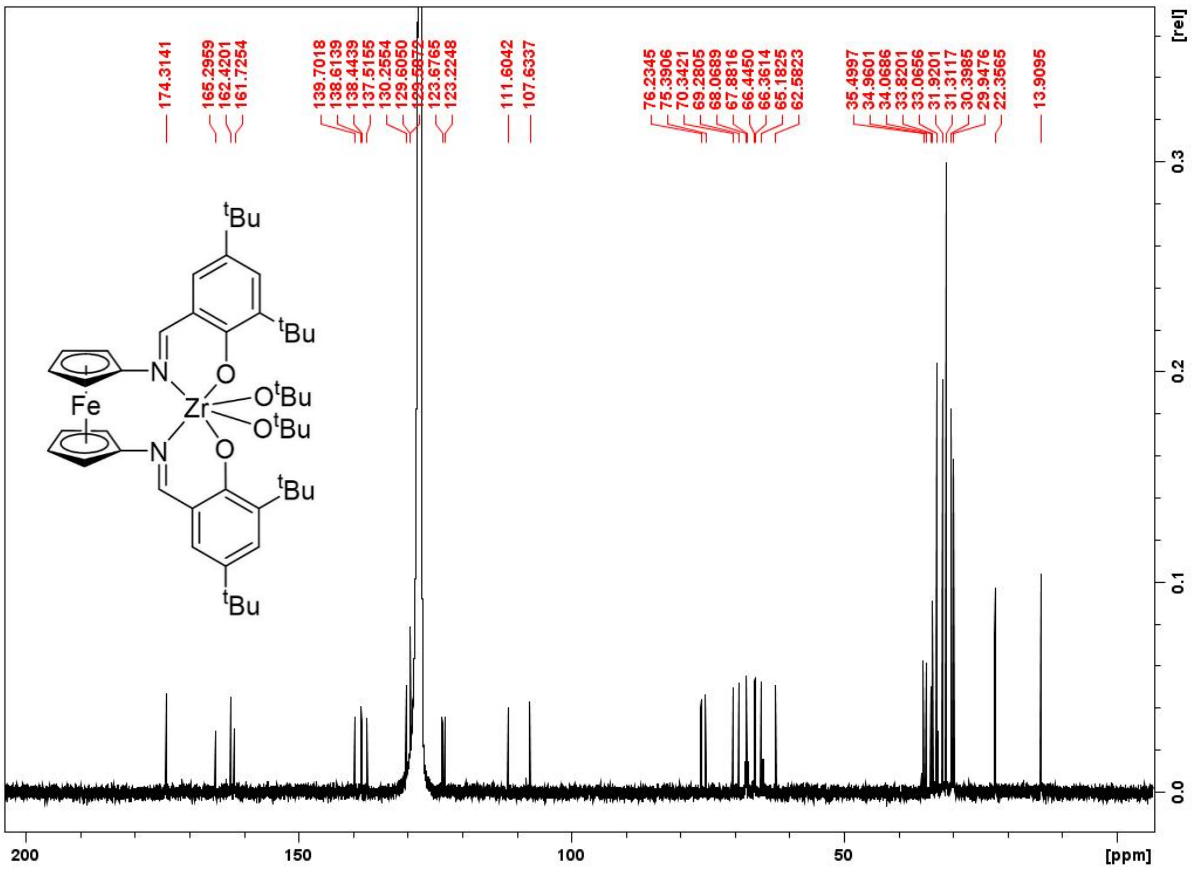

Figure 2.B2. ^{13}C NMR (500 MHz, C_6D_6, 298 K) spectrum of (salfen)Zr(O^{t}Bu)$_2$. δ, ppm: 174.3 (N=*C*), 165.3 (N=*C*), 162.4 (*m*-O*C*$_6$H$_2$), 161.7 (*m*-O*C*$_6$H$_2$), 139.7 (*m*-O*C*$_6$H$_2$), 138.6 (*m*-O*C*$_6$H$_2$), 138.4 (*m*-O*C*$_6$H$_2$), 137.5 (*m*-O*C*$_6$H$_2$), 130.3 (*m*-O*C*$_6$H$_2$), 129.6 (*m*-O*C*$_6$H$_2$), 129.5 (*m*-O*C*$_6$H$_2$), 127.3 (*m*-O*C*$_6$H$_2$), 123.7 (*m*-O*C*$_6$H$_2$), 123.2 (*m*-O*C*$_6$H$_2$), 111.6 (*m*-O*C*$_6$H$_2$), 107.6 (*C*$_5$H$_4$), 76.2 (*C*$_5$H$_4$), 75.4 (*C*$_5$H$_4$), 70.3 (*C*$_5$H$_4$), 69.2 (*C*$_5$H$_4$), 68.1 (*C*$_5$H$_4$), 67.9 (*C*$_5$H$_4$), 66.4 (*C*$_5$H$_4$), 66.3 (*C*$_5$H$_4$), 65.2 (O*C*(CH$_3$)$_3$), 62.6 (O*C*(CH$_3$)$_3$), 35.5 (C(*C*H$_3$)$_3$), 34.9 (C(*C*H$_3$)$_3$), 34.1 (C(*C*H$_3$)$_3$), 33.8 (C(*C*H$_3$)$_3$), 33.1 (C(*C*H$_3$)$_3$), 31.9 (C(*C*H$_3$)$_3$), 31.3 (C(*C*H$_3$)$_3$), 30.4 (C(*C*H$_3$)$_3$), 29.9 (C(*C*H$_3$)$_3$).

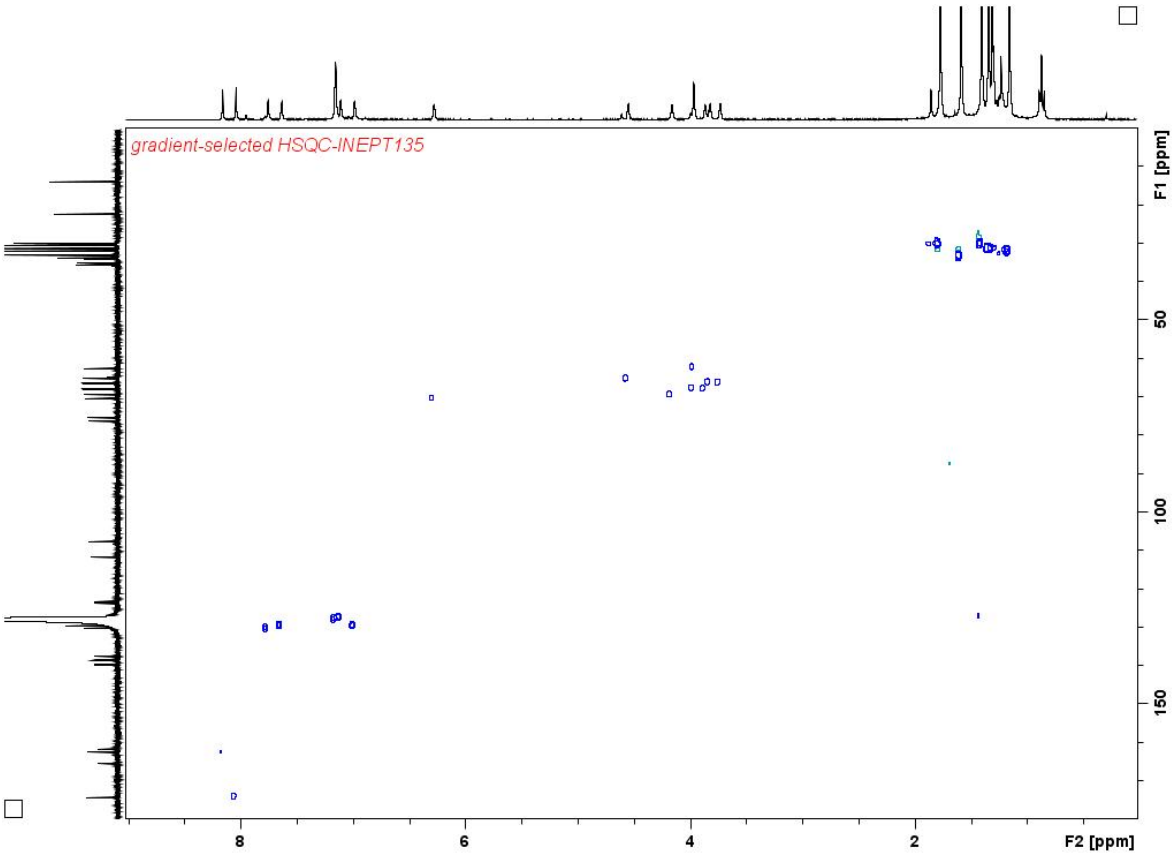

Figure 2.B3. 2D HSQC NMR (500 MHz, C_6D_6, 298 K) spectrum of (salfen)Zr(O^tBu)$_2$.

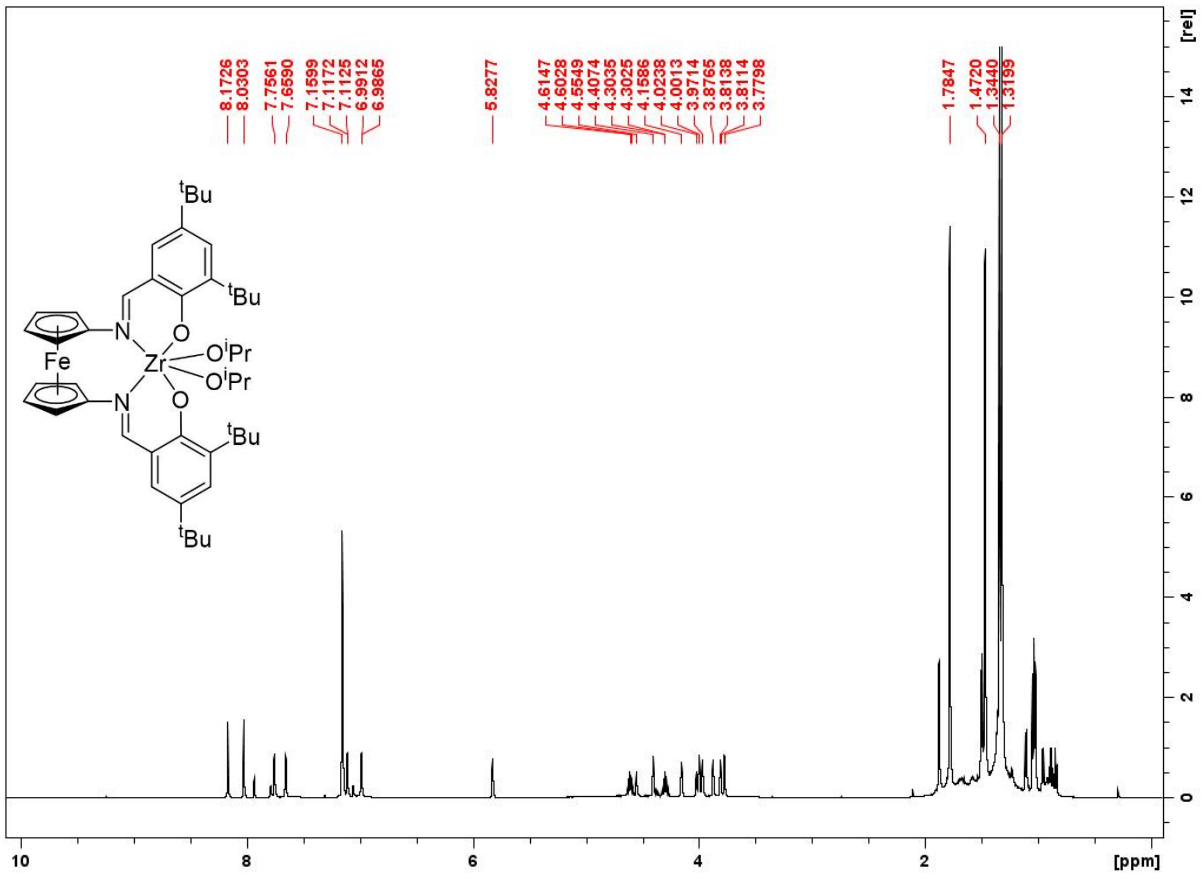

Figure 2.B4. ^{1}H NMR (300 MHz, C_6D_6, 298 K) spectrum of (salfen)Zr(O^iPr)$_2$. δ, ppm: 8.17 (s, 1H, N=C*H*), 8.03 (s, 1H, N=C*H*), 7.76 (d, 1H, *m*-OC_6H_2), 7.66 (d, 1H, *m*-OC_6H_2), 7.11 (d, 1H, *m*-OC_6H_2), 6.99 (d, 1H, *m*-OC_6H_2), 5.83 (s, 1H, C_5H_4), 4.60 (m, 1H, $OCH(CH_3)_2$), 4.30 (m, 1H, $OCH(CH_3)_3$), 4.4-3.8 (m, 7H, C_5H_4), 1.78 (s, 6H, $OCH(CH_3)_2$), 1.47 (s, 6H, $OCH(CH_3)_2$), 1.34 (s, 18H, $C(CH_3)_3$), 1.32 (s, 18H, $C(CH_3)_3$).

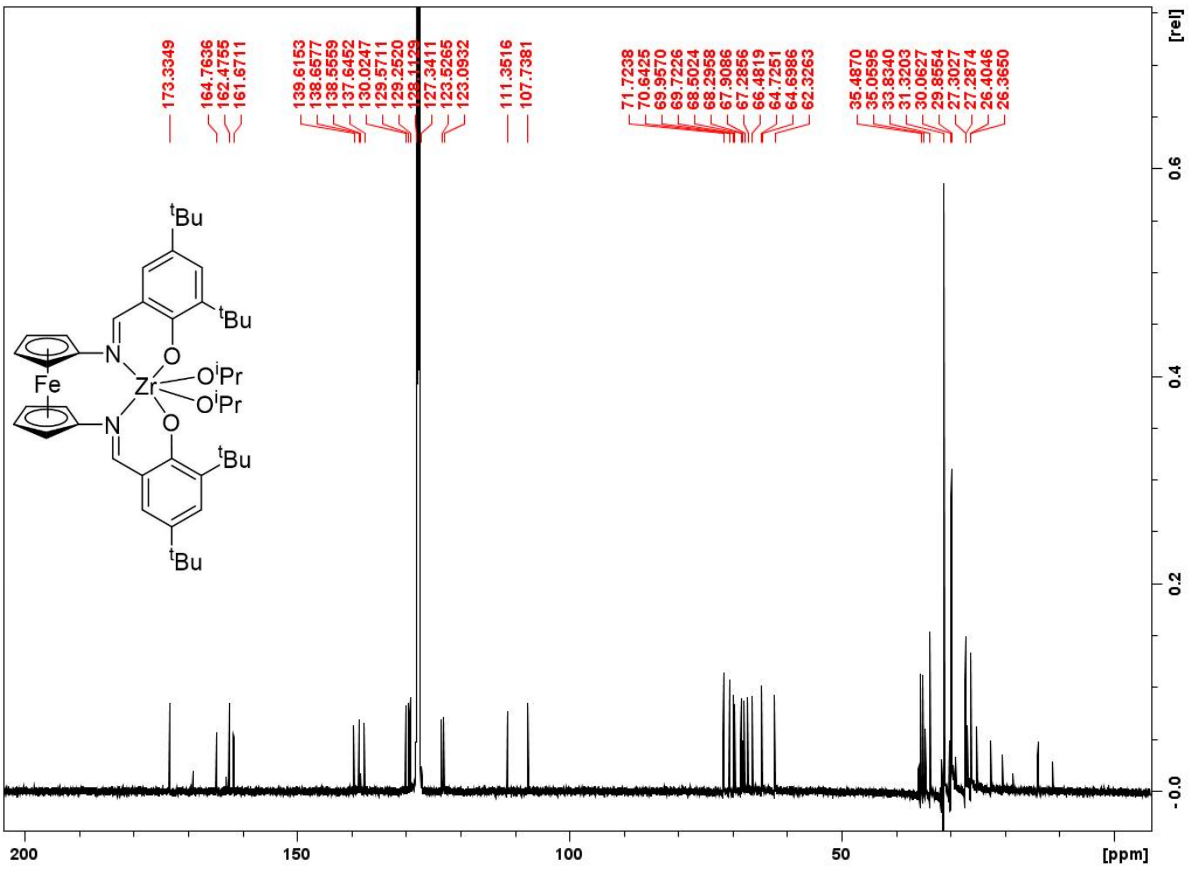

Figure 2.B5. ^{13}C NMR (500 MHz, C_6D_6, 298 K) spectrum of (salfen)Zr(O^{i}Pr)$_2$. δ, ppm: 173.3 (N=*C*), 164.8 (N=*C*), 162.5 (*m*-O*C*$_6$H$_2$), 161.7 (*m*-O*C*$_6$H$_2$), 139.6 (*m*-O*C*$_6$H$_2$), 138.7 (*m*-O*C*$_6$H$_2$), 138.6 (*m*-O*C*$_6$H$_2$), 137.6 (*m*-O*C*$_6$H$_2$), 130.0 (*m*-O*C*$_6$H$_2$), 129.6 (*m*-O*C*$_6$H$_2$), 129.3 (*m*-O*C*$_6$H$_2$), 123.5 (*m*-O*C*$_6$H$_2$), 123.1 (*m*-O*C*$_6$H$_2$), 111.4, 107.7 (*C*$_5$H$_4$), 71.7 (*C*$_5$H$_4$), 70.6 (*C*$_5$H$_4$), 70.0 (*C*$_5$H$_4$), 69.7 (*C*$_5$H$_4$), 68.5 (*C*$_5$H$_4$), 67.9 (*C*$_5$H$_4$), 67.3 (*C*$_5$H$_4$), 66.5, (*C*$_5$H$_4$), 64.7, 62.3 (O*C*H(CH$_3$)$_2$), 35.5 (C(*C*H$_3$)$_3$), 35.1 (C(*C*H$_3$)$_3$), 34.6 (C(*C*H$_3$)$_3$), 33.8 (C(*C*H$_3$)$_3$), 31.3 (C(*C*H$_3$)$_3$), 30.1 (C(*C*H$_3$)$_3$), 29.9 (C(*C*H$_3$)$_3$), 27.3 (C(*C*H$_3$)$_3$), 26.4 (OCH(*C*H$_3$)$_2$), 26.3 (OCH(*C*H$_3$)$_2$).

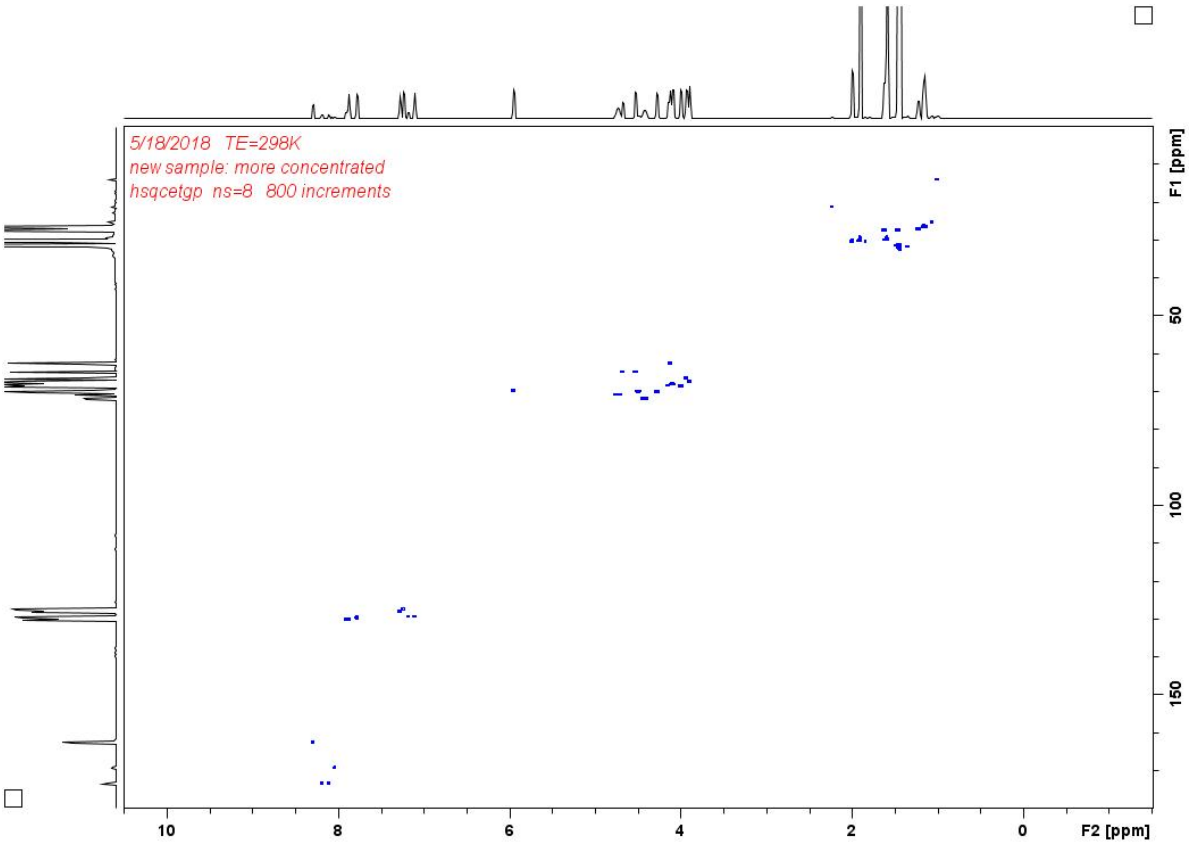

Figure 2.B6. 2D HSQC NMR (500 MHz, C_6D_6, 298 K) spectrum of (salfen)Zr(O^iPr)$_2$.

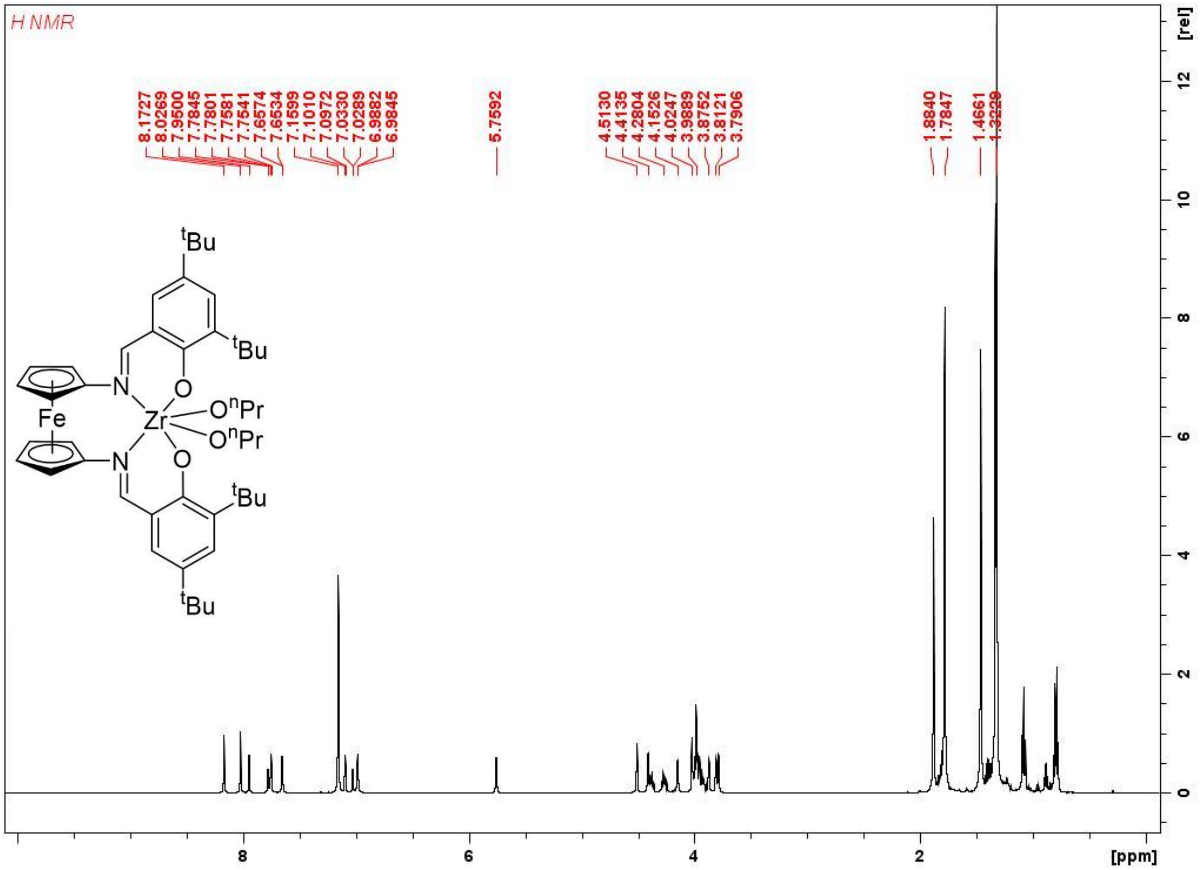

Figure 2.B7. ^{1}H NMR (500 MHz, C_6D_6, 298 K) spectrum of (salfen)Zr(O^nPr)$_2$. δ, ppm: 8.17 (s, 1H, N=C*H*), 8.03 (s, 1H, N=C*H*), 7.76 (d, 1H, *m*-OC_6H_2), 7.65 (d, 1H, *m*-OC_6H_2), 7.10 (d, 1H, *m*-OC_6H_2), 6.98 (d, 1H, *m*-OC_6H_2), 5.76 (s, 1H, C_5H_4), 4.38 (m, 2H, $OCH_2CH_2CH_3$), 4.28 (m, 2H, $OCH_2CH_2CH_3$), 4.5-3.8 (m, 7H, C_5H_4), 1.88 (m, 4H, $OCH_2CH_2CH_3$), 1.78 (m, 6H, $OCH_2CH_2CH_3$), 1.47 (s, 18H, $C(CH_3)_3$), 1.33 (s, 18H, $C(CH_3)_3$).

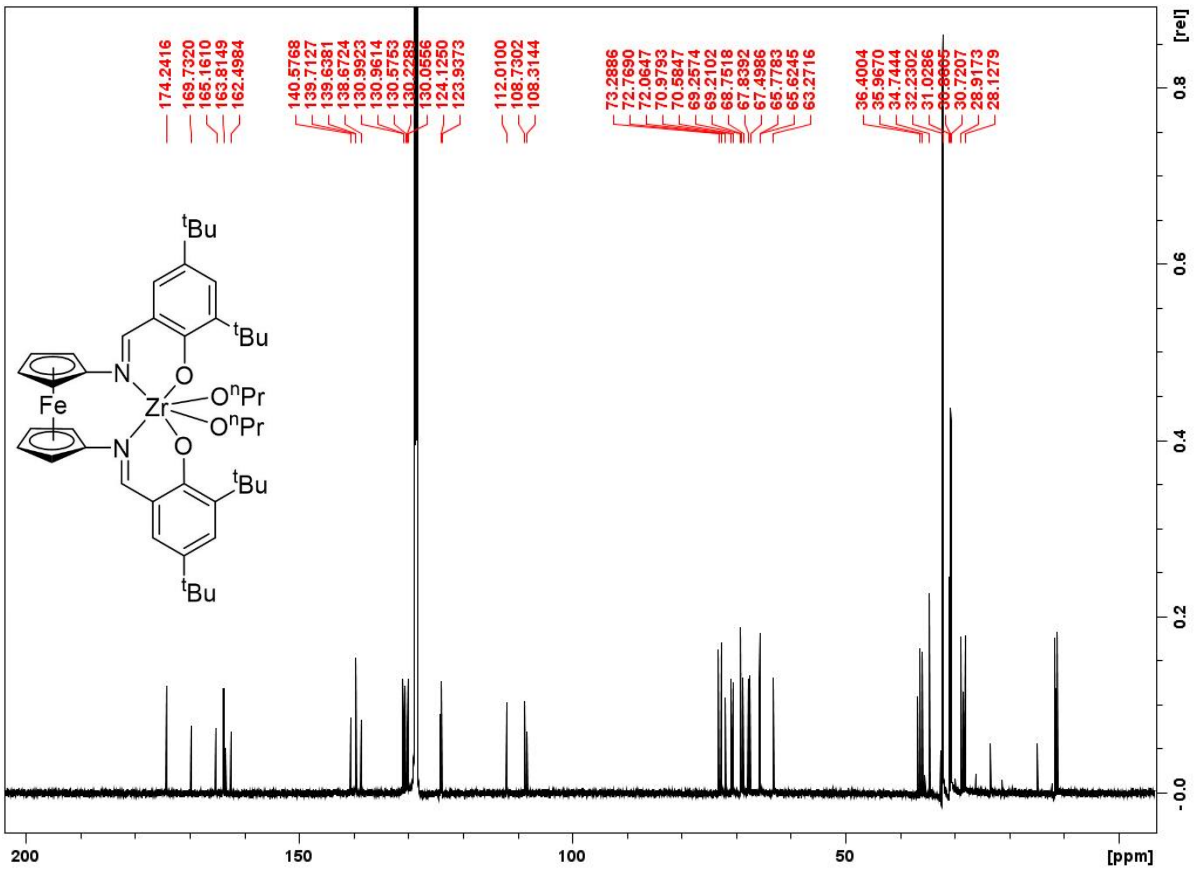

Figure 2.B8. ^{13}C NMR (500 MHz, C_6D_6, 298 K) spectrum of (salfen)Zr(O^{n}Pr)$_2$. δ, ppm: 174.2 (N=*C*), 169.7 (N=*C*), 163.4 (*m*-O*C*$_6$H$_2$), 162.5 (*m*-O*C*$_6$H$_2$), 140.6 (*m*-O*C*$_6$H$_2$), 138.7 (*m*-O*C*$_6$H$_2$), 138.6 (*m*-O*C*$_6$H$_2$), 137.6 (*m*-O*C*$_6$H$_2$), 129.9 (*m*-O*C*$_6$H$_2$), 129.6 (*m*-O*C*$_6$H$_2$), 129.4 (*m*-O*C*$_6$H$_2$), 124.1 (*m*-O*C*$_6$H$_2$), 123.9 (*m*-O*C*$_6$H$_2$), 112.0 (*C*$_5$H$_4$), 108.7 (*C*$_5$H$_4$), 73.3 (*C*$_5$H$_4$), 72.8 (*C*$_5$H$_4$), 72.1 (*C*$_5$H$_4$), 71.0 (*C*$_5$H$_4$), 68.5 (*C*$_5$H$_4$), 67.9 (*C*$_5$H$_4$), 67.3 (*C*$_5$H$_4$), 65.8 (*C*$_5$H$_4$), 65.6 (O*C*H$_2$CH$_2$CH$_3$), 63.3 (O*C*H$_2$CH$_2$CH$_3$), 36.8 (OCH$_2$*C*H$_2$CH$_3$), 36.4 (OCH$_2$*C*H$_2$CH$_3$), 34.6 (OCH$_2$CH$_2$*C*H$_3$), 33.8 (OCH$_2$CH$_2$*C*H$_3$), 31.3 (C(*C*H$_3$)$_3$), 30.1 (C(*C*H$_3$)$_3$), 29.9 (C(*C*H$_3$)$_3$), 28.9 (C(*C*H$_3$)$_3$), 28.5 (C(*C*H$_3$)$_3$), 28.1 (C(*C*H$_3$)$_3$).

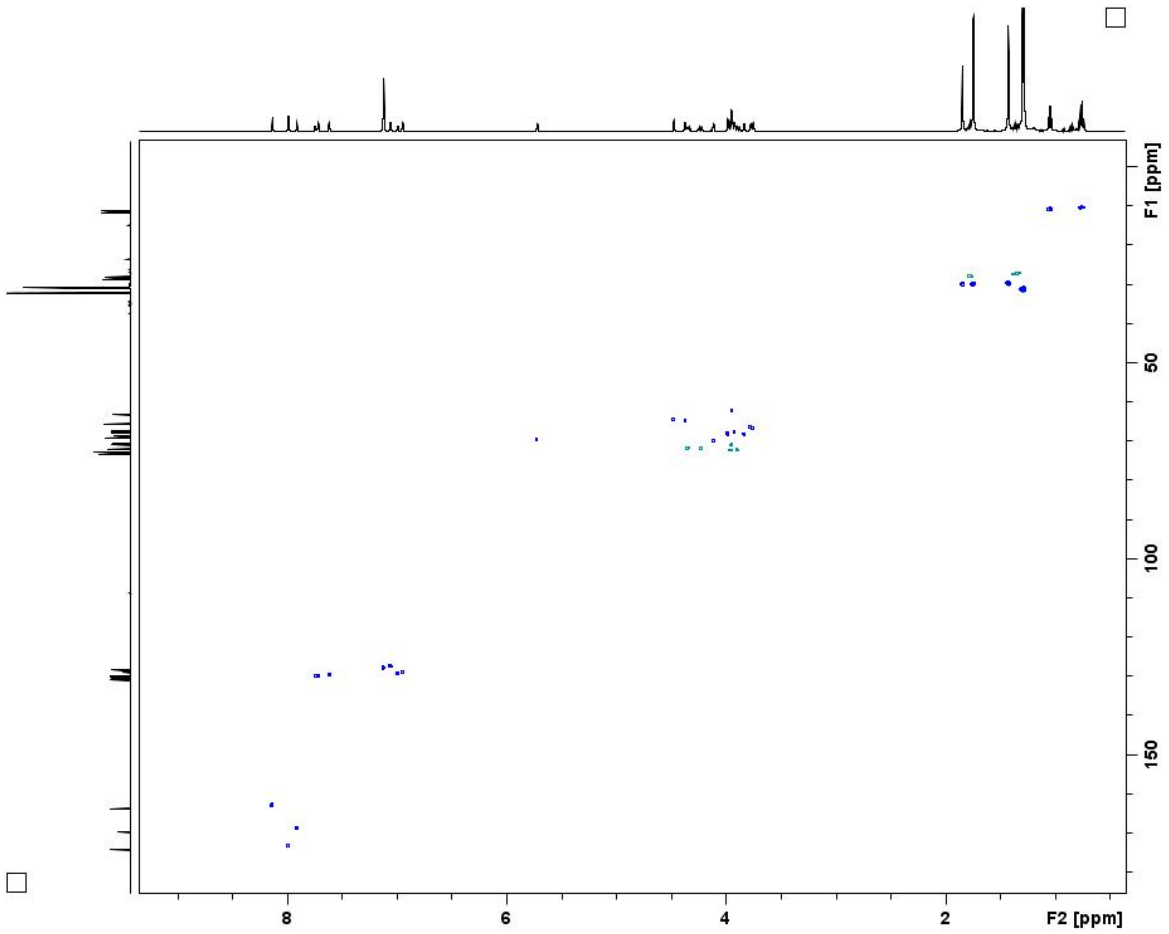

Figure 2.B9. 2D HSQC NMR (500 MHz, C_6D_6, 298 K) spectrum of (salfen)Zr(O^nPr)$_2$.

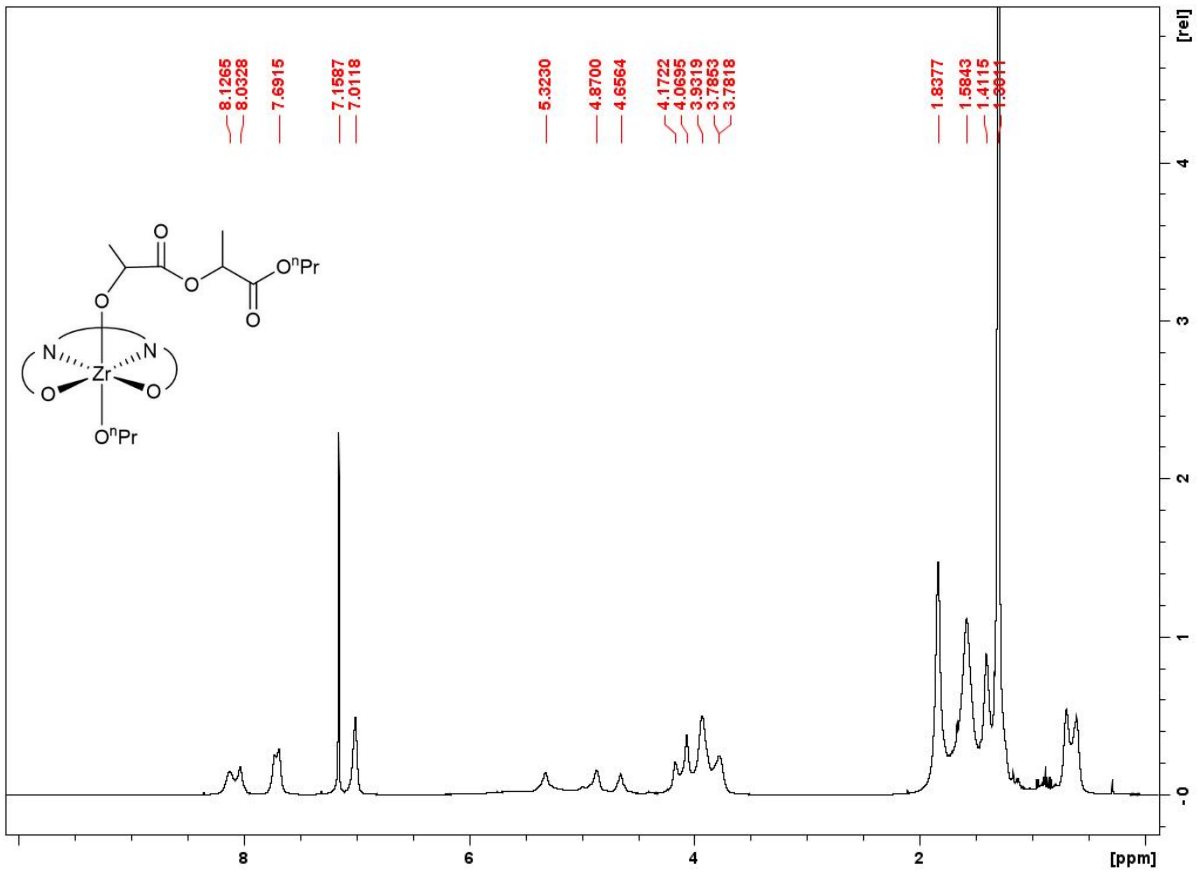

Figure 2.B10. ^{1}H NMR (500 MHz, C_6D_6, 298 K) spectrum of (salfen)Zr(O^nPr)$_2$-LA. δ, ppm: 8.11 (s, 2H, N=C*H*), 7.71 (s, 2H, *m*-OC_6H_2), 7.02 (s, 2H, *m*-OC_6H_2), 5.33 (br, 2H, C_5H_4), 4.66 (br, 2H, C_5H_4), 4.16 (br, 2H, C_5H_4), 4.07 (br, 2H, C_5H_4), 4.88 (s, 2H, OC*H*(CH_3)COO), 3.81 (br, 2H, O$CH_2CH_2CH_3$), 3.79 (br, 2H, O$CH_2CH_2CH_3$), 1.84 (br, 3H, OCH(CH_3)COO), 1.59 (br, 3H, OCH(CH_3)COO), 1.41 (br, 2H, $OCH_2CH_2CH_2CH_3$), 1.23 (br, 2H, $OCH_2CH_2CH_2CH_3$), 1.30 (br, 36H, C(CH_3)$_3$), 0.89 (br, 6H, $OCH_2CH_2CH_3$).

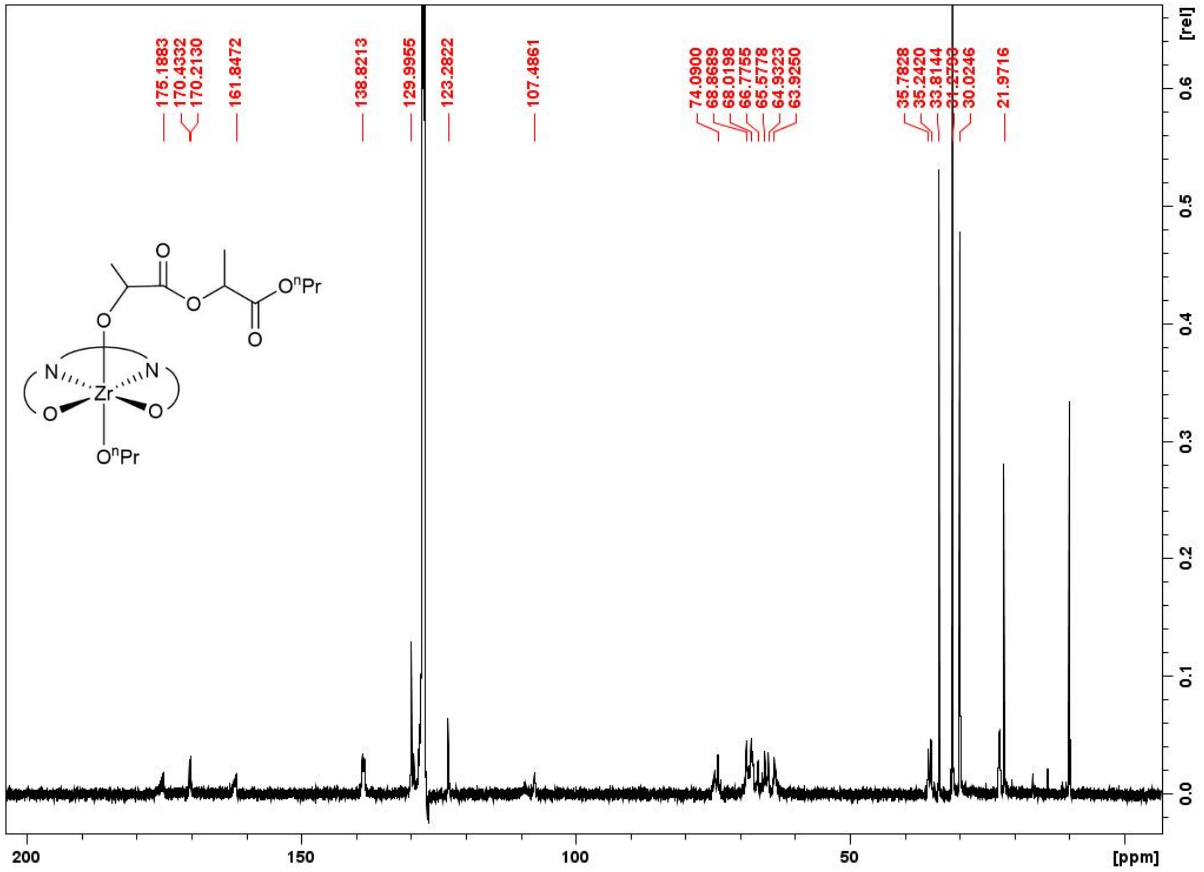

Figure 2.B11. ^{13}C NMR (500 MHz, C_6D_6, 298 K) spectrum for (salfen)Zr(O^nPr)$_2$-LA. δ, ppm: 176.1 (*C*OO), 171.3 (N=*C*), 162.8 (*m*-O*C*$_6$H$_2$), 139.8 (*m*-O*C*$_6$H$_2$), 139.5 (*m*-O*C*$_6$H$_2$), 130.9 (*m*-O*C*$_6$H$_2$), 128.0 (*m*-O*C*$_6$H$_2$), 124.2 (*m*-O*C*$_6$H$_2$), 108.4 (*C*$_5$H$_4$), 75.0 (O*C*HCOO), 69.8 (*C*$_5$H$_4$), 69.3 (*C*$_5$H$_4$), 68.9 (*C*$_5$H$_4$), 68.7 (*C*$_5$H$_4$), 67.7 (*C*$_5$H$_4$), 66.5 (*C*$_5$H$_4$), 65.9 (*C*$_5$H$_4$), 64.8 (*C*$_5$H$_4$), 34.7 (*C*(CH$_3$)$_3$), 32.2 (C(*C*H$_3$)$_3$), 31.0 (OCH$_2$*C*H$_2$CH$_3$), 22.9 (OCH$_2$CH$_2$*C*H$_3$).

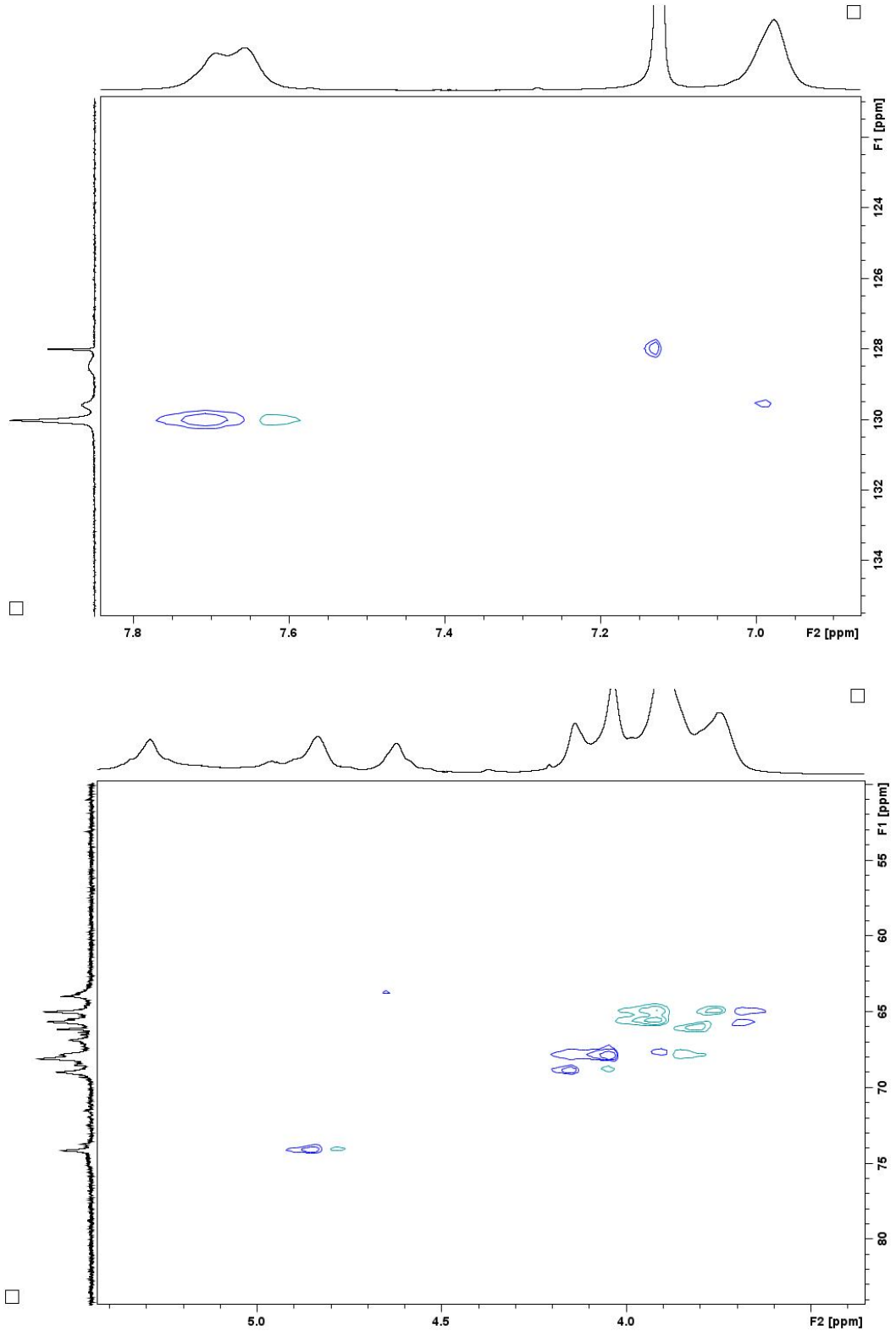

Figure 2.B12. 2D HSQC NMR (500 MHz, C_6D_6, 298 K) spectra of (salfen)Zr(O^nPr)$_2$-LA.

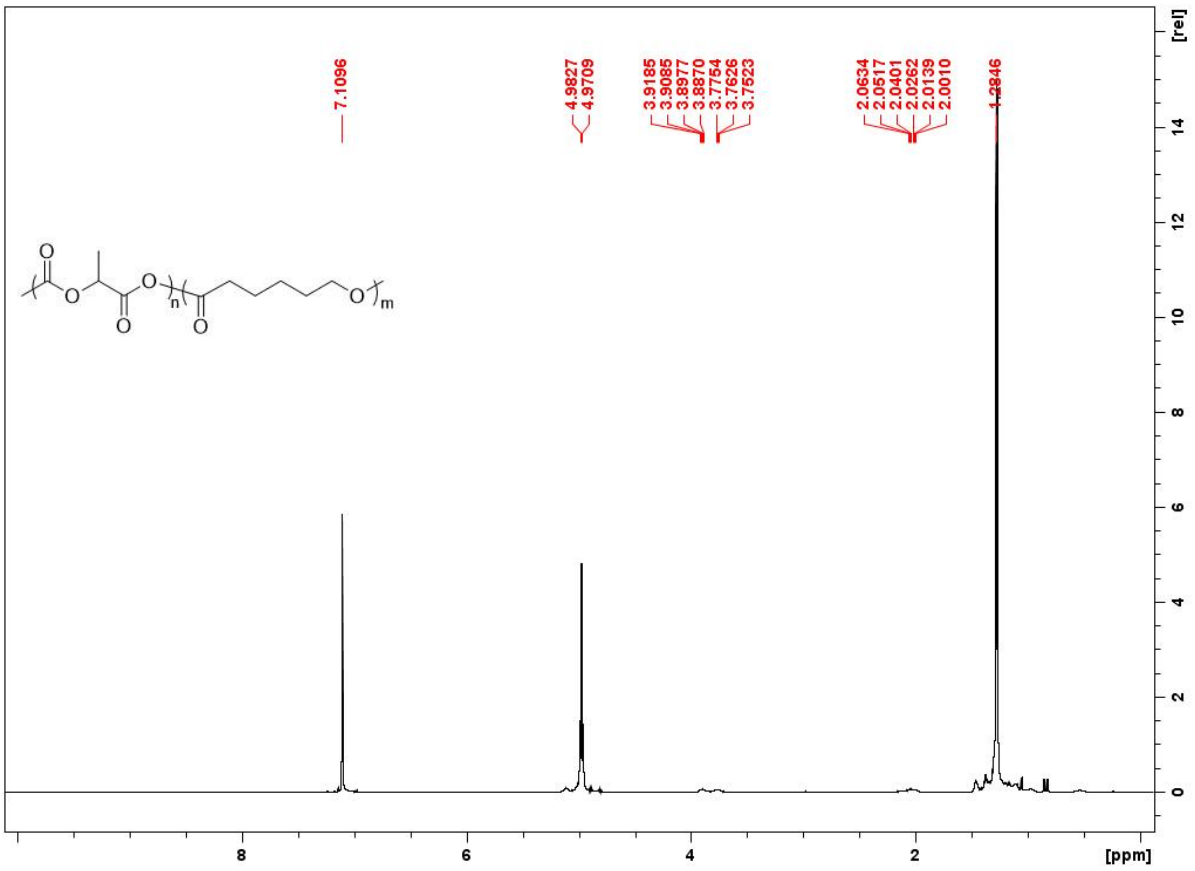

Figure 2.B13. ^{1}H NMR (600 MHz, C_6D_6, 298 K) spectrum of the LA-CL block copolymer. δ, ppm: 4.98 (d, 1H, C*H*(CH_3)-LA), 3.89 (m, 2H, COC*H*$_2$$CH_2$-CL), 3.76 (m, 2H, C*H*$_2$COO-CL), 2.04 (m, 6H, CH_2C*H*$_2$$CH_2$-CL), 1.28 (d, 3H, CH(C*H*$_3$)-LA).

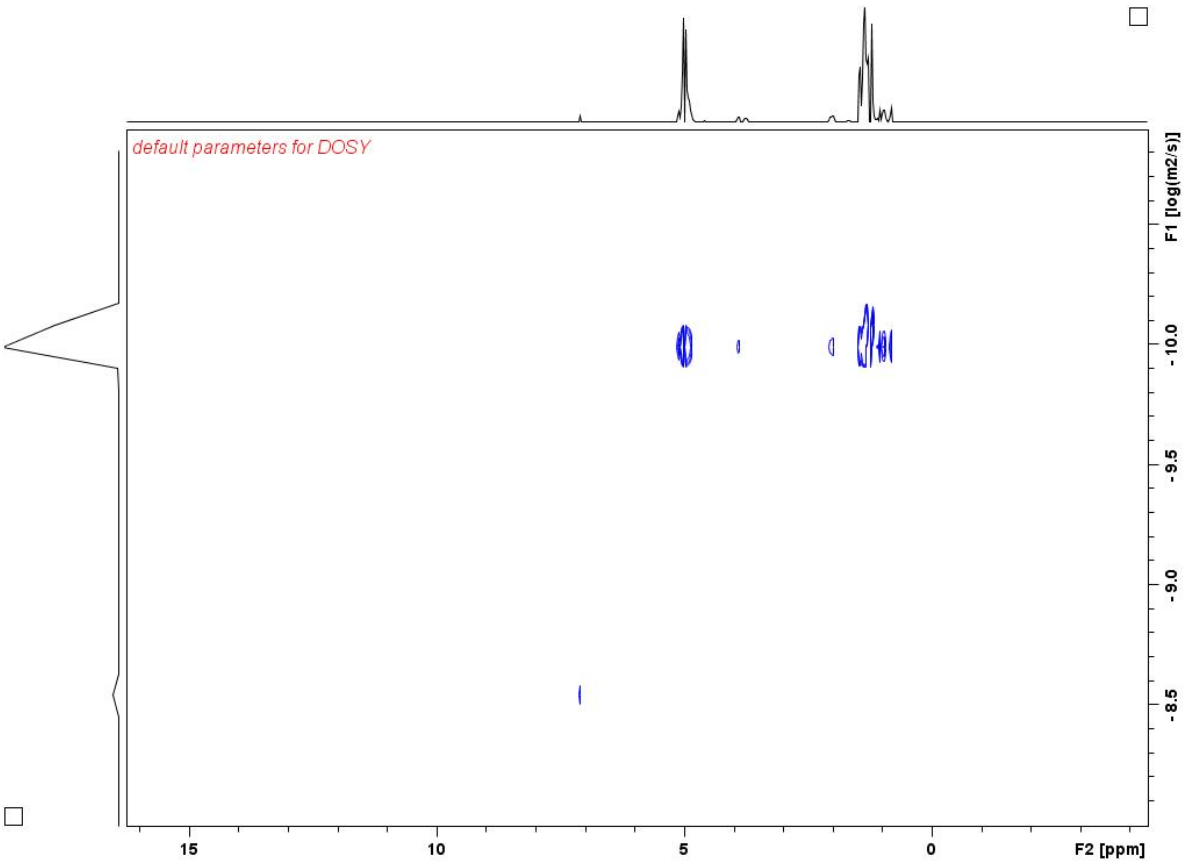

Figure 2.B14. 2D DOSY NMR (600 MHz, C_6D_6, 298 K) spectrum of the LA-CL copolymer.

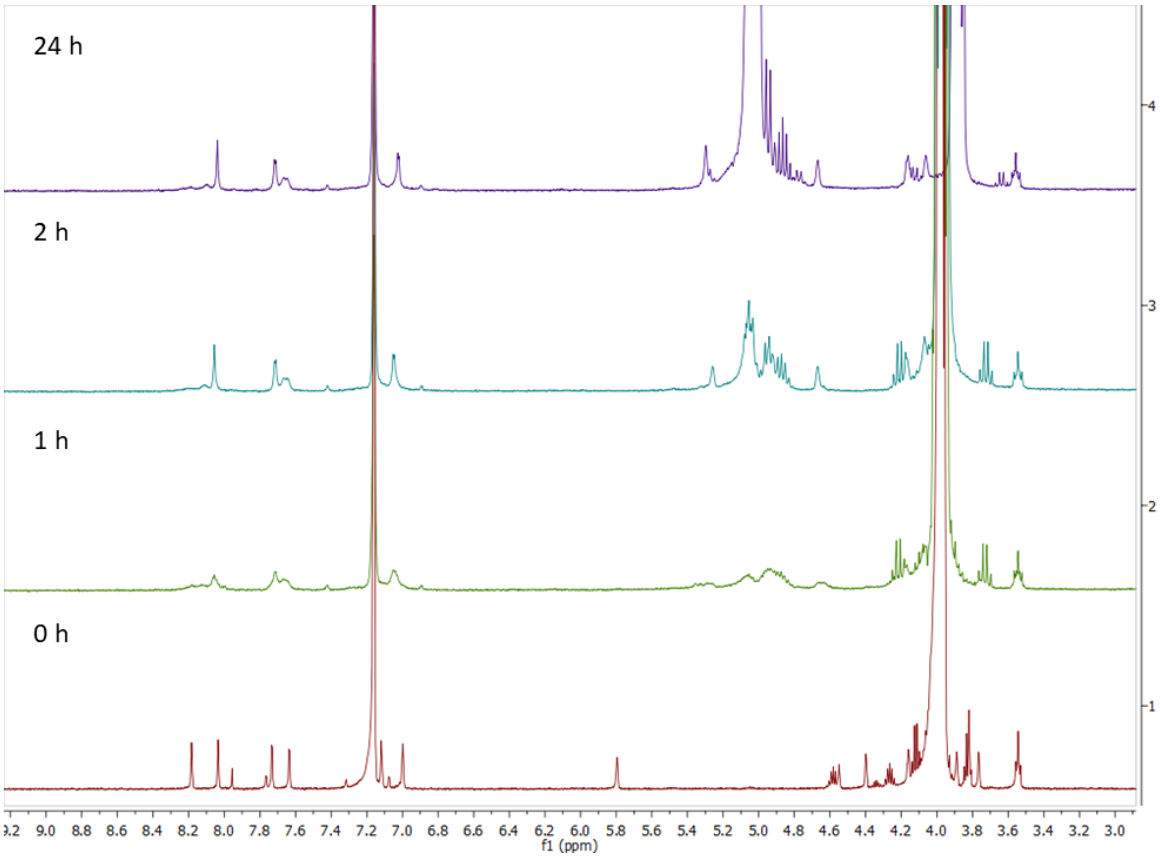

Figure 2.B15. ^{1}H NMR (300 MHz, C_6D_6, 25 ^{o}C) spectra of the reaction between (salfen)Zr($O^{i}Pr$)$_2$ and 100 equivalents of LA at 100 ^{o}C.

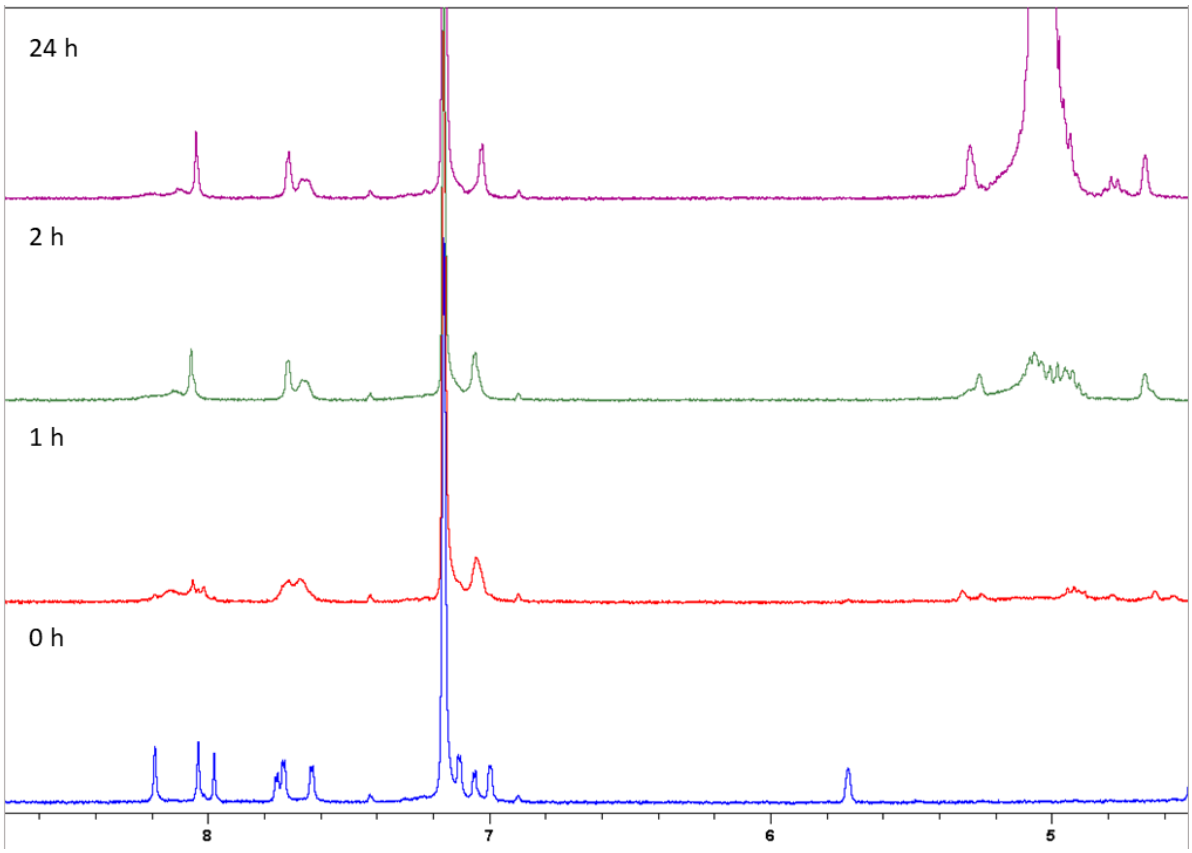

Figure 2.B16. ^{1}H NMR (300 MHz, C_6D_6, 25 ^{o}C) spectra of the reaction between (salfen)Zr($O^{n}Pr$)$_2$ and 100 equivalents of LA at 100 ^{o}C.

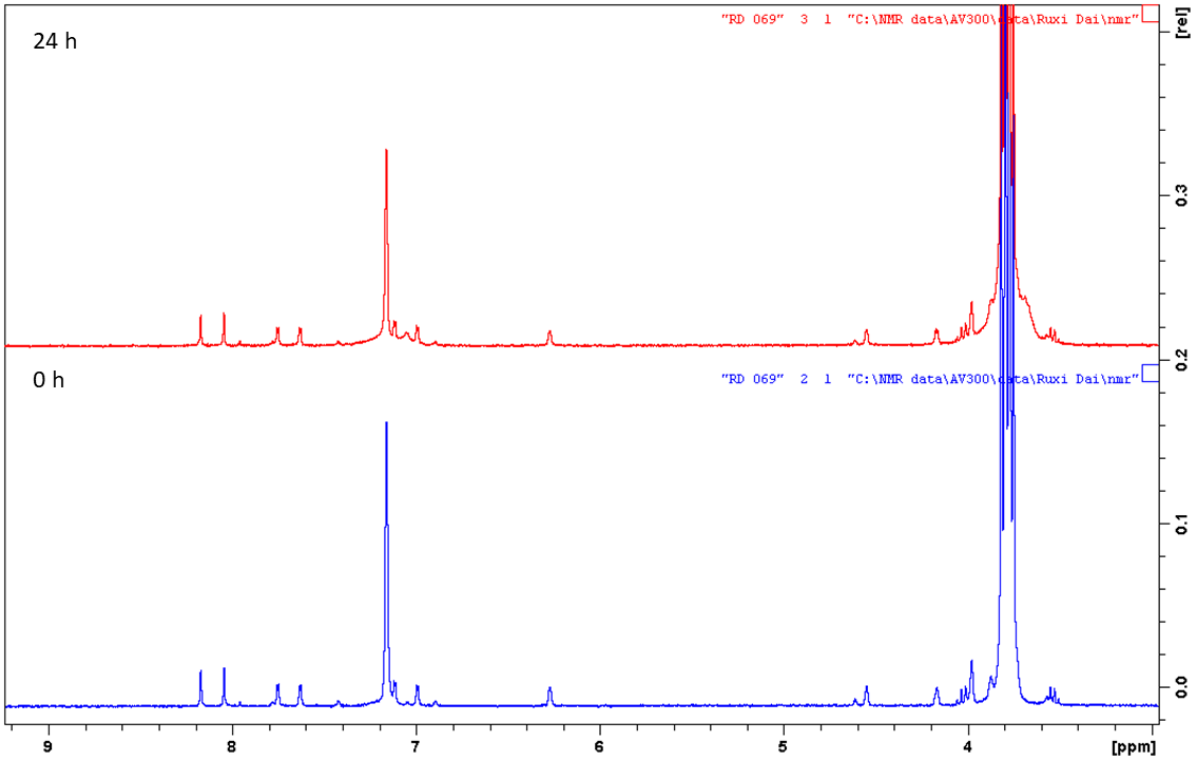

Figure 2.B17. ^{1}H NMR (300 MHz, C_6D_6, 25 ^{o}C) spectra of the reaction between (salfen)Zr($O^{t}Bu$)$_2$ and 100 equivalents of LA at 100 ^{o}C, no geometry change and no reaction after 24 hours.

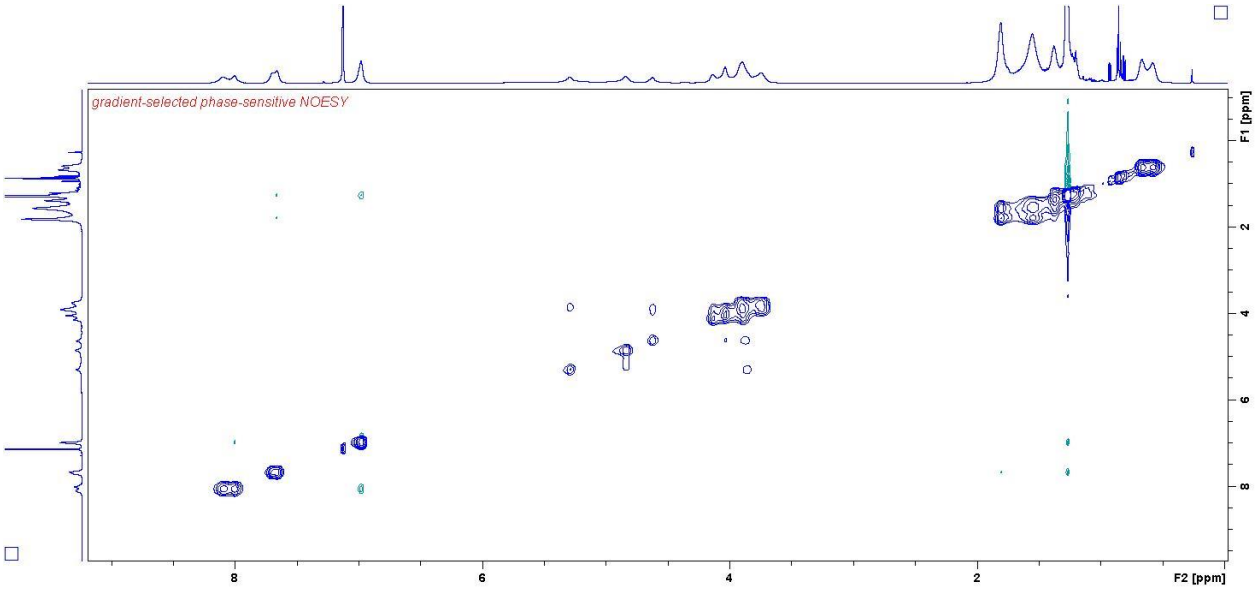

Figure 2.B18. 2D NOESY NMR (500 MHz, C_6D_6, 298 K) spectrum of (salfen)Zr(O^nPr)$_2$-LA.

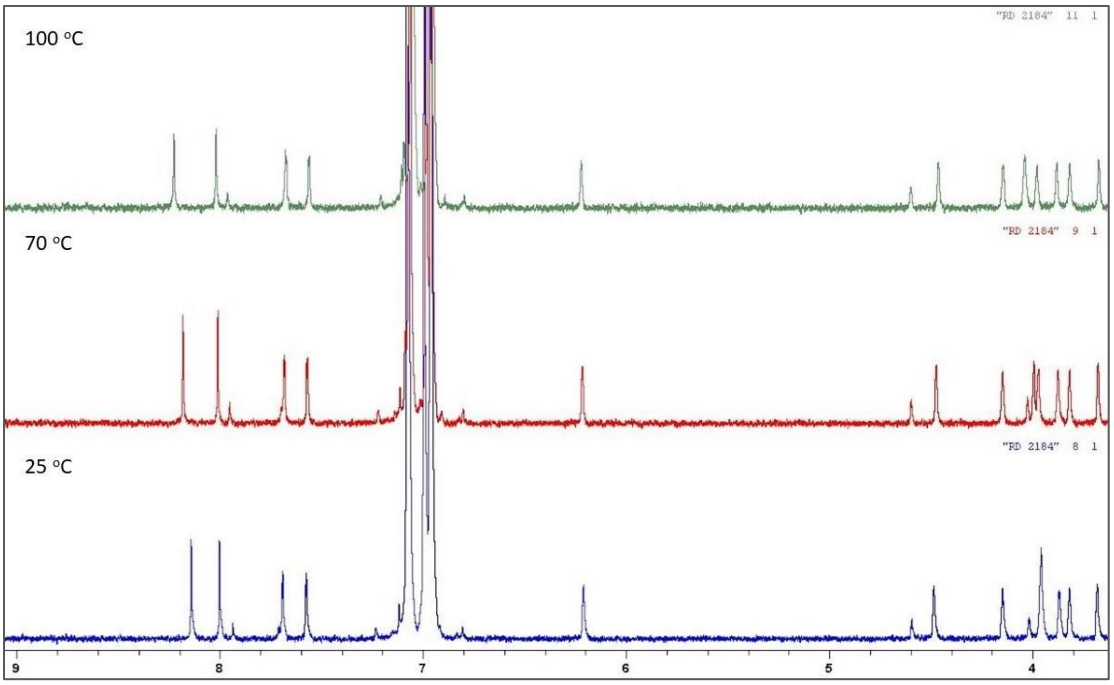

Figure 2.B19. ^{1}H NMR spectra (500 MHz, d_8-toluene) of (salfen)Zr(O^tBu)$_2$ at 25 °C (bottom), 70 °C (middle) and 100 °C (top).

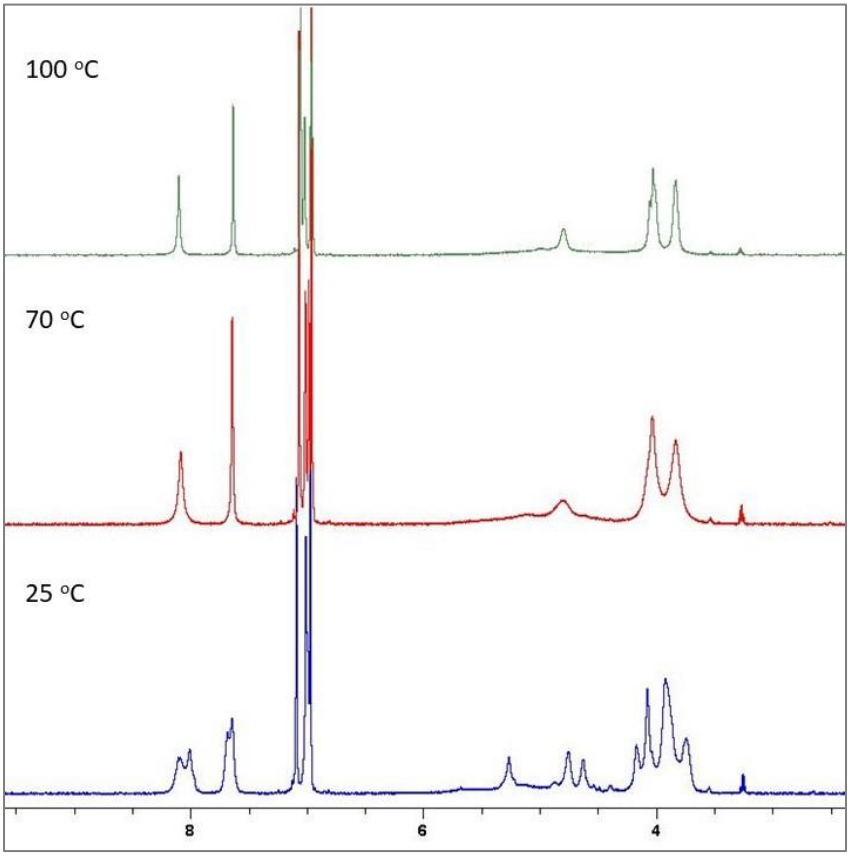

Figure 2.B20. ^{1}H NMR spectra (500 MHz, d_8-toluene) of (salfen)Zr(O^{n}Pr)$_2$-LA at 25 °C (bottom), 70 °C (middle) and 100 °C (top).

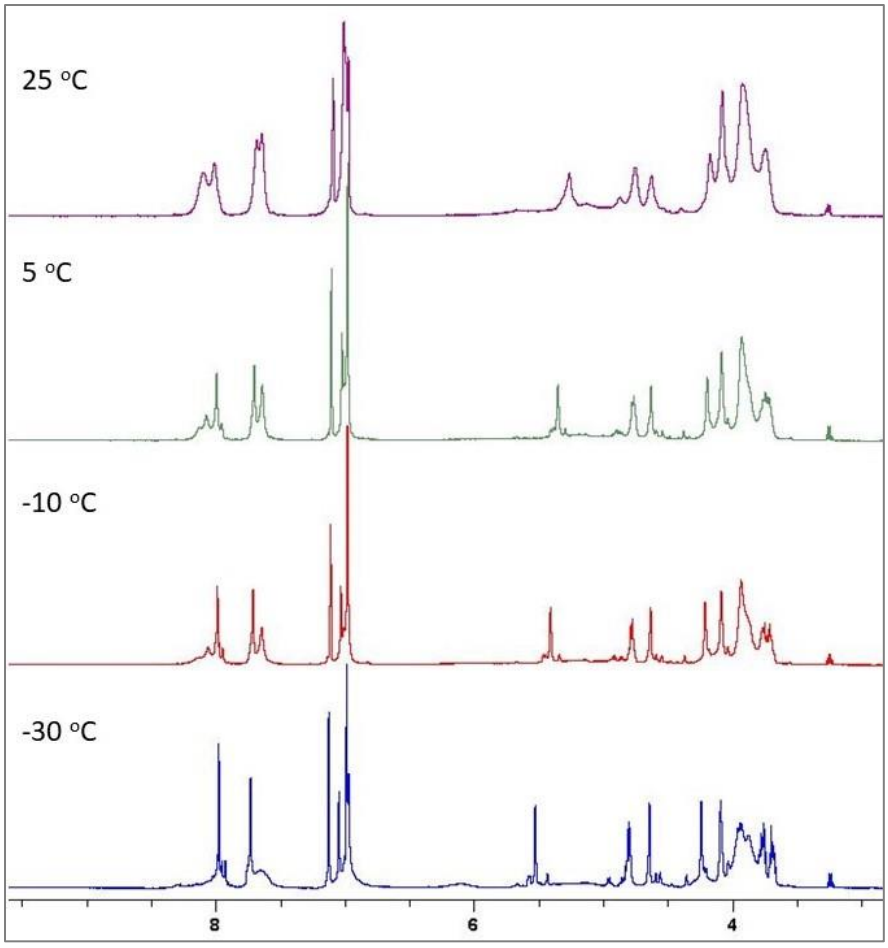

Figure 2.B21. ^{1}H NMR spectra (500 MHz, d_8-toluene) of (salfen)Zr(O^{n}Pr)$_2$-LA at -30 °C, -10 °C, 5 °C and 25 °C.

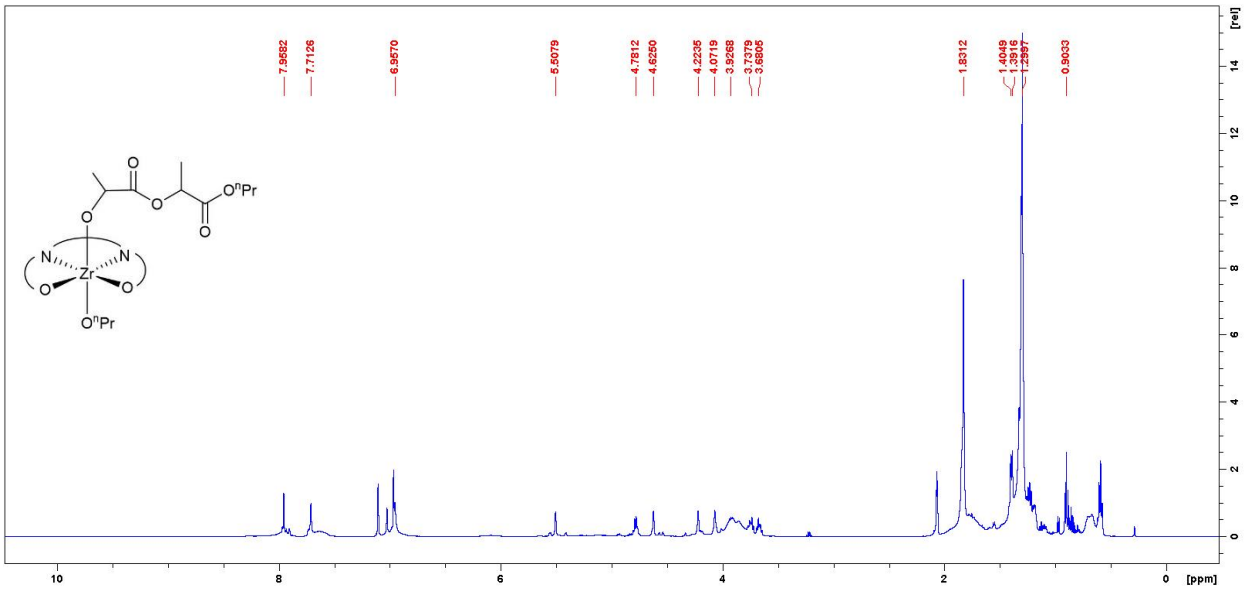

Figure 2.B22. ^{1}H NMR spectra (500 MHz, d_8-toluene) of (salfen)Zr(O^{n}Pr)$_2$-LA at -30 ^{o}C. δ, ppm: 7.96 (s, 2H, N=C*H*), 7.71 (s, 2H, *m*-OC$_6$*H*$_2$), 6.96 (s, 2H, *m*-OC$_6$*H*$_2$), 5.51 (s, 1H, C$_5$*H*$_4$), 4.78 (s, 2H, C$_5$*H*$_4$), 4.63 (s, 2H, C$_5$*H*$_4$), 4.22 (t, 2H, OC*H*$_2$CH$_2$CH$_3$), 4.07 (t, 2H, OC*H*$_2$CH$_2$CH$_3$), 3.92 (br, 3H, C$_5$*H*$_4$), 3.73 (q, 1H, OC*H*(CH$_3$)COO), 3.68 (q, 1H, OC*H*(CH$_3$)COO), 1.83 (br, 6H, OCH(C*H*$_3$)COO), 1.39 (d, 4H, OCH$_2$C*H*$_2$CH$_3$), 1.30 (s, 36H, C(C*H*$_3$)$_3$), 0.90 (m, 6H, OCH$_2$CH$_2$C*H*$_3$).

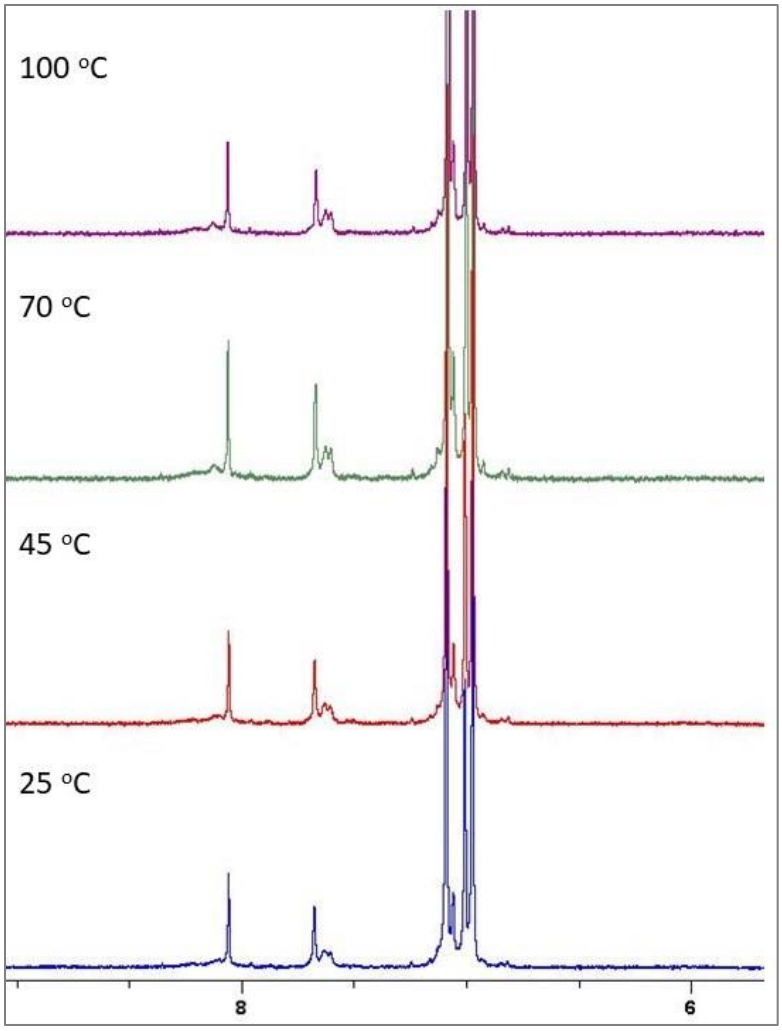

Figure 2.B23. 100 equivalent LA polymerization catalyzed by (salfen)Zr(O^nPr)$_2$ at 100 °C and then stopped at 40% conversion. ^{1}H NMR spectra (500 MHz, d_8-toluene) was taken of the mixture of at 25 °C, 45 °C, 70 °C and 100 °C.

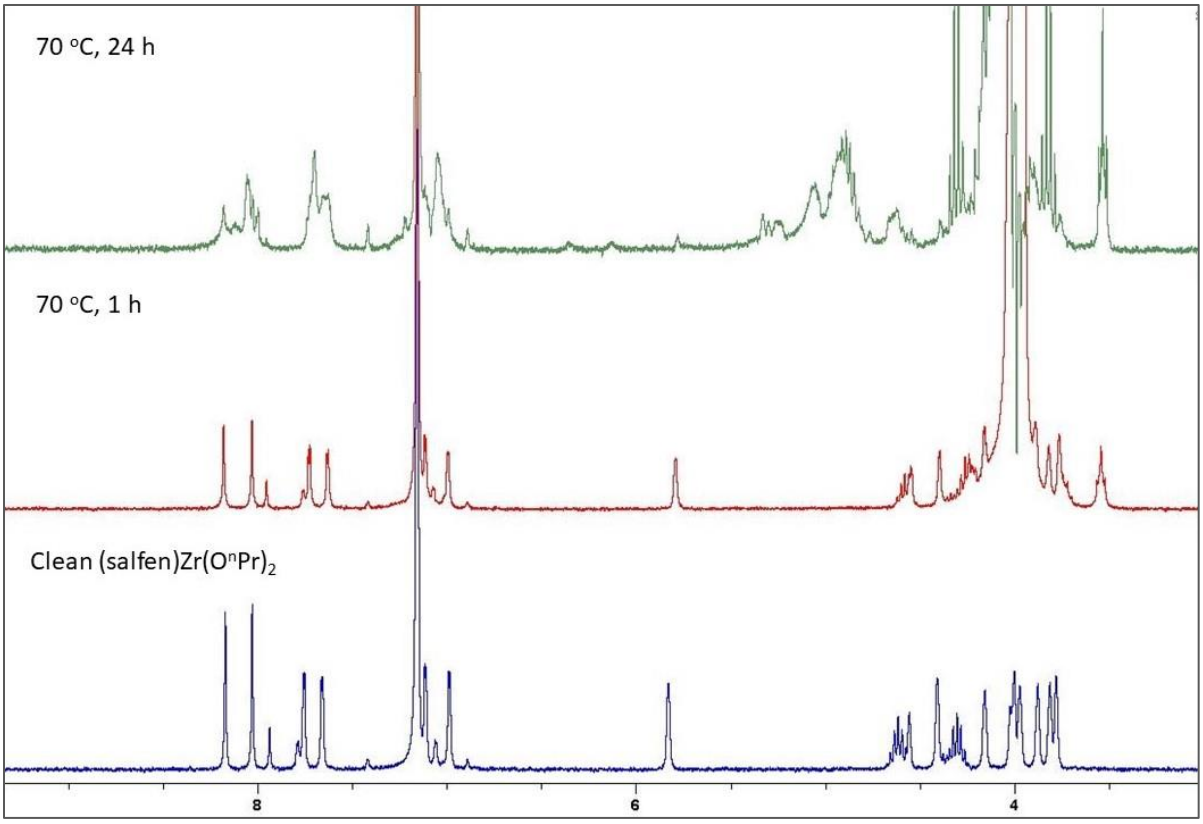

Figure 2.B24. ^{1}H NMR spectra (500 MHz, d_6-benzene, 25 °C) of 100 equivalent LA polymerization catalyzed by (salfen)Zr(O^{i}Pr)$_2$ at 70 °C, time 0 (middle) and after 24 hours (top). ^{1}H NMR spectra (500 MHz, d_6-benzene, 25 °C) of only (salfen)Zr(O^{i}Pr)$_2$ (bottom).

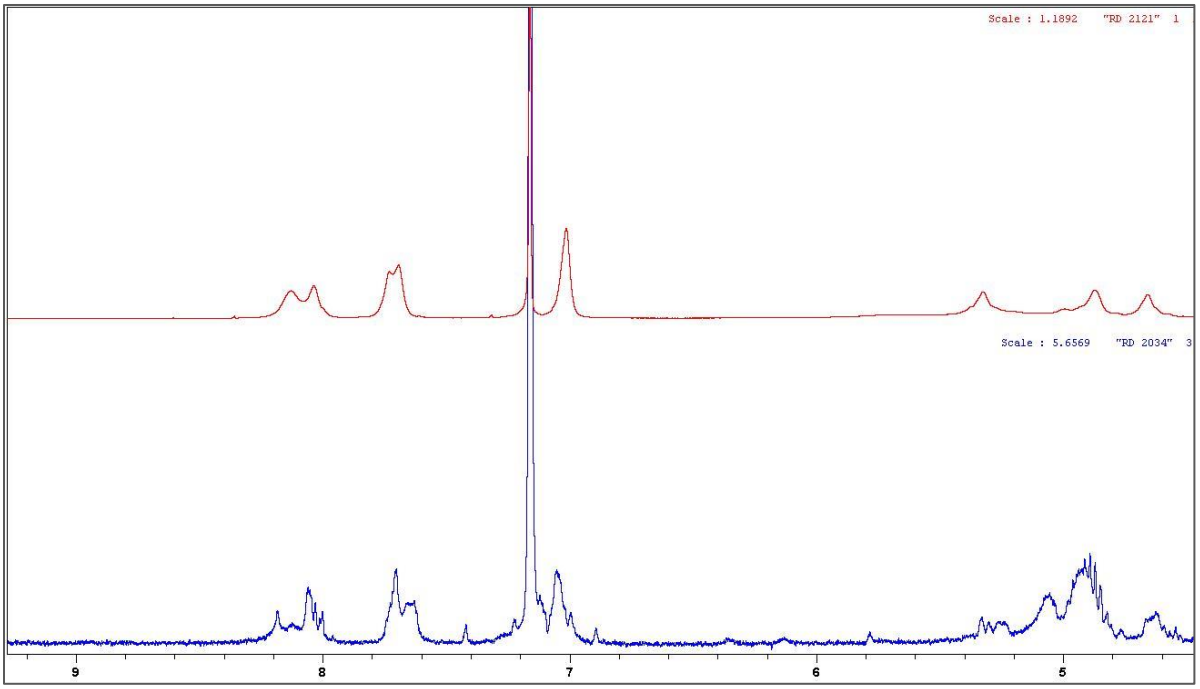

Figure 2.B25. ^{1}H NMR spectra (500 MHz, d_6-benzene) of 100 equivalent LA polymerization catalyzed by (salfen)Zr(O^{i}Pr)$_2$ at 70 ^{o}C for 24 hours (bottom). ^{1}H NMR spectra (500 MHz, d_6-benzene, 25 ^{o}C) of (salfen)Zr(O^{n}Pr)$_2$-LA (top).

Table 2.B1. LA polymerization by (salfen)Zr(O^iPr)$_2$.[a]

Entry	LA equiv.	Conv.[b]	Mn (calc., 10^3)[c]	Mn (GPC, 10^3)	*Đ*
1	75	55%	3.0	3.5	1.04
2	100	70%	5.2	6.4	1.02
3	150	68%	7.3	7.5	1.02

[a] All experiments were conducted in 0.8 mL of C_6D_6, with 0.004 mmol zirconium compound and different equivalents of LA at 100 ^oC, and hexamethylbenzene as an internal standard; [b] the conversion was calculated from the integration of ^1H NMR peaks against those of hexamethylbenzene. [c] Molar masses were calculated from ^1H NMR spectra based on integration compared to the internal standard.

Table 2.B2. Conversion vs. time data for LA polymerization by (salfen)Zr(O^iPr)$_2$.[a]

Time (h)	0	1	2	3	4	5	6	7	9	24
Conv. (%)	/	4.1	7.9	11.0	15.7	20	23.6	27.9	33	70

[a] The experiments were conducted in 0.8 mL of C_6D_6, with 0.004 mmol zirconium compound and 100 equivalents of LA at 100 ^oC, and hexamethylbenzene as an internal standard; the conversion was calculated from the integration of ^1H NMR peaks against those of hexamethylbenzene.

SEC Data

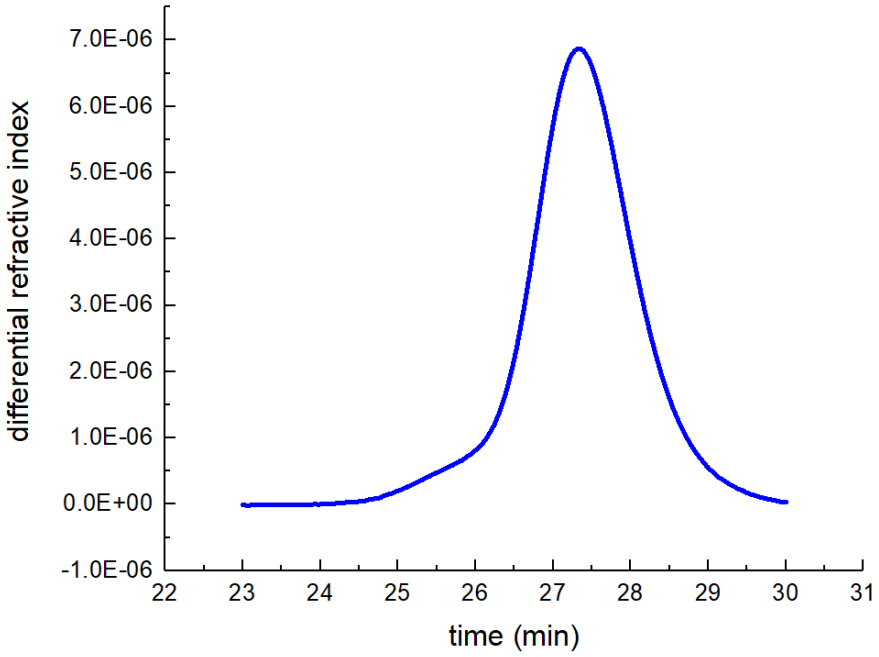

Figure 2.B26. GPC trace of PLA (Table 2.2, entry 2 and Table S1, entry 2). Mn = 6.4*10^3 Da, *Đ* = 1.02.

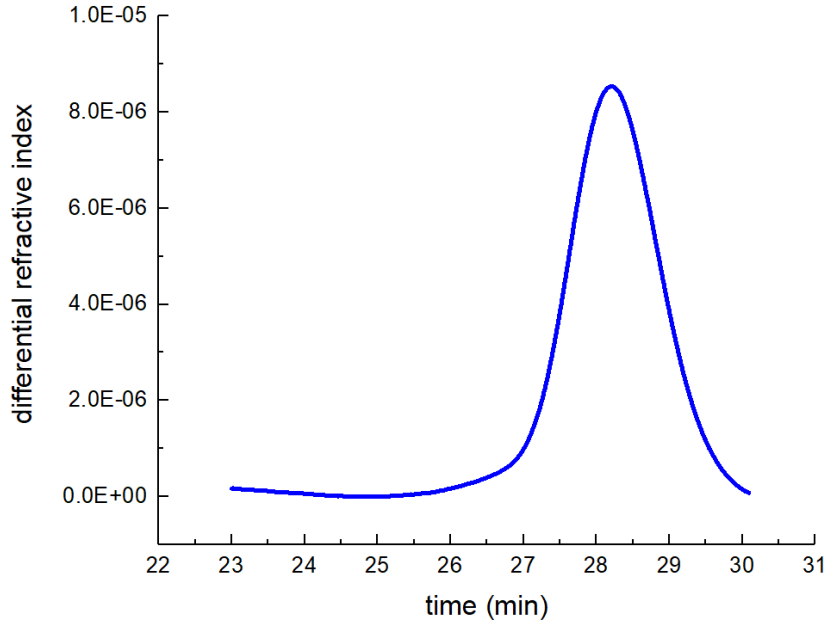

Figure 2.B27. GPC trace of PLA (Table 2.B1, entry 3). Mn = 3.5*10^3 Da, *Đ* = 1.04.

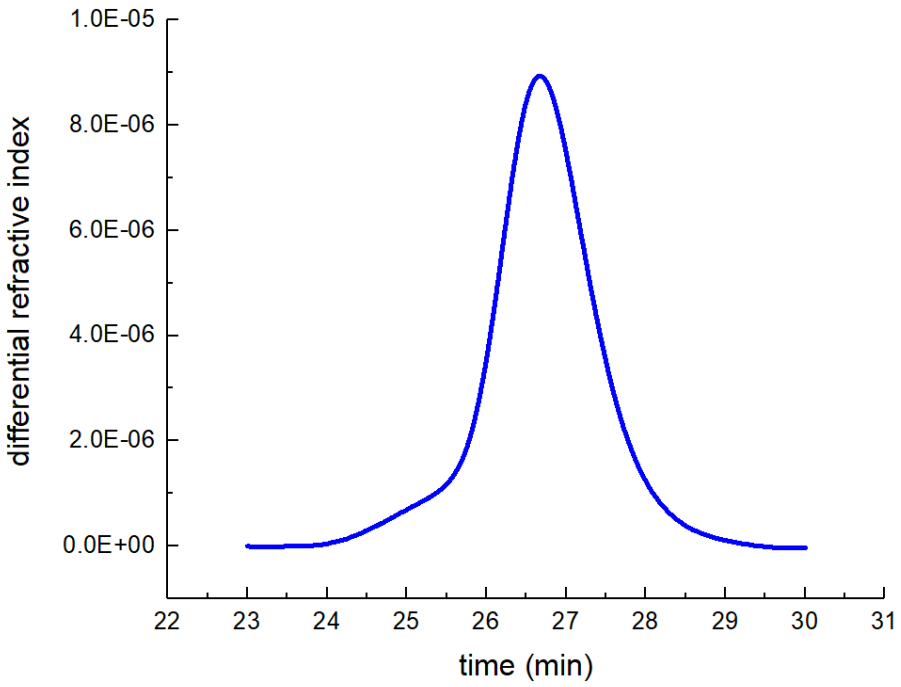

Figure 2.B28. GPC trace of PLA (Table 2.B1, entry 1). Mn = 7.5*10^3 Da, $Đ$ = 1.04.

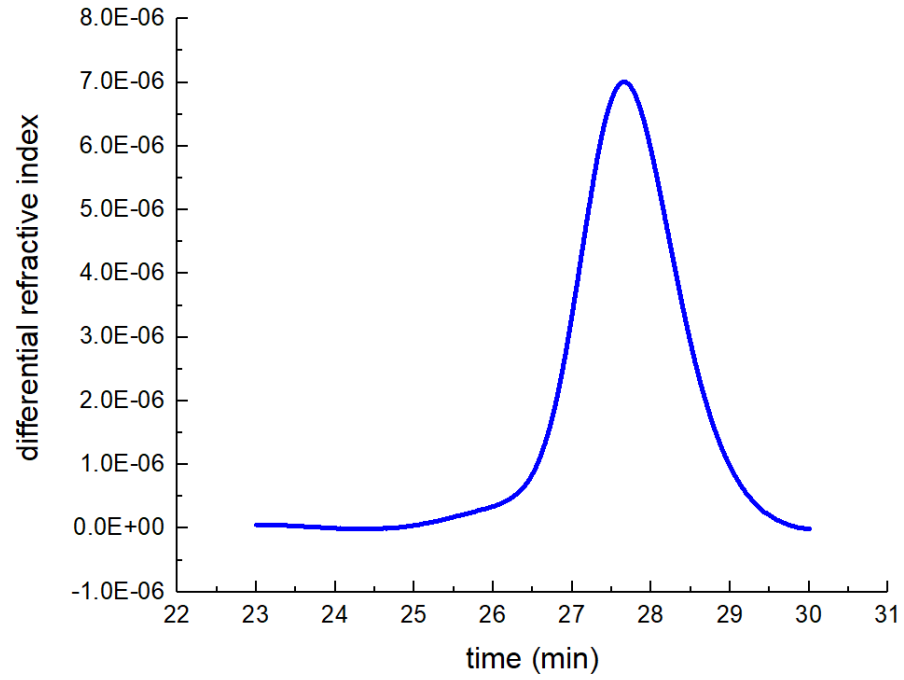

Figure 2.B29. GPC trace of PLA (Table 2.2, entry 3). Mn = 5.5*10^3 Da, $Đ$ = 1.05.

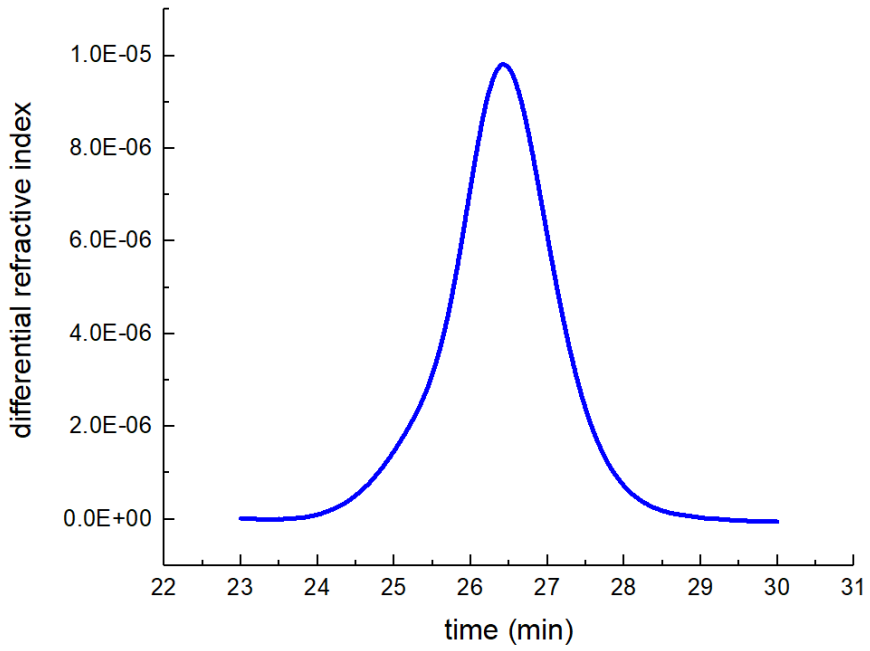

Figure 2.B30. GPC trace of PLA-PCL. Mn = $8.2*10^3$ Da, $Đ$ = 1.02.

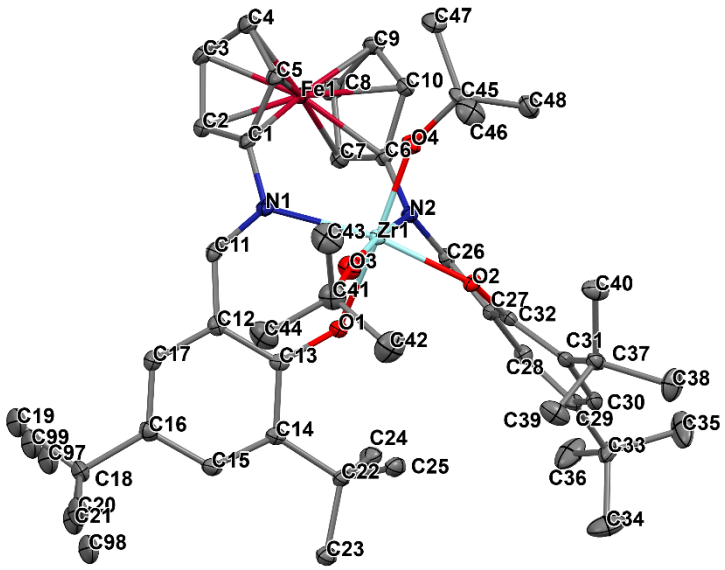

Figure 2.B31. Thermal ellipsoid (50% probability) representation of one of the two crystallographically independent molecules in the unit cell of (salfen)Zr(O^{t}Bu)$_2$; hydrogen atoms were omitted for clarity.

Crystal data for $C_{48}H_{68}FeN_2O_4Zr$; M_r = 1768.22; Triclinic; space group P-1; *a* = 14.6933(12) Å; *b* = 17.3842(14) Å; *c* = 19.1228(15) Å; α = 87.070(1)°; β = 72.275(1)°; γ = 85.012(1)°; V = 4633.5(6) Å^3; Z = 2; T = 100(2) K; λ = 0.71073 Å; μ = 0.580 mm^{-1}; d_{calc} = 1.267 g.cm^{-3}; 30946 reflections collected; 27548 unique; giving R_1 = 0.0327 for 27548 data with [I>2σ(I)] and R_1 = 0.0431, wR_2 = 0.0748 for all data. Residual electron density (e$^-$.Å^{-3}) max/min: 0.83/-0.50.

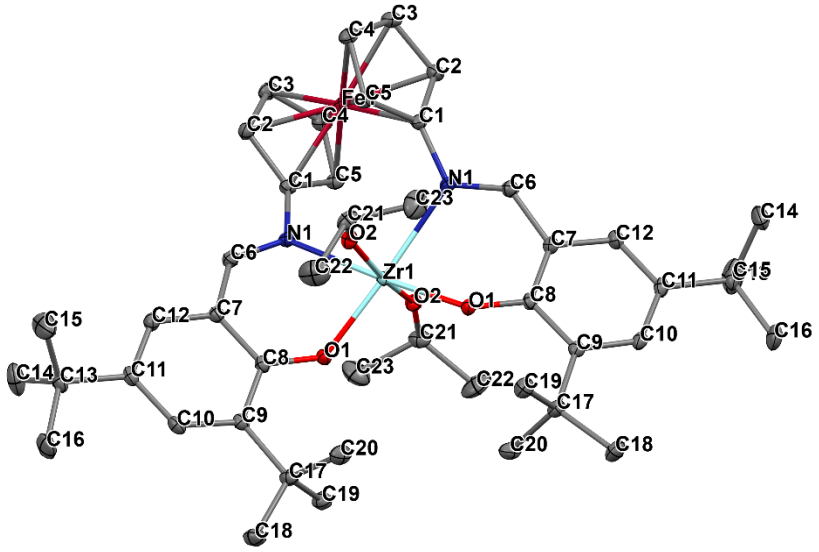

Figure 2.B32. Thermal ellipsoid (50% probability) representation of (salfen)Zr(O^iPr)$_2$; hydrogen atoms were omitted for clarity.

Crystal data for $C_{23}H_{32}Fe_{0.5}NO_2Zr_{0.5}$; M_r = 428.03; Monoclinic; space group P2/c; *a* = 12.986(5) Å; *b* = 16.183(6) Å; *c* = 11.714(5) Å; β = 104.927(6)°; V = 2378.8(16) Å^3; Z = 4; T = 100(2) K; λ = 0.71073 Å; μ = 0.563 mm^{-1}; d_{calc} = 1.195 g.cm^{-3}; 7030 reflections collected; 6059 unique; giving R_1 = 0.0264 for 6059 data with [I>2σ(I)] and R_1 = 0.0331, wR_2 = 0.0828 for all data. Residual electron density (e$^-$.Å^{-3}) max/min: 0.50/-0.56.

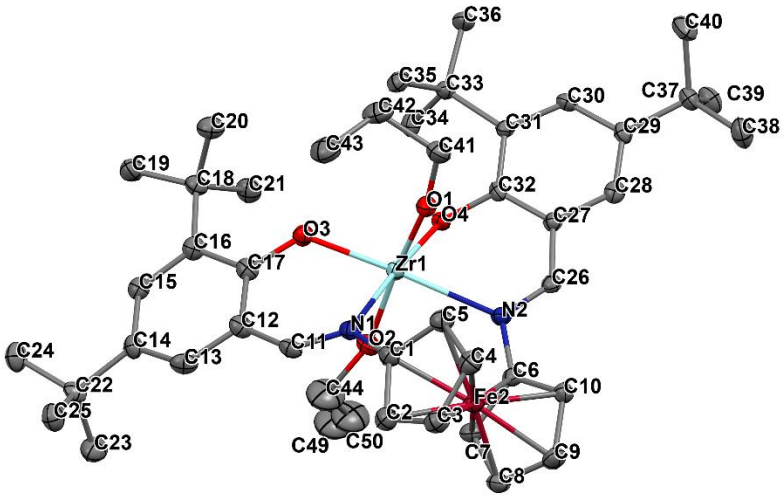

Figure 2.B33. Thermal ellipsoid (50% probability) representation of (salfen)Zr(O^nPr)$_2$; hydrogen atoms were omitted for clarity.

Crystal data for $C_{46}H_{64}FeN_2O_4Zr$; M_r = 856.06; Orthorhombic; space group $P2_12_12_1$; *a* = 11.6255(9) Å; *b* = 18.3632(14) Å; *c* = 20.0355(15) Å; V = 4277.2(6) Å^3; Z = 4; T = 100(2) K; λ = 0.71073 Å; μ = 0.626 mm^{-1}; d_{calc} = 1.329 g.cm^{-3}; 10620 reflections collected; 9226 unique; giving R_1 = 0.0459 for 9226 data with [I>2σ(I)] and R_1 = 0.0555, wR_2 = 0.1102 for all data. Residual electron density (e^-.Å^{-3}) max/min: 2.31/-1.07.

DFT Calculations

Table 2.B3. Calculated energies of Zr model compounds for precatalysts and products. The Gibbs free energy was calculated as the sum of the following contributions:

$G = E_{el} + G_{solv} + E_{ZPE} - RT \ln(q_{trans}\, q_{rot}\, q_{vib})$

where E_{el} is the in vacuo energy of the system, G_{solv} is the solvation free energy, E_{ZPE} is the zero-point energy, and $-RT \ln(q_{trans}\, q_{rot}\, q_{vib})$ accounts for the entropic terms and the thermal correction to the enthalpy obtained from a frequency calculation at 298 K and 1 atm using the ideal-gas approximation.[67] Chemical potential is $E_{ZPE} - RT \ln(q_{trans}\, q_{rot}\, q_{vib})$.

Entry	E_{el} (Hartree)	G_{solv} (Hartree)	Chemical potential (kJ/mol)	Final G (Hartree)	G - $G_{cis-\beta}$ (kcal/mol)
1 cis-β (salfen)Zr(OMe)$_2$	-2727.411201	-0.007817	988.29	-2727.043468	--
2 trans (salfen)Zr(OMe)$_2$	-2727.407065	-0.008624	986.69	-2727.036146	1.7
3 cis-β (salfen)Zr(OMe)$_2$-LA	-3262.040332	-0.011795	1315.04	-3261.552412	-2.4
4 trans (salfen)Zr(OMe)$_2$-LA	-3262.047135	-0.010995	1314.3	-3261.558697	-6.3

2.6. References

1. *The New Plastics Economy – Rethinking the future of plastics*; World Economic Forum, Ellen MacArthur Foundation, McKinsey & Company, 2016; p http://www.ellenmacarthurfoundation.org/publications.

2. Haward, M., Plastic pollution of the world's seas and oceans as a contemporary challenge in ocean governance. *Nat. Commun.* **2018,** *9*, 667.

3. Zhu, J.-B.; Watson, E. M.; Tang, J.; Chen, E. Y.-X., A synthetic polymer system with repeatable chemical recyclability. *Science* **2018,** *360*, 398-403.

4. Hong, M.; Chen, E. Y. X., Chemically recyclable polymers: a circular economy approach to sustainability. *Green Chem.* **2017,** *19*, 3692-3706.

5. Hong, M.; Chen, E. Y. X., Towards Truly Sustainable Polymers: A Metal-Free Recyclable Polyester from Biorenewable Non-Strained γ-Butyrolactone. *Angew. Chem. Int. Ed.* **2016,** *55*, 4188-4193.

6. Watts, A.; Kurokawa, N.; Hillmyer, M. A., Strong, Resilient, and Sustainable Aliphatic Polyester Thermoplastic Elastomers. *Biomacromolecules* **2017,** *18*, 1845-1854.

7. Schneiderman, D. K.; Hillmyer, M. A., Aliphatic Polyester Block Polymer Design. *Macromolecules* **2016,** *49*, 2419-2428.

8. Zhu, Y.; Romain, C.; Williams, C. K., Sustainable polymers from renewable resources. *Nature* **2016,** *540*, 354-362.

9. Williams, C. K.; Hillmyer, M. A., Polymers from Renewable Resources: A Perspective for a Special Issue of Polymer Reviews. *Polym. Rev.* **2008,** *48*, 1-10.

10. Ragauskas, A. J.; Williams, C. K.; Davison, B. H.; Britovsek, G.; Cairney, J.; Eckert, C. A.; Frederick, W. J.; Hallett, J. P.; Leak, D. J.; Liotta, C. L.; Mielenz, J. R.; Murphy, R.; Templer, R.; Tschaplinski, T., The Path Forward for Biofuels and Biomaterials. *Science* **2006,** *311*, 484-489.

11. Tian, H.; Tang, Z.; Zhuang, X.; Chen, X.; Jing, X., Biodegradable synthetic polymers: Preparation, functionalization and biomedical application. *Prog. Polym. Sci.* **2012,** *37*, 237-280.

12. Kaihara, S.; Matsumura, S.; Mikos, A. G.; Fisher, J. P., Synthesis of poly(L-lactide) and polyglycolide by ring-opening polymerization. *Nat. Protoc.* **2007,** *2*, 2767.

13. O'Keefe, B. J.; Hillmyer, M. A.; Tolman, W. B., Polymerization of lactide and related cyclic esters by discrete metal complexes. *J. Chem. Soc., Dalton Trans.* **2001**, 2215-2224.

14. Zhang, X.; Jones, G. O.; Hedrick, J. L.; Waymouth, R. M., Fast and selective ring-opening polymerizations by alkoxides and thioureas. *Nat. Chem.* **2016,** *8*, 1047.

15. Sauer, A.; Kapelski, A.; Fliedel, C.; Dagorne, S.; Kol, M.; Okuda, J., Structurally well-defined group 4 metal complexes as initiators for the ring-opening polymerization of lactide monomers. *Dalton Trans.* **2013,** *42*, 9007-9023.

16. Guillaume, S. M.; Kirillov, E.; Sarazin, Y.; Carpentier, J.-F., Beyond Stereoselectivity, Switchable Catalysis: Some of the Last Frontier Challenges in Ring-Opening Polymerization of Cyclic Esters. *Chem. Eur. J.* **2015,** *21*, 7988-8003.

17. Kricheldorf, H. R.; Berl, M.; Scharnagl, N., Poly(lactones). 9. Polymerization mechanism of metal alkoxide initiated polymerizations of lactide and various lactones. *Macromolecules* **1988,** *21*, 286-293.

18. Miola-Delaite, C.; Hamaide, T.; Spitz, R., Anionic coordinated polymerization of ε-caprolactone with aluminium, zirconium and some rare earths alkoxides as initiators in the presence of alcohols. *Macromolecular Chemistry and Physics* **1999,** *200*, 1771-1778.

19. Gendler, S.; Segal, S.; Goldberg, I.; Goldschmidt, Z.; Kol, M., Titanium and Zirconium Complexes of Dianionic and Trianionic Amine−Phenolate-Type Ligands in Catalysis of Lactide Polymerization. *Inorg. Chem.* **2006,** *45*, 4783-4790.

20. Saha, T. K.; Ramkumar, V.; Chakraborty, D., Salen Complexes of Zirconium and Hafnium: Synthesis, Structural Characterization, Controlled Hydrolysis, and Solvent-Free Ring-Opening Polymerization of Cyclic Esters and Lactides. *Inorg. Chem.* **2011,** *50*, 2720-2722.

21. Stopper, A.; Okuda, J.; Kol, M., Ring-Opening Polymerization of Lactide with Zr Complexes of {ONSO} Ligands: From Heterotactically Inclined to Isotactically Inclined Poly(lactic acid). *Macromolecules* **2012,** *45*, 698-704.

22. Buffet, J.-C.; Okuda, J., Group 4 metal initiators for the controlled stereoselective polymerization of lactide monomers. *Chem. Commun.* **2011,** *47*, 4796-4798.

23. Buffet, J.-C.; Martin, A. N.; Kol, M.; Okuda, J., Controlled stereoselective polymerization of lactide monomers by group 4 metal initiators that contain an (OSSO)-type tetradentate bis(phenolate) ligand. *Polym. Chem.* **2011,** *2*, 2378-2384.

24. Gregson, C. K. A.; Blackmore, I. J.; Gibson, V. C.; Long, N. J.; Marshall, E. L.; White, A. J. P., Titanium–salen complexes as initiators for the ring opening polymerisation of rac-lactide. *Dalton Trans.* **2006**, 3134-3140.

25. Chmura, A. J.; Davidson, M. G.; Jones, M. D.; Lunn, M. D.; Mahon, M. F.; Johnson, A. F.; Khunkamchoo, P.; Roberts, S. L.; Wong, S. S. F., Group 4 Complexes with

Aminebisphenolate Ligands and Their Application for the Ring Opening Polymerization of Cyclic Esters. *Macromolecules* **2006,** *39*, 7250-7257.

26. Kim, S. H.; Lee, J.; Kim, D. J.; Moon, J. H.; Yoon, S.; Oh, H. J.; Do, Y.; Ko, Y. S.; Yim, J.-H.; Kim, Y., Titanium complexes containing new dianionic tetradentate [ONNO]-type ligands with benzyl substituents on bridging nitrogen atoms: Syntheses, X-ray structures, and catalytic activities in ring opening polymerization of lactide. *J. Organomet. Chem.* **2009,** *694*, 3409-3417.

27. Jones, M. D.; Davidson, M. G.; Kociok-Kohn, G., New titanium and zirconium initiators for the production of polylactide. *Polyhedron* **2010,** *29*, 697-700.

28. Cameron, P. A.; Jhurry, D.; Gibson, V. C.; White, A. J. P.; Williams, D. J.; Williams, S., Controlled polymerization of lactides at ambient temperature using [5-Cl-salen]AlOMe. *Macromol. Rapid Commun.* **1999,** *20*, 616-618.

29. Yeori, A.; Gendler, S.; Groysman, S.; Goldberg, I.; Kol, M., Salalen: a hybrid Salan/Salen tetradentate [ONNO]-type ligand and its coordination behavior with group IV metals. *Inorg. Chem. Commun.* **2004,** *7*, 280-282.

30. Brown, L. A.; Rhinehart, J. L.; Long, B. K., Effects of Ferrocenyl Proximity and Monomer Presence during Oxidation for the Redox-Switchable Polymerization of l-Lactide. *ACS Catal.* **2015,** *5*, 6057-6060.

31. Gregson, C. K. A.; Gibson, V. C.; Long, N. J.; Marshall, E. L.; Oxford, P. J.; White, A. J. P., Redox Control within Single-Site Polymerization Catalysts. *J. Am. Chem. Soc.* **2006,** *128*, 7410-7411.

32. Hermans, C.; Rong, W.; Spaniol, T. P.; Okuda, J., Lanthanum complexes containing a bis(phenolate) ligand with a ferrocene-1,1'-diyldithio backbone: synthesis, characterization, and ring-opening polymerization of rac-lactide. *Dalton Trans.* **2016,** *45*, 8127-8133.

33. Sauer, A.; Buffet, J.-C.; Spaniol, T. P.; Nagae, H.; Mashima, K.; Okuda, J., Switching the Lactide Polymerization Activity of a Cerium Complex by Redox Reactions. *ChemCatChem* **2013,** *5*, 1088-1091.

34. Biernesser, A. B.; Li, B.; Byers, J. A., Redox-Controlled Polymerization of Lactide Catalyzed by Bis(imino)pyridine Iron Bis(alkoxide) Complexes. *J. Am. Chem. Soc.* **2013,** *135*, 16553-16560.

35. Wei, J.; Riffel, M. N.; Diaconescu, P. L., Redox Control of Aluminum Ring-Opening Polymerization: A Combined Experimental and DFT Investigation. *Macromolecules* **2017,** *50*, 1847-1861.

36. Quan, S. M.; Wei, J.; Diaconescu, P. L., Mechanistic Studies of Redox-Switchable Copolymerization of Lactide and Cyclohexene Oxide by a Zirconium Complex. *Organometallics* **2017,** *36*, 4451-4457.

37. Lowe, M. Y.; Shu, S.; Quan, S. M.; Diaconescu, P. L., Investigation of redox switchable titanium and zirconium catalysts for the ring opening polymerization of cyclic esters and epoxides. *Inorg. Chem. Front.* **2017,** *4*, 1798-1805.

38. Quan, S. M.; Wang, X.; Zhang, R.; Diaconescu, P. L., Redox Switchable Copolymerization of Cyclic Esters and Epoxides by a Zirconium Complex. *Macromolecules* **2016,** *49*, 6768-6778.

39. Wang, X.; Thevenon, A.; Brosmer, J. L.; Yu, I.; Khan, S. I.; Mehrkhodavandi, P.; Diaconescu, P. L., Redox Control of Group 4 Metal Ring-Opening Polymerization Activity toward l-Lactide and ε-Caprolactone. *J. Am. Chem. Soc.* **2014,** *136*, 11264-11267.

40. Broderick, E. M.; Thuy-Boun, P. S.; Guo, N.; Vogel, C. S.; Sutter, J.; Miller, J. T.; Meyer, K.; Diaconescu, P. L., Synthesis and Characterization of Cerium and Yttrium Alkoxide Complexes Supported by Ferrocene-Based Chelating Ligands. *Inorg. Chem.* **2011,** *50*, 2870-2877.

41. Broderick, E. M.; Guo, N.; Wu, T.; Vogel, C. S.; Xu, C.; Sutter, J.; Miller, J. T.; Meyer, K.; Cantat, T.; Diaconescu, P. L., Redox control of a polymerization catalyst by changing the oxidation state of the metal center. *Chem. Commun.* **2011,** *47*, 9897-9899.

42. Broderick, E. M.; Guo, N.; Vogel, C. S.; Xu, C.; Sutter, J.; Miller, J. T.; Meyer, K.; Mehrkhodavandi, P.; Diaconescu, P. L., Redox Control of a Ring-Opening Polymerization Catalyst. *J. Am. Chem. Soc.* **2011,** *133*, 9278–9281.

43. Abubekerov, M.; Wei, J.; Swartz, K. R.; Xie, Z.; Pei, Q.; Diaconescu, P. L., Preparation of multiblock copolymers via step-wise addition of l-lactide and trimethylene carbonate. *Chem. Sci.* **2018,** *9*, 2168-2178.

44. Abubekerov, M.; Khan, S. I.; Diaconescu, P. L., Ferrocene-bis(phosphinimine) Nickel(II) and Palladium(II) Alkyl Complexes: Influence of the Fe–M (M = Ni and Pd) Interaction on Redox Activity and Olefin Coordination. *Organometallics* **2017,** *36*, 4394-4402.

45. Shepard, S. M.; Diaconescu, P. L., Redox-Switchable Hydroelementation of a Cobalt Complex Supported by a Ferrocene-Based Ligand. *Organometallics* **2016,** *35*, 2446–2453.

46. Huang, W.; Diaconescu, P. L., Reactivity and Properties of Metal Complexes Enabled by Flexible and Redox-Active Ligands with a Ferrocene Backbone. *Inorg. Chem.* **2016,** *55*, 10013–10023.

47. Abubekerov, M.; Shepard, S. M.; Diaconescu, P. L., Switchable Polymerization of Norbornene Derivatives by a Ferrocene-Palladium(II) Heteroscorpionate Complex. *Eur. J. Inorg. Chem.* **2016,** *2016*, 2634-2640.

48. Wang, X.; Brosmer, J. L.; Thevenon, A.; Diaconescu, P. L., Highly Active Yttrium Catalysts for the Ring-Opening Polymerization of ε-Caprolactone and δ-Valerolactone. *Organometallics* **2015,** *34*, 4700–4706.

49. Quan, S. M.; Diaconescu, P. L., High activity of an indium alkoxide complex toward ring opening polymerization of cyclic esters. *Chem. Commun.* **2015,** *51*, 9643 - 9646.

50. Broderick, E. M.; Diaconescu, P. L., Cerium(IV) Catalysts for the Ring-Opening Polymerization of Lactide. *Inorg. Chem.* **2009,** *48*, 4701-4706.

51. Clarkson, G. J.; Gibson, V. C.; Goh, P. K. Y.; Hammond, M. L.; Knight, P. D.; Scott, P.; Smit, T. M.; White, A. J. P.; Williams, D. J., Group 4 catalysts for ethene polymerization containing tetradentate salicylaldiminato ligands. *Dalton Trans.* **2006**, 5484-5491.

52. Chen, H.; White, P. S.; Gagné, M. R., Synthesis and Reactivity of Titanium(IV)−Salen Complexes Containing Oxygen and Chloride Ligands. *Organometallics* **1998,** *17*, 5358-5366.

53. Pangborn, A. B.; Giardello, M. A.; Grubbs, R. H.; Rosen, R. K.; Timmers, F. J., Safe and Convenient Procedure for Solvent Purification. *Organometallics* **1996,** *15*, 1518-1520.

54. Dhar, D.; Yee, G. M.; Spaeth, A. D.; Boyce, D. W.; Zhang, H.; Dereli, B.; Cramer, C. J.; Tolman, W. B., Perturbing the Copper(III)–Hydroxide Unit through Ligand Structural Variation. *J. Am. Chem. Soc.* **2016,** *138*, 356-368.

55. Ahlrichs, R.; Bär, M.; Häser, M.; Horn, H.; Kölmel, C., Electronic structure calculations on workstation computers: The program system turbomole. *Chemical Physics Letters* **1989,** *162*, 165-169.

56. Treutler, O.; Ahlrichs, R., Efficient molecular numerical integration schemes. *J. Chem. Phys.* **1995,** *102*, 346-354.

57. Dirac, P. A. M., Quantum mechanics of many-electron systems. *Proc. Royal Soc. Lond.* **1929,** *123*, 714-733.

58. Slater, J. C., A Simplification of the Hartree-Fock Method. *Phys. Rev.* **1951,** *81*, 385-390.

59. Perdew, J. P.; Wang, Y., Accurate and simple analytic representation of the electron-gas correlation energy. *Phys. Rev. B* **1992,** *45*, 13244-13249.

60. Tao, J.; Perdew, J. P.; Staroverov, V. N.; Scuseria, G. E., Climbing the Density Functional Ladder: Nonempirical Meta--Generalized Gradient Approximation Designed for Molecules and Solids. *Phys. Rev. Lett.* **2003,** *91*, 146401.

61. Weigend, F.; Häser, M.; Patzelt, H.; Ahlrichs, R., RI-MP2: optimized auxiliary basis sets and demonstration of efficiency. *Chemical Physics Letters* **1998,** *294*, 143-152.

62. Weigend, F.; Ahlrichs, R., Balanced basis sets of split valence, triple zeta valence and quadruple zeta valence quality for H to Rn: Design and assessment of accuracy. *Phys. Chem. Chem. Phys.* **2005,** *7*, 3297-3305.

63. Staroverov, V. N.; Scuseria, G. E.; Tao, J.; Perdew, J. P., Comparative assessment of a new nonempirical density functional: Molecules and hydrogen-bonded complexes. *J. Chem. Phys.* **2003,** *119*, 12129-12137.

64. Grimme, S.; Antony, J.; Ehrlich, S.; Krieg, H., A consistent and accurate ab initio parametrization of density functional dispersion correction (DFT-D) for the 94 elements H-Pu. *J. Chem. Phys.* **2010,** *132*, 154104.

65. Klamt, A.; Schüürmann, G., COSMO: a new approach to dielectric screening in solvents with explicit expressions for the screening energy and its gradient. *J. Chem. Soc., Perkin Trans. 2* **1993**, 799-805.

66. Schäfer, A.; Klamt, A.; Sattel, D.; Lohrenz, J. C. W.; Eckert, F., COSMO Implementation in TURBOMOLE: Extension of an efficient quantum chemical code towards liquid systems. *Phys. Chem. Chem. Phys.* **2000,** *2*, 2187-2193.

67. Jensen, F., *Introduction to Computational Chemistry*. Wiley: New York, 1999.

Chapter 3. Homopolymerization and copolymerization studies using (salfen)Zr(O^iPr)$_2$

3.1. Introduction

Polymers are playing an important role in our society's everyday life, their applications ranging from plastic bags to smart phone screen protectors, and from artificial tissues to electronic wire covers.[1-4] As the polymer consumption increases every year, the "white pollution" is becoming a more and more serious environmental issue in the world.[5-8] Biodegradable polymers, as a promising alternative to the plastics in use now, have been researched intensely in the past few decades.[9-13] Poly-lactide (PLA) is an example of a material that has been proved to be environmentally friendly.[14, 15] However, the properties of the homopolymers are not as diverse as those of its possible copolymers.

Block copolymerization is a method to regulate the properties of copolymers, and it is considered one of the most feasible approaches among the large number of methods available.[16-18] Although anionic or atom transfer radical polymerization can be used for the synthesis of block copolymers, these methods require additional modification steps, for example, end group modification and bifunctional initiators, especially when different types of monomers, such as LA (lactide) and CHO (cyclohexene oxide), need to be combined.[19-21] Therefore, researching methods to build block copolymers with few or no additional modification steps is necessary.

Switchable catalysis is a promising method for the construction of sequence controlled block copolymers.[22-29] In such reactions, an external trigger, such as electron transfer,[30-36] chemical reagents,[37-43] or light,[43-45] is used to toggle between two or more catalyst states, which each show orthogonal reactivity toward different monomers. In redox switchable catalysis, the oxidation state of the catalyst can be changed by using electron transfer; different polymer blocks are synthesized

by the different oxidation states of the catalyst. This method has been best applied to the ring opening polymerization of cyclic esters and ethers.[30-36, 46-50]

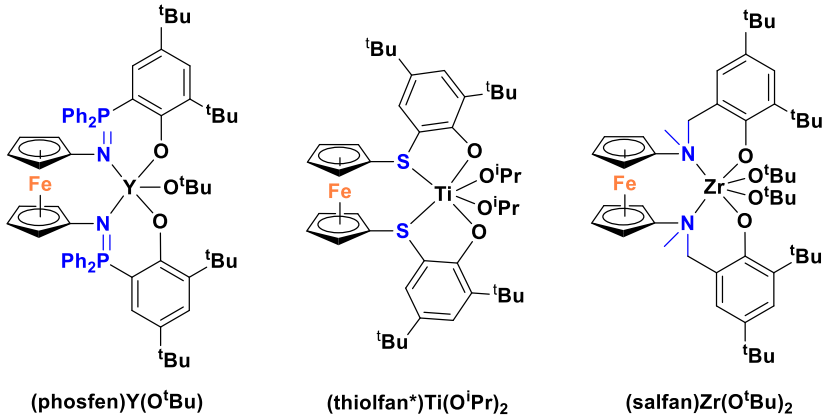

Figure 3.1. Previously reported metal complexes supported by ferrocene chelating ligands that perform redox switchable ring opening polymerization.

The first example of a redox controlled ring opening polymerization was first reported in 2006 by N. Long and coworkers,[51] who showed that a titanium Schiff base complex, featuring ferrocene groups appended at the periphery of the molecule, has a different activity in the polymerization of *rac*-lactide depending on the oxidation state of the ferrocene units. In 2011, our group reported a complementary study, showing that while a yttrium complex, (phosfen)Y(O^{t}Bu) (phosfen = 1,1'-di(2-*tert*-butyl-6-diphenylphosphiniminophenoxy)ferrocene, Figure 3.1), mimicked the results observed with the previous titanium complex, an indium analogue showed the opposite activity.[48] Further, in 2014, we reported the first example of a redox switchable polymerization system, where reversible oxidation and reduction could be done on a single precatalyst, (salfan)Zr(O^{t}Bu)$_2$ (salfan = 1,1′-di(2-*tert*-butyl-6-N-methylmethylenephenoxy)ferrocene, Figure 3.1), and each oxidation state could polymerize

different monomers.[36] A copolymerization study based on this redox switchable system was reported in 2016, demonstrating an orthogonal monomer selectivity under different precatalyst oxidation states.[35] The precatalyst, (salfan)Zr(O^tBu)$_2$ (Figure 3.1), had a ferrocene unit in the ligand backbone such that iron could be reduced and oxidized *in situ*, while the zirconium center showed a different ring opening polymerization activity depending on the monomer of choice. Mechanistic studies were reported in 2017.[33] Based on those results, we became interested in whether a compound featuring a fully conjugated ligand, (salfen)Zr(O^iPr)$_2$ (salfen = N,N′-bis(2,4-di-*tert*-butylphenoxy)-1,1′-ferrocenediimine),[52] could behave similarly in redox switchable polymerization. Herein, we report its redox properties and polymerization behavior toward cyclic esters and ethers.

3.2. Results and Discussion

Redox properties of (salfen)Zr(O^iPr)$_2$

(salfen)Zr(O^iPr)$_2$ ([Zr]^{red}) was synthesized according to the reported procedures.[52] It can be oxidized *in situ* by ^{Ac}FcBAr^F (^{Ac}Fc = acetylferrocene, BAr^F = tetrakis(3,5-bis(trifluoromethyl)-phenyl)borate) to give [(salfen)Zr(O^iPr)$_2$][BAr^F] ([Zr]^{ox}) and then reduced back cleanly by $CoCp_2$ (Scheme 3.1, Figure 3.C2). Cyclic voltammetry experiments were carried out, with 1,2-difluorobenzene as the solvent and TPABAr^F (TPA = tetra-*n*-propylammonium) as the electrolyte, showing that the compound has a redox potential of $E_{1/2}$ = 0.10 V vs ferrocene (Figure 3.2). When the chemical oxidation reaction was done on a 25 mg scale, a dark-red oil was collected and characterized to be [(salfen)Zr(O^iPr)$_2$][BAr^F]. Such an observation of the viscous oil-like liquid appearance is consistent with several previous reports on similar ionic compounds.[32, 36, 53] Attempts

were made to grow crystals of [(salfen)Zr(O^iPr)$_2$][BAr^F] from benzene/hexanes, but single crystals could not be obtained.

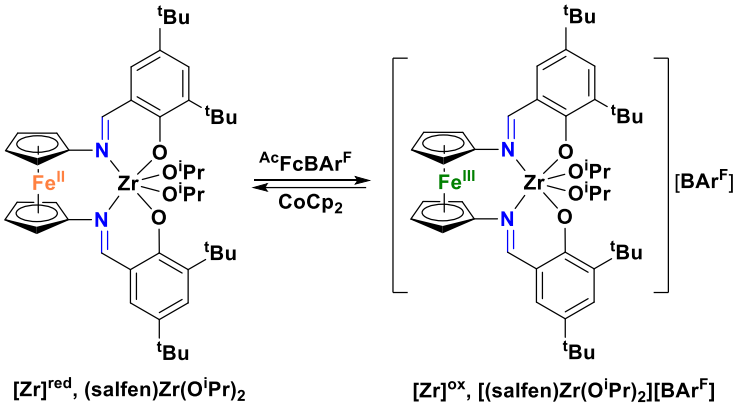

Scheme 3.1. Redox interconversions between $[Zr]^{red}$ and $[Zr]^{ox}$.

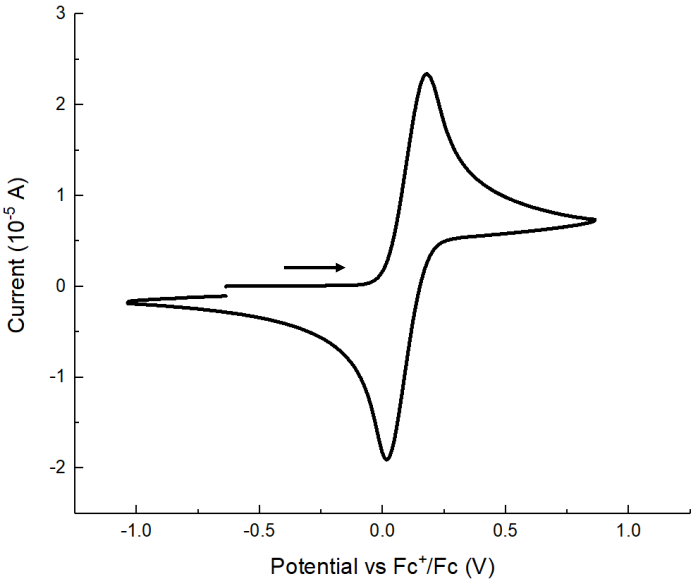

Figure 3.2. Cyclic voltammogram recorded at a glassy carbon electrode at 100 mV/s in 1,2-difluorobenzene, 0.10 M $TPABAr^F$ containing 5.0 mM (salfen)Zr(O^iPr)$_2$.

Homopolymerizations

The activity of five different cyclic esters in the presence of (salfen)Zr(O^iPr)$_2$ ([Zr]^{red}) or the *in situ* generated oxidized species ([Zr]^{ox}) was tested. LA (L-lactide) and VL (δ-valerolactone) could be polymerized by [Zr]^{red} but not by [Zr]^{ox} (Table 3.1, entries 1-4). When [Zr]^{red} was added to 100 equivalents of VL, 39% conversion was achieved after heating at 100 ^oC for 24 hours (Table 3.C1, entry 3). However, the polymer product could not be precipitated out with methanol, as was done in the PLA (poly-L-lactide) work up. Increasing the monomer feeding to 250 equivalents gave a higher conversion of 64%, resulting in a product that could be precipitated out from methanol as a white powder (Table 3.1, entry 3). TMC (1,3-trimethylene carbonate) worked with both the reduced and oxidized species (Table 3.1, entries 5-6). PC (propylene carbonate) and BL (β-butyrolactone) did not work with either the reduced nor oxidized species (Table 3.1, entries 7-10).

With regard to epoxide homopolymerization, both CHO and PO (propylene oxide) showed no conversion with [Zr]^{red}. However, CHO polymerization went very fast upon adding [Zr]^{ox}, similarly to the CHO homopolymerization catalyzed by [(salfan)Zr(O^tBu)$_2$][BAr^F].[35] PO polymerization was not as fast, 100 equivalents of monomer led to a 51% conversion after 24 hours (Table 3.C1, entry 15), but these results indicate a higher activity of (salfen)Zr(O^iPr)$_2$ than (salfan)Zr(O^tBu)$_2$ toward PO.[35] Unlike PCHO, PPO (poly-propylene oxide) is usually a liquid[54, 55] and could not be precipitated from methanol as a solid product. Therefore, an increased feeding of PO (1000 equivalents, Table 3.1, entry 14) was used and, after 24 hours at room temperature, the reaction mixture was quenched with methanol, stirring with activated carbon for 3 hours. The mixture was then filtered through Celite and the volatiles were removed under a reduced pressure, giving a viscous liquid as the product. The molecular weight obtained was much lower than the

theoretical value, and the SEC (size exclusion chromatography) measurement (Figure 3.C21) showed multiple traces, indicating that the polymerization process was not controlled.

Comparing the aforementioned results to the homopolymerizations previously reported for (salfan)Zr(O^tBu)$_2$ (Figure 3.1), we were able to probe the ligand affect on the polymerization catalysis. For cyclic ester polymerization, LA was polymerized faster with (salfan)Zr(O^tBu)$_2$ (3 hours) than (salfen)Zr(O^iPr)$_2$. However, for epoxide polymerizations, CHO and PO were polymerized slower with (salfan)Zr(O^tBu)$_2$ (4 hours for CHO and 24 hours for PO) than (salfen)Zr(O^iPr)$_2$.[35]

Table 3.1. Homopolymerization of different monomers with $[Zr]^{red}$ and $[Zr]^{ox}$.[a]

Entry	Monomer [d]	cat.	Time (h)	Conv. (%)	Mn[e] (10^3 Da)	Đ
1	LA	red	24	71	6.4	1.02
2	LA	ox	24	<3	--	--
3 [b]	VL	red	24	64	10.8	1.13
4	VL	ox	24	<3	--	--
5	TMC	red	24	92	10.0	1.29
6	TMC	ox	24	88	8.7	1.13
7	PC	red	24	<3	--	--
8	PC	ox	24	<3	--	--
9	BL	red	24	<3	--	--
10	BL	ox	24	<3	--	--
11	CHO	red	24	<3	--	--
12	CHO	ox	0.2	100	22.0	1.23
13	PO	red	24	<3	--	--
14 [c]	PO	ox	24	88	1.8	1.62

[a] All polymerization reactions were carried out with 4 μmol precatalysts, 0.6 mL of C_6D_6 as the solvent and hexamethylbenzene as an internal standard. 100 equivalents of monomer was used unless otherwise mentioned. All reactions with $[Zr]^{red}$ were done at 100 °C and all reactions with $[Zr]^{ox}$ were done at 25 °C. [b] 250 equivalents of monomer was used. [c] 1000 equivalents of monomer was used. [d] VL stands for δ-valerolactone, TMC stands for 1,3-trimethylene carbonate, BL stands for β-butyrolactone, PC stands for propylene carbonate and PO stands for propylene oxide. [e] Molar masses were derived from SEC measurements.

Copolymerizations with redox control

Based on the results of the monomer screening, LA, TMC, and CHO are the three active monomers that could be used for a copolymerization study. VL was not chosen due to a too low conversion in a relatively long time. PO was not chosen because of the uncontrollable polymerization process. A diblock-copolymer, PCHO-PLA, and a triblock-copolymer, PLA-PCHO-PLA, were prepared. LA was first polymerized with $[Zr]^{red}$, and then $^{Ac}FcBAr^F$ was added to the solution to give $[Zr]^{ox}$, after which, CHO was added and the PCHO-PLA copolymer was formed after an hour. The reaction time for the second block, PCHO, was much shorter than that in the previously reported system of (salfan)Zr(O^tBu)$_2$ (17 hours).[35] A sequential addition was needed because the oxidant, $^{Ac}FcBAr^F$, can also polymerize CHO. Therefore, in each oxidation reaction, only 0.97 equivalents of $^{Ac}FcBAr^F$ with respect to $[Zr]^{red}$ was added to avoid an excess of oxidant. A discussion on the roles of the oxidant was reported by us previously.[35] Both PLA-PCHO diblock-copolymers and PLA-PCHO-PLA triblock-copolymers were characterized by SEC and DOSY NMR spectroscopy to confirm that their copolymeric nature (DOSY NMR spectra showed in Figures 3.C13, 3.C14; SEC traces in Figures 3.C23 and 3.C25). A mixture of PLA and

PCHO homopolymers (from Table 3.1, entry 1 and entry 12, respectively) was also characterized by SEC and DOSY NMR spectroscopy. The SEC trace of this mixture showed two peaks and the DOSY NMR spectrum showed two species with different diffusion rates (Figures 3.C24 and 3.C15, respectively). Those characterizations further supported that the aforementioned PCHO-PLA and PLA-PCHO-PLA were copolymers and not mixtures of homopolymers. A comparison between SEC traces of PLA, PCHO-PLA, PLA-PCHO-PLA is shown in Figure 3.3.

TMC and LA is another possible combination for a copolymerization study. When TMC was polymerized first, followed by the addition of LA (Table 3.2, entry 3), the PLA-PTMC copolymer was formed as expected. But when LA was polymerized first followed by adding TMC to the system, TMC showed no conversion over 24 hours. Such results were consistent with previous reports that TMC cannot open the ring formed by the metal-lactide coordination-insertion intermediate.[56-60] Since TMC could be polymerized by either $[Zr]^{ox}$ or $[Zr]^{red}$, attempts were made to form the PTMC block by $[Zr]^{ox}$ (Table 3.2, entry 5), but the experiment did not go as expected, with the TMC conversion still 0%. These results demonstrated that the Zr-LA coordination is strong and that TMC could not be incorporated into the polymer.

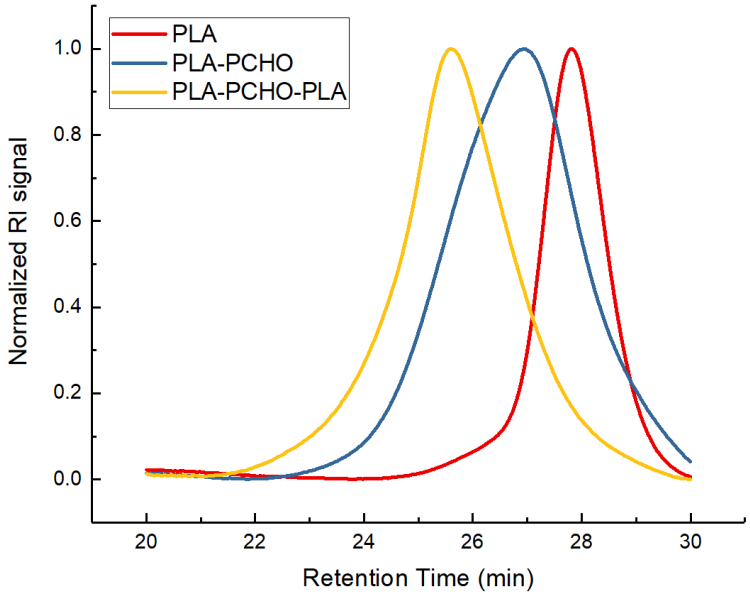

Figure 3.3. SEC traces of PLA homopolymers, PLA-PCHO diblock and PLA-PCHO-PLA triblock copolymers.

Table 3.2. Redox controlled copolymerization studies.[a]

Entry	Monomer	Catalyst[b]	Conv. (%)	Time (h)	Đ
1	LA-CHO	red-ox	70-100	24-1	1.37
2	LA-CHO-LA	red-ox-red	66-100-88	24-1-16	1.55
3	TMC-LA	red-red	60-87	16-24	1.09
4	LA-TMC	red-red	70-0	24-24	--
5	LA-TMC	red-ox	70-0	24-24	--

[a] All polymerization reactions were carried out with 4 μmol precatalyst, 0.6 mL of C_6D_6 as a solvent and hexamethylbenzene as an internal standard. 100 equivalents of monomer were used unless otherwise mentioned. All reactions with the reduced species, (salfen)Zr(O^iPr)$_2$, were done at 100 ^oC and all reactions with the oxidized species, [(salfen)Zr(O^iPr)$_2$][BAr^F], were done at 25

^{o}C. [b] "red" means that $[Zr]^{red}$ was used as a precatalyst, "ox" means that $[Zr]^{ox}$ was generated *in situ*.

3.3. Conclusions

Compound (salfen)Zr($O^{i}Pr$)$_2$ was tested as a redox switchable precatalyst for the ring opening polymerization and copolymerization of cyclic esters and ethers. Different monomers were tested for homopolymerization reactions with oxidized and reduced states of the precatalysts. LA, VL and TMC could be polymerized by $[Zr]^{red}$, while CHO, PO could be polymerized by $[Zr]^{ox}$. A PCHO-PLA diblock copolymer and a PLA-PCHO-PLA triblock copolymer were prepared and characterized by SEC and DOSY NMR spectroscopy. The preparation of PLA-PTMC copolymers was attempted but it was not successful.

Comparing with (salfan)Zr($O^{t}Bu$)$_2$, LA homopolymerization was slower with (salfen)Zr($O^{i}Pr$)$_2$, while PO and CHO homopolymerizations were faster with [(salfen)Zr($O^{i}Pr$)$_2$][BAr^{F}]. Such difference was more significant in PLA-PCHO copolymerization scenario, where with (salfan)Zr($O^{t}Bu$)$_2$ the PLA block was finished in 3 h and the CHO block in 17 h, while with (salfen)Zr($O^{i}Pr$)$_2$ the LA block was prepared in 24 h and the CHO block in 1 h.

3.4. Experimental Section

General considerations

All experiments were performed in an Mbraun inert gas glovebox or under a dry nitrogen atmosphere using standard Schlenk techniques. Solvents were purified with a two-state solid-state purification system by the method of Grubbs and transferred to the glovebox inside a Schlenk flask

without exposure to air. NMR solvents were obtained from Cambridge Isotope Laboratories, degassed, and stored over activated molecular sieves prior to use. ^{1}H NMR spectra were recorded on Bruker 300, Bruker 500, or Bruker 600 spectrometers at room temperature in C_6D_6. Chemical shifts are reported with respect to the residual solvent peaks, 7.16 ppm (C_6D_6) for ^{1}H NMR spectra. Liquid monomers and 1,2-difluorobenzene were distilled over CaH_2 and brought into the glovebox without exposure to air. Solid monomers and 1,3,5-trimethoxybenzene were recrystallized from toluene at least twice before use. 2,4-di-*tert*-butylphenol, *n*-BuLi, and $CoCp_2$ were purchased from Sigma-Aldrich and used as received. ^{Ac}FcBAr^{F} (^{Ac}Fc = acetylferrocene, BAr^{F} = tetrakis(3,5-bis(trifluoromethyl)-phenyl)borate)[61] and (salfen)Zr(O^{i}Pr)$_2$[52] were synthesized following previously published procedures. Molar masses of polymers were determined by size exclusion chromatography using a SEC-MALS instrument at UCLA. SEC-MALS uses a Shimazu Prominence-i LC 2030C 3D equipped with an autosampler, two MZ Analysentechnik MZ-Gel SDplus LS 5 μm, 300 × 8 mm linear columns, a Wyatt DAWN HELEOS-II, and a Wyatt Optilab T-rEX. The column temperature was set at 40 ^{o}C. A flow rate of 0.70 mL/min was used and samples were dissolved in THF. The number average molar mass and dispersity values were found using the known concentration of the sample in THF with the assumption of 100% mass recovery to calculate dn/dc from the RI signal. Cyclic voltammograms were acquired with a CH Instruments CHI630D potentiostat and recorded with CH Instruments software (version 13.04). All potentials are given with respect to the ferrocene-ferrocenium couple. CHN analyses were performed on an Exeter Analytical, Inc. CE-440 Elemental Analyzer.

Isolation of [(salfen)Zr(O^{i}Pr)$_2$][BAr^{F}] ([Zr]^{ox})

(salfen)Zr(O^{i}Pr)$_2$ (25.7 mg, 0.03 mmol) and ^{Ac}FcBAr^{F} (32.7 mg, 0.03 mmol) were each dissolved in 5 mL diethyl ether. ^{Ac}FcBAr^{F} was added to (salfen)Zr(O^{i}Pr)$_2$ dropwise. A dark red

solution was generated instantly, then the mixture was stirred at room temperature for 1 hour. The solution was filtered through a Celite plug and concentrated under a reduced pressure. Hexanes was layered on the top of the diethyl ether solution, and the mixture was kept in the freezer for 18 hours (overnight). The top layer was removed, leaving a dark colour viscous liquid at the bottom of the vial as the product. The oil was dried under a reduced pressure for 2 hours to remove the volatiles; the product was still an oil-like, viscous liquid after drying. Yield: 49.8 mg (97%). Crystals feasible for elemental analysis were grown from benzene/hexanes solutions. ^{1}H NMR (300 MHz, C_6D_6, 25 ^{o}C), δ, ppm: 8.40 (s, 8H, *m*-C_6H_3, BAr^F), 7.68 (s, 4H, *m*-C_6H_3, BAr^F), 7.95 (s, 2H, N=C*H*), 7.82 (s, 2H, *m*-C_6H_2), 7.11 (s, 2H, *m*-C_6H_2), 4.34 (br, 8H, C_5H_4), 4.02 (s, 6H, $CH(CH_3)_2$), 3.53 (s, 6H, $CH(CH_3)_2$), 1.78 (s, 2H, $CH(CH_3)_2$), 1.62 (s, 18H, $C(CH_3)_3$), 1.25 (s, 18H, $C(CH_3)_3$). Elemental analysis for $C_{78}H_{76}N_2O_4FeZrBF_{24}$, Calcd: C, 54.49%, H, 4.45%, N, 1.63%; Found: C, 54.50%, H, 3.81%, N, 1.23%.

NMR scale polymerizations with (salfen)Zr(O^iPr)$_2$ ([Zr]^{red})

Under an inert atmosphere, (salfen)Zr(O^iPr)$_2$ (4 μmol), the monomer, C_6D_6 (0.6 mL), and an internal standard (hexamethylbenzene) were added to a J-Young NMR tube. The reaction mixture was left at room temperature for 5 minutes while being shaken occasionally. The tube was sealed and brought out of the glovebox and heated to the specified temperature with an oil bath. The NMR tube was taken out of the oil bath and analyzed periodically by ^{1}H NMR spectroscopy. When the reaction was done, CH_2Cl_2 was added to the mixture and then the resulting solution was poured into 10 mL of cold methanol to precipitate the polymer. The mixture was centrifuged 3 x 5 minutes, decanted, and dried under a reduced pressure to give the final polymer product.

NMR scale polymerizations with [(salfen)Zr(O^iPr)$_2$][BAr^F] ([Zr]^{ox})

Under an inert atmosphere, (salfen)Zr(O^iPr)$_2$ (4 μmol), C_6D_6 (0.3 mL), and an internal standard (hexamethylbenzene) were added to a J-Young NMR tube. The $^{Ac}FcBAr^F$ solution (0.1 mL, 40 mM in 1,2-difluorobenzene) was added and the NMR tube was shaken for 5 minutes before adding the monomer. The tube was sealed and brought out of the glovebox and left at room temperature. The NMR tube was monitored periodically by ^{1}H NMR spectroscopy. When the reaction was done, CH_2Cl_2 was added to the mixture and then the resulting solution was poured into 10 mL of cold methanol to precipitate the polymer. The mixture was centrifuged 3 x 5 minutes, decanted, and dried under a reduced pressure to give the final polymer product.

General procedure for copolymerizations

Redox switchable polymerization starting with [Zr]^{red}

Under an inert atmosphere, (salfen)Zr(O^iPr)$_2$ (4 μmol), the monomer, C_6D_6 (0.6 mL) and the internal standard (hexamethylbenzene) were added to a J-Young NMR tube. The reaction mixture was left at room temperature for 5 minutes while being shaken occasionally. The tube was sealed and brought out of the glovebox and heated to the specified temperature with an oil bath. The NMR tube was taken out of the oil bath and monitored periodically by ^{1}H NMR spectroscopy. After the first block of the copolymer was made, the NMR tube was brought back into the glovebox. An $^{Ac}FcBAr^F$ solution (0.1 mL, 40 mM in 1,2-difluorobenzene) was added and the NMR tube was shaken for 5 min before adding the second monomer. The tube was sealed and brought out of the glovebox, left at room temperature and monitored periodically by ^{1}H NMR spectroscopy. When the reaction was done, CH_2Cl_2 was added to the reaction mixture and then the solution was poured into 10 mL cold methanol to precipitate the polymer. The mixture was centrifuged for 3x5 minutes, decanted, and dried under a reduced pressure to give the final polymer product.

Two redox switches starting with [Zr]^{red}

Under an inert atmosphere, (salfen)Zr(O^iPr)$_2$ (4 μmol), the monomer, C_6D_6 (0.6 mL) and the internal standard (hexamethylbenzene) were added to a J-Young NMR tube. The reaction mixture was left at room temperature for 5 minutes while being shaken occasionally. The tube was sealed and brought out of the glovebox and heated to the specified temperature with an oil bath. The NMR tube was taken out of the oil bath and monitored periodically by ^{1}H NMR spectroscopy. After the first block of the copolymer was made, the NMR tube was brought back into the glovebox. An ^{Ac}FcBAr^F solution (0.1 mL, 40 mM in 1,2-difluorobenzene) was added and the NMR tube was shaken for 5 min before adding the second monomer. The tube was sealed and brought out of the glovebox, left at room temperature and monitored periodically by ^{1}H NMR spectroscopy. After the second block was made, the NMR tube was brought back into the glovebox. A $CoCp_2$ solution (0.1 mL, 40 mM in C_6D_6) was added to the reaction mixture and the third monomer was added. The reaction mixture was left at room temperature for 5 minutes while being shaken occasionally. The tube was sealed and brought out of the glovebox and heated to the specified temperature with an oil bath. The NMR tube was taken out of the oil bath and monitored periodically by ^{1}H NMR spectroscopy. When the reaction was done, CH_2Cl_2 was added to the reaction mixture and then the solution was poured into 10 mL cold methanol to precipitate the polymer. The mixture was centrifuged for 3x5 minutes, decanted, and dried under a reduced pressure to give the final polymer product.

Cyclic voltammetry studies of (salfen)Zr(O^iPr)$_2$

Cyclic voltammetry studies were carried out in a 20 mL scintillation vial with electrodes fixed in position by a rubber stopper, in a 0.10 M TPABAr^F (TPA = tetra-*n*-propylammonium) solution in 1,2-difluorobenzene. A glassy carbon working electrode, a platinum reference electrode, and a silver-wire pseudoreference electrode were purchased from CH Instruments. Before each

cyclic voltammogram was recorded, the working and auxiliary electrodes were polished with an aqueous suspension of 0.05 μm alumina on a Microcloth polishing pad.

3.5. Appendix C

NMR Spectra

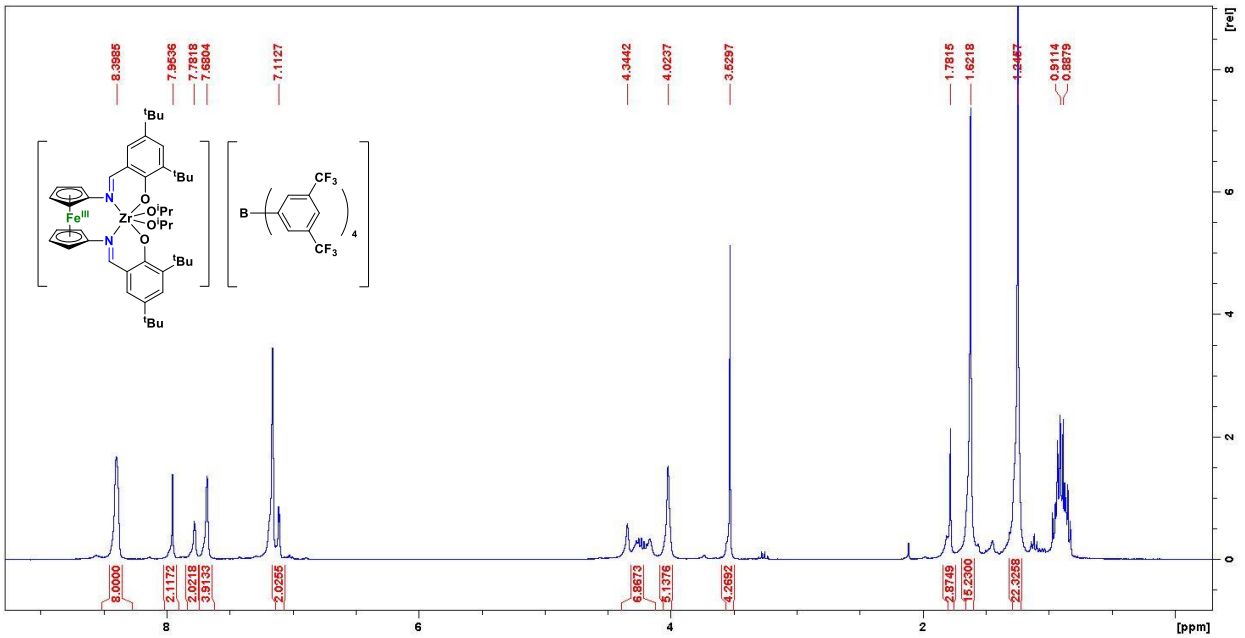

Figure 3.C1. ^{1}H NMR (300 MHz, C_6D_6, 25 ^{o}C) spectrum of [(salfen)Zr($O^{i}Pr$)$_2$][BAr^{F}]. δ, ppm: 8.40 (s, 8H, *m*-C_6H_3, BAr^{F}), 7.68 (s, 4H, *m*-C_6H_3, BAr^{F}), 7.95 (s, 2H, N=C*H*), 7.82 (s, 2H, *m*-C_6H_2), 7.11 (s, 2H, *m*-C_6H_2), 4.34 (br, 8H, C_5H_4), 4.02 (s, 6H, CH(CH_3)$_2$), 3.53 (s, 6H, CH(CH_3)$_2$), 1.78 (s, 2H, C*H*(CH_3)$_2$), 1.62 (s, 18H, C(CH_3)$_3$), 1.25 (s, 18H, C(CH_3)$_3$), 0.90 (hexanes). The other hexanes peaks are blocked by the 1.25 ppm product peak.

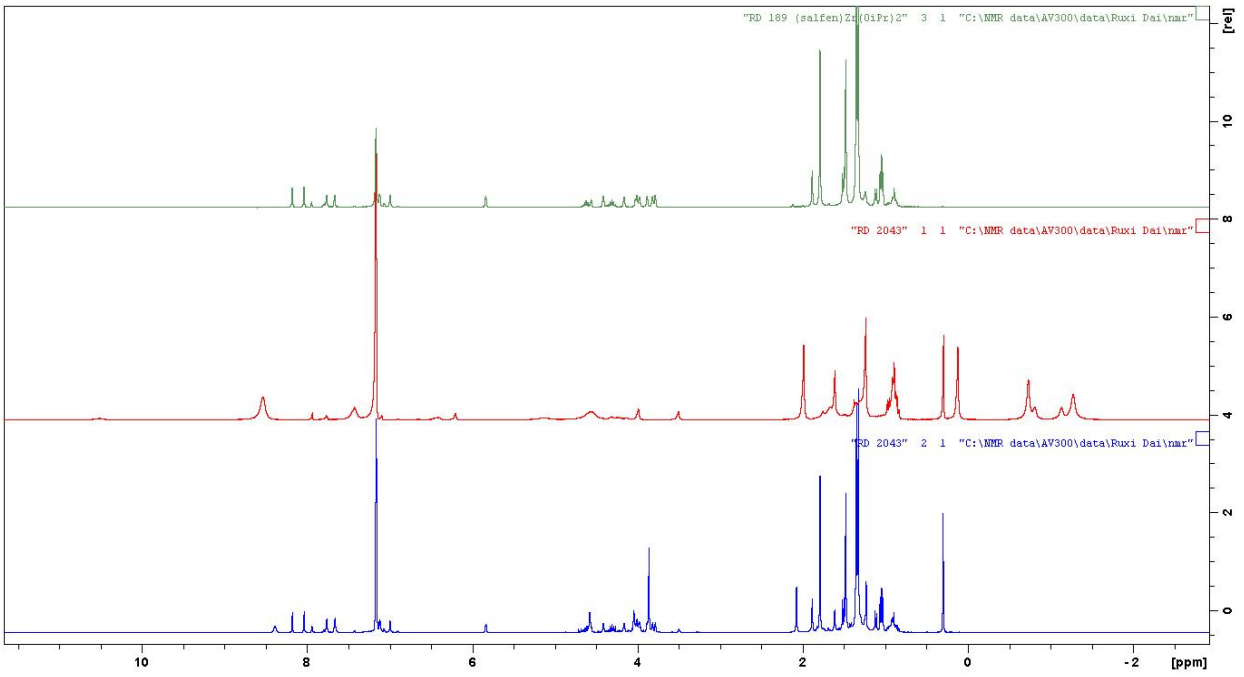

Figure 3.C2. ^{1}H NMR (300 MHz, C_6D_6, 25 ^{o}C) spectrum of (salfen)Zr($O^{i}Pr$)$_2$ (top), [(salfen)Zr($O^{i}Pr$)$_2$][BAr^{F}] (middle) and (salfen)Zr($O^{i}Pr$)$_2$ (reduced back, bottom). All the peaks in top spectrum could be found in bottom spectrum. The extra peaks in the bottom spectrum are residues of the oxidant $^{Ac}FcBAr^{F}$ and reductant $CoCp_2$.

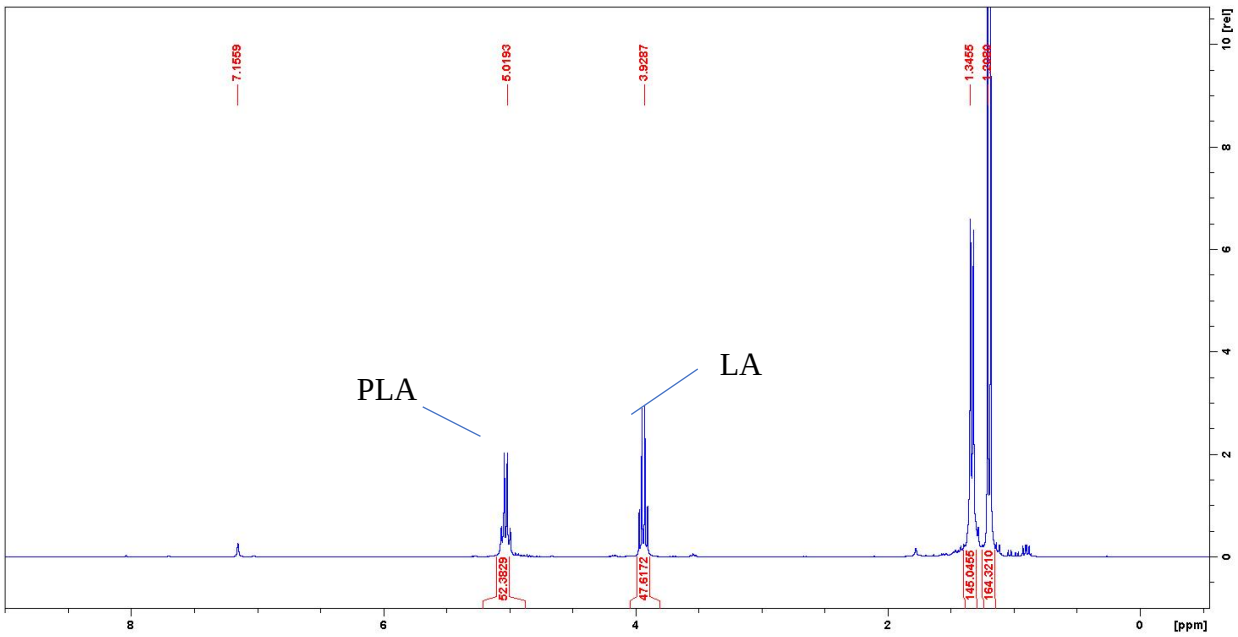

Figure 3.C3. ^{1}H NMR (300 MHz, C_6D_6, 25 ^{o}C) spectrum of 100 equivalents of LA polymerization by (salfen)Zr($O^{i}Pr$)$_2$ (Table 3.1 entry 1). δ, ppm: 5.02 (t, 1H, C*H*(CH_3)COO, PLA), 3.91 (t, 1H, C*H*(CH_3)COO, LA), 1.34 (d, 3H, CH(C*H*$_3$)COO, PLA), 1.21 (d, 3H, CH(C*H*$_3$)COO, LA).

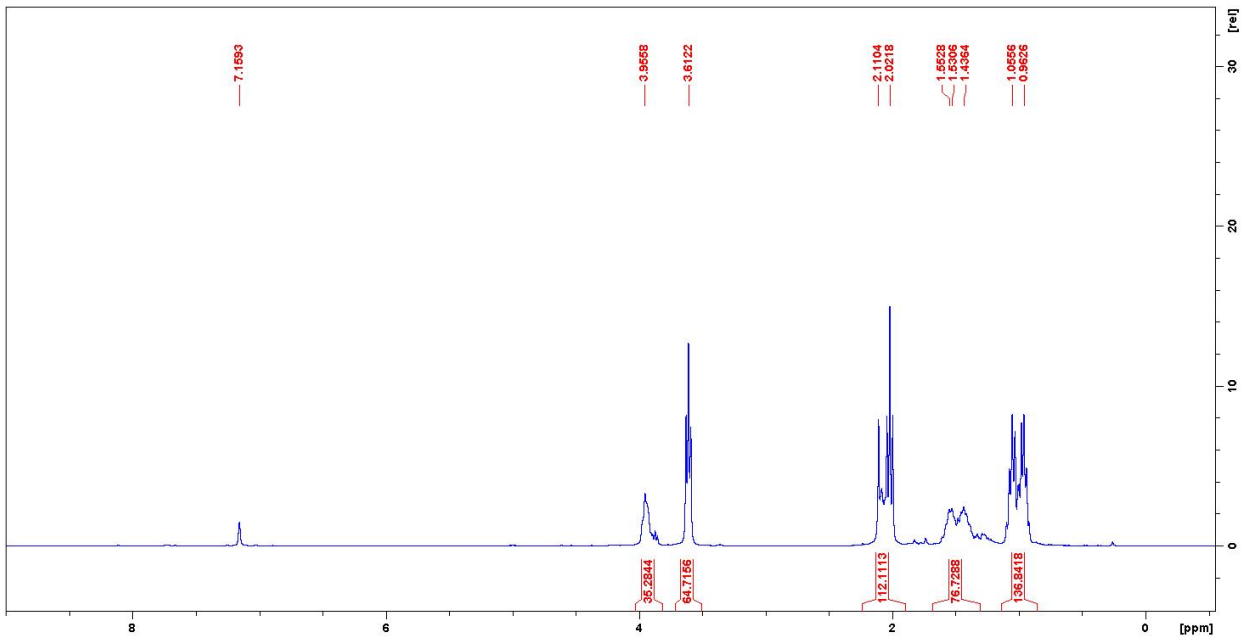

Figure 3.C4. ^{1}H NMR (300 MHz, C_6D_6, 25 ^{o}C) spectrum of 100 equivalents of VL polymerization by (salfen)Zr($O^{i}Pr$)$_2$ (Table 3.1 entry 3). δ, ppm: 3.96 (br, 2H, C*H*$_2$COO, PVL), 3.61 (t, 2H, C*H*$_2$COO, VL), 2.11 (m, 2H, C*H*$_2$CH$_2$COO, VL), 2.02 (m, 2H, COOC*H*$_2$CH$_2$, VL) , 1.55 (br, 2H, C*H*$_2$CH$_2$COO, PVL), 1.43 br, 2H, COOC*H*$_2$CH$_2$, PVL), 1.06 (m, 2H, COOCH$_2$C*H*$_2$, VL), 0.96 (m, 2H, COOCH$_2$C*H*$_2$, PVL).

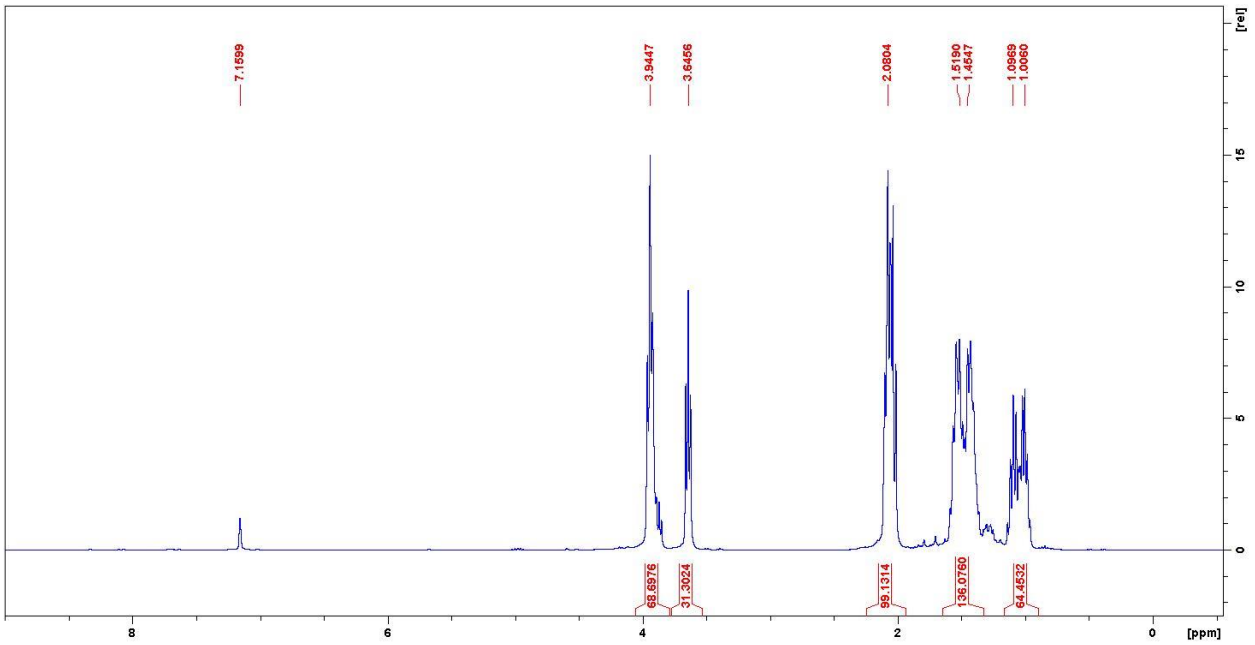

Figure 3.C5. ^{1}H NMR (300 MHz, C_6D_6, 25 ^{o}C) spectrum of 250 equivalents of VL polymerization by (salfen)Zr($O^{i}Pr$)$_2$ (Table 3.1 entry 4). δ, ppm: 3.94 (br, 2H, C*H*$_2$COO, PVL), 3.65 (t, 2H, C*H*$_2$COO, VL), 2.08 (m, 2H, C*H*$_2$CH$_2$COO, VL), 1.52 (br, 2H, C*H*$_2$CH$_2$COO, PVL), 1.45(br, 2H, COOC*H*$_2$CH$_2$, PVL), 1.10 (m, 2H, COOCH$_2$C*H*$_2$, VL), 1.01 (m, 2H, COOCH$_2$C*H*$_2$, PVL).

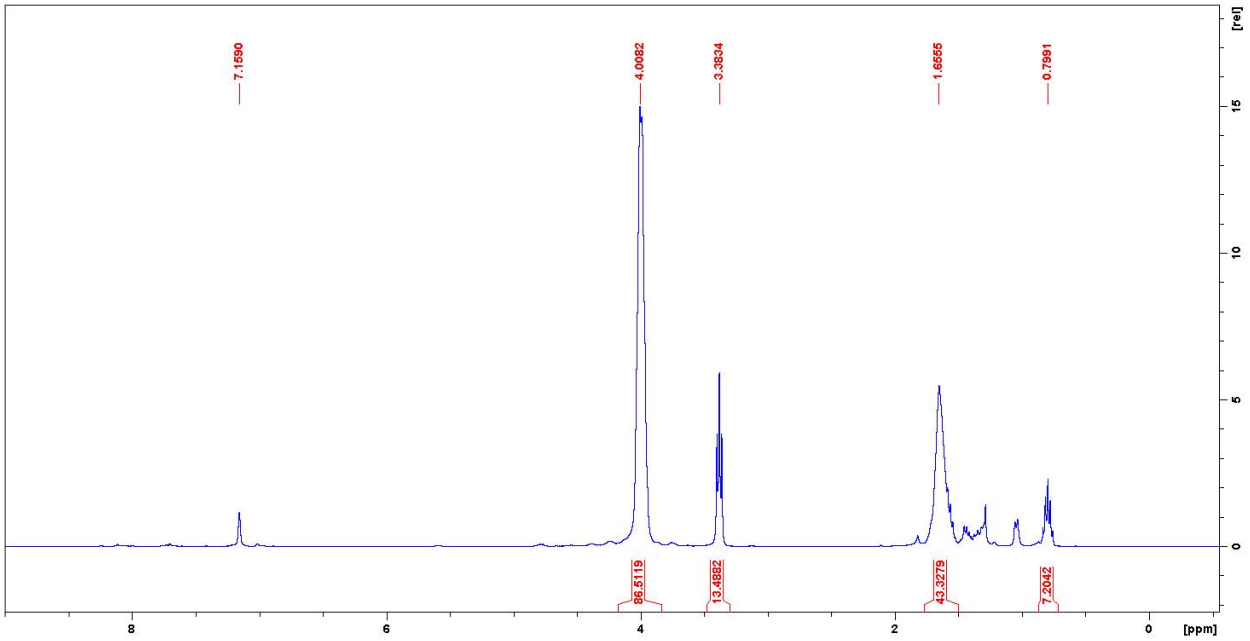

Figure 3.C6. ^{1}H NMR (300 MHz, C_6D_6, 25 ^{o}C) spectrum of 100 equivalents of TMC polymerization by (salfen)Zr($O^{i}Pr$)$_2$ (Table 3.1 entry 5). δ, ppm: 4.01 (s, 4H, OC*H*$_2$CH$_2$C*H*$_2$O, PTMC), 3.38 (t, 4H, OC*H*$_2$CH$_2$C*H*$_2$O, TMC), 1.66 (br, 2H, OCH$_2$C*H*$_2$CH$_2$O, PTMC), 0.80 (m, 2H, OCH$_2$C*H*$_2$CH$_2$O, TMC).

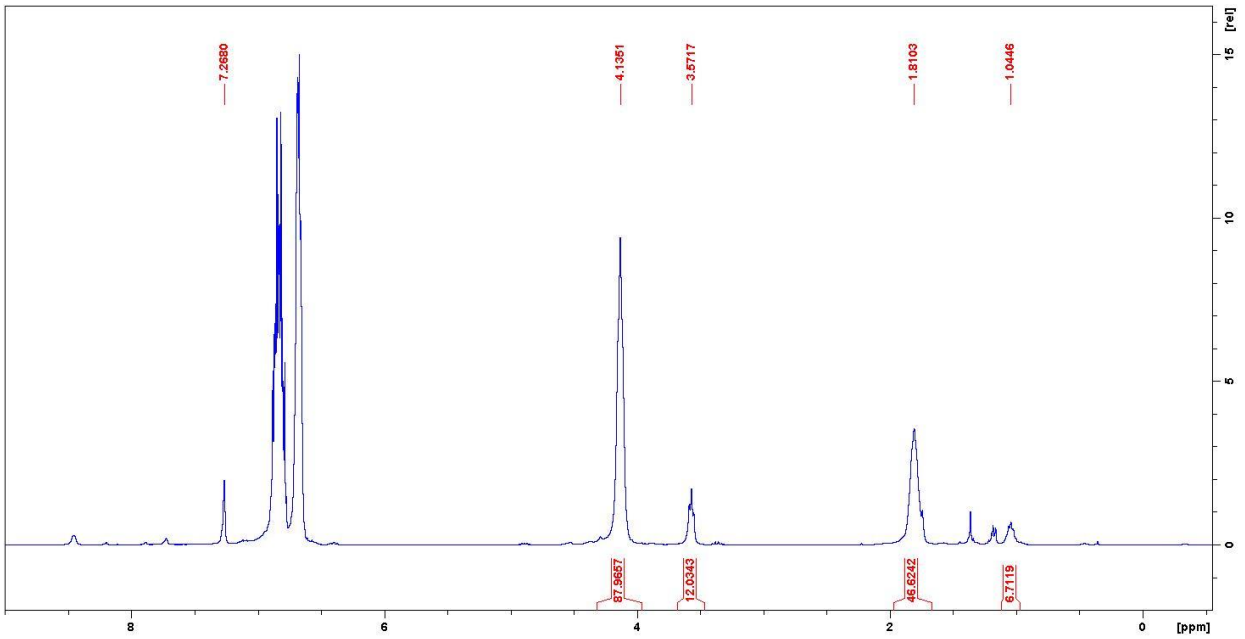

Figure 3.C7. ^{1}H NMR (300 MHz, C_6D_6, 25 ^{o}C) spectrum of 100 equivalents of TMC polymerization by *in situ* generated [(salfen)Zr($O^{i}Pr$)$_2$][BAr^{F}] (Table 3.1 entry 6). δ, ppm: 4.14 (s, 4H, OC*H*$_2$CH$_2$C*H*$_2$O, PTMC), 3.57 (t, 4H, OC*H*$_2$CH$_2$C*H*$_2$O, TMC), 1.81 (br, 2H, OCH$_2$C*H*$_2$CH$_2$O, PTMC), 1.04 (m, 2H, OCH$_2$C*H*$_2$CH$_2$O, TMC).

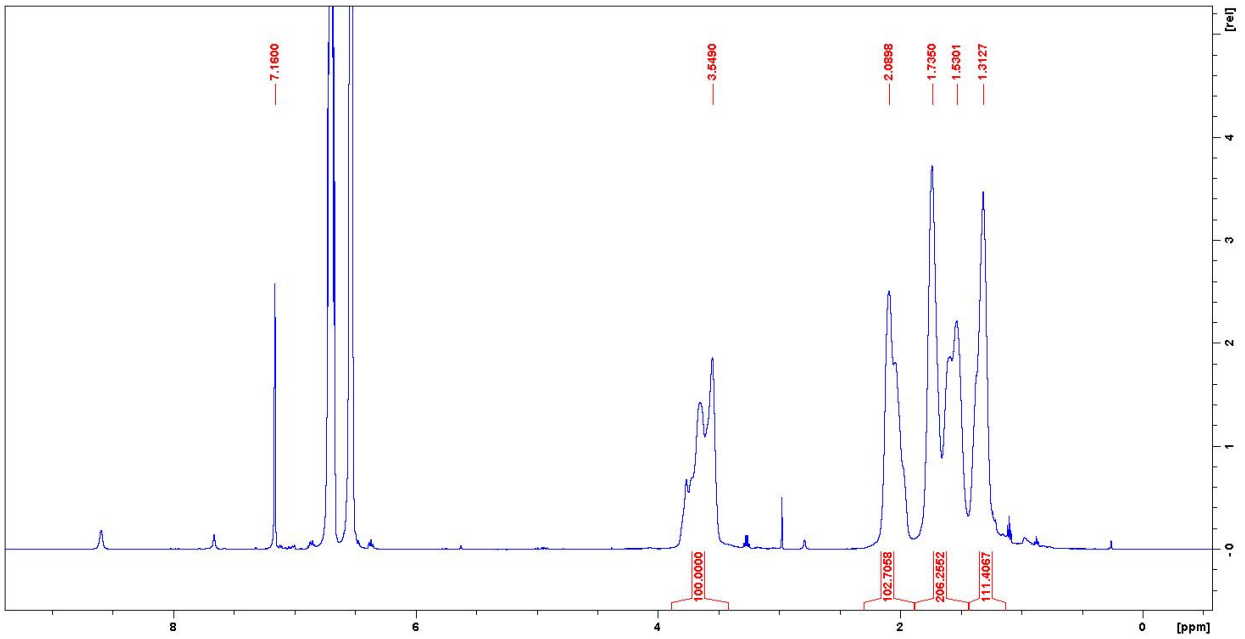

Figure 3.C8. ^{1}H NMR (300 MHz, C_6D_6, 25 ^{o}C) spectrum of 100 equivalents of CHO polymerization by *in situ* generated [(salfen)Zr($O^{i}Pr$)$_2$][BAr^{F}] (Table 3.1 entry 12). δ, ppm: 3.55 (br, 2H, CH_2CH_2CH(O), PCHO), 2.09 (br, 2H, CH_2CH_2CH(O), PCHO), 1.74 (br, 2H, CH_2CH_2CH(O), PCHO), 1.53 (br, 2H, CH_2CH_2CH(O), PCHO), 1.31 (br, 2H, CH_2CH_2CH(O), PCHO).

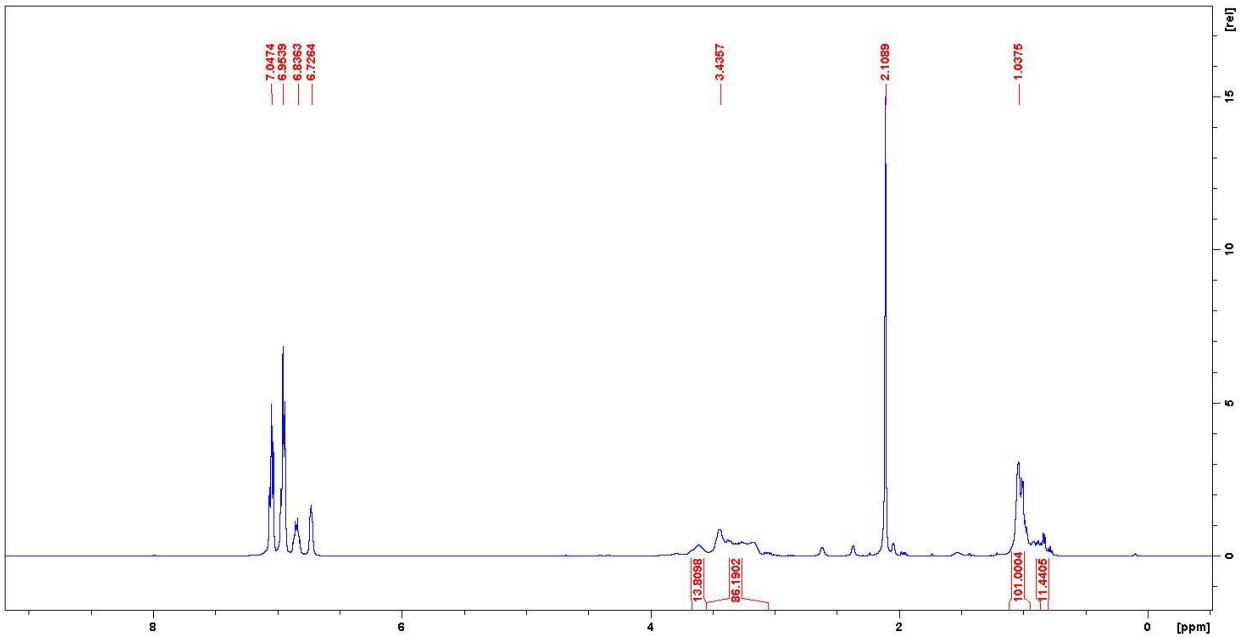

Figure 3.C9. ^{1}H NMR (300 MHz, C_6D_6, 25 ^{o}C) spectrum of 1000 equivalents of PO polymerization by *in situ* generated [(salfen)Zr($O^{i}Pr$)$_2$][BAr^{F}] (Table 3.1 entry 14). δ, ppm: 7.05 (m, 2H, *m*-C_6H_4, difluorobenzene), 6.95 (m, 2H, *m*-C_6H_4, difluorobenzene), 6.84 (br, 2H, CH_3-C_6H_5, toluene), 6.73 (br, 3H, CH_3-C_6H_5, toluene),3.44 (br, 3H, OC*H*(CH_3)C*H*$_2$O, PPO), 2.11 (s, 3H, C*H*$_3$-C_6H_5, toluene), 1.04 (br, 3H, OCH(C*H*$_3$)CH_2O, PPO).

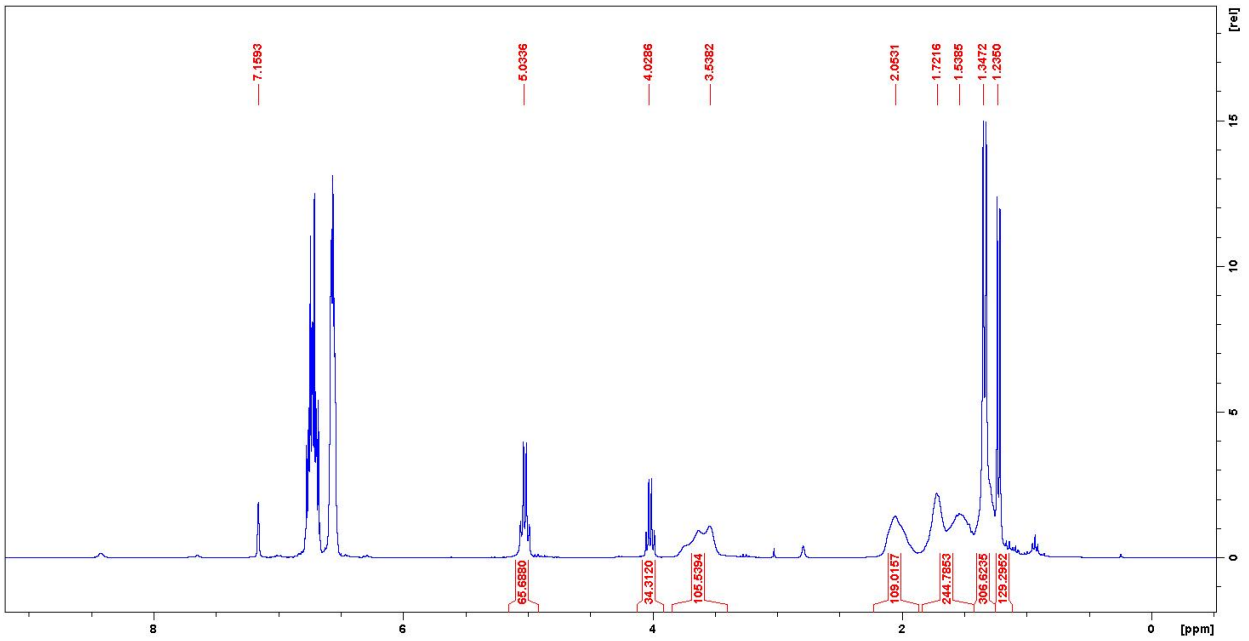

Figure 3.C10. ^{1}H NMR (300 MHz, C_6D_6, 25 ^{o}C) spectrum of PLA-PCHO copolymerization (Table 3.2 entry 1). δ, ppm: 5.03 (t, 1H, C*H*(CH_3)COO, PLA), 4.03 (t, 1H, C*H*(CH_3)COO, LA), 1.35 (d, 3H, CH(C*H*$_3$)COO, PLA), 1.24 (d, 3H, CH(C*H*$_3$)COO, LA), 3.54 (br, 2H, CH_2CH_2CH(O), PCHO), 2.05 (br, 2H, CH_2CH_2CH(O), PCHO), 1.72 (br, 2H, CH_2CH_2CH(O), PCHO), 1.54 (br, 2H, CH_2CH_2CH(O), PCHO).

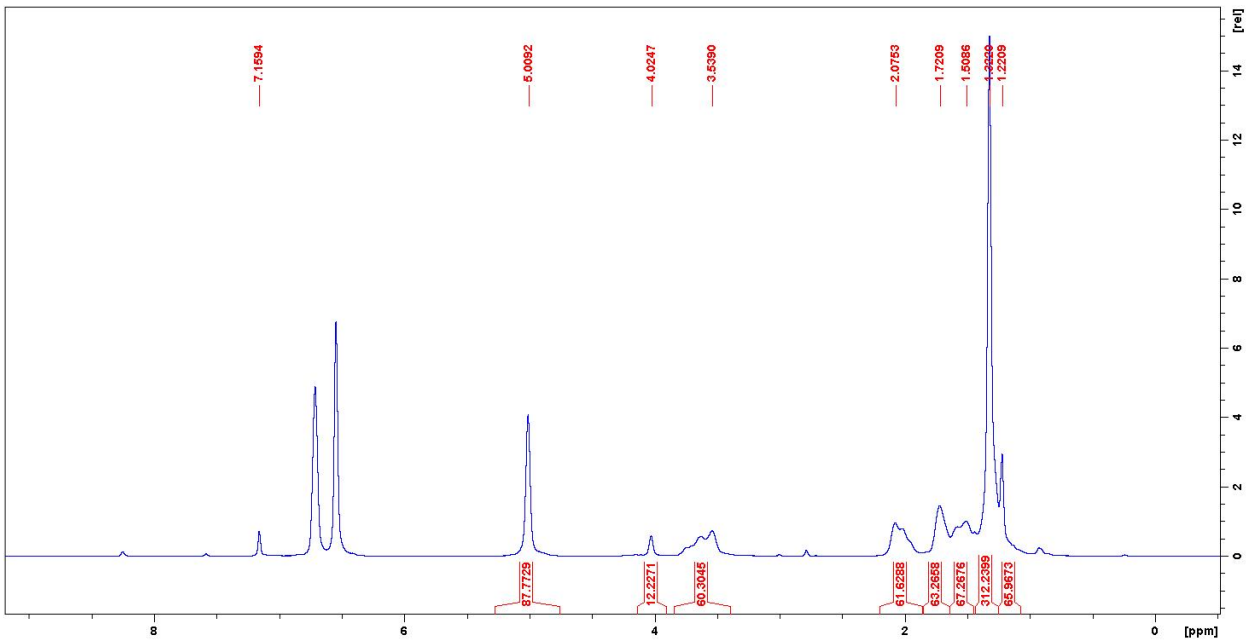

Figure 3.C11. ^{1}H NMR (300 MHz, C_6D_6, 25 ^{o}C) spectrum of PLA-PCHO-PLA copolymerization (Table 3.2 entry 2). δ, ppm: 5.04 (t, 1H, C*H*(CH_3)COO, PLA), 4.10 (t, 1H, C*H*(CH_3)COO, LA), 1.33 (d, 3H, CH(C*H*$_3$)COO, PLA), 1.25 (d, 3H, CH(C*H*$_3$)COO, LA), 3.54 (br, 2H, CH_2CH_2CH(O), PCHO), 2.05 (br, 2H, CH_2CH_2CH(O), PCHO), 1.71 (br, 2H, CH_2CH_2CH(O), PCHO).

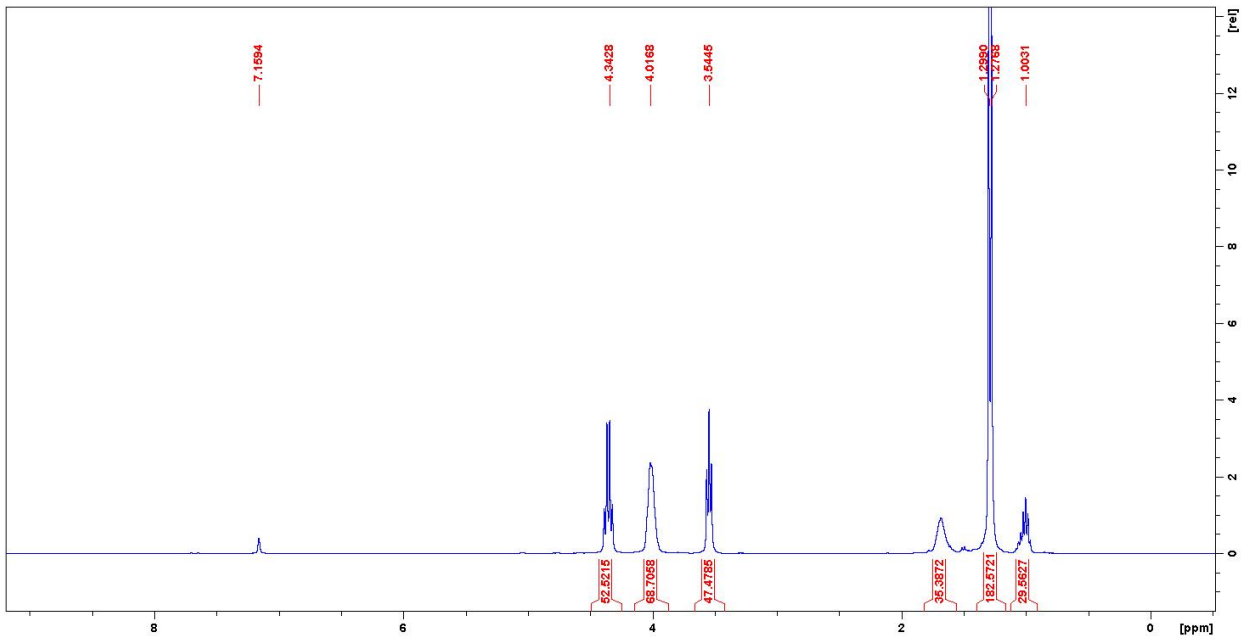

Figure 3.C12. ^{1}H NMR (300 MHz, C_6D_6, 25 ^{o}C) spectrum of PTMC-PLA copolymerization (Table 3.1 entry 3). δ, ppm: 4.34 (t, 1H, C*H*(CH_3)COO, PLA), 3.54 (t, 1H, C*H*(CH_3)COO, LA), 1.30 (d, 3H, CH(C*H*$_3$)COO, PLA), 1.28 (d, 3H, CH(C*H*$_3$)COO, LA), 4.02 (s, 4H, OC*H*$_2$CH$_2$C*H*$_2$O, PTMC), 3.54 (t, 4H, OC*H*$_2$CH$_2$C*H*$_2$O, TMC), 1.68 (br, 2H, OCH$_2$C*H*$_2$CH$_2$O, PTMC), 1.00 (m, 2H, OCH$_2$C*H*$_2$CH$_2$O, TMC).

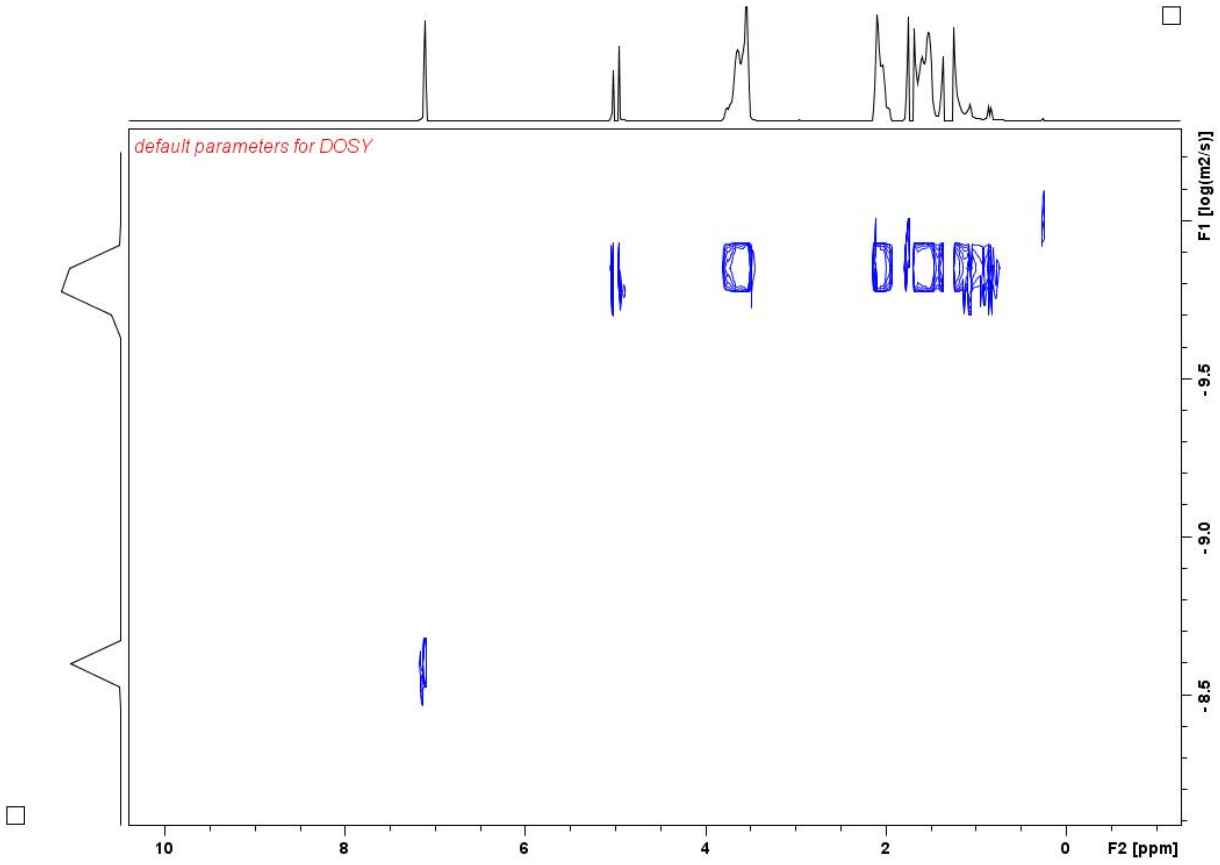

Figure 3.C13. DOSY NMR for PLA-PCHO copolymer (Table 3.2 entry 1).

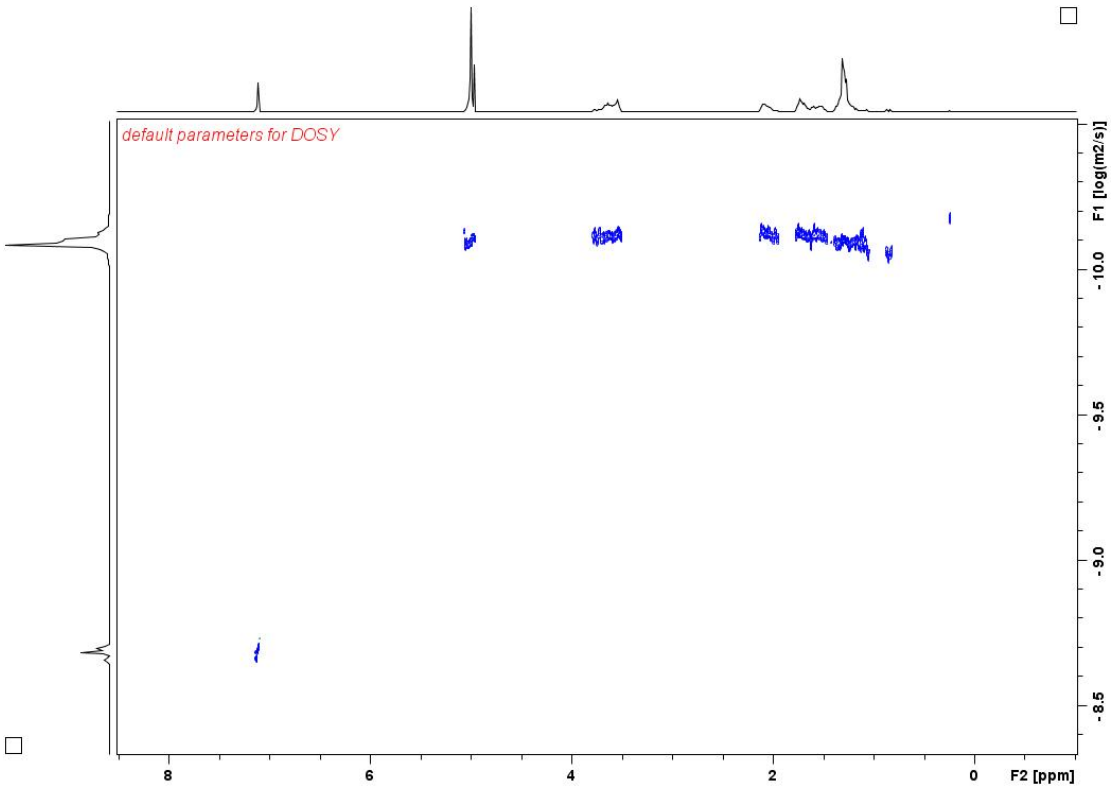

Figure 3.C14. DOSY NMR for PLA-PCHO-PLA copolymer (Table 3.2 entry 2).

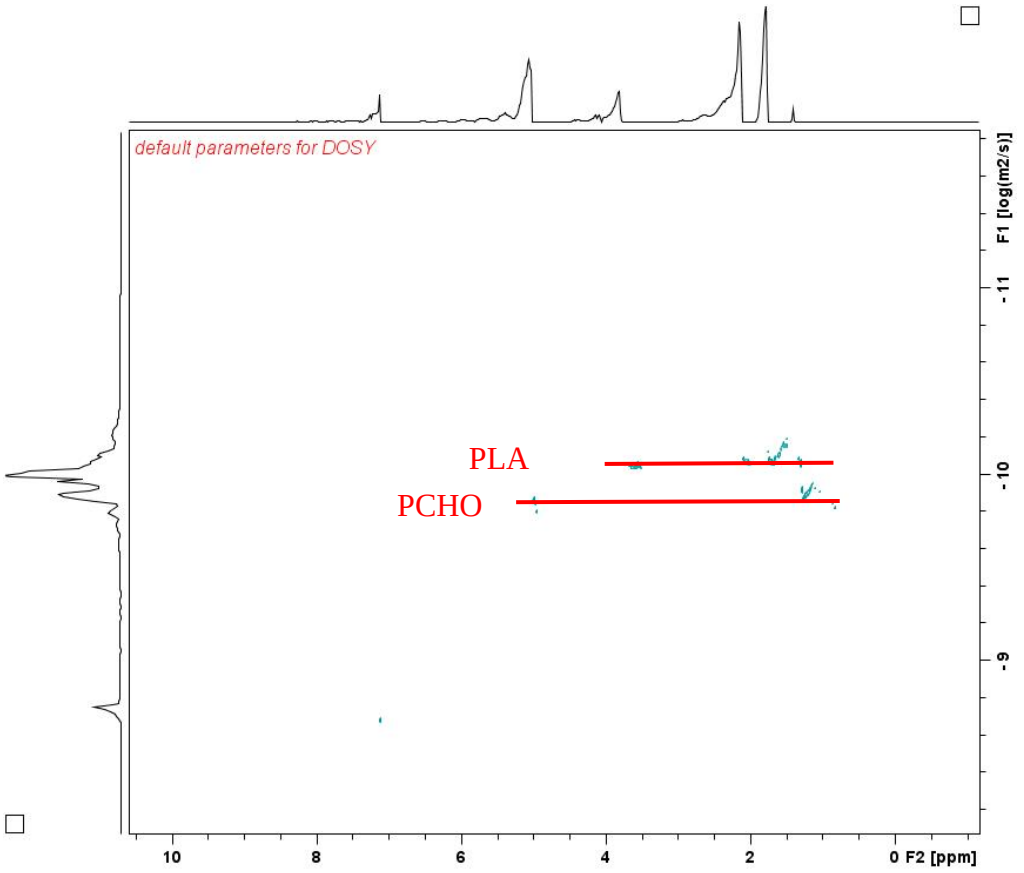

Figure 3.C15. DOSY NMR for a mixture of PLA and PCHO homopolymers.

Table 3.C1. Homopolymerizations by [(salfen)Zr(O^iPr)$_2$] or [(salfen)Zr(O^iPr)$_2$][BAr^F].[a]

Entry	Monomer[b]	catalyst oxidation state	Equiv. monomer	Time (h)	Temp. (°C)	Conv. (%)	Exp. Mw (10^3 g/mol)	Calcd. Mw (10^3 g/mol)	Đ
1	LA	red	100	24	100	71	6.4	5.5	1.02
2		ox	100	24	25	<3	--	--	--
3	VL	red	100	24	100	39	--	--	--
4		red	250	24	100	64	10.8	8.7	1.13
5		ox	100	14	25	<3	--	--	--
6	TMC	red	100	24	100	92	10.0	9.4	1.29
7		ox	100	24	25	88	8.7	9.0	1.13
8	PC	red	100	24	100	<3	--	--	--
9		ox	100	24	25	<3	--	--	--
10	BL	red	100	24	100	<3	--	--	--
11		ox	100	24	25	<3	--	--	--
12	CHO	red	100	24	100	<3	--	--	--
13		ox	100	0.1	25	100	22	5.0	1.23
14	PO	red	100	24	100	<3	--	--	--
15		ox	100	24	25	51	--	--	--
16		ox	1000	24	25	88	1.8	30	1.62

[a] All polymerization reactions were done with 4 μmol precatalysts, 0.6 mL of C_6D_6 as a solvent and hexamethylbenzene as an internal standard. [b]VL stands for δ-valerolactone, TMC stands for 1,3-trimethylene carbonate, BL stands for β-butyrolactone, PC stands for propylene carbonate and PO stands for propylene oxide.

Table 3.C2. Redox-controlled copolymerizations.[a]

Entry	Monomer 1 (conv. %)	Monomer 2 (conv. %)	Monomer 3 (conv. %)	catalyst oxidation state	Exp. Mw (10^3 g/mol)	Calcd. Mw (10^3 g/mol)	Đ
1	LA (70 %)	CHO (100 %)	--	red-ox	14.0	9.8	1.37
2	LA (66 %)	CHO (100 %)	LA (88%, overall)	red-ox-red	1.72	1.69	1.55
3	TMC (60 %)	LA (87 %)	--	red-red	14.7	12.4	1.09
4	LA (70 %)	TMC (0 %)	--	red-red	--	--	--
5	LA (70 %)	TMC (0 %)	--	red-ox	--	--	--

[a] All polymerization reactions were done with 4 µmol precatalysts, 0.6 mL of C_6D_6 as the solvent and hexamethylbenzene as an internal standard. 100 equivalents of monomer was used unless otherwise mentioned. All reactions with $[Zr]^{red}$ were done at 100 ^oC and all reactions with $[Zr]^{ox}$ were done at 25 ^oC.

SEC

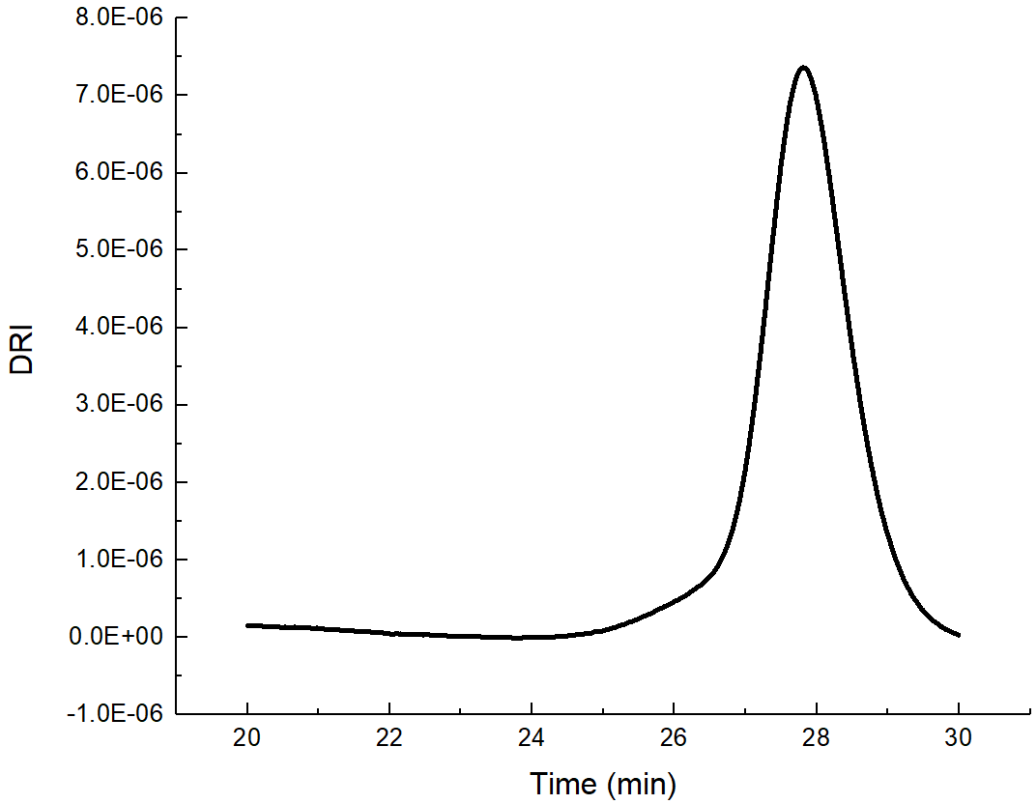

Figure 3.C16. SEC trace for the reaction between 100 equivalents of LA and (salfen)Zr(O^iPr)$_2$ (Table 3.1, entry 1).

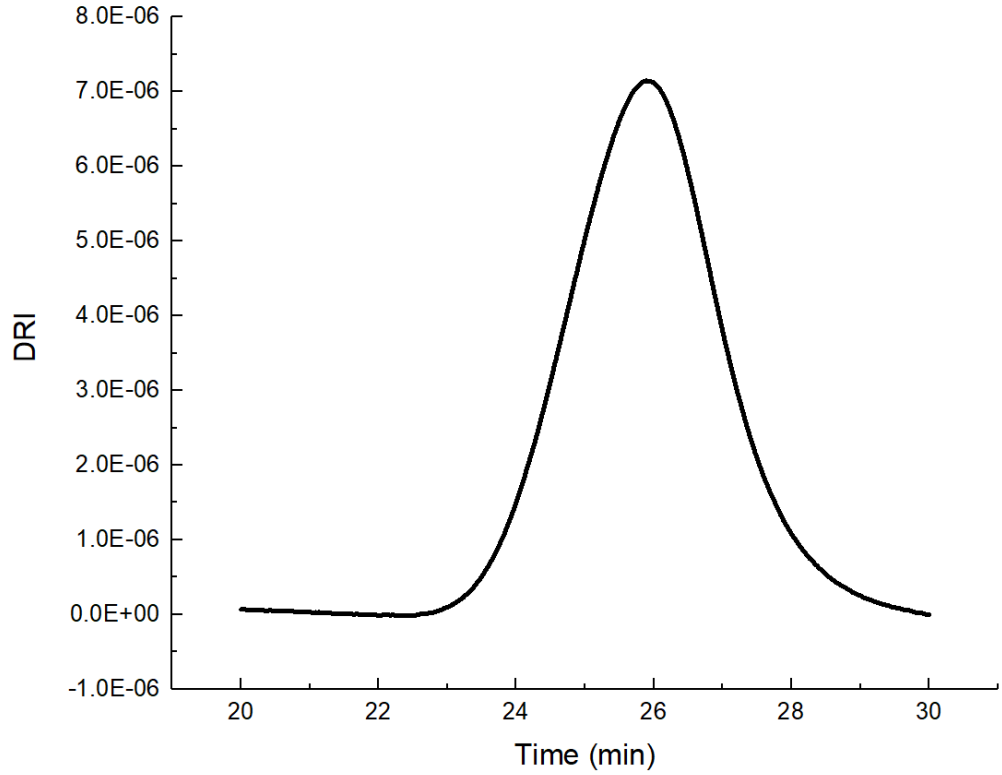

Figure 3.C17. SEC trace for the reaction between 250 equivalents of VL and (salfen)Zr(O^iPr)$_2$ (Table 3.1, entry 4).

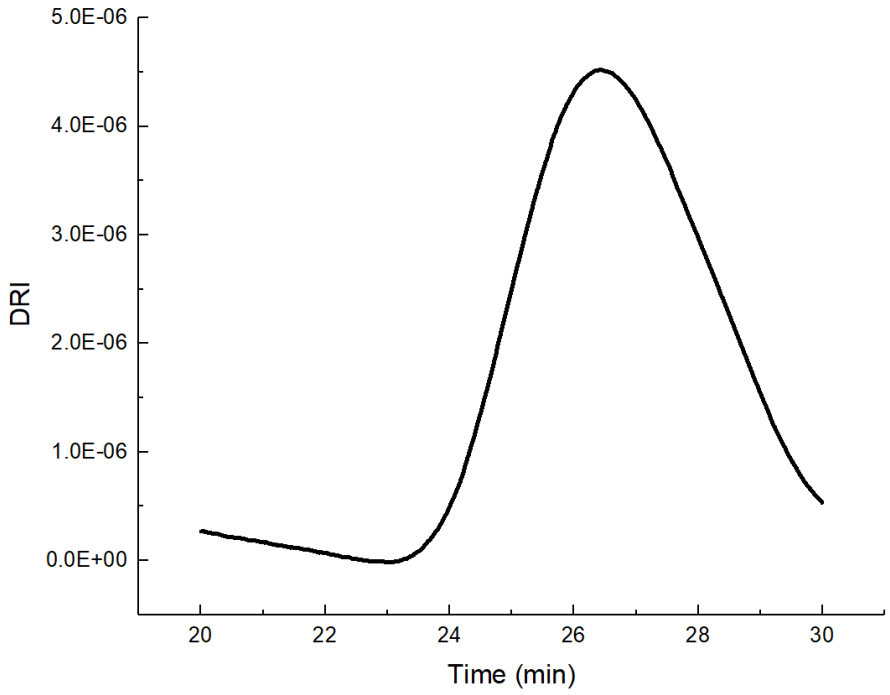

Figure 3.C18. SEC trace for the reaction between 100 equivalents of TMC and (salfen)Zr(O^iPr)$_2$ (Table 3.1, entry 5).

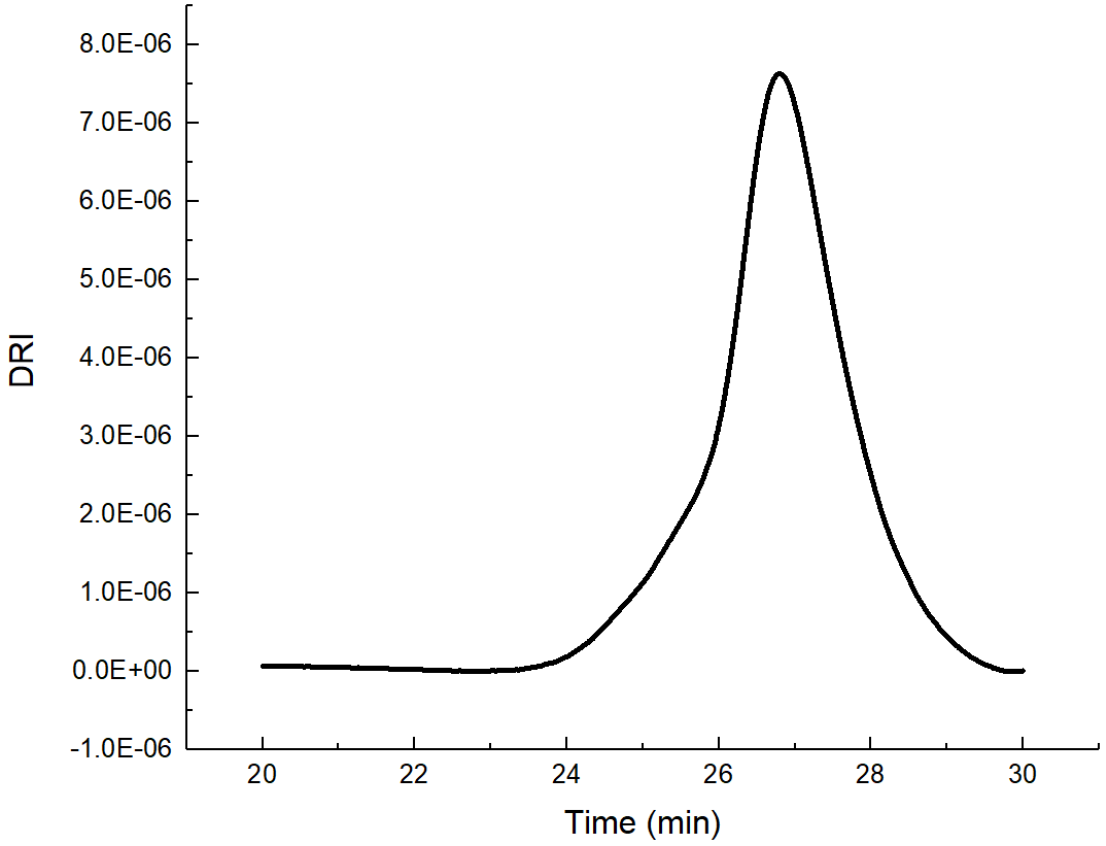

Figure 3.C19. SEC trace for the reaction between of 100 equivalents of TMC and in situ generated [(salfen)Zr(O^iPr)$_2$][BAr^F] (Table 3.1, entry 6).

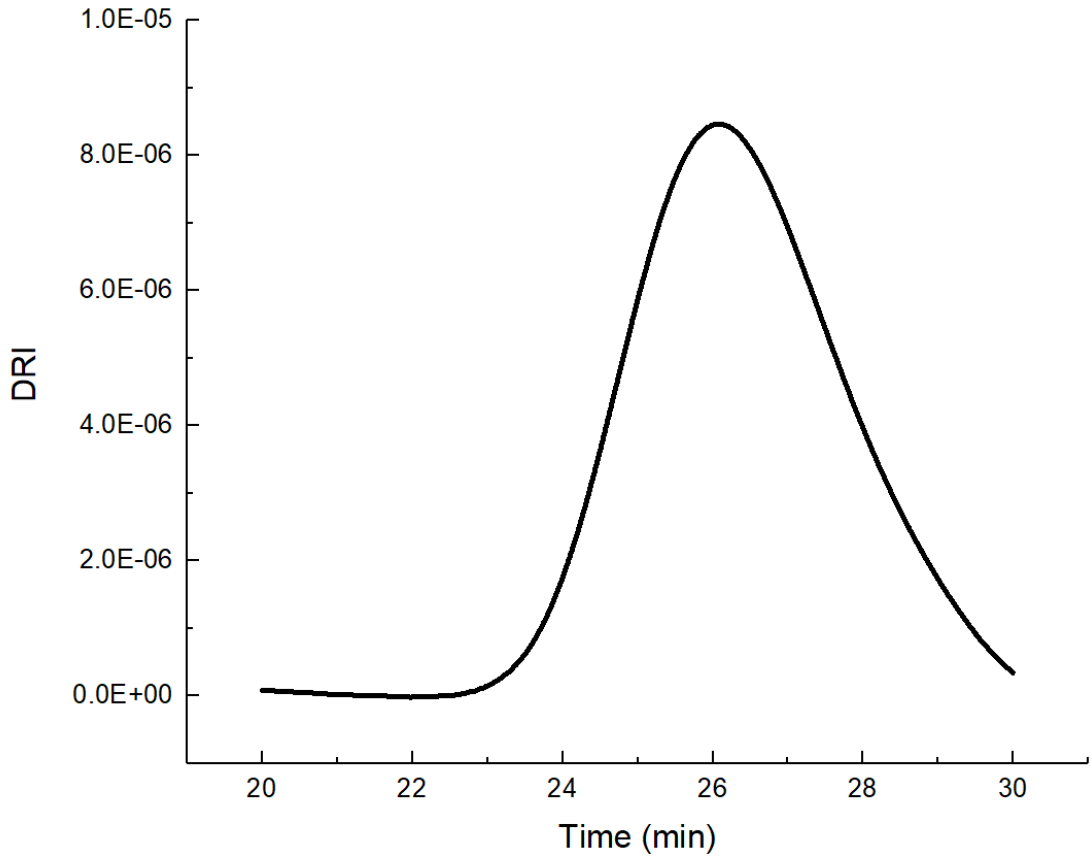

Figure 3.C20. SEC trace for the reaction between 100 equivalents of CHO and in situ generated [(salfen)Zr(O^iPr)$_2$][BAr^F] (Table 3.1, entry 12).

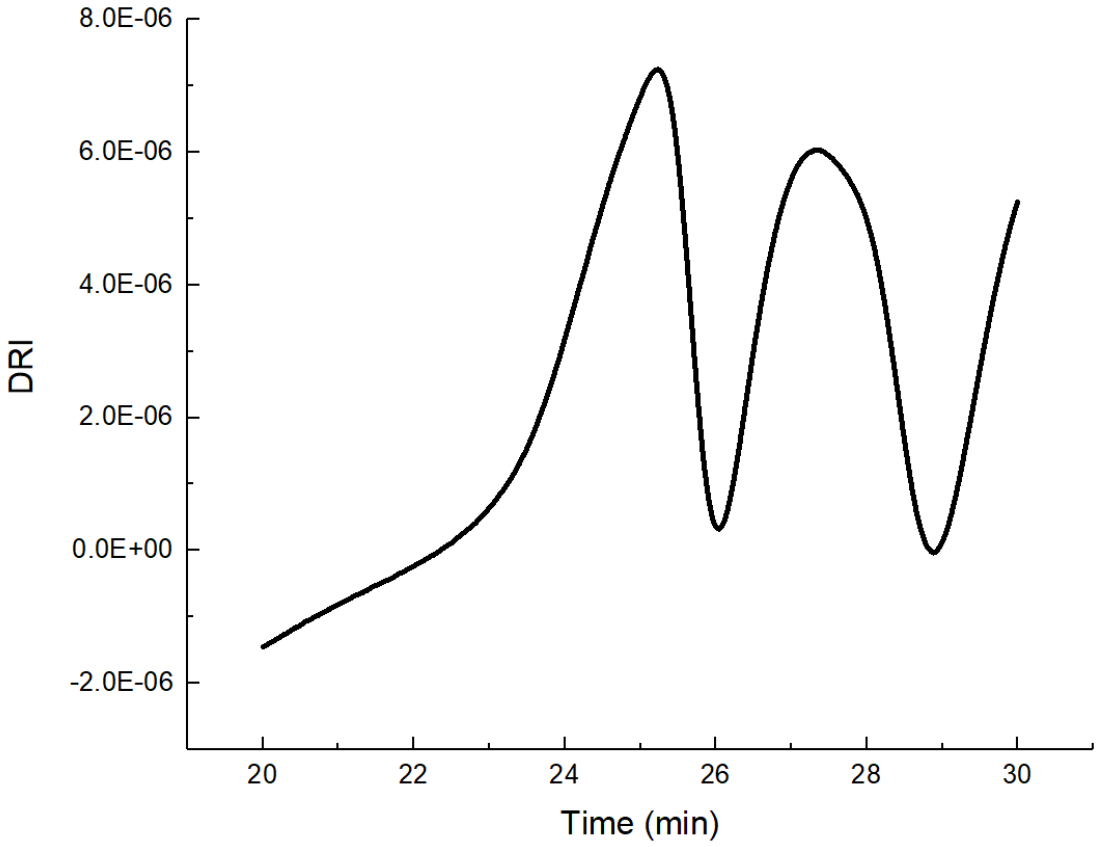

Figure 3.C21. SEC trace for the reaction between 1000 equivalents of PO and in situ generated [(salfen)Zr(O^iPr)$_2$][BAr^F] (Table 3.1, entry 14).

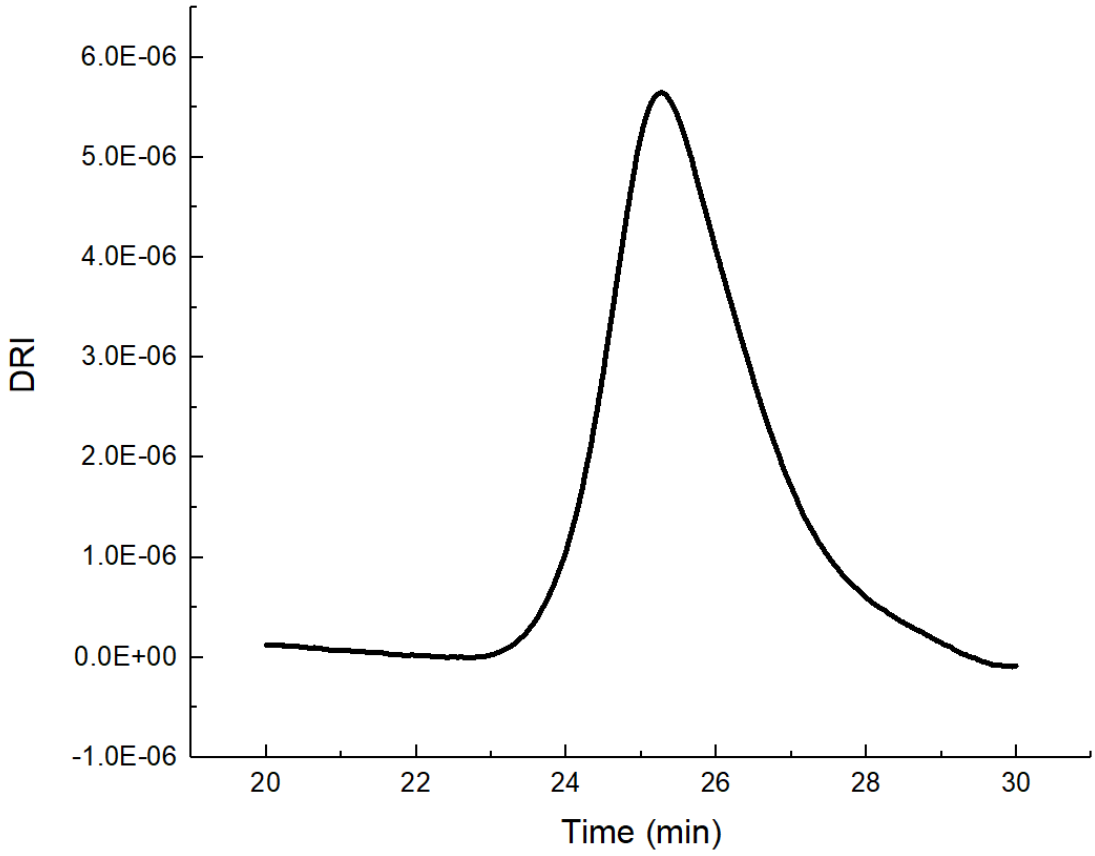

Figure 3.C22. SEC trace for the PTMC-PLA copolymer by (salfen)Zr(O^iPr)$_2$ (Table 3.2, entry 3).

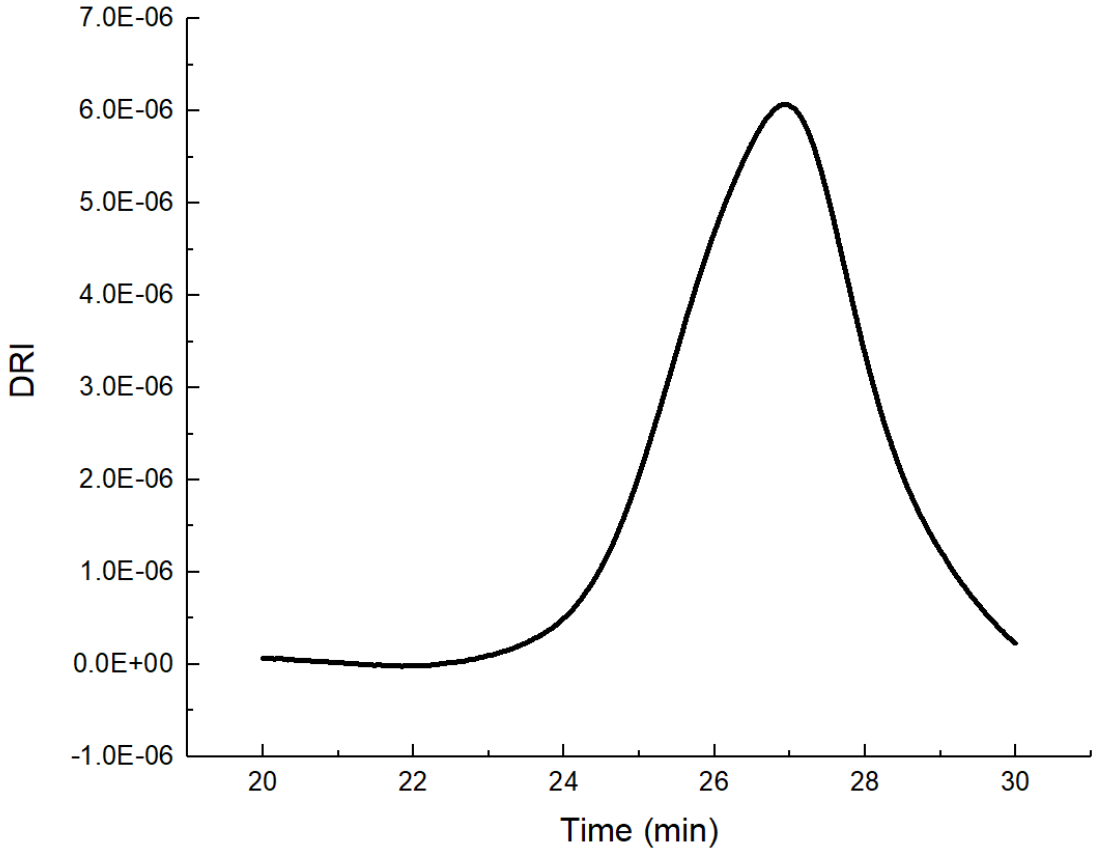

Figure 3.C23. SEC trace for the PLA-PCHO copolymers (Table 3.2, entry 1).

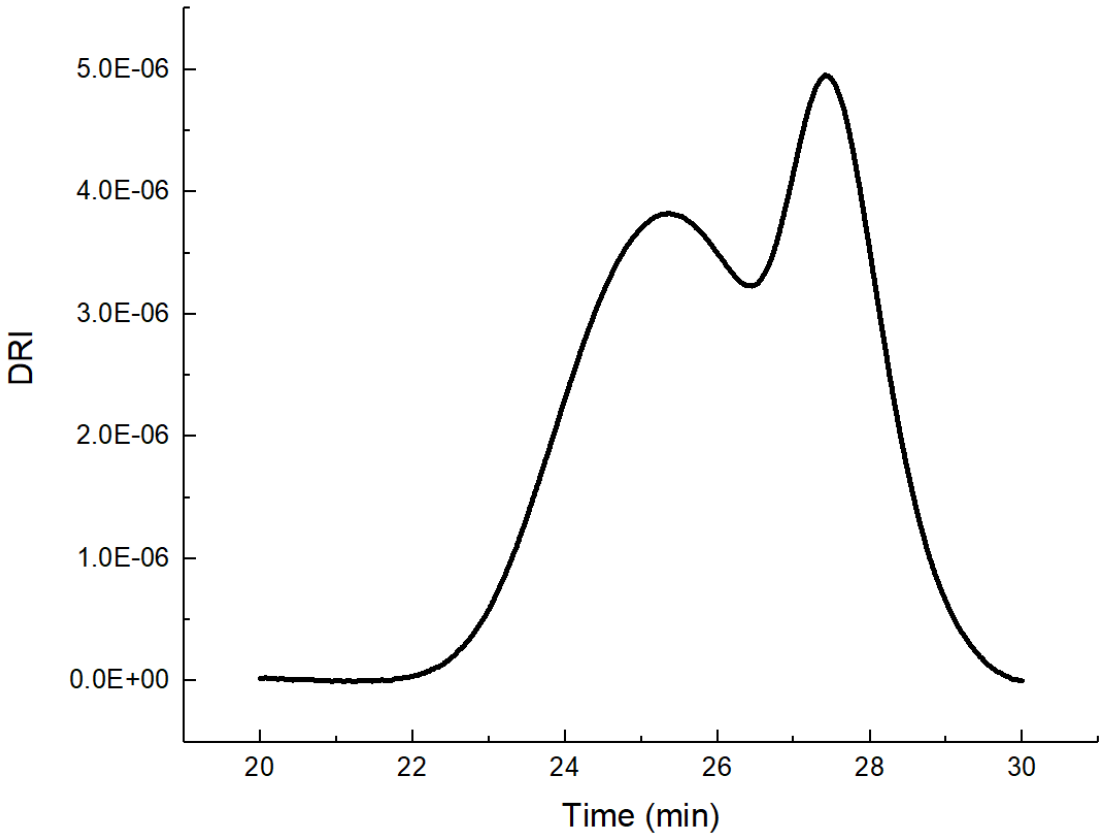

Figure 3.C24. SEC trace for a mixture of PLA homopolymers and PCHO homopolymers.

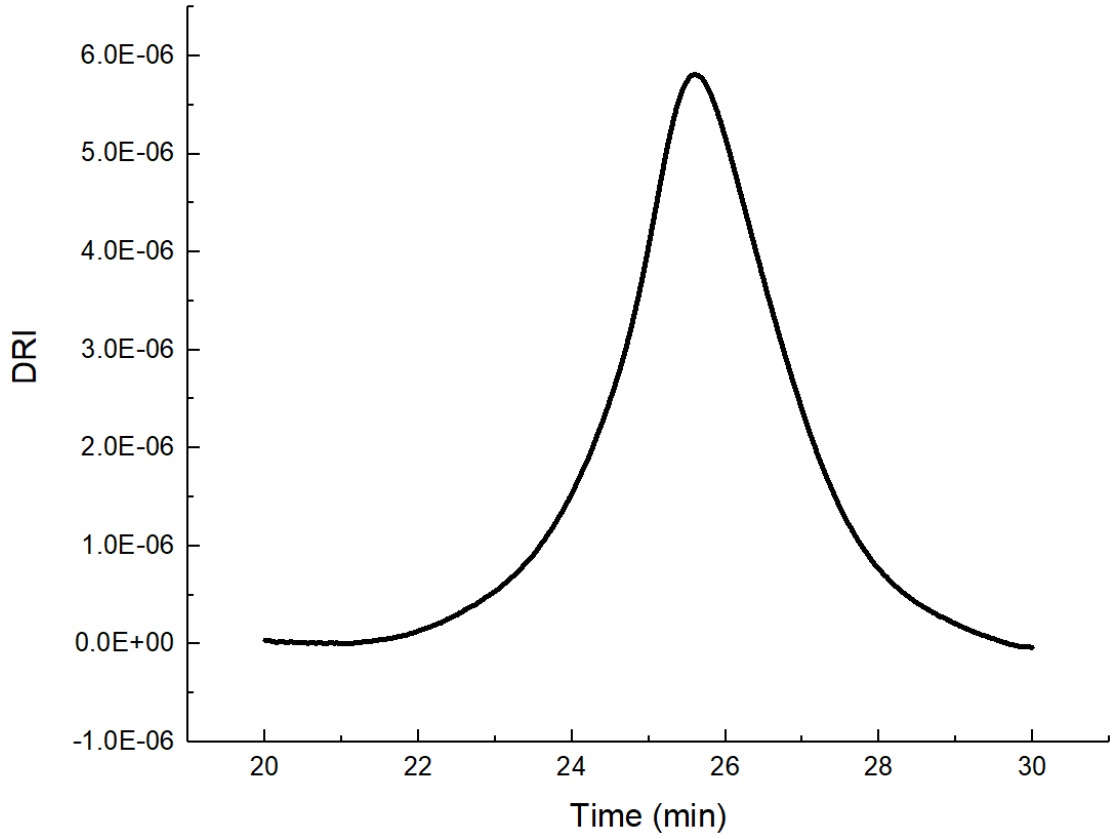

Figure 3.C25. SEC trace for the PLA-PCHO-PLA triblock copolymer (Table 3.2, entry 2).

Polymerization Kinetics Study: Mn vs Conversion

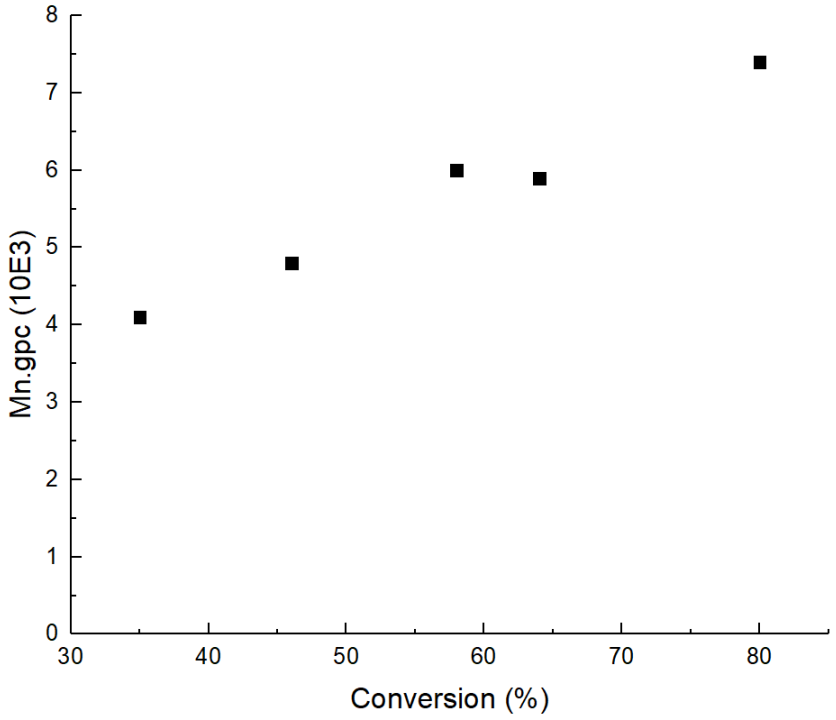

Figure 3.C26. Mn vs conversion plot for LA polymerization by (salfen)Zr(O^iPr)$_2$.

Table 3.C3 Kinetics study: Mn vs conversion for LA polymerization by (salfen)Zr(O^iPr)$_2$.

Entry	Conversion	Exp. Mn (10^3 Da)	Calcd. Mn (10^3 Da)	Đ
1	35%	4.1	3.1	1.06
2	46%	4.8	4.0	1.03
3	58%	6.0	5.0	1.01
4	64%	5.9	5.5	1.03
5	80%	7.4	6.9	1.05

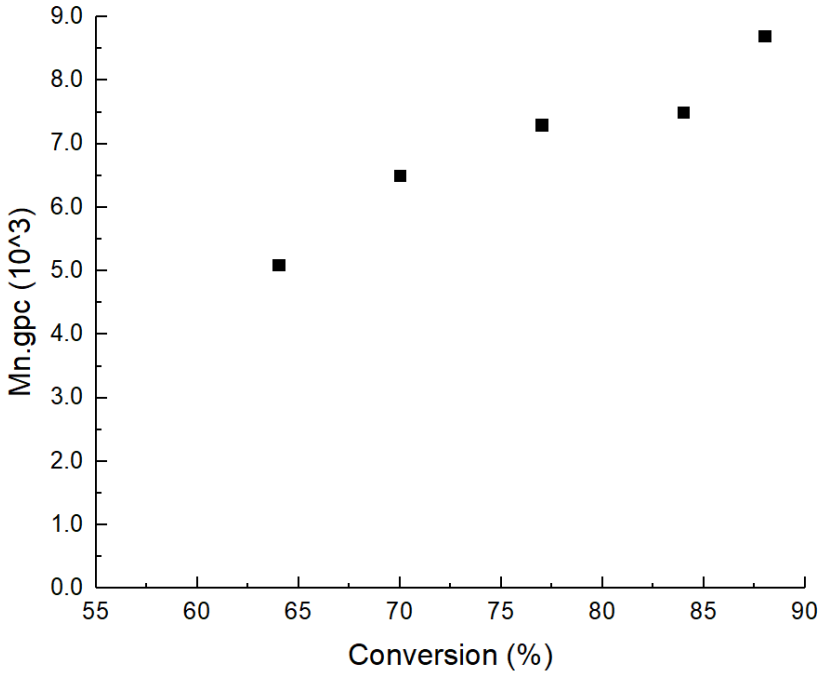

Figure 3.C27. Mn vs conversion plot for TMC polymerization by [(salfen)Zr(O^iPr)$_2$][BAr^F].

Table 3.C4. Kinetics study: Mn vs conversion for TMC polymerization by [(salfen)Zr(O^iPr)$_2$][BAr^F].

Entry	Conversion	Exp. Mn (10^3 Da)	Calcd. Mn (10^3 Da)	Đ
1	64%	5.1	6.5	1.03
2	70%	6.5	7.1	1.09
3	77%	7.3	7.8	1.11
4	84%	7.5	8.4	1.06
5	88%	8.7	9.0	1.13

3.6. References

1. Ruzette, A.-V.; Leibler, L., Block copolymers in tomorrow's plastics. *Nat. Mater.* **2005,** *4*, 19-31.

2. Suriano, F.; Coulembier, O.; Hedrick, J. L.; Dubois, P., Functionalized cyclic carbonates: from synthesis and metal-free catalyzed ring-opening polymerization to applications. *Polym. Chem.* **2011,** *2*, 528-533.

3. Vert, M., Aliphatic Polyesters: Great Degradable Polymers That Cannot Do Everything. *Biomacromolecules* **2005,** *6*, 538-546.

4. Place, E. S.; George, J. H.; Williams, C. K.; Stevens, M. M., Synthetic polymer scaffolds for tissue engineering. *Chem. Soc. Rev.* **2009,** *38*, 1139-1151.

5. Lebreton, L.; Slat, B.; Ferrari, F.; Sainte-Rose, B.; Aitken, J.; Marthouse, R.; Hajbane, S.; Cunsolo, S.; Schwarz, A.; Levivier, A.; Noble, K.; Debeljak, P.; Maral, H.; Schoeneich-Argent, R.; Brambini, R.; Reisser, J., Evidence that the Great Pacific Garbage Patch is rapidly accumulating plastic. *Sci. Rep.* **2018,** *8*, 4666.

6. Romera-Castillo, C.; Pinto, M.; Langer, T. M.; Álvarez-Salgado, X. A.; Herndl, G. J., Dissolved organic carbon leaching from plastics stimulates microbial activity in the ocean. *Nat. Commun.* **2018,** *9*, 1430.

7. Lebreton, L. C. M.; van der Zwet, J.; Damsteeg, J.-W.; Slat, B.; Andrady, A.; Reisser, J., River plastic emissions to the world's oceans. *Nat. Commun.* **2017,** *8*, 15611.

8. Galloway, T. S.; Cole, M.; Lewis, C., Interactions of microplastic debris throughout the marine ecosystem. *Nat. Ecol. Evol.* **2017,** *1*, 0116.

9. Chen, G.-Q.; Patel, M. K., Plastics Derived from Biological Sources: Present and Future: A Technical and Environmental Review. *Chem. Rev.* **2012,** *112*, 2082-2099.

10. Dechy-Cabaret, O.; Martin-Vaca, B.; Bourissou, D., Controlled Ring-Opening Polymerization of Lactide and Glycolide. *Chem. Rev.* **2004,** *104*, 6147-6176.

11. Nair, L. S.; Laurencin, C. T., Biodegradable polymers as biomaterials. *Prog. Polym. Sci.* **2007,** *32*, 762-798.

12. Zhu, Y.; Romain, C.; Williams, C. K., Sustainable polymers from renewable resources. *Nature* **2016,** *540*, 354-362.

13. Hillmyer, M. A.; Tolman, W. B., Aliphatic Polyester Block Polymers: Renewable, Degradable, and Sustainable. *Acc. Chem. Res.* **2014,** *47*, 2390-2396.

14. Platel, R. H.; Hodgson, L. M.; Williams, C. K., Biocompatible Initiators for Lactide Polymerization. *Polym. Rev.* **2008,** *48*, 11-63.

15. Shogren, R. L.; Doane, W. M.; Garlotta, D.; Lawton, J. W.; Willett, J. L., Biodegradation of starch/polylactic acid/poly(hydroxyester-ether) composite bars in soil. *Polym. Degrad. Stab.* **2003,** *79*, 405-411.

16. Tamboli, V.; Mishra, G. P.; Mitra, A. K., Novel pentablock copolymer (PLA–PCL–PEG–PCL–PLA)-based nanoparticles for controlled drug delivery: effect of copolymer compositions on the crystallinity of copolymers and in vitro drug release profile from nanoparticles. *Colloid Polym. Sci.* **2012,** *291*, 1235-1245.

17. Guillaume, S. M., Recent advances in ring-opening polymerization strategies toward α,ω-hydroxy telechelic polyesters and resulting copolymers. *Eur. Polym. J.* **2013,** *49*, 768-779.

18. Wang, Y.; Hillmyer, M. A., Synthesis of Polybutadiene−Polylactide Diblock Copolymers Using Aluminum Alkoxide Macroinitiators. Kinetics and Mechanism. *Macromolecules* **2000,** *33*, 7395-7403.

19. Jing, R.; Wang, G.; Zhang, Y.; Huang, J., One-Pot Synthesis of PS-b-PEO-b-PtBA Triblock Copolymers via Combination of SET-LRP and "Click" Chemistry Using Copper(0)/PMDETA as Catalyst System. *Macromolecules* **2011,** *44*, 805-810.

20. Chagneux, N.; Camerlynck, S.; Hamilton, E.; Vilela, F. M. L.; Sherrington, D. C., Synthesis of Laterally Linked Poly(tetrahydrofuran)−Poly(methyl methacrylate) Block Copolymers via Use of a "Jekyll and Hyde" Comonomer. *Macromolecules* **2007,** *40*, 3183-3189.

21. Mecerreyes, D.; Moineau, G.; Dubois, P.; Jérôme, R.; Hedrick, J. L.; Hawker, C. J.; Malmström, E. E.; Trollsas, M., Simultaneous Dual Living Polymerizations: A Novel One-Step Approach to Block and Graft Copolymers. *Angew. Chem. Int. Ed.* **1998,** *37*, 1274-1276.

22. Teator, A. J.; Lastovickova, D. N.; Bielawski, C. W., Switchable Polymerization Catalysts. *Chem. Rev.* **2016,** *116*, 1969-1992.

23. Blanco, V.; Leigh, D. A.; Marcos, V., Artificial switchable catalysts. *Chem. Soc. Rev.* **2015,** *44*, 5341-5370.

24. Guillaume, S. M.; Kirillov, E.; Sarazin, Y.; Carpentier, J.-F., Beyond Stereoselectivity, Switchable Catalysis: Some of the Last Frontier Challenges in Ring-Opening Polymerization of Cyclic Esters. *Chem. Eur. J.* **2015,** *21*, 7988-8003.

25. Leibfarth, F. A.; Mattson, K. M.; Fors, B. P.; Collins, H. A.; Hawker, C. J., External Regulation of Controlled Polymerizations. *Angew. Chem. Int. Ed.* **2013,** *52*, 199-210.

26. Chen, C., Redox-Controlled Polymerization and Copolymerization. *ACS Catal.* **2018,** *8*, 5506-5514.

27. Kaiser, J. M.; Long, B. K., Recent developments in redox-active olefin polymerization catalysts. *Coord. Chem. Rev.* **2018,** *372*, 141-152.

28. Stößer, T.; Chen, T. T. D.; Zhu, Y.; Williams, C. K., 'Switch' catalysis: from monomer mixtures to sequence-controlled block copolymers. *Philos. Trans. Royal Soc. A* **2018,** *376*.

29. Wei, J.; Diaconescu, P. L., Redox-switchable Ring-opening Polymerization with Ferrocene Derivatives. *Acc. Chem. Res.* **2019**, in press.

30. Qi, M.; Dong, Q.; Wang, D.; Byers, J. A., Electrochemically Switchable Ring-Opening Polymerization of Lactide and Cyclohexene Oxide. *J. Am. Chem. Soc.* **2018,** *140*, 5686-5690.

31. Biernesser, A. B.; Delle Chiaie, K. R.; Curley, J. B.; Byers, J. A., Block Copolymerization of Lactide and an Epoxide Facilitated by a Redox Switchable Iron-Based Catalyst. *Angew. Chem. Int. Ed.* **2016,** *55*, 5251–5254.

32. Wei, J.; Riffel, M. N.; Diaconescu, P. L., Redox Control of Aluminum Ring-Opening Polymerization: A Combined Experimental and DFT Investigation. *Macromolecules* **2017,** *50*, 1847-1861.

33. Quan, S. M.; Wei, J.; Diaconescu, P. L., Mechanistic Studies of Redox-Switchable Copolymerization of Lactide and Cyclohexene Oxide by a Zirconium Complex. *Organometallics* **2017,** *36*, 4451-4457.

34. Lowe, M. Y.; Shu, S.; Quan, S. M.; Diaconescu, P. L., Investigation of redox switchable titanium and zirconium catalysts for the ring opening polymerization of cyclic esters and epoxides. *Inorg. Chem. Front.* **2017,** *4*, 1798-1805.

35. Quan, S. M.; Wang, X.; Zhang, R.; Diaconescu, P. L., Redox Switchable Copolymerization of Cyclic Esters and Epoxides by a Zirconium Complex. *Macromolecules* **2016,** *49*, 6768-6778.

36. Wang, X.; Thevenon, A.; Brosmer, J. L.; Yu, I.; Khan, S. I.; Mehrkhodavandi, P.; Diaconescu, P. L., Redox Control of Group 4 Metal Ring-Opening Polymerization Activity toward l-Lactide and ε-Caprolactone. *J. Am. Chem. Soc.* **2014,** *136*, 11264-11267.

37. Chen, T. T. D.; Zhu, Y.; Williams, C. K., Pentablock Copolymer from Tetracomponent Monomer Mixture Using a Switchable Dizinc Catalyst. *Macromolecules* **2018,** *51*, 5346-5351.

38. Romain, C.; Williams, C. K., Chemoselective Polymerization Control: From Mixed-Monomer Feedstock to Copolymers. *Angew. Chem. Int. Ed.* **2014,** *53*, 1607-1610.

39. Satoh, K.; Hashimoto, H.; Kumagai, S.; Aoshima, H.; Uchiyama, M.; Ishibashi, R.; Fujiki, Y.; Kamigaito, M., One-shot controlled/living copolymerization for various comonomer sequence distributions via dual radical and cationic active species from RAFT terminals. *Polym. Chem.* **2017,** *8*, 5002-5011.

40. Aoshima, H.; Uchiyama, M.; Satoh, K.; Kamigaito, M., Interconvertible Living Radical and Cationic Polymerization through Reversible Activation of Dormant Species with Dual Activity. *Angew. Chem. Int. Ed.* **2014,** *53*, 10932-10936.

41. Romain, C.; Zhu, Y.; Dingwall, P.; Paul, S.; Rzepa, H. S.; Buchard, A.; Williams, C. K., Chemoselective Polymerizations from Mixtures of Epoxide, Lactone, Anhydride, and Carbon Dioxide. *J. Am. Chem. Soc.* **2016,** *138*, 4120-4131.

42. Paul, S.; Romain, C.; Shaw, J.; Williams, C. K., Sequence Selective Polymerization Catalysis: A New Route to ABA Block Copoly(ester-b-carbonate-b-ester). *Macromolecules* **2015,** *48*, 6047-6056.

43. Peterson, B. M.; Kottisch, V.; Supej, M. J.; Fors, B. P., On Demand Switching of Polymerization Mechanism and Monomer Selectivity with Orthogonal Stimuli. *ACS Cent. Sci.* **2018,** *4*, 1228-1234.

44. Eisenreich, F.; Kathan, M.; Dallmann, A.; Ihrig, S. P.; Schwaar, T.; Schmidt, B. M.; Hecht, S., A photoswitchable catalyst system for remote-controlled (co)polymerization in situ. *Nat. Catal.* **2018,** *1*, 516-522.

45. Kottisch, V.; Michaudel, Q.; Fors, B. P., Photocontrolled Interconversion of Cationic and Radical Polymerizations. *J. Am. Chem. Soc.* **2017,** *139*, 10665-10668.

46. Abubekerov, M.; Vlček, V.; Wei, J.; Miehlich, M. E.; Quan, S. M.; Meyer, K.; Neuhauser, D.; Diaconescu, P. L., Exploring Oxidation State-Dependent Selectivity in Polymerization of Cyclic Esters and Carbonates with Zinc(II) Complexes. *iScience* **2018,** *7*, 120-131.

47. Broderick, E. M.; Guo, N.; Wu, T.; Vogel, C. S.; Xu, C.; Sutter, J.; Miller, J. T.; Meyer, K.; Cantat, T.; Diaconescu, P. L., Redox control of a polymerization catalyst by changing the oxidation state of the metal center. *Chem. Commun.* **2011,** *47*, 9897-9899.

48. Broderick, E. M.; Guo, N.; Vogel, C. S.; Xu, C.; Sutter, J.; Miller, J. T.; Meyer, K.; Mehrkhodavandi, P.; Diaconescu, P. L., Redox Control of a Ring-Opening Polymerization Catalyst. *J. Am. Chem. Soc.* **2011,** *133*, 9278–9281.

49. Biernesser, A. B.; Li, B.; Byers, J. A., Redox-Controlled Polymerization of Lactide Catalyzed by Bis(imino)pyridine Iron Bis(alkoxide) Complexes. *J. Am. Chem. Soc.* **2013,** *135*, 16553-16560.

50. Sauer, A.; Buffet, J.-C.; Spaniol, T. P.; Nagae, H.; Mashima, K.; Okuda, J., Switching the Lactide Polymerization Activity of a Cerium Complex by Redox Reactions. *ChemCatChem* **2013,** *5*, 1088-1091.

51. Gregson, C. K. A.; Gibson, V. C.; Long, N. J.; Marshall, E. L.; Oxford, P. J.; White, A. J. P., Redox Control within Single-Site Polymerization Catalysts. *J. Am. Chem. Soc.* **2006,** *128*, 7410-7411.

52. Dai, R.; Lai, A.; Alexandrova, A. N.; Diaconescu, P. L., Geometry Change in a Series of Zirconium Compounds during Lactide Ring-Opening Polymerization. *Organometallics* **2018,** *37*, 4040-4047.

53. Abubekerov, M.; Shepard, S. M.; Diaconescu, P. L., Switchable Polymerization of Norbornene Derivatives by a Ferrocene-Palladium(II) Heteroscorpionate Complex. *Eur. J. Inorg. Chem.* **2016,** *2016*, 2634-2640.

54. Emig, N.; Nguyen, H.; Krautscheid, H.; Réau, R.; Cazaux, J.-B.; Bertrand, G., Neutral and Cationic Tetracoordinated Aluminum Complexes Featuring Tridentate Nitrogen Donors: Synthesis, Structure, and Catalytic Activity for the Ring-Opening Polymerization of Propylene Oxide and (d,l)-Lactide. *Organometallics* **1998,** *17*, 3599-3608.

55. Morris, L. S.; Childers, M. I.; Coates, G. W., Bimetallic Chromium Catalysts with Chain Transfer Agents: A Route to Isotactic Poly(propylene oxide)s with Narrow Dispersities. *Angew. Chem. Int. Ed.* **2018,** *57*, 5731-5734.

56. Darensbourg, D. J.; Choi, W.; Karroonnirun, O.; Bhuvanesh, N., Ring-Opening Polymerization of Cyclic Monomers by Complexes Derived from Biocompatible Metals. Production of Poly(lactide), Poly(trimethylene carbonate), and Their Copolymers. *Macromolecules* **2008,** *41*, 3493-3502.

57. Kim, J.-H.; Lee, S. Y.; Chung, D. J., Synthesis and Properties of Triblock Copolymers from L-Lactide and Trimethylene Carbonate. *Polym. J.* **2000,** *32*, 1056.

58. Wang, L.; Kefalidis, C. E.; Sinbandhit, S.; Dorcet, V.; Carpentier, J.-F.; Maron, L.; Sarazin, Y., Heteroleptic Tin(II) Initiators for the Ring-Opening (Co)Polymerization of Lactide and Trimethylene Carbonate: Mechanistic Insights from Experiments and Computations. *Chem. Eur. J.* **2013,** *19*, 13463-13478.

59. Kricheldorf, H. R.; Rost, S., Biodegradable Multiblock Copolyesters Prepared from ε-Caprolactone, l-Lactide, and Trimethylene Carbonate by Means of Bismuth Hexanoate. *Macromolecules* **2005,** *38*, 8220-8226.

60. Abubekerov, M.; Wei, J.; Swartz, K. R.; Xie, Z.; Pei, Q.; Diaconescu, P. L., Preparation of multiblock copolymers via step-wise addition of l-lactide and trimethylene carbonate. *Chem. Sci.* **2018,** *9*, 2168-2178.

61. Dhar, D.; Yee, G. M.; Spaeth, A. D.; Boyce, D. W.; Zhang, H.; Dereli, B.; Cramer, C. J.; Tolman, W. B., Perturbing the Copper(III)–Hydroxide Unit through Ligand Structural Variation. *J. Am. Chem. Soc.* **2016,** *138*, 356-368.

Chapter 4. Preparation and solid state self-assembly study of LA-LO copolymers

4.1. Introduction

Limonene oxide (LO, Figure 4.1a) is one of the bio-renewable materials that can be used as a candidate for constructing a green polymer, which will be depolymerized in nature and minimize the post-usage "white pollution".[1-8] LO can be easily prepared from limonene, an abundant terpene extracted from citrus, and has already gained wide application in the industry as a solvent and insecticide.[9-14] LO is largely used as a monomer to be copolymerized with CO_2 and form poly(limonene carbonate) (PLC, Figure 4.1b).[15-22] However, few reports exist on the homopolymerization of LO. In 1985, poly(limonene oxide) (PLO) was prepared for the first time by a radiation-induced cationic polymerization manner, with a molar mass averaging 2.0 kDa.[23] The only other report of PLO synthesis used the metal-catalyzed ring opening polymerization mechanism, giving a molar mass of 1.2 kDa.[24] The limited number of reports available and the low molar mass of the PLO suggest that the homopolymerization of LO is difficult, also indicating that the preparation of LO based block copolymers other than PLC might not be straightforward. In order to determine if LO based block copolymers have value and potential applications, preparation methods are needed. Once prepared, the LO based copolymers can be tested for further applications. For example, they might self-assemble into bio-compatible permeable films or particles, or could be used as coatings or drug deliver capsules.[24-31]

Redox switchable catalysis is a novel method for synthesizing block copolymers; a metal catalyst can have orthogonal activity toward different monomers depending on its oxidation state.[32-36] Upon adding an external oxidant or reductant, different monomers can be selectively polymerized and added to the polymer chain, therefore, a block copolymer can be prepared.

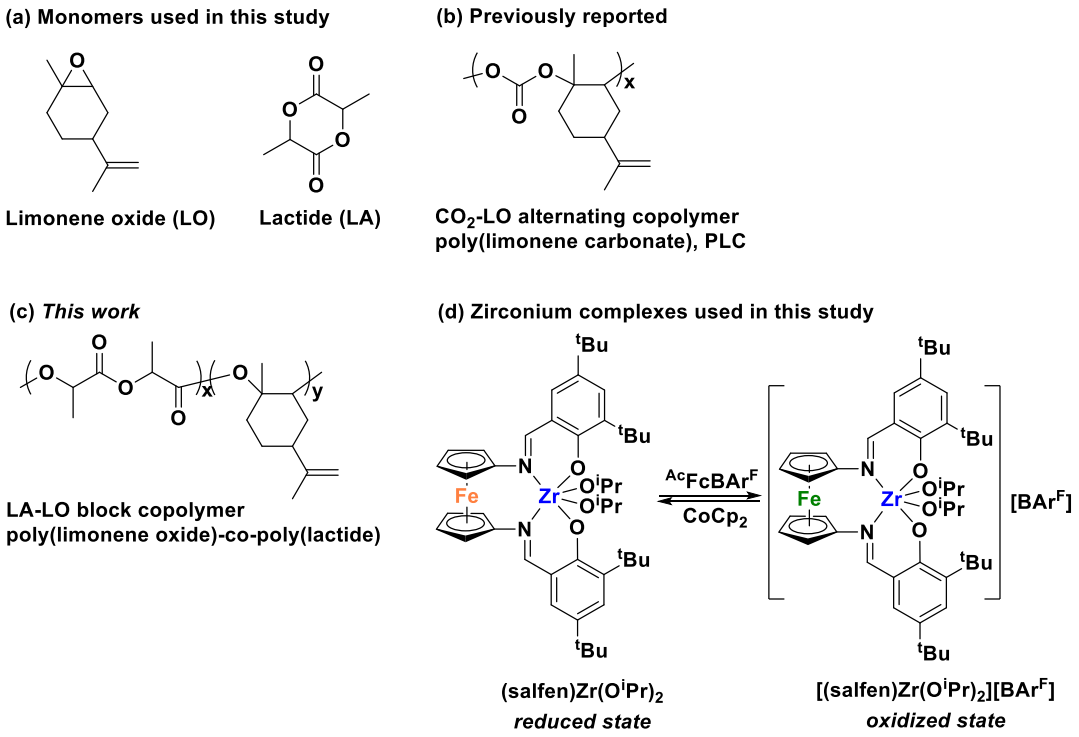

Figure 4.1. (a) Monomers used in this study: LO is (+)-limonene oxide, mixture of *cis* and *trans*, LA is L-lactide; (b) previously reported poly(limonene carbonate); (c) an example of a LO copolymer reported in this work; (d) redox switching of (salfen)Zr(O^iPr)$_2$.

Our group has studied ferrocene-based metal compounds that can perform redox switchable ring opening polymerization.[37-51] The ferrocene unit in the ligand backbone is the redox center, while the other metal is the catalytic center (Figure 4.1d). For example, (salfen)Zr(O^iPr)$_2$ (salfen = N,N'-bis(2,4-di-*tert*-butylphenoxy)-1,1'-ferrocenediimine) can polymerize lactones in the reduced state and epoxides in its oxidized state, and such redox switches can be repeated multiple times.[40] The compound was used to prepare L-lactide (LA) and cyclohexene oxide copolymers, so we reasoned it could be a good candidate for LO polymerization, too. Herein, we report the use of (salfen)Zr(O^iPr)$_2$ to prepare the largest LO homopolymer, and the first LO block

copolymer with LA, another bio-renewable monomer. The self-assembly properties of the copolymers were probed by rheology measurements and small angle X-ray scattering (SAXS).

4.2. Results and Discussions

LO Homopolymerization

[(salfen)Zr(O^iPr)$_2$][BAr^F] (BAr^F = tetrakis(3,5-bis(trifluoromethyl)-phenyl)borate), the precatalyst in the oxidized state, was used for the LO homopolymerization. The reactions reached near full conversion within 1 h (Figure 4.D1), but the molar mass obtained from the size exclusion chromatography (SEC) was less than the theoretical value. Therefore, we tried to optimize the reaction conditions by modifying the reaction time, temperature, monomer to precatalyst ratio, and concentration (Table 4.1).The molar mass of the homopolymers did not vary too much among all the 12 entries in Table 4.1, falling in the range of 2.9 to 4.0 kDa. The reaction time did not have a significant impact on the molar mass of the homopolymers (Table 4.1, entry 1-4), nor did the amount of monomer (Table 4.1, entry 5-6). The solvent volume, or the general concentration, did not show a great impact on the molar mass (Table 4.1, entry 11-12), either. The only factor that impacted the molar mass, though slightly, was the temperature. A temperature as low as 0 ^oC gave a higher molar mass (Table 4.1, entry 7-8), and an elevated temperature as 50 ^oC gave a lower molar mass (Table 4.1, entry 10) than the unoptimized reaction, respectively. We postulated that the LO homopolymerization is affected by some back-biting side reaction, and the polymer chain gets “locked” at certain lengths. Thermodynamics may favor the back-biting over polymer propagation over a certain chain length, which is about 3-4 kDa in our case. The low temperature can slow down the back-biting, leading to a higher degree of polymerization, thus a higher molar mass.

Table 4.1. LO homopolymerization studies[a]

Entry	Monomer equiv.	Time (h)	Temp. (°C)	Solvent volume (mL)	Mn SEC (kDa) [b]	Mn calcd. (kDa) [c]	*Đ*
1	100	1	25	0.6	3.0	7.5	1.13
2	100	2	25	0.6	3.0	7.5	1.14
3	100	4	25	0.6	3.4	7.5	1.08
4	100	6	25	0.6	2.9	7.5	1.13
5	75	2	25	0.6	3.6	5.6	1.05
6	200	2	25	0.6	3.4	15.1	1.11
7	100	2	0	0.6	4.0	7.5	1.15
8	100	6	0	0.6	3.9	7.5	1.11
9	100	2	40	0.6	3.4	7.5	1.06
10	100	2	50	0.6	2.3	7.5	1.08
11	100	2	25	0.3	3.0	7.5	1.12
12	100	2	25	1.2	3.8	7.5	1.05

[a] All polymerization reactions were carried out with 4 μmol precatalyst, C_6D_6 was used as the solvent and hexamethylbenzene as an internal standard. All reactions achieved 100% conversion. [b] Molar masses were derived from SEC measurements. [c] The theoretical molar mass was calculated based on two initiating groups in the precatalyst.

Copolymerization of LO and LA

The preparation of a LO-LA copolymer (Figure 4.1c), a fully bio renewable block copolymer, was studied using the redox switchable polymerization method. The precatalyst, (salfen)Zr(O^iPr)$_2$ can polymerize L-LA in its reduced state, and polymerize LO in the oxidized

state following the addition of an external oxidant, giving a PLO-PLA copolymer. The LO block polymerization time was first set at 5 h, since the (salfen)Zr(O^iPr)$_2$ catalytic system was reported to have a slower reaction rate of epoxide copolymerization compared to epoxide homopolymerization.[40] However, simply following the sequence "LA polymerization, catalyst oxidation, LO polymerization" gave a polymer mixture (Table 4.D1, entry 1), with a bimodal SEC trace (Figure 4.2a). After comparing the SEC trace of the product and those of PLA and PLO homopolymers, we realized that a new PLO-PLA copolymer was made, but the PLO homopolymer was also generated. Such a PLO biproduct would also affect the further copolymerization to triblock and tetrablock copolymers.

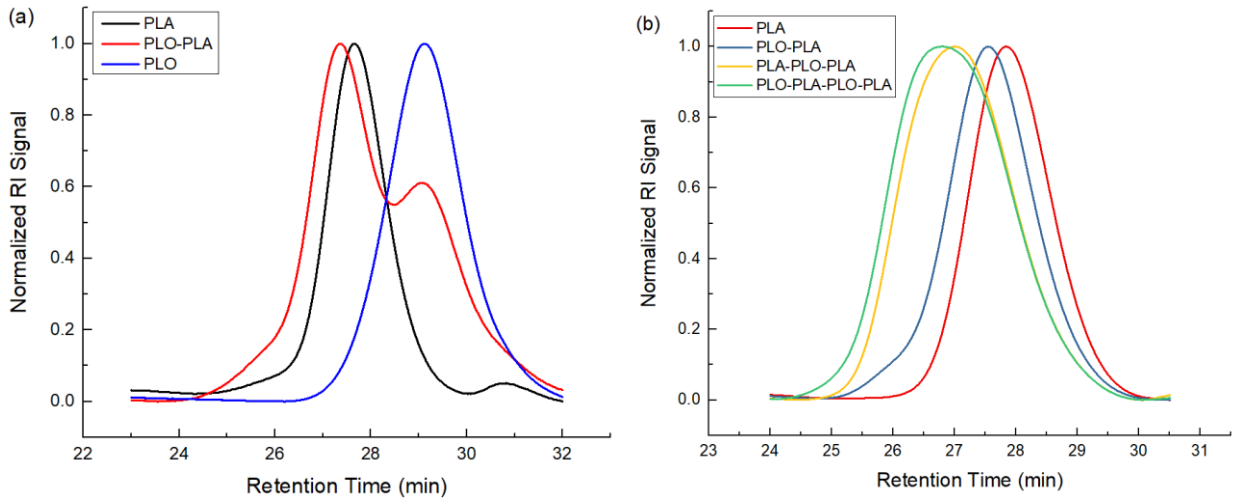

Figure 4.2. (a) SEC trace of the unsuccessful attempt of LO-LA copolymerization comparing with PLA and PLO homopolymer traces. The PLO-PLA trace was bimodal, with the right peak assigned as a PLO peak, and the left peak probably coming from the new copolymer. (b) SEC traces of the real-time monitoring of a tetrablock copolymer preparation.

We reasoned that the LA polymerization was fine as the first block of the copolymerization. During the preparation of the second block, the LO block, the copolymerization was likely going well in the beginning, and then back-biting occurred, leading to the formation of extra PLO homopolymer biproduct. Therefore, the copolymerization conditions needed to be optimized, with the idea of stopping the LO polymerization before the back-biting point was reached.

Firstly, the LO monomer feeding was reduced from 100 to 75 and then to 50 (Table 4.D1, entry 1-3), hoping the back-biting would not occur before the monomer was fully consumed. The traces of the three copolymerization products were all bimodal, but the PLO homopolymer peak at around 29.3 min experienced a decrease in height (Figure 4.D10). The trace for the copolymerization reaction with 50 equiv LO showed no legible shoulder, though the trace has a tail at the end. Finally, the LO polymerization time was optimized from 5 h to 2 h, then to 1 h (Table 4.D1, entries 3-5). The SEC traces showed that a fine distribution was achieved in the 1h LO polymerization product (Figure 4.D11), meaning the PLO-PLA diblock copolymer could be made without the PLO homopolymer biproduct. DOSY studies supported the claim that 1 h LO polymerization product was a copolymer, while the 2 h LO polymerization product was still a mixture of different polymers (Figures 4.D4, 4.D5).

With the optimized conditions, a PLA-PLO-PLA triblock and a PLO-PLA-PLO-PLA tetrablock copolymer were prepared (Table 4.2, Figures 4.2b, 4.D6, 4.D7).

Table 4.2. Real-time monitoring of the tetrablock copolymer preparation [a]

Block No.	Monomer of this block	Mn of the entire polymer so far (kDa) [b]	*Đ*	Mn of this block (kDa) [c]	Polymer formula [d]

1st block	LA	3.3	1.02	3.3	LA_{23}
2nd block	LO	5.5	1.09	2.2	LO_{15}-LA_{23}
3rd block	LA	6.8	1.08	1.3	LA_9-LO_{15}-LA_{23}
4th block	LO	7.9	1.12	1.1	LO_8-LA_9-LO_{15}-LA_{23}

[a] All polymerization reactions were carried out with 4 μmol precatalysts, C_6D_6 was used as the solvent and hexamethylbenzene as an internal standard. LA block polymerization: 100 equiv LA, heating for 20 h in 100 ^oC; LO block polymerization: 50 equiv LO, 1 h at room temperature. Data points were taken at the end of the preparation of each block. [b] Molar masses were obtained from SEC measurements. [c] Molar masses were calculated from the total Mn of the current data point minus the total Mn of the last data point. [d] Formula for each block was calculated by the Mn of this block divided by the molar mass of the corresponding monomer.

Rheology measurements

To investigate the self-assembly properties of the prepared block copolymers, a rheology study was conducted to test the phase separation or microphase domain in the solid state copolymers. Both triblock and tetrablock copolymers exhibited an extended rubbery plateau over the frequencies of 0.1-100 rad/s (Figure 4.3b, 4.3c). This extended rubbery plateau was observed even above the melting temperature of the material. The presence of the rubbery plateau suggests that the materials are phase separated into domains and display similar behavior as thermoplastic elastomers. Even though these materials displayed substantial decrease in G' and G" as a result of losing structural rigidity, they continued to display rubbery plateaus even at temperatures significantly greater than their glass transition temperature (T_g). This indicates that a microphase

separated domain structure is retained even above the T_g of the hard block, an evidence of self-assembly in the solid state.

In contrast to the triblock and tetrablock, the diblock copolymer displayed a shorter rubbery plateau prior to the T_g (Figure 4.3a). Further, at 160 °C the material had a low storage and loss modulus that were similar to each other, suggesting a weakly structured material or one close to the boundary of rheological liquid and rheological solid.

Overall, the data suggests that the triblock and tetrablock copolymers contain mechanically percolated phase separated structures, which were not observed in the diblock copolymer. This is likely because the triblock and tetrablock structures can form microphase separated domains, where individual polymer chains straddle multiple domains and thereby create an extended, mechanically percolated structure. The diblock copolymer, even if microphase separated, does not have an effective mechanical percolation and hence the mechanical properties above the melting temperature approximate a rheological liquid. Since the existence of the copolymers self-assembly were supported by the rheology test, SAXS measurements were performed to investigate further the size of the self-assembly domain.

Small angle X-ray scattering (SAXS) measurements

In the SAXS experiments, the scattering vector is calculated as:

$$q = \frac{4\pi \text{ Sin } (\vartheta)}{\lambda}$$

We used the Debye model for the analysis of SAXS data. Unlike the familiar nanostructures that have well defined shapes, block copolymers are considered to have no specific shape and the scattering originates from shape independent two-phase regions of the polymer of different electron densities. Even if the two phases have irregular shapes, the correlation length

between the two domains can be obtained from the analysis. Debye's model calculates the scattering intensity over the entire volume as:

$$I(q) = \int e^{-\left(\frac{R}{\xi}\right)^{2h}} \frac{4\pi R}{q} \sin(qR)\, dR$$

Here, the correlation function includes the *correlation length (ξ)* and the *fractal coefficient h*. The correlation between two phases is represented by the probability of having a region of the same electron density at a distance *R* away. Thus, when the probability becomes (*1/e*), the distance is referred to as the correlation length, or the self-assembly domain radius. Although two domains may have the same electron density at a distance, the shape of the domains may be irregular. The *fractal coefficient h* is taking into account the shape irregularities. As observed from the above equation, the correlation function is heavily dependent on the fractal coefficient. When the shape irregularity is increased, *h* decreases and the domains become correlated only at longer distances (ξ increases), resulting in an increase of the radius of the self-assembly domain.

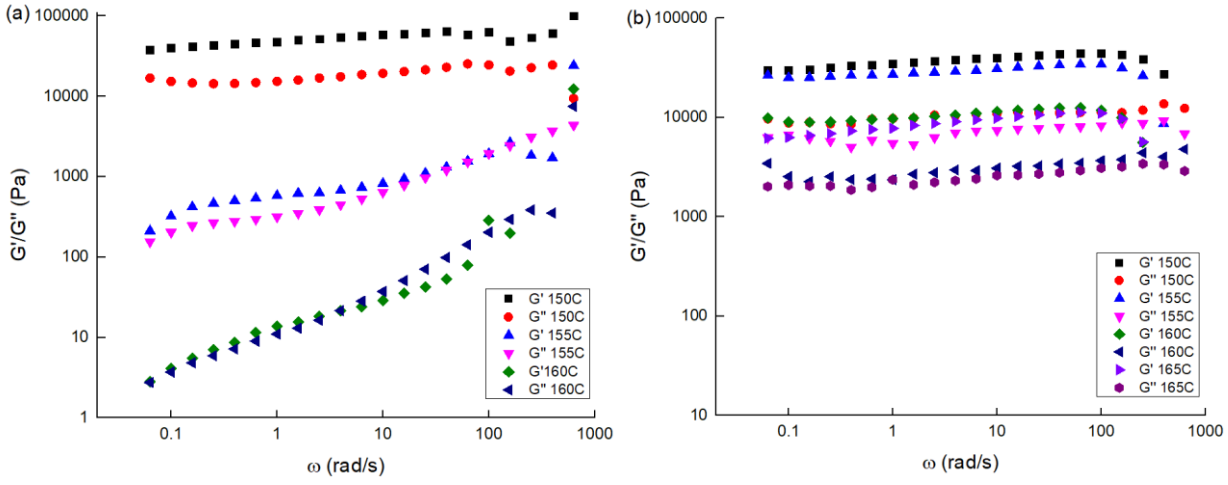

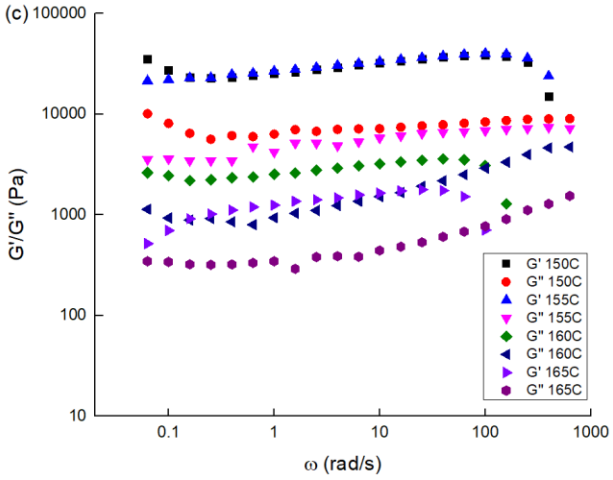

Figure 4.3. (a) Storage (G') and loss (G") moduli of the PLO-PLA diblock copolymer at different temperatures. (b) Storage (G') and loss (G") moduli of the PLA-PLO-PLA triblock copolymer at different temperatures. (c) Storage (G') and loss (G") moduli of the PLO-PLA-PLO-PLA tetrablock copolymer at different temperatures.

Figure 4.4 depicts the SAXs data and the best fits obtained using the Debye model. The correlation lengths (ξ), or self-assembly domain radius, obtained from the fits are given in the plot. The diblock, triblock and tetrablock copolymers have a domain radius of 11, 25, and 35 nm, respectively. The domain radius value increased with the number of blocks, consistent with the fact that a larger polymer should have a larger self-assembly domain. The experimental data also showed an additional small peak around q = 0.008 $Å^{-1}$, corresponding to a length scale of 80 nm. The fractal parameter *h* from the fit for all the samples was around 0.35.

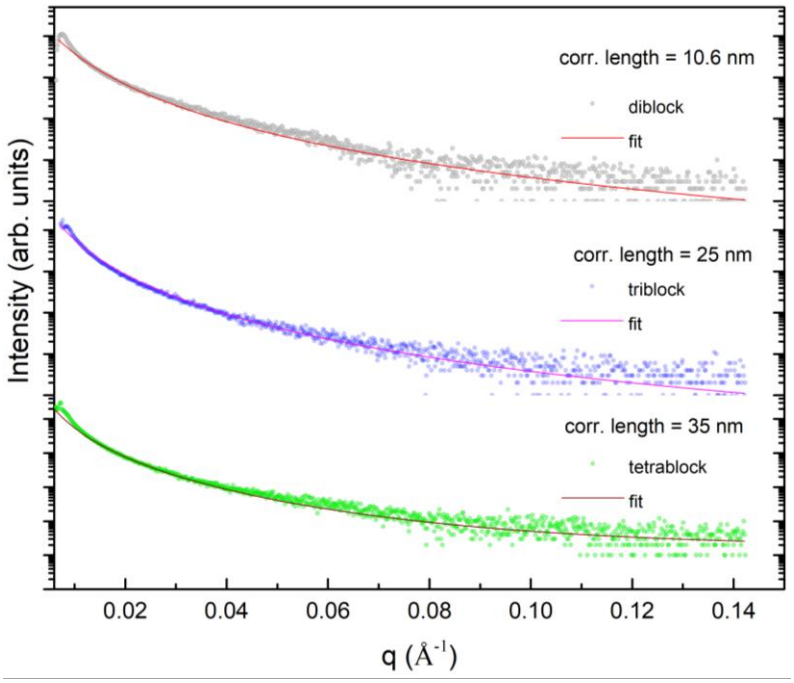

Figure 4.4. The log intensity vs. scattering vector (q) plots of the PLO-PLA diblock, triblock, and tetrablock copolymers.

4.3. Conclusions

PLO homopolymers were prepared with a zirconium catalyst developed by our group, with a molar mass up to 4.0 kDa, the largest ever reported in the literature. Furthermore, multi-block copolymers of LO and LA were prepared through redox switchable catalysis. Upon the optimization of polymerization conditions, LO-LA copolymer series were prepared for the first time. The self-assembly properties of the copolymers were investigated in the solid state. Rheology tests showed that there was a clear phase separation in the triblock and tetrablock copolymers, suggesting the existence of a self-assembly domain. SAXS experiments were then performed to give a quantified measurement of the self-assembly domain. Using the Debye model, the correlation length, or the self-assembly domain radius were fitted to be 11, 25, and 35 nm for the

diblock, triblock and tetrablock copolymers, respectively. This study marks a breakthrough in the LO chemistry and indicates potential applications in nanoparticle and drug delivery based on the LO copolymer self-assembly properties.

4.4. Experimental section

General considerations

All experiments were performed in an Mbraun inert gas glovebox or under a dry nitrogen atmosphere using standard Schlenk techniques. Solvents were purified with a two-state solid-state purification system by the method of Grubbs and transferred to the glovebox inside a Schlenk flask without exposure to air. NMR solvents were obtained from Cambridge Isotope Laboratories, degassed, and stored over activated molecular sieves prior to use. ^{1}H NMR spectra were recorded on Bruker 300, Bruker 500, or Bruker 600 spectrometers at room temperature in C_6D_6. Chemical shifts are reported with respect to the residual solvent peaks, 7.16 ppm (C_6D_6) for ^{1}H NMR spectra. Limonene oxide and 1,2-difluorobenzene were distilled over CaH_2 and brought into the glovebox without exposure to air. Solid monomers and hexamethylbenzene were recrystallized from toluene at least twice before use. $CoCp_2$ was purchased from Sigma-Aldrich and used as received. $^{Ac}FcBAr^{F}$ (^{Ac}Fc = acetylferrocene, BAr^{F} = tetrakis(3,5-bis(trifluoromethyl)-phenyl)borate)[52] and (salfen)Zr($O^{i}Pr$)$_2$[41] were synthesized following previously published procedures. Molar masses of polymers were determined by size exclusion chromatography (SEC) using a SEC-MALS instrument at UCLA. SEC-MALS uses a Shimazu Prominence-i LC 2030C 3D equipped with an autosampler, two MZ Analysentechnik MZ-Gel SDplus LS 5 μm, 300 × 8 mm linear columns, a Wyatt DAWN HELEOS-II, and a Wyatt Optilab T-rEX. The column temperature was set at 40 ^{o}C. A flow rate of 0.70 mL/min was used and samples were dissolved in THF. The number average

molar mass and dispersity values were found using the known concentration of the sample in THF with the assumption of 100% mass recovery to calculate dn/dc from the RI signal. Transmission small angle X-ray scattering (SAXS) and wide-angle X-ray scattering (WAXS) experiments were conducted on the block copolymers using a Rigaku Smartlab diffractometer (Rigaku Corp., Japan) equipped with Cu-Kα radiation (λ = 1.541 Å) at 40 kV, 44 mA setting. The setup uses a linearly collimated parallel X-ray beam delivered by a multilayer mirror and a SAXS-selection slit and a divergence slit shapes the incident beam to achieve SAXS resolution and limit the parasitic scattering from slit.

LO homopolymerization

Under an inert atmosphere, (salfen)Zr(O^iPr)$_2$ (4 μmol), C_6D_6 (0.3 mL), and an internal standard (hexamethylbenzene) were added to a J-Young NMR tube. The $^{Ac}FcBAr^F$ solution (0.1 mL, 40 mM in 1,2-difluorobenzene) was added and the NMR tube was shaken for 5 minutes before adding the LO monomer. The tube was sealed and brought out of the glovebox and left at room temperature. The reaction was monitored periodically by ^{1}H NMR spectroscopy. When the reaction was done, CH_2Cl_2 was added to the mixture and the resulting solution was poured into 10 mL of cold methanol to precipitate the polymer. The mixture was centrifuged 3 x 5 minutes, decanted, and dried under a reduced pressure to give the final polymer product.

Redox switchable copolymerization

PLA-PLO diblock copolymer preparation. Under an inert atmosphere, (salfen)Zr(O^iPr)$_2$ (16 μmol), LA, C_6D_6 (2.5 mL), and the internal standard (hexamethylbenzene) were added to a 50 mL Schlenk tube. The reaction mixture was left at room temperature for 5 min while stirring. The tube was sealed and brought out of the glovebox and heated to 100 ^{o}C with an oil bath. After 20 h, the 1st block of the copolymer was made. Then the Schlenk tube was brought back into the

glovebox. An $^{Ac}FcBAr^{F}$ solution (0.4 mL, 40 mM in 1,2-difluorobenzene) was added and the tube was stirred for 5 min before adding the LO monomer. The tube was sealed and brought out of the glovebox, and left at room temperature for 1 h. The progress of the reaction was monitored by taking a sample from the reactor and measured by NMR spectroscopy.

PLA-PLO-PLA triblock copolymer preparation. After the diblock copolymer was prepared, the Schlenk tube was brought into the glovebox, $CoCp_2$ (0.4 mL, 40 mM in C_6D_6) was added and the mixture stirred for 5 min. The LA monomer was added and the tube was sealed, brought out of the glovebox, and heated to 100 ^{o}C with an oil bath. After 20 h, the 3rd block of the copolymer was made. The progress of the reaction was monitored by taking a sample from the reactor and measured by NMR spectroscopy.

PLA-PLO-PLA-PLO tetrablock copolymer preparation. After the triblock copolymer was prepared, the Schlenk tube was brought into the glovebox, and $^{Ac}FcBAr^{F}$ solution (0.4 mL, 40 mM in 1,2-difluorobenzene) was added and the mixture stirred for 5 min. The LO monomer was added, the tube was sealed, brought out of the glovebox, and left at room temperature for 1 h. The progress of the reaction was monitored by taking a sample from the reactor and measured by NMR spectroscopy.

Rheology measurements

Frequency sweep experiments of triblock and tetrablock copolymers were performed at a temperature ranging from +5 °C and -5 °C from the glass transition temperatures (T_g). The triblock copolymer displayed a T_g around 155 °C and the tetrablock copolymer displayed a T_g around 160 °C. Hence, the experiments were performed in the range of 150-160 °C and 155-165 °C for the triblock and tetrablock copolymers, respectively. A 20 mm crosshatched plate geometry was used

to perform the experiments. The experiments were performed at a frequency range of 10^{-2} to 10^{2} Hz at 0.1% applied strain.

SAXS measurements

A powder sample was sandwiched between very thin sheets of Mylar and mounted vertically on the sample stage for experiments in the transmission mode. The small angle scattering data from the sample was extracted by subtracting the scattering contribution due to air and the Mylar sheets. An evacuated beam path inserted on the receiving side limit the air scattering contribution in the SAXs signal and a combination of receiving and scatter slits were used to achieve the required resolution at the detector. The data was collected by performing detector scans.

4.5. Appendix D

NMR Spectra

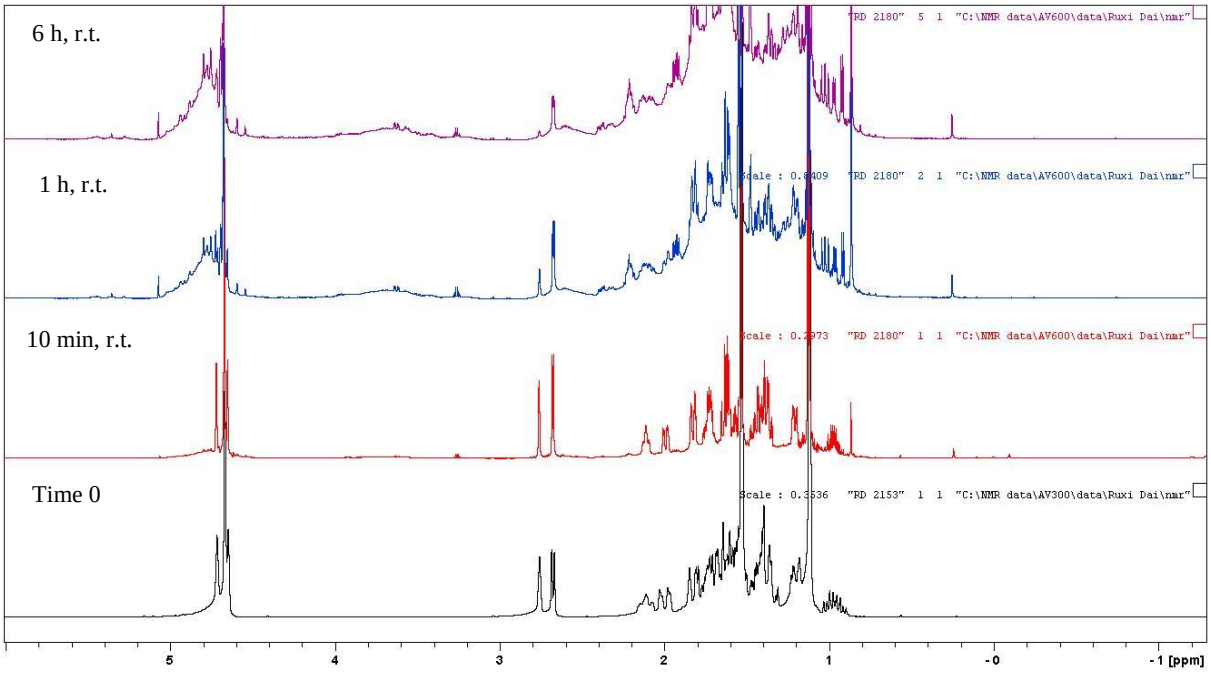

Figure 4.D1. Limonene oxide (LO) homopolymerization at room temperature (r. t.) monitored by ^{1}H NMR (300 MHz, C_6D_6, 25 ^{o}C) spectroscopy.

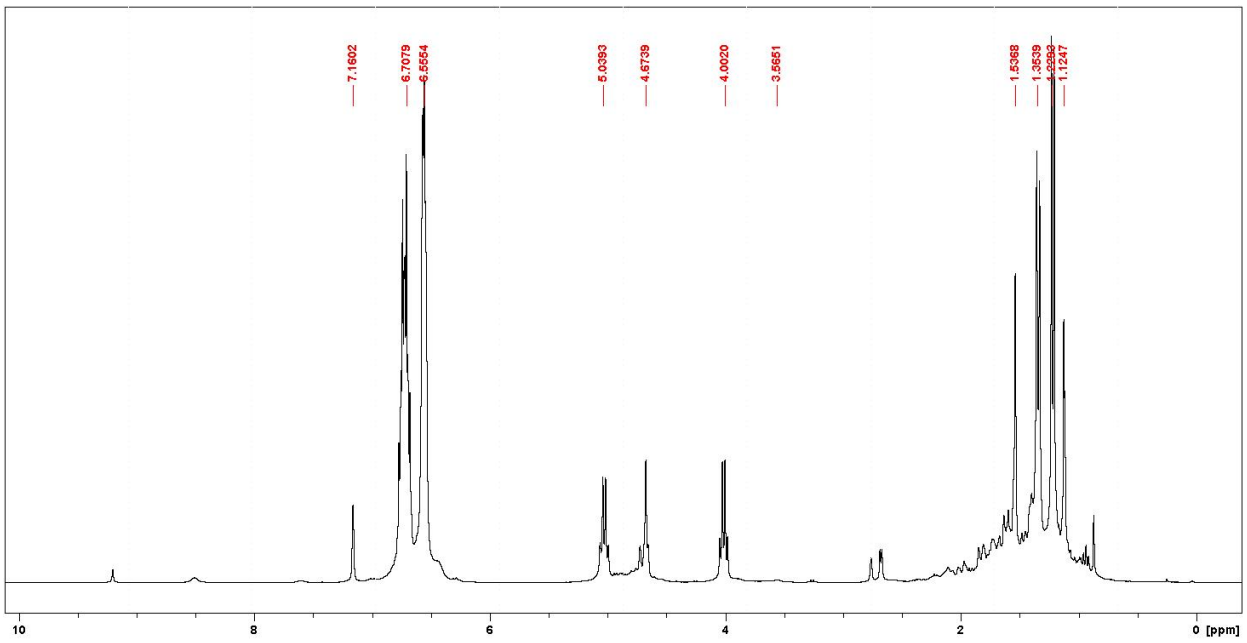

Figure 4.D2. ^{1}H NMR (600 MHz, C_6D_6, 25 ^{o}C) of the reaction mixture of lactide (LA) and LO copolymerization, at the end of the LO block preparation (Table 2, entry 5). δ, ppm: 7.16 (s, C_6D_6), 6.71 (m, 1,2-difluorobenzene), 6.56 (m, 1,2-difluorobenzene), 5.04 (d, polylactide, PLA), 4.67 (s, poly(limonene oxide), PLO), 4.00 (d, free LA), 3.57 (br, PLO), 1.54 (s, PLO), 1.35 (d, PLA), 1.22 (d, free LA), 1.12 (s, PLO).

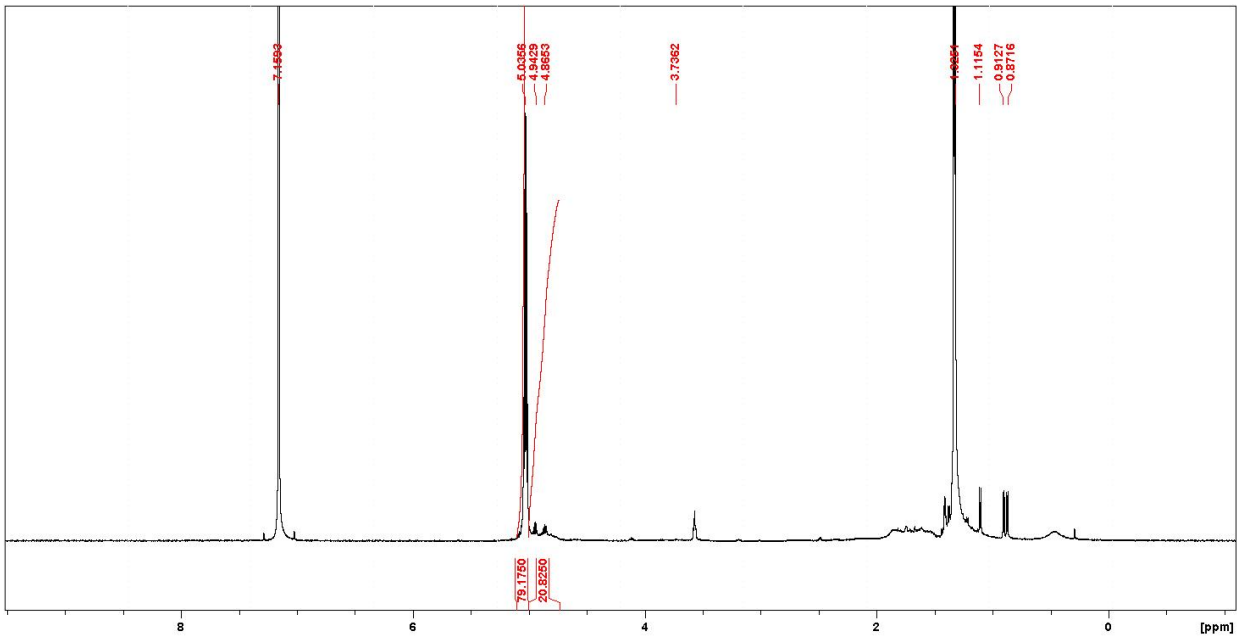

Figure 4.D3. ^{1}H NMR (600 MHz, C_6D_6, 25 ^{o}C) of isolated PLA-PLO diblock copolymer (Table 2, entry 5). δ, ppm: 7.16 (s, C_6D_6), 5.04 (d, PLA), 4.94 (m, PLO vinyl group), 4.87 (m, PLO vinyl group), 3.74 (br, PLO ether region), 1.52 (d, PLA), 1.12 (d, PLO), 0.91 (d, PLO), 0.87 (d, PLO).

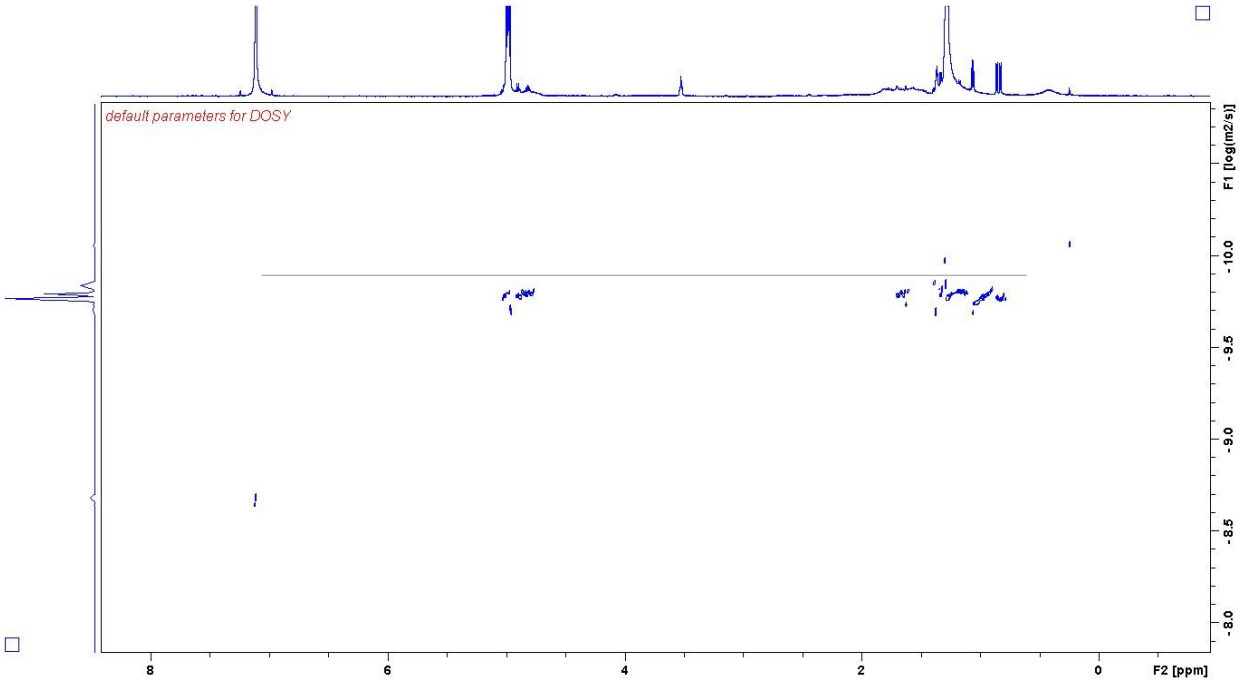

Figure 4.D4. DOSY (600 MHz, C_6D_6, 25 ^oC) of LA and LO copolymerization product (Table 4.D1, entry 5). The diffusion pattern indicated the copolymer nature of the product.

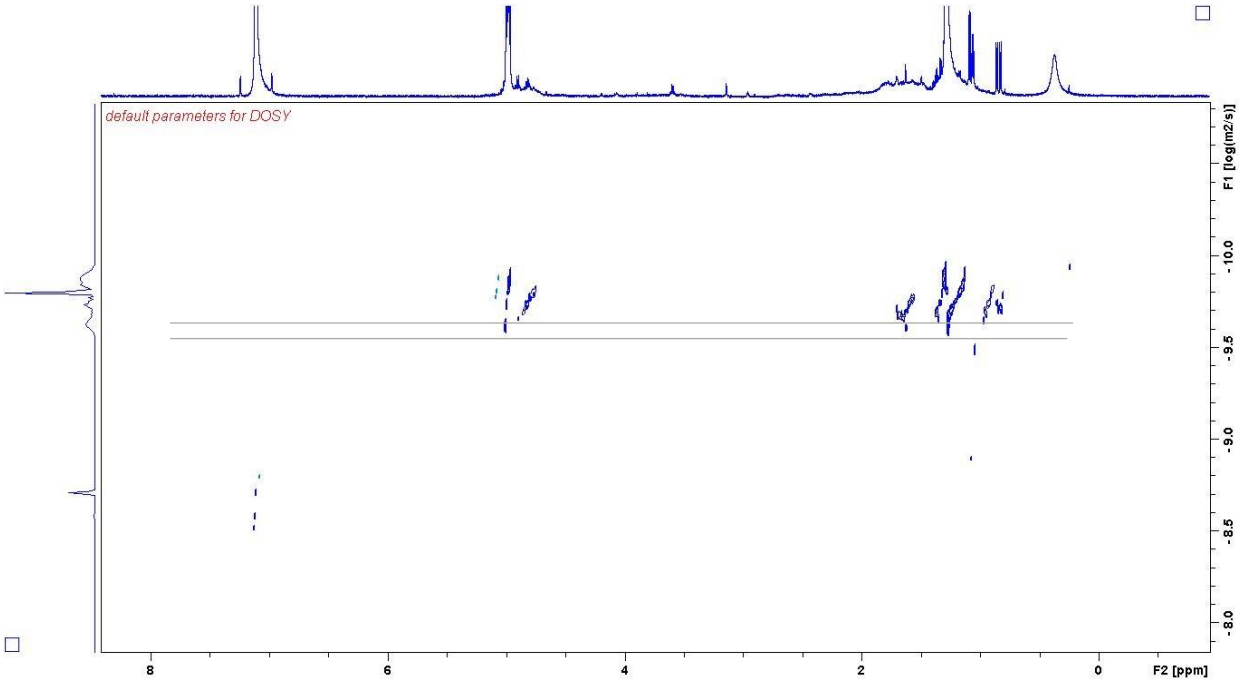

Figure 4.D5. DOSY NMR (600 MHz, C_6D_6, 25 ^oC) of LA and LO copolymerization product (Table 4.D1, entry 4). The diffusion pattern indicated there were homopolymer biproduct besides the copolymer.

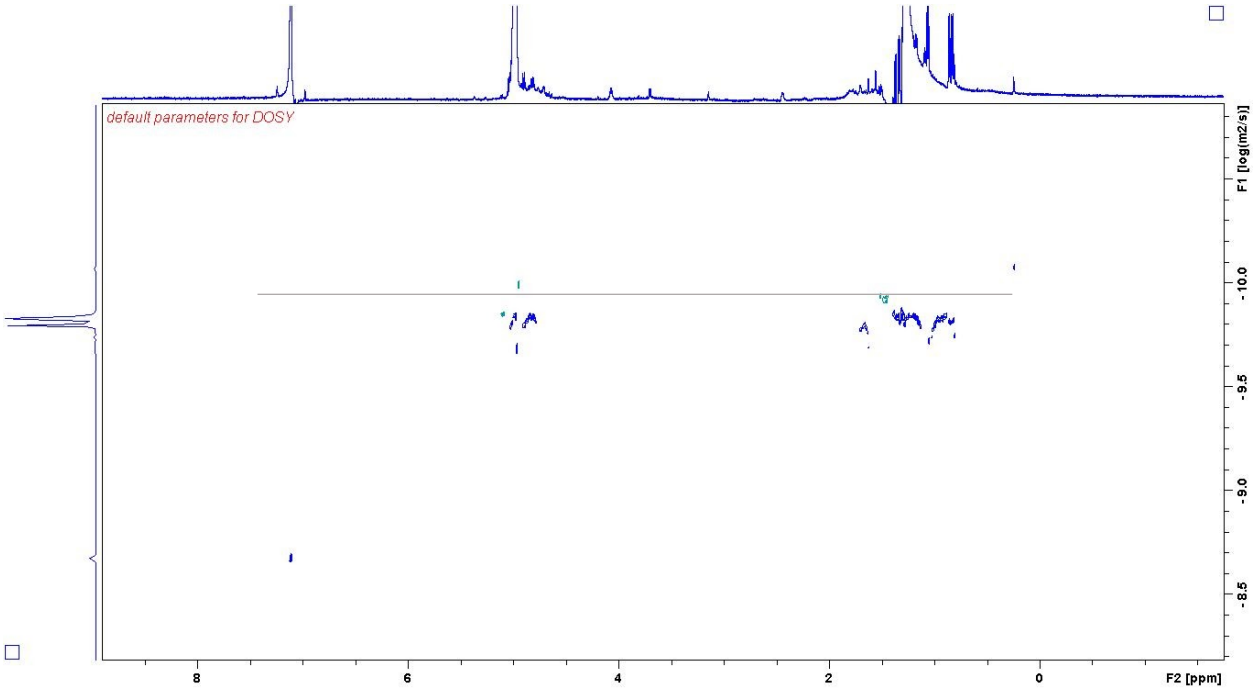

Figure 4.D6. DOSY NMR (600 MHz, C_6D_6, 25 ^oC) of PLA-PLO-PLA triblock copolymer.

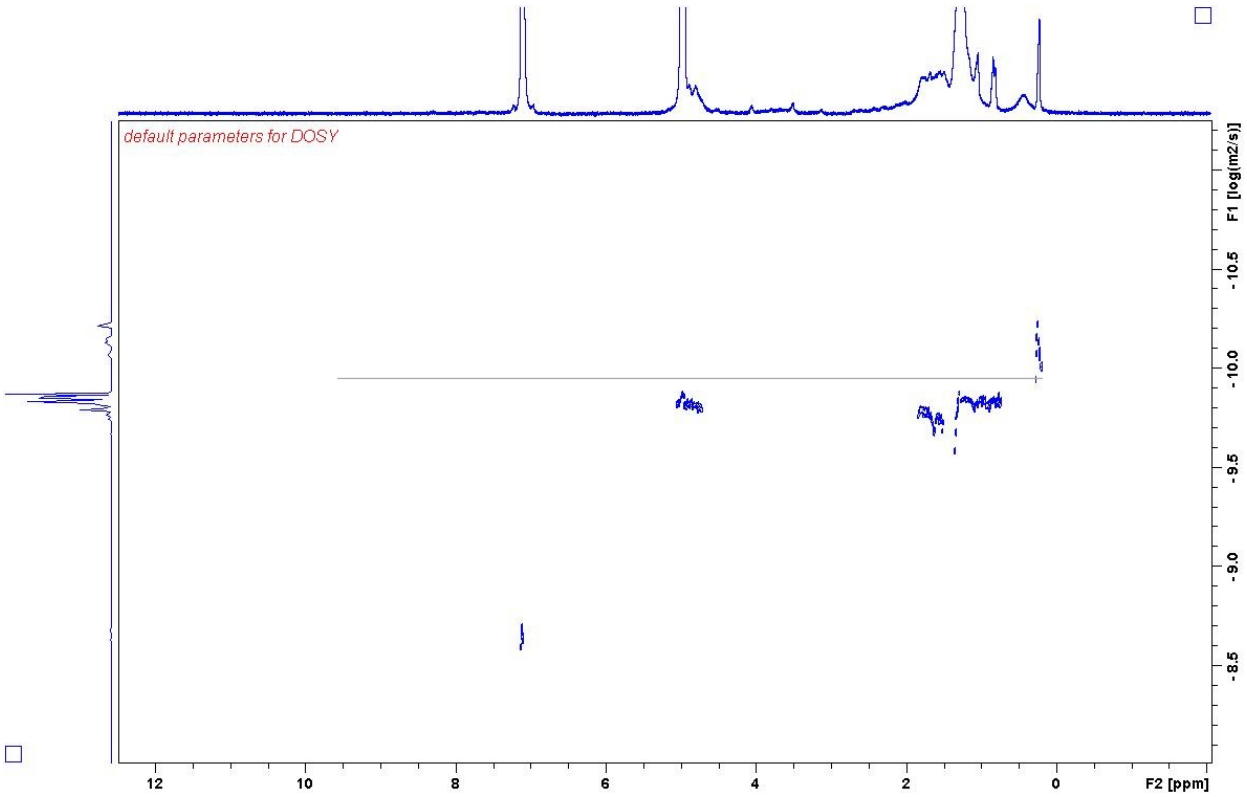

Figure 4.D7. DOSY NMR (600 MHz, C_6D_6, 25 ^oC) of PLA-PLO-PLA-PLO tetrablock copolymer.

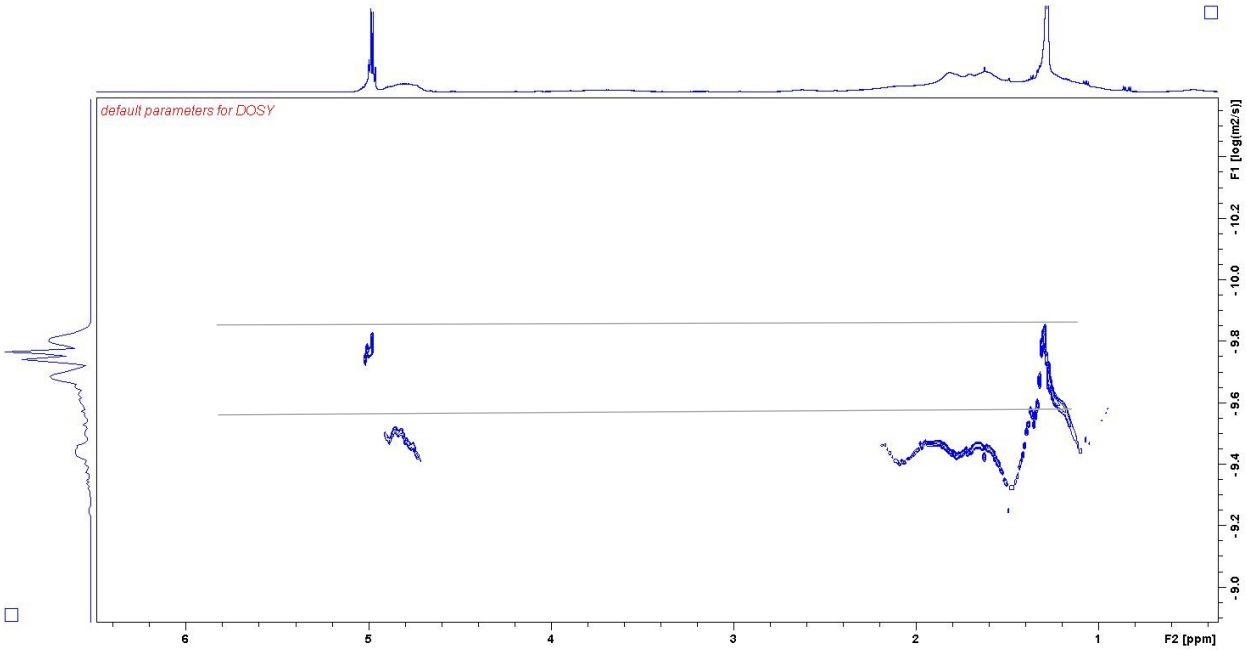

Figure 4.D8. DOSY NMR (600 MHz, C_6D_6, 25 ^oC) of a mixture of PLA homopolymer and PLO homopolymer.

SEC Measurements

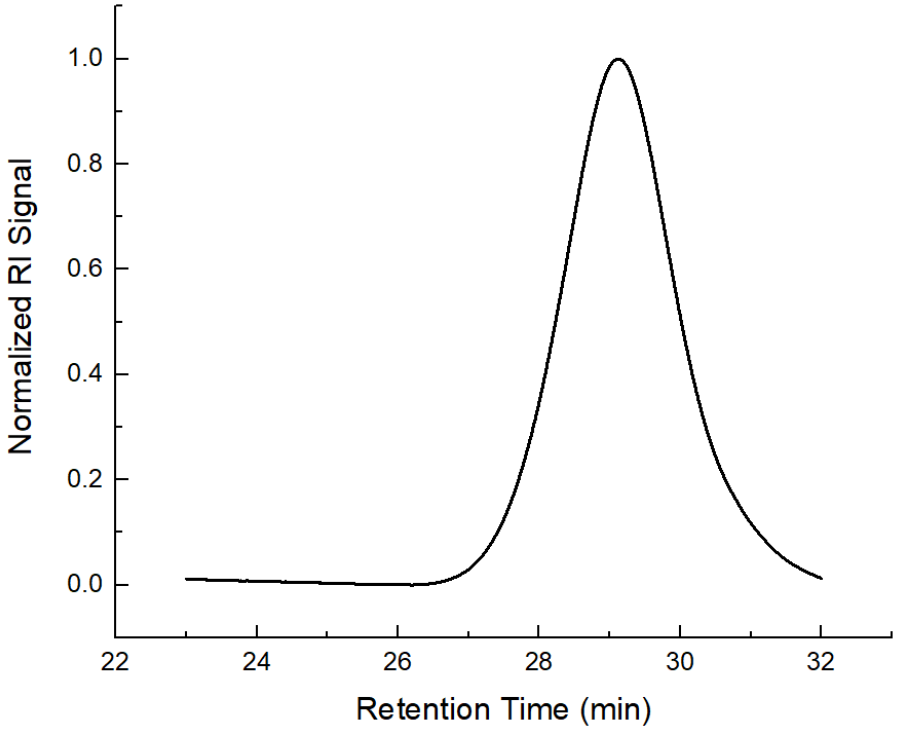

Figure 4.D9. SEC trace of PLO homopolymer (Table 1, entry 2).

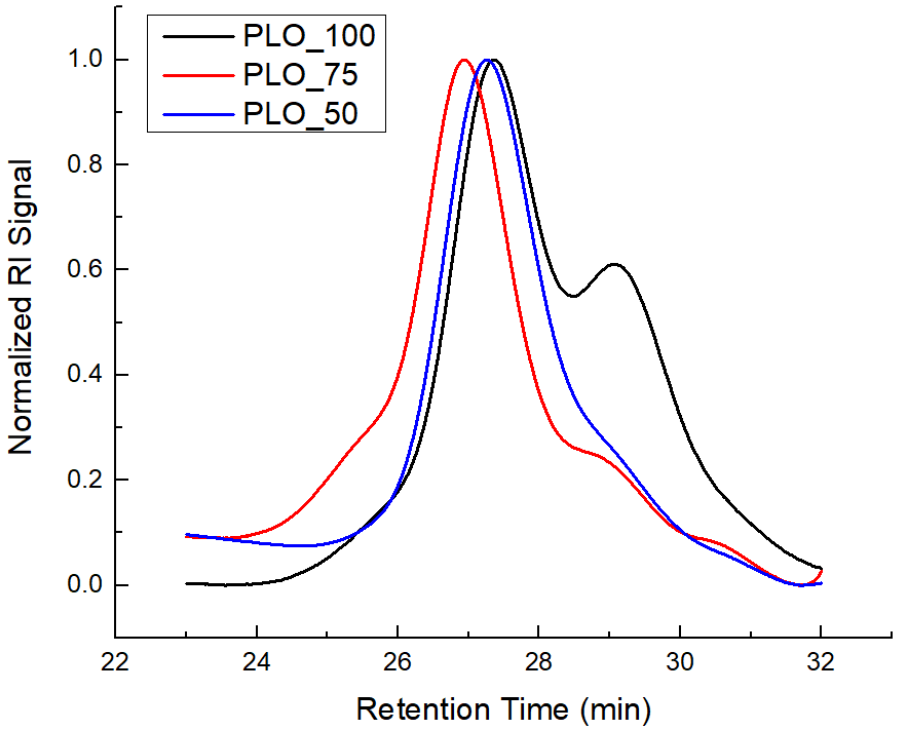

Figure 4.D10. SEC traces of three PLA-PLO copolymerization attempts, with 100, 75 and 50 equiv. LO monomer fed. The PLO homopolymer peak at around 29.3 min decreased in height.

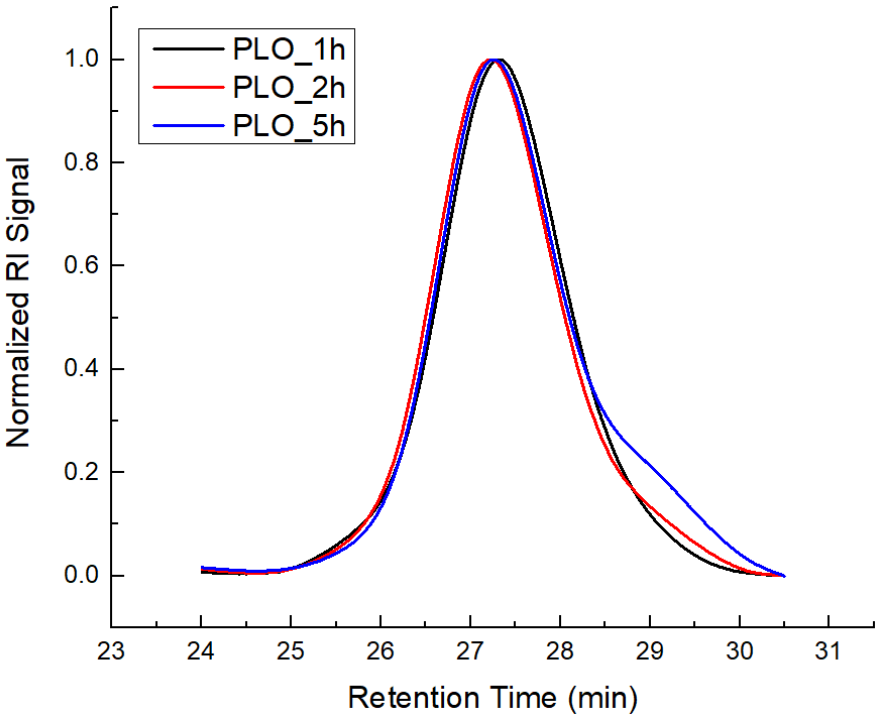

Figure 4.D11. SEC traces of three LO-LA copolymerization attempts, with LO polymerization time decreased from 5 h to 2 h then to 1 h. The "tail" of the trace decreased as the LO polymerization time shortened.

Table 4.D1. LO-LA copolymerization condition optimization [a]

Entry	LO feeding (equiv.)	LO time (h)	SEC trace
1	100	5	Bimodal
2	75	5	Bimodal
3	50	5	Bimodal
4	50	2	Bimodal
5	50	1	Unimodal

[a] All polymerization reactions were carried out with 4 μmol precatalysts, C_6D_6 was used as the solvent and hexamethylbenzene as an internal standard. LA polymerization for all entries were the same: 100 equiv. LA monomers, heating for 20 h in 100 ^oC. The temperature for LO polymerization was 25 ^oC for all entries.

DSC measurement

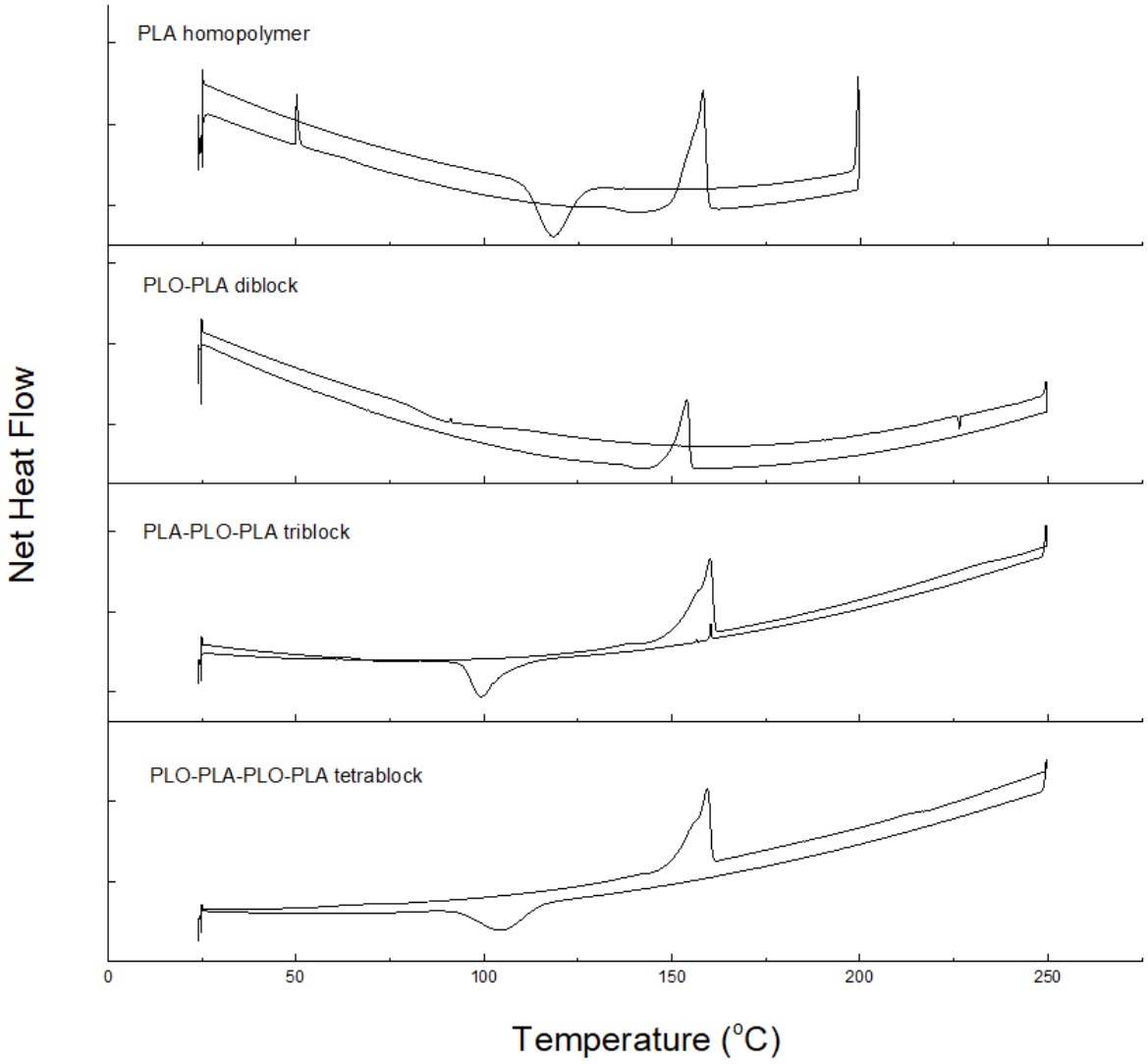

Figure 4.D12. DSC measurement of PLA homopolymer and diblock, triblock and tetrablock copolymers

Table 4.D2. Glass transition temperature of the copolymers

Polymer	Glass transition temperature (°C)
PLA homopolymer	158
PLO-PLA diblock	153
PLO-PLA-PLO triblock	160
PLO-PLA-PLO-PLA tetrablock	159

Small Angle X-ray Scattering (SAXs) Measurements

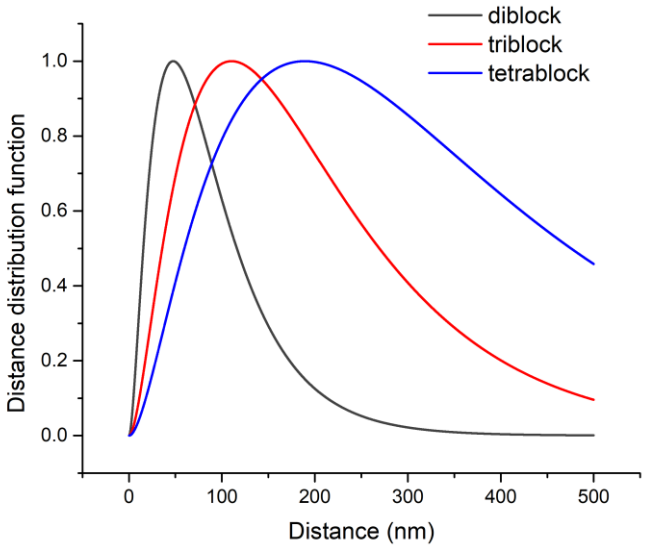

Figure 4.D13. Self-assembly domain radius distribution of the diblock, triblock and tetrablock copolymers.

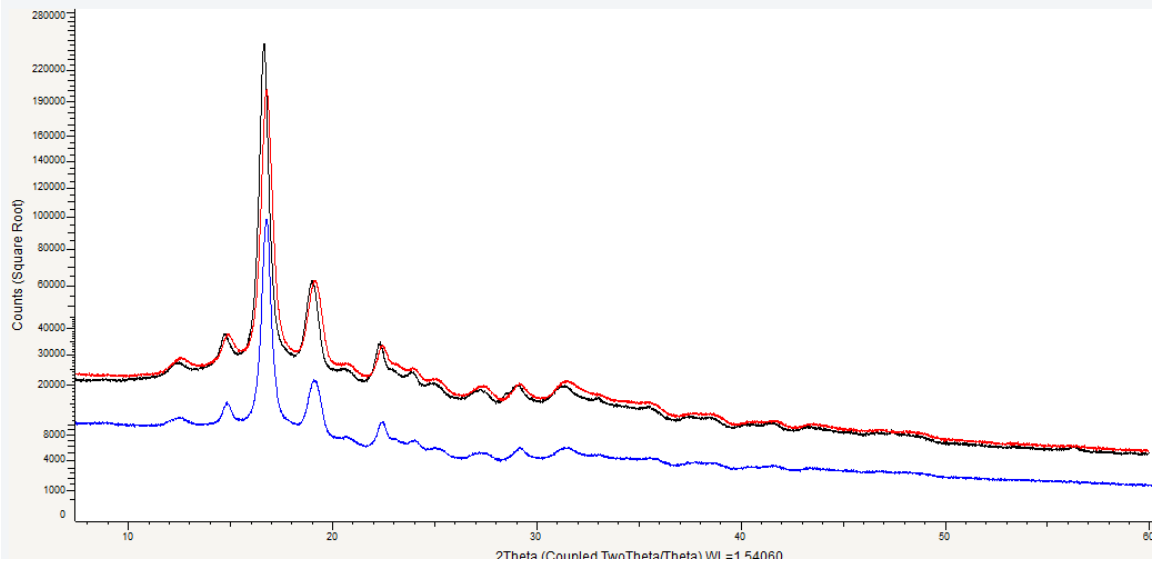

Figure 4.D14. Screenshot of the SAXS pattern.

4.6. References

1. Meier, M. A. R.; Metzger, J. O.; Schubert, U. S., Plant oil renewable resources as green alternatives in polymer science. *Chem. Soc. Rev.* **2007,** *36*, 1788-1802.

2. Grignard, B.; Gennen, S.; Jérôme, C.; Kleij, A. W.; Detrembleur, C., Advances in the use of CO2 as a renewable feedstock for the synthesis of polymers. *Chem. Soc. Rev.* **2019,** *48*, 4466-4514.

3. Platel, R. H.; Hodgson, L. M.; Williams, C. K., Biocompatible Initiators for Lactide Polymerization. *Polymer Reviews* **2008,** *48*, 11-63.

4. Nair, L. S.; Laurencin, C. T., Biodegradable polymers as biomaterials. *Progress in Polymer Science* **2007,** *32*, 762-798.

5. Borrelle, S. B.; Ringma, J.; Law, K. L.; Monnahan, C. C.; Lebreton, L.; McGivern, A.; Murphy, E.; Jambeck, J.; Leonard, G. H.; Hilleary, M. A.; Eriksen, M.; Possingham, H. P.; De Frond, H.; Gerber, L. R.; Polidoro, B.; Tahir, A.; Bernard, M.; Mallos, N.; Barnes, M.; Rochman, C. M., Predicted growth in plastic waste exceeds efforts to mitigate plastic pollution. *Science* **2020,** *369*, 1515.

6. Lau, W. W. Y.; Shiran, Y.; Bailey, R. M.; Cook, E.; Stuchtey, M. R.; Koskella, J.; Velis, C. A.; Godfrey, L.; Boucher, J.; Murphy, M. B.; Thompson, R. C.; Jankowska, E.; Castillo Castillo, A.; Pilditch, T. D.; Dixon, B.; Koerselman, L.; Kosior, E.; Favoino, E.; Gutberlet, J.; Baulch, S.; Atreya, M. E.; Fischer, D.; He, K. K.; Petit, M. M.; Sumaila, U. R.; Neil, E.; Bernhofen, M. V.; Lawrence, K.; Palardy, J. E., Evaluating scenarios toward zero plastic pollution. *Science* **2020,** *369*, 1455.

7. Chen, G.-Q.; Patel, M. K., Plastics Derived from Biological Sources: Present and Future: A Technical and Environmental Review. *Chemical Reviews* **2012,** *112*, 2082-2099.

8. Dechy-Cabaret, O.; Martin-Vaca, B.; Bourissou, D., Controlled Ring-Opening Polymerization of Lactide and Glycolide. *Chemical Reviews* **2004,** *104*, 6147-6176.

9. Ciriminna, R.; Lomeli-Rodriguez, M.; Demma Carà, P.; Lopez-Sanchez, J. A.; Pagliaro, M., Limonene: a versatile chemical of the bioeconomy. *Chem. Commun.* **2014,** *50*, 15288-15296.

10. Karr, L. L.; Coats, J. R., リモネンの殺虫作用. *Journal of Pesticide Science* **1988,** *13*, 287-290.

11. Kim, Y. W.; Kim, M. J.; Chung, B. Y.; Bang, D. Y.; Lim, S. K.; Choi, S. M.; Lim, D. S.; Cho, M. C.; Yoon, K.; Kim, H. S.; Kim, K. B.; Kim, Y. S.; Kwack, S. J.; Lee, B.-M., Safety Evaluation And Risk Assessment Of d-Limonene. *Journal of Toxicology and Environmental Health, Part B* **2013,** *16*, 17-38.

12. Pourbafrani, M.; Forgács, G.; Horváth, I. S.; Niklasson, C.; Taherzadeh, M. J., Production of biofuels, limonene and pectin from citrus wastes. *Bioresource Technology* **2010,** *101*, 4246-4250.

13. Thomas, A. F.; Bessière, Y., Limonene. *Natural Product Reports* **1989,** *6*, 291-309.

14. Jongedijk, E.; Cankar, K.; Buchhaupt, M.; Schrader, J.; Bouwmeester, H.; Beekwilder, J., Biotechnological production of limonene in microorganisms. *Applied Microbiology and Biotechnology* **2016,** *100*, 2927-2938.

15. Della Monica, F.; Kleij, A. W., From terpenes to sustainable and functional polymers. *Polym. Chem.* **2020,** *11*, 5109-5127.

16. Byrne, C. M.; Allen, S. D.; Lobkovsky, E. B.; Coates, G. W., Alternating Copolymerization of Limonene Oxide and Carbon Dioxide. *J. Am. Chem. Soc.* **2004,** *126*, 11404-11405.

17. Li, C.; van Berkel, S.; Sablong, R. J.; Koning, C. E., Post-functionalization of fully biobased poly(limonene carbonate)s: Synthesis, characterization and coating evaluation. *European Polymer Journal* **2016,** *85*, 466-477.

18. Li, C.; Sablong, R. J.; Koning, C. E., Synthesis and characterization of fully-biobased α,ω-dihydroxyl poly(limonene carbonate)s and their initial evaluation in coating applications. *European Polymer Journal* **2015,** *67*, 449-458.

19. Stößer, T.; Li, C.; Unruangsri, J.; Saini, P. K.; Sablong, R. J.; Meier, M. A. R.; Williams, C. K.; Koning, C., Bio-derived polymers for coating applications: comparing poly(limonene carbonate) and poly(cyclohexadiene carbonate). *Polymer Chemistry* **2017,** *8*, 6099-6105.

20. Auriemma, F.; De Rosa, C.; Di Caprio, M. R.; Di Girolamo, R.; Ellis, W. C.; Coates, G. W., Stereocomplexed Poly(Limonene Carbonate): A Unique Example of the Cocrystallization of Amorphous Enantiomeric Polymers. *Angewandte Chemie International Edition* **2015,** *54*, 1215-1218.

21. Peña Carrodeguas, L.; González-Fabra, J.; Castro-Gómez, F.; Bo, C.; Kleij, A. W., AlIII-Catalysed Formation of Poly(limonene)carbonate: DFT Analysis of the Origin of Stereoregularity. *Chemistry – A European Journal* **2015,** *21*, 6115-6122.

22. Auriemma, F.; De Rosa, C.; Di Caprio, M. R.; Di Girolamo, R.; Coates, G. W., Crystallization of Alternating Limonene Oxide/Carbon Dioxide Copolymers:

Determination of the Crystal Structure of Stereocomplex Poly(limonene carbonate). *Macromolecules* **2015,** *48*, 2534-2550.

23. Aikins, J. A.; Williams, F., Radiation-Induced Cationic Polymerization of Limonene Oxide, α-Pinene Oxide, and β-Pinene Oxide. In *Ring-Opening Polymerization*, American Chemical Society: 1985; Vol. 286, pp 335-359.

24. Sessini, V.; Palenzuela, M.; Damián, J.; Mosquera, M. E. G., Bio-based polyether from limonene oxide catalytic ROP as green polymeric plasticizer for PLA. *Polymer* **2020,** *210*, 123003.

25. Rösler, A.; Vandermeulen, G. W. M.; Klok, H.-A., Advanced drug delivery devices via self-assembly of amphiphilic block copolymers. *Adv. Drug Deliv. Rev.* **2012,** *64*, 270-279.

26. Albert, J. N. L.; Epps, T. H., Self-assembly of block copolymer thin films. *Mater. Today* **2010,** *13*, 24-33.

27. Li, C.; Johansson, M.; Sablong, R. J.; Koning, C. E., High performance thiol-ene thermosets based on fully bio-based poly(limonene carbonate)s. *European Polymer Journal* **2017,** *96*, 337-349.

28. Hauenstein, O.; Reiter, M.; Agarwal, S.; Rieger, B.; Greiner, A., Bio-based polycarbonate from limonene oxide and CO2 with high molecular weight, excellent thermal resistance, hardness and transparency. *Green Chemistry* **2016,** *18*, 760-770.

29. Carrodeguas, L. P.; Chen, T. T. D.; Gregory, G. L.; Sulley, G. S.; Williams, C. K., High elasticity, chemically recyclable, thermoplastics from bio-based monomers: carbon dioxide, limonene oxide and ε-decalactone. *Green Chemistry* **2020,** *22*, 8298-8307.

30. Neumann, S.; Leitner, L.-C.; Schmalz, H.; Agarwal, S.; Greiner, A., Unlocking the Processability and Recyclability of Biobased Poly(limonene carbonate). *ACS Sustainable Chemistry & Engineering* **2020,** *8*, 6442-6448.

31. Parrino, F.; Fidalgo, A.; Palmisano, L.; Ilharco, L. M.; Pagliaro, M.; Ciriminna, R., Polymers of Limonene Oxide and Carbon Dioxide: Polycarbonates of the Solar Economy. *ACS Omega* **2018,** *3*, 4884-4890.

32. Lai, A.; Hern, Z. C.; Shen, Y.; Dai, R.; Diaconescu, P. L., Metal Complexes for Redox Switching and Control of Reactivity. In *Reference Module in Chemistry, Molecular Sciences and Chemical Engineering*, Elsevier: 2021.

33. Wei, J.; Diaconescu, P. L., Redox-switchable Ring-opening Polymerization with Ferrocene Derivatives. *Acc. Chem. Res.* **2019,** *52*, 415-424.

34. Qi, M.; Dong, Q.; Wang, D.; Byers, J. A., Electrochemically Switchable Ring-Opening Polymerization of Lactide and Cyclohexene Oxide. *J. Am. Chem. Soc.* **2018,** *140*, 5686-5690.

35. Biernesser, A. B.; Delle Chiaie, K. R.; Curley, J. B.; Byers, J. A., Block Copolymerization of Lactide and an Epoxide Facilitated by a Redox Switchable Iron-Based Catalyst. *Angew. Chem. Int. Ed.* **2016,** *55*, 5251–5254.

36. Teator, A. J.; Lastovickova, D. N.; Bielawski, C. W., Switchable Polymerization Catalysts. *Chem. Rev.* **2016,** *116*, 1969-1992.

37. Xu, X.; Luo, G.; Hou, Z.; Diaconescu, P. L.; Luo, Y., Theoretical insight into the redox-switchable activity of group 4 metal complexes for the ring-opening polymerization of ε-caprolactone. *Inorg. Chem. Front.* **2020,** *7*, 961-971.

38. Lai, A.; Hern, Z. C.; Diaconescu, P. L., Switchable Ring-Opening Polymerization by a Ferrocene Supported Aluminum Complex. *ChemCatChem* **2019,** *11*, 4210-4218.

39. Lai, A.; Clifton, J.; Diaconescu, P. L.; Fey, N., Computational mapping of redox-switchable metal complexes based on ferrocene derivatives. *Chem. Commun.* **2019,** *55*,, 7021-7024

40. Dai, R.; Diaconescu, P. L., Investigation of a Zirconium Compound for Redox Switchable Ring Opening Polymerization. *Dalton Trans.* **2019,** *48*, 2996-3002.

41. Dai, R.; Lai, A.; Alexandrova, A. N.; Diaconescu, P. L., Geometry Change in a Series of Zirconium Compounds during Lactide Ring-Opening Polymerization. *Organometallics* **2018,** *37*, 4040-4047.

42. Abubekerov, M.; Wei, J.; Swartz, K. R.; Xie, Z.; Pei, Q.; Diaconescu, P. L., Preparation of multiblock copolymers via step-wise addition of l-lactide and trimethylene carbonate. *Chem. Sci.* **2018,** *9*, 2168-2178.

43. Abubekerov, M.; Vlček, V.; Wei, J.; Miehlich, M. E.; Quan, S. M.; Meyer, K.; Neuhauser, D.; Diaconescu, P. L., Exploring Oxidation State-Dependent Selectivity in Polymerization of Cyclic Esters and Carbonates with Zinc(II) Complexes. *iScience* **2018,** *7*, 120-131.

44. Wei, J.; Riffel, M. N.; Diaconescu, P. L., Redox Control of Aluminum Ring-Opening Polymerization: A Combined Experimental and DFT Investigation. *Macromolecules* **2017,** *50*, 1847-1861.

45. Quan, S. M.; Wei, J.; Diaconescu, P. L., Mechanistic Studies of Redox-Switchable Copolymerization of Lactide and Cyclohexene Oxide by a Zirconium Complex. *Organometallics* **2017,** *36*, 4451-4457.

46. Lowe, M. Y.; Shu, S.; Quan, S. M.; Diaconescu, P. L., Investigation of redox switchable titanium and zirconium catalysts for the ring opening polymerization of cyclic esters and epoxides. *Inorg. Chem. Front.* **2017,** *4*, 1798-1805.

47. Quan, S. M.; Wang, X.; Zhang, R.; Diaconescu, P. L., Redox Switchable Copolymerization of Cyclic Esters and Epoxides by a Zirconium Complex. *Macromolecules* **2016,** *49*, 6768-6778.

48. Quan, S. M.; Diaconescu, P. L., High activity of an indium alkoxide complex toward ring opening polymerization of cyclic esters. *Chem. Commun.* **2015,** *51*, 9643 - 9646.

49. Wang, X.; Thevenon, A.; Brosmer, J. L.; Yu, I.; Khan, S. I.; Mehrkhodavandi, P.; Diaconescu, P. L., Redox Control of Group 4 Metal Ring-Opening Polymerization Activity toward l-Lactide and ε-Caprolactone. *J. Am. Chem. Soc.* **2014,** *136*, 11264-11267.

50. Broderick, E. M.; Guo, N.; Wu, T.; Vogel, C. S.; Xu, C.; Sutter, J.; Miller, J. T.; Meyer, K.; Cantat, T.; Diaconescu, P. L., Redox control of a polymerization catalyst by changing the oxidation state of the metal center. *Chem. Commun.* **2011,** *47*, 9897-9899.

51. Broderick, E. M.; Guo, N.; Vogel, C. S.; Xu, C.; Sutter, J.; Miller, J. T.; Meyer, K.; Mehrkhodavandi, P.; Diaconescu, P. L., Redox Control of a Ring-Opening Polymerization Catalyst. *J. Am. Chem. Soc.* **2011,** *133*, 9278–9281.

52. Dhar, D.; Yee, G. M.; Spaeth, A. D.; Boyce, D. W.; Zhang, H.; Dereli, B.; Cramer, C. J.; Tolman, W. B., Perturbing the Copper(III)–Hydroxide Unit through Ligand Structural Variation. *J. Am. Chem. Soc.* **2016,** *138*, 356-368.

Chapter 5. Post-functionalization of LA-CHDO copolymers to enhance the mechanical properties

5.1. Introduction

Polyester and polyether are two classes of synthetic polymers that draw the attention of scientists for a long time.[1-4] Both of them are biodegradable, and can help to reduce the worldwide plastic waste and mitigate the "white pollution" issue.[5-13] However, both of them have certain limitations when used as a substituent of the daily plastic. Polyester is usually described as a hard, brittle and hydrophobic material,[14-18] while polyether is soft and hydrophilic in some cases.[19-21] One potential solution is to tune the properties when preparing the polyester-*co*-polyether copolymers, to finely adjust the elasticity, hydrophilicity and other properties to meet the specific requirement of the material.[22, 23] The copolymerization method for precisely controlling the composition and property of polyester-*co*-polyether has been widely studied during the past decade.[24-26]

Redox switchable polymerization is a promising synthetic method for ring-opening copolymerization of cyclic lactones and epoxides. Invented in 2006, the method was well studied and many redox switchable complexes have been developed by our group.[27-40] The Zr, Ti or Al based precatalysts bearing a ferrocene unit in the ligand backbone can be oxidized and reduced back *in situ* (Scheme 1a), and demonstrate different catalytic behaviors in the reduced and oxidized states.[30, 34, 38] The synthesis and redox switchable catalytic behavior of a Zr complex, (salfen)Zr(O^iPr)$_2$ (salfen = N,N'-bis(2,4-di-tert-butylphenoxy)-1,1'-ferrocenediimine) was investigated and published by our group (Scheme 5.1a).[30, 40] In its reduced form, the complex can polymerize lactone monomers, such as l-lactide (LA), ε-caprolactone and δ-valerolactone, while in the oxidized form, the complex can polymerize epoxide monomers such as cyclohexene oxide

(CHO) and propylene oxide. This was proved to be a successful redox switchable copolymerization system, where diblock copolymers and a triblock copolymer PLA-PCHO-PLA (poly(lactide)-*co*-poly(cyclohexene oxide)-*co*-poly(lactide)) were prepared.

LA is well-known as a promising lactone monomer because it is bio-renewable and compatible to human beings.[41-43] However, the PLA is very brittle, making it not versatile for many applications.[44, 45] Given that LA can be polymerized in our redox switchable copolymerization system, we would like to see if it is possible to tune the mechanical property of PLA by making a copolymer with polyether.[46] Apart from copolymerization, post-functionalization is another possible approach, since there have been cases where post-functionalization can alter the mechanical property of polymers.[47-49] Therefore, we chose cyclohexadiene oxide (CHDO, Scheme 5.1b) as the epoxide monomer, which is an unsaturated derivative of CHO. The unsaturated bond in CHDO can be used for post-functionalization to further tune the mechanical property of the copolymer. Here we report the first CHDO-LA block copolymerization using the redox switchable method (Scheme 5.1b), along with the post-functionalization to study how those reactions would affect the mechanical property of the polymer.

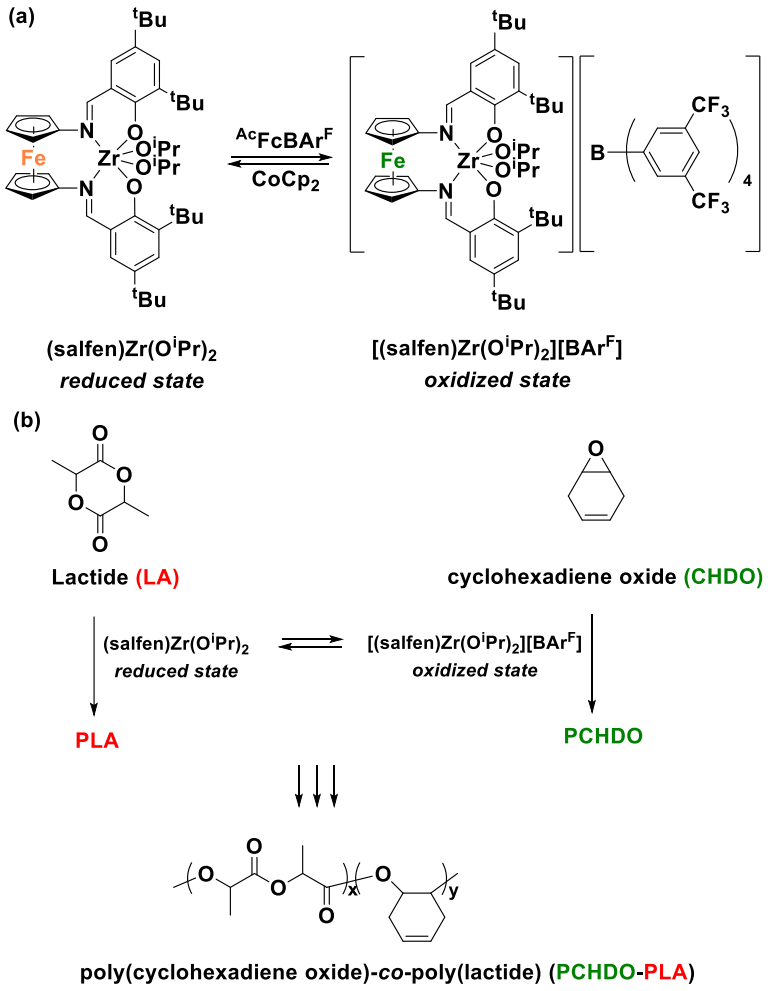

Scheme 5.1. (a) Redox switch of (salfen)Zr(O^iPr)$_2$ (b) LA and CHDO monomers used in this study, and the flow chart of block copolymer preparation using redox switchable copolymerization in this work.

5.2. Results and Discussion

CHDO homopolymerization

CHDO was synthesized from cyclohexadiene, following a published procedure.[50] The homopolymerization of CHDO was tested. (salfen)Zr(O^iPr)$_2$, and its *in situ* oxidized form,

[(salfen)Zr(O^iPr)$_2$][BAr^F] (BAr^F = tetrakis(3,5-bis(trifluoromethyl)-phenyl)borate) were both tested as the precatalyst for the homopolymerization. CHDO can only be polymerized under the oxidized state of the precatalyst, with a 99% conversion (Table 5.E2, entry 2). Then the kinetics of the polymerization was monitored by NMR and size exclusive chromatography (SEC), with the conversion and molar mass data listed in Table 5.E3. The result showed that at 60 min the conversion already reached 90.6% (Table 5.E3, entry 4). Therefore, a one-hour reaction time should be enough for the homopolymerization.

CHDO and LA copolymerization

Since CHDO can be polymerized with the oxidized form of precatalyst, and LA can be polymerized with the reduced form of the precatalyst, we tried to combine the two reactions together to prepare copolymers in a redox switchable manner. First, the PCHDO-PLA diblock copolymer was prepared. The precatalyst (salfen)Zr(O^iPr)$_2$ was first added to a Schlenk tube in its reduced form, then LA was added to construct a PLA block. 1 equiv oxidant, $^{Ac}FcBAr^F$, was added to oxidize the catalyst *in situ*, followed by the addition of CHDO monomers to construct the PCHDO block. A real-time monitor was performed by taking a reaction aliquot after the preparation of each polymer block. The molar mass of each block was put in Table 5.1, entry 1. A polymer formula $CHDO_{69}$- LA_{40} can be derived using the molar mass of each block divided by the molecular weight of the corresponding monomer. SEC traces (Figure 5.E15) and DOSY NMR (Figure 5.E6) confirmed that it is a copolymer.

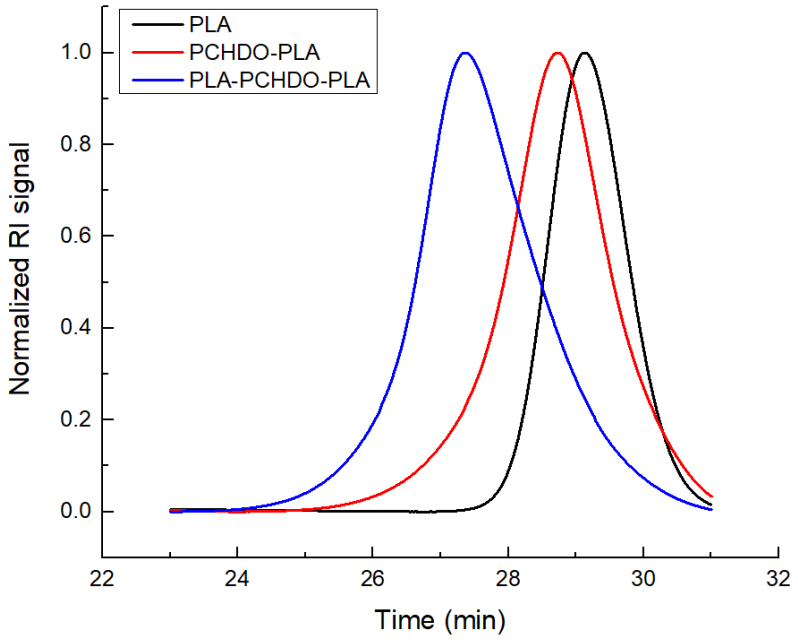

Figure 5.1. The real-time monitor SEC traces of the PLA-PCHDO-PLA triblock copolymer. The molar mass increased as new blocks were added.

Table 5.1. Real-time monitor of the diblock and triblock copolymers [a]

Entry	Copolymer class	1st block Mn (kDa) [b]	2nd block Mn (kDa)	3rd block Mn (kDa)	Total Mn (kDa)	Đ	Copolymer formula [c]
1	PCHDO-PLA	5.7	6.6	--	12.3	1.2	LA_{40}-$CHDO_{69}$
2	PLA-PCHDO-PLA	4.2	3.8	4.1	12.1	1.3	LA_{29}-$CHDO_{39}$-LA_{30}
3	PCHDO-PLA-PCHDO	9.2	4.6	2.4	16.2	1.5	$CHDO_{25}$-LA_{32}-$CHDO_{96}$

[a] 100 equiv LA/CHDO monomer was used for preparing each block during the copolymerization.

The polymerization was conducted at 25 ^{o}C for 1 hour with the oxidized form of precatalyst, and at 100 ^{o}C for around 20 h with the reduced form of precatalyst. [b] All the molar mass in this table was derived from SEC. [c] The number of repeating units was calculated from the molar mass of each block, divided by the molecular weight of the corresponding monomer. The triblock copolymers were prepared in a similar way. To prepare the PLA-PCHDO-PLA triblock copolymer, the reduced form of the precatalyst, (salfen)Zr($O^{i}Pr$)$_2$, was firstly used to construct the 1st PLA block, then the catalyst was oxidized to synthesize the PCHDO block, and then it was reduced back to perform the 2nd PLA block polymerization. In the case of preparing the PCHDO-PLA-PCHDO triblock copolymer, the precatalyst was firstly oxidized to [(salfen)Zr($O^{i}Pr$)$_2$][BAr^{F}] *in situ* to polymerize the 1st PCHDO block, following by a reduction for PLA block, then an oxidation for the 2nd PCHDO block. The molar mass real-time monitor data was listed in Table 5.1, entry 2-3 for both triblock copolymers. The SEC traces from the real-time monitor of PLA-PCHDO-PLA triblock copolymer was shown in Figure 5.1, where the traces were all unimodal, suggesting the nature of a copolymer. DOSY NMR (Figure 5.E9) result also confirmed that it was a copolymer.

Post-functionalization of the copolymers

All the copolymers prepared were then post-functionalized with a thiol-ene click reaction. Azobisisobutyronitrile (AIBN) was used as the radical initiator to catalyse the addition of methyl thioglycolate to the C=C double bond in the CHDO units in the copolymer (Scheme 5.2). The reaction was sensitive to oxygen, so air was removed before the reaction started. The reaction was stirred at 75 ^{o}C for 20 hours in THF, followed by a workup in cold methanol. The molar mass of the functionalized copolymer was significantly higher than the corresponding plain copolymer (Table 4). In ^{1}H NMR spectra, the C=C double bond peak disappeared after the post-functionalization, and new peaks formed at the meantime (Figure 5.E13). Both evidences

confirmed the success of the post-functionalization reaction. The post-functionalization rate was then calculated, from the number of units functionalized divided by the number of CHDO units originally in the plain copolymer. In all cases, the post-functionalization rate was higher than 50%.

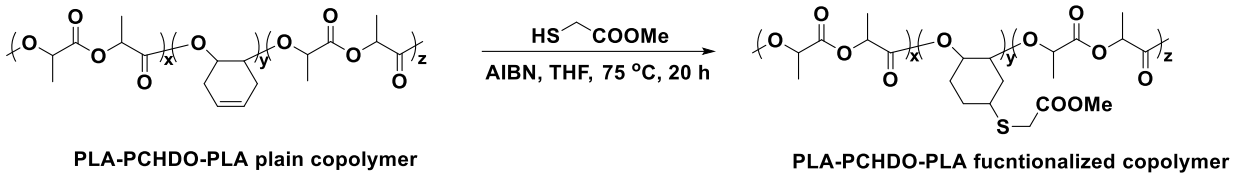

PLA-PCHDO-PLA plain copolymer

PLA-PCHDO-PLA fucntionalized copolymer

Scheme 5.2. Post-functionalization of the PLA-PCHDO-PLA triblock copolymer.

Table 5.2. The molar mass of before and after functionalization of the copolymers, and the functionalization rate. [a]

Entry	Copolymer formula	Mn of plain copolymer (kDa) [b]	Mn of functionalized copolymer (kDa)	Number of units functionalized [c]	Post-functionalization rate [d]
1	$CHDO_{69}$-LA_{40}	12.3	19.4	67	97%
2	LA_{29}-$CHDO_{39}$-LA_{30}	12.1	15.7	34	87%
3	$CHDO_{25}$-LA_{32}-$CHDO_{96}$	16.2	24.7	78	55%

[a] 1:200:10 of AIBN (Azobisisobutyronitrile) to methyl thioglycolate to C=C double bond ratio was used for the reaction. [b] All the molar mass data was derived from SEC measurement. [c] The number of functionalized units was calculated from subtracting the molar mass of the plain copolymer from that of the corresponding functionalized copolymer, then divided by the molecular weight of the methyl thioglycolate. [d] The post-functionalization rate was calculated by the number of functionalized units divided by the number of CHDO units originally in the copolymer.

Table 5.3. The dynamic mechanical analysis (DMA) of the plain and functionalized copolymers.

Entry	Copolymer class	LA unit ratio [a]	Plain (P) or functionalized (F)	Mn (kDa)	Young's modulus (MPa)	Max stress (MPa)	Elongation at break
1	PCHDO-PLA	0.2	P	14.3	9.0	2.8	36%
2			F	22.5	2.2	1.5	55%
3		0.4	P	12.3	1.2	2.5	21%
4			F	19.4	3.1	1.1	30%
5	PLA-PCHDO-PLA	0.2	P	14.8	6.5	1.5	330%
6			F	26.3	4.4	1.4	940%
7		0.4	P	14.5	4.2	2.7	130%
8			F	20.1	4.0	5.0	270%
9	PCHDO-PLA-PCHDO	0.2	P	16.2	5.1	1.3	170%
10			F	24.7	1.9	7.9	650%
11		0.4	P	15.9	2.1	1.6	72%
12			F	21.9	2.0	2.4	110%

a The LA unit ratio is calculated from the total number of LA units in the copolymer divided by the sum of LA units and CHDO units in the copolymer. This is not a mass ratio. The breakdown of the polymer formula and molar mass for individual blocks in each entry is listed in Table 5.E1.

Elasticity measurement of the plain and functionalized copolymer

The elasticity properties were measured by the dynamic mechanical analysis for both the plain and the functionalized copolymers (Table 5.3). All the three classes of copolymers, PCHDO-PLA, PCHDO-PLA-PCHDO and PLA-PCHDO-PLA were measured. To do the study properly, we controlled the molar mass of every plain copolymer into the region of (14.3±2.0) kDa. We also put the LA unit ratio as a variable, since it would be unfair to compare two copolymers from different classes with different LA to CHDO ratio. Within each copolymer class, two copolymers

with LA unit ratio of 0.2 and 0.4 were prepared, so that it became easier to compare the copolymers with the same LA ratio from different classes. Therefore, more copolymers were prepared from the aforementioned redox switchable polymerization method, with slight modification of the monomer feeding. All the copolymers were post-functionalized and characterized by SEC (Table 5.E1). Then every copolymer sample was dissolved in THF and cast into a film for the dynamic mechanical analysis (DMA).

The Young's modulus was calculated, and the maximum stress and elongation at break point were read from the stress strain curve (Figure 5.2 and 5.E20 to 5.E31). All the data was listed in Table 5.3 and several conclusions can be drawn here. First, among all the copolymers, regardless of plain or functionalized, the Young's modulus and maximum stress were all in the same magnitude, and no obvious trends can be observed. However, the elongation percentage at break differed from each entry, and this can represent the difference in toughness (or the amount of energy it can absorb before breaking) between the copolymers.

Second, the functionalized copolymer always had a larger elongation percentage compared to the corresponding plain copolymer, demonstrating that the post-functionalization did alter the elasticity property of the copolymer. Third, within the same copolymer class, lower LA ratio resulted to a larger elongation percentage. This means that in the LA-CHDO copolymer system, the LA is the "rigid monomer" and the CHDO is the "soft monomer".

Last but not least, for the plain copolymers from different classes but with the same LA unit ratio, the elongation at break is always PCHDO-PLA < PCHDO-PLA-PCHDO < PLA-PCHDO-PLA. It seems the diblock copolymer is inherently having a lower elongation percentage than the triblock copolymers, which is similar to a previous study from our group.[46] The difference between the two triblock copolymer classes can be interpreted by the length of a single PCHDO

block. As the CHDO is the "soft monomer", a longer PCHDO block might bring a larger overall elongation percentage. At the same LA unit ratio, the PLA-PCHDO-PLA copolymer has all the CHDO in one block, while the PCHDO-PLA-PCHDO has the CHDO in two blocks, resulting in a shorter single PCHDO block in the latter copolymer.

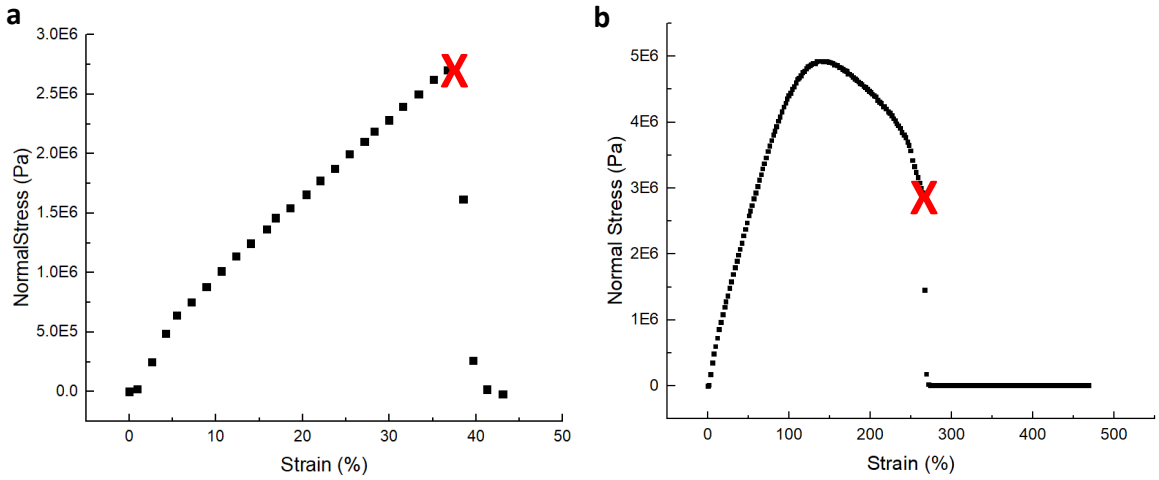

Figure 5.2. The stress strain curves of (a) PLA-PCHDO/0.2LA plain copolymer (Table 5.3, entry 1) and (b) PLA-PCHDO-PLA/0.4LA functionalized copolymer (Table 5.3, entry 8). The red cross marks the break point of the polymer film. The stress strain curves for other copolymers are in the SI.

5.3. Conclusion

The biodegradable copolymers, PCHDO-PLA diblock, PLA-PCHDO-PLA triblock and PCHDO-PLA-PCHDO triblock copolymers were synthesized following a redox switchable copolymerization method. Then the copolymer was post-functionalized by a thiol-ene click reaction. Methyl thioglycolate was added to the CHDO units in the copolymer, and the success of this functionalization was supported by the increase of the polymer molar mass and the C=C

double bond peak diminish from NMR. All plain and functionalized copolymers were characterized by the dynamic mechanical analysis. The elongation percentage at break, or the toughness of the copolymer, is lower in the plain copolymer compared to the corresponding functionalized copolymer, and is lower when the copolymer has a higher LA unit ratio. The general trend of elongation percentage is PCHDO-PLA < PCHDO-PLA-PCHDO < PLA-PCHDO-PLA. This means we can improve the mechanical property of the copolymer by altering the composition of the copolymer and by post-functionalization. Overall, the study will help the biodegradable polyesters and polyethers gain more applications as daily plastic. Further investigations into other post-functionalization methods will be carried out by our group, in the future.

5.4 Experimental Section

General considerations

All experiments were performed in an Mbraun inert gas glovebox or under a dry nitrogen atmosphere using standard Schlenk techniques. Solvents were purified with a two-state solid-state purification system by the method of Grubbs and transferred to the glovebox inside a Schlenk flask without exposure to air. NMR solvents were obtained from Cambridge Isotope Laboratories, degassed, and stored over activated molecular sieves prior to use. ^{1}H NMR spectra were recorded on Bruker 300, Bruker 500, or Bruker 600 spectrometers at room temperature in C_6D_6. Chemical shifts are reported with respect to the residual solvent peaks, 7.16 ppm (C_6D_6) for ^{1}H NMR spectra. CHDO were synthesized from cyclohexadiene following a published procedure [50]and brought into the glovebox without exposure to air. 1,2-difluorobenzene was distilled over CaH_2 and brought into the glovebox without exposing to air. L-lactide (LA) and hexamethylbenzene were recrystallized from THF at least twice before use. $CoCp_2$ were purchased from Sigma-Aldrich and

used as received. ^{Ac}FcBAr^{F} (^{Ac}Fc =acetoferrocenyl, BAr^{F} = tetrakis(3,5-bis(trifluoromethyl)-phenyl)borate) and (salfen)Zr(O^{i}Pr)$_2$ were synthesized following previously published procedures.[30, 51] Molecular weights of polymers were determined by size exclusion chromatography using a GPC-MALS instrument at UCLA. GPC-MALS uses a Shimazu Prominence-i LC 2030C 3D equipped with an autosampler, two MZ Analysentechnik MZ-Gel SDplus LS 5 µm, 300 × 8 mm linear columns, a Wyatt DAWN HELEOS-II, and a Wyatt Optilab T-rEX. The column temperature was set at 40 °C. A flow rate of 0.70 mL/min was used and samples were dissolved in THF. The number average molar mass and dispersity values were found using the known concentration of the sample in THF with the assumption of 100% mass recovery to calculate dn/dc from the DRI signal.

Tensile tests were carried out on a TA RSA3 dynamic mechanical analyzer (DMA) at a strain rate of 0.5 mm s^{-1}. Samples with a measured thickness of 300 µm were cut in 5-mm wide strips with a razor blade and loaded onto the thin film grips. At least three repetitive samples were tested for each formulation.

NMR scale polymerizations with (salfen)Zr(O^{i}Pr)$_2$

Under an inert atmosphere, (salfen)Zr(O^{i}Pr)$_2$ (4 µmol), the monomer, C_6D_6 (0.6 mL), and an internal standard (hexamethylbenzene) were added to a J-Young NMR tube. The reaction mixture was left at room temperature for 5 minutes while being shaken occasionally. The tube was sealed and brought out of the glovebox and heated to the specified temperature with an oil bath. The NMR tube was taken out of the oil bath and analyzed periodically by ^{1}H NMR spectroscopy. When the reaction was done, CH_2Cl_2 was added to the mixture and then the resulting solution was poured into 10 mL of cold methanol to precipitate the polymer. The mixture was centrifuged for 3x5 minutes, decanted, and dried under a reduced pressure to give the final polymer product.

NMR scale polymerizations with [(salfen)Zr(O^iPr)$_2$][BAr^F]

Under an inert atmosphere, (salfen)Zr(O^iPr)$_2$ (4 μmol), C_6D_6 (0.3 mL), and an internal standard (hexamethylbenzene) were added to a J-Young NMR tube. The $^{Ac}FcBAr^F$ solution (0.1 mL, 40 mM in 1,2-difluorobenzene) was added and the NMR tube was shaken for 5 minutes before adding the monomer. The tube was sealed and brought out of the glovebox and left at room temperature. The NMR tube was monitored periodically by ^1H NMR spectroscopy. When the reaction was done, CH_2Cl_2 was added to the mixture and then the resulting solution was poured into 10 mL of cold methanol to precipitate the polymer. The mixture was centrifuged for 3x5 minutes, decanted, and dried under a reduced pressure to give the final polymer product.

Preparation of PLA-PCHDO diblock copolymer

Under an inert atmosphere, (salfen)Zr(O^iPr)$_2$ (16 μmol), LA (100 equiv), C_6D_6 (2.5 mL) and the internal standard (hexamethylbenzene) were added to a 25 mL Schlenk tube. The reaction mixture was left at room temperature to stir for 5 minutes. The tube was sealed and brought out of the glovebox and heated to 100 ^oC with an oil bath. After heating for 20 h, the first block of the copolymer was made, and the tube was brought back into the glovebox. An $^{Ac}FcBAr^F$ solution (0.4 mL, 40 mM in 1,2-difluorobenzene) was added and the Schlenk tube was shaken for 5 min before adding the CHDO (100 equiv). The tube was sealed and brought out of the glovebox, left at room temperature and shaken every 30 minutes. After 1 h reaction time, the polymerization was completed. The solution was poured into 20 mL cold methanol to precipitate the polymer. The mixture was centrifuged for 3x5 minutes, decanted, and dried under a reduced pressure to give the final polymer product. For real-time monitor, a reaction aliquot was taken in the glovebox at the completion of each polymer block. The volume of the aliquot should be carefully measured and the amount of subsequently added reagents should be fixed accordingly.

Preparation of PLA-PCHDO-PLA triblock copolymer

Under an inert atmosphere, (salfen)Zr(O^iPr)$_2$ (16 μmol), LA (100 equiv), C_6D_6 (2.5 mL) and the internal standard (hexamethylbenzene) were added to a 25 mL Schlenk tube. The reaction mixture was left at room temperature to stir for 5 minutes. The tube was sealed and brought out of the glovebox and heated to 100 ^oC with an oil bath. After heating for 20 h, the first block of the copolymer was made, and the tube was brought back into the glovebox. An $^{Ac}FcBAr^F$ solution (0.4 mL, 40 mM in 1,2-difluorobenzene) was added and the Schlenk tube was shaken for 5 min before adding the CHDO (100 equiv). The tube was sealed, left at room temperature, and shaken every 30 minutes. After 1 h reaction time, the polymerization was completed. Then $CoCp_2$ solution (0.4 mL, 40 mM in C_6D_6) was added to the reaction mixture. The tube was shaken for 5 minutes, then another 100 equiv LA was added. The tube was sealed and brought out of the glovebox and heated to 100 ^oC with an oil bath. After heating for 20 h, the third block of the copolymer was made. The solution was poured into 20 mL cold methanol to precipitate the polymer. The mixture was centrifuged for 3x5 minutes, decanted, and dried under a reduced pressure to give the final polymer product. For real-time monitor, a reaction aliquot was taken in the glovebox at the completion of each polymer block. The volume of the aliquot should be carefully measured and the amount of subsequently added reagents should be fixed accordingly.

Preparation of PLA-PCHDO-PLA triblock copolymer

Under an inert atmosphere, (salfen)Zr(O^iPr)$_2$ (16 μmol), C_6D_6 (2.5 mL) and an internal standard (hexamethylbenzene) were added to a 25 mL Schlenk tube. An $^{Ac}FcBAr^F$ solution (0.4 mL, 40 mM in 1,2-difluorobenzene) was added and the Schlenk tube was shaken for 5 min before adding the CHDO (100 equiv). The tube was sealed, left at room temperature, and shaken every 30 minutes. After 1 h reaction time, the polymerization was completed. Then $CoCp_2$ solution (0.4

mL, 40 mM in C_6D_6) was added to the reaction mixture. The tube was shaken for 5 minutes, then another 100 equiv LA was added. The tube was sealed and brought out of the glovebox and heated to 100 ^oC with an oil bath. After heating for 20 h, the second block of the copolymer was made. The tube was brought back into the glovebox. An $^{Ac}FcBAr^F$ solution (0.4 mL, 40 mM in 1,2-difluorobenzene) was added and the Schlenk tube was shaken for 5 min before adding another 100 equiv CHDO. The tube was sealed, left at room temperature, and shaken every 30 minutes. After 1 h reaction time, the polymerization of third block was completed. The solution was poured into 20 mL cold methanol to precipitate the polymer. The mixture was centrifuged for 3x5 minutes, decanted, and dried under a reduced pressure to give the final polymer product. For real-time monitor, a reaction aliquot was taken in the glovebox at the completion of each polymer block. The volume of the aliquot should be carefully measured and the amount of subsequently added reagents should be fixed accordingly.

Post-functionalization of the copolymer

Around 100 mg copolymers were added to 4.0 mL degassed THF in a Schlenk tube. 20 equiv methyl thioglycolate and 0.3 equiv AIBN were added and the reactor was sealed. The reactor was kept at 75^oC and stirred for 20 h. Then the reaction mixture was concentrated and added to cold methanol for precipitation. The resulting polymer was dried under a reduced pressure.

Preparation of polymer film for dynamic mechanical analysis

Completely dried copolymer sample (around 100 mg) was dissolved into THF (2 mL) and stirred to make a transparent solution. About 5 drops of the copolymer solution were applied on a glass slide and spread to a 2*2 cm^2 square, and then wait for air-dry. The procedure was repeated until all the solution was consumed. The polymer film was cut from the glass slide on the next day for dynamic mechanical analysis.

5.5. Appendix E

Table 5.E1. Summary of copolymerization and post-functionalization [a]

Entry	Copolymer type	1st block Mn (kDa) [b]	2nd block Mn (kDa)	3rd block Mn (kDa)	Total Mn (kDa)	Đ	Copolymer formula [c]	LA unit ratio	Post-functionalization Mn (kDa)	Post-functionalization ratio
1	PCHDO-PLA	4.4	9.8	--	14.3	1.3	$CHDO_{102}$-LA_{31}	0.2	22.5	75%
2		5.7	6.6	--	12.3	1.2	$CHDO_{69}$-LA_{40}	0.4	19.4	97%
3	PLA-PCHDO-PLA	(1.7) [d]	(12.4)	3.5	14.8	1.5	LA_{24}-$CHDO_{129}$-$LA1_2$	0.2	26.3	84%
4		4.7	7.4	2.4	14.5	1.4	LA_{17}-$CHDO_{77}$-LA_{33}	0.4	20.1	69%
5		4.2	3.8	4.1	12.1	1.3	LA_{29}-$CHDO_{39}$-LA_{30}	0.6	15.7	87%
6	PCHDO-PLA-PCHDO	9.2	4.6	2.4	16.2	1.5	$CHDO_{25}$-LA_{32}-$CHDO_{96}$	0.2	24.7	55%
7		6.9	7.6	1.4	15.9	1.5	$CHDO_{15}$-LA_{53}-$CHDO_{71}$	0.4	21.9	66%

[a] The polymerization was conducted at 25 ^{o}C for 1 hour with the oxidized form of precatalyst, and at 100 ^{o}C for 20 h with the reduced form of precatalyst. [b] All the molar mass in this table was derived from SEC. [c] the number of repeating units was calculated from the molar mass of each block, divided by the molecular weight of the corresponding monomer. [d] this molar mass data was calculated from ^{1}H NMR, as we could not precipitate the polymer from the reaction mixture and measure with SEC at the low molar mass.

Table 5.E2. CHDO homopolymerization[a] with the reduced or oxidized form of prectalalyst

Entry	Precatalyst	Time	Conversion [b]
1	(salfen)Zr(O^iPr)$_2$	20 h	0%
2	[(salfen)Zr(O^iPr)$_2$][BAr^F]	2 h	99%

[a] 100 equiv CHDO monomer was used in each polymerization. The polymerization was conducted at 100 ^oC with the reduced form of precatalyst, and 25 ^oC with the oxidized form of precatalyst, consistent with our previous publication.[30] [b] The conversion was monitored by ^1H NMR.

Table 5.E3. Kinetics study of CHDO homopolymerization[a]

Entry	Time	Conversion	Mn SEC (kDa) [b]	Mn calcd. (kDa) [c]
1 [d]	35 min	67.1%	--	--
2	40 min	75.0%	10.1	7.4
3	50 min	86.4%	13.1	8.6
4	60 min	90.6%	12.9	9.0
5	70 min	93.6%	13.4	9.3
6	80 min	95.6%	13.7	9.4

[a] 100 equiv CHDO monomer was used in the polymerization. The polymerization was performed at 25 ^oC with the oxidized form of precatalyst. [b] The molar mass derived from SEC. [c] The theoretical molar mass at the corresponding conversion. [d] No polymer sample could be obtained for SEC measurement at this low conversion.

NMR Spectra

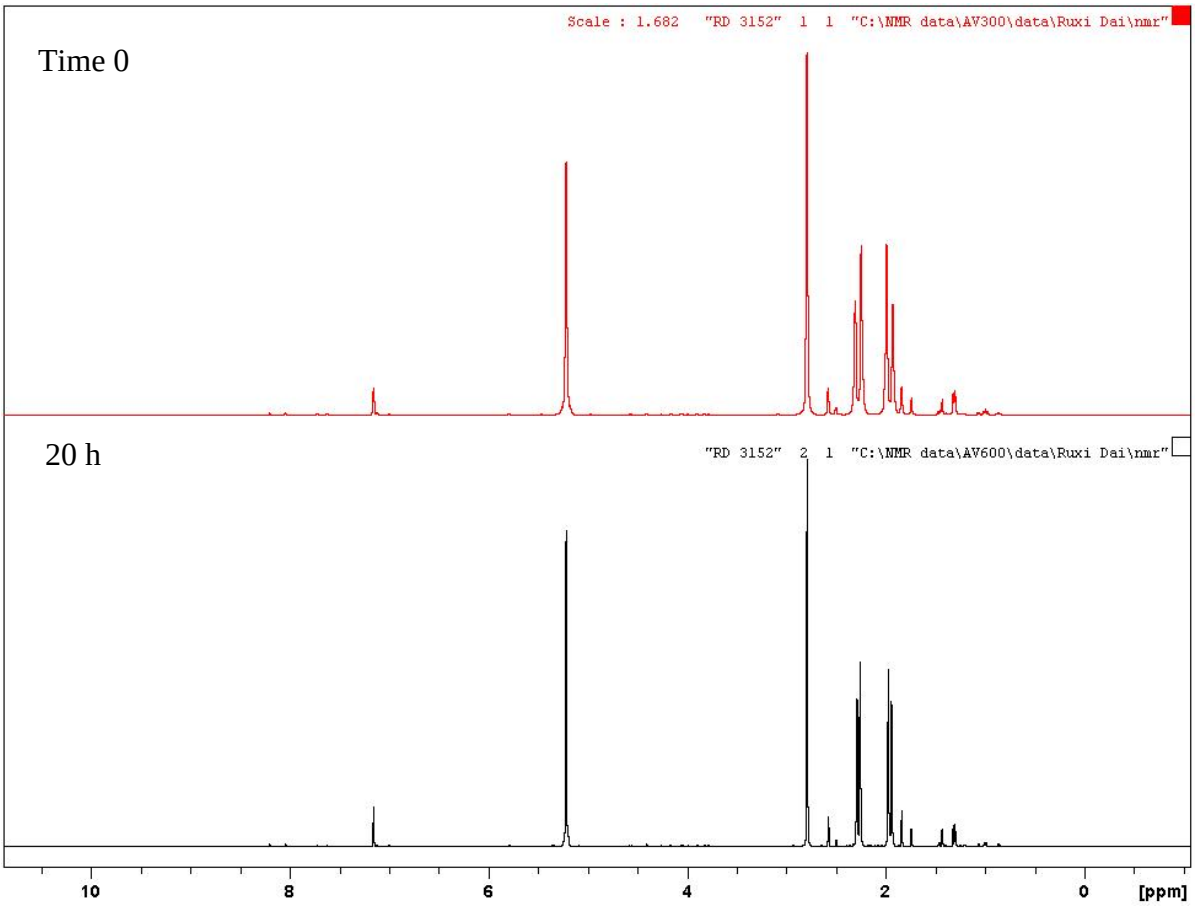

Figure 5.E1. CHDO homopolymerization by (salfen)Zr(O^iPr)$_2$. No conversion was observed after 20 hours.

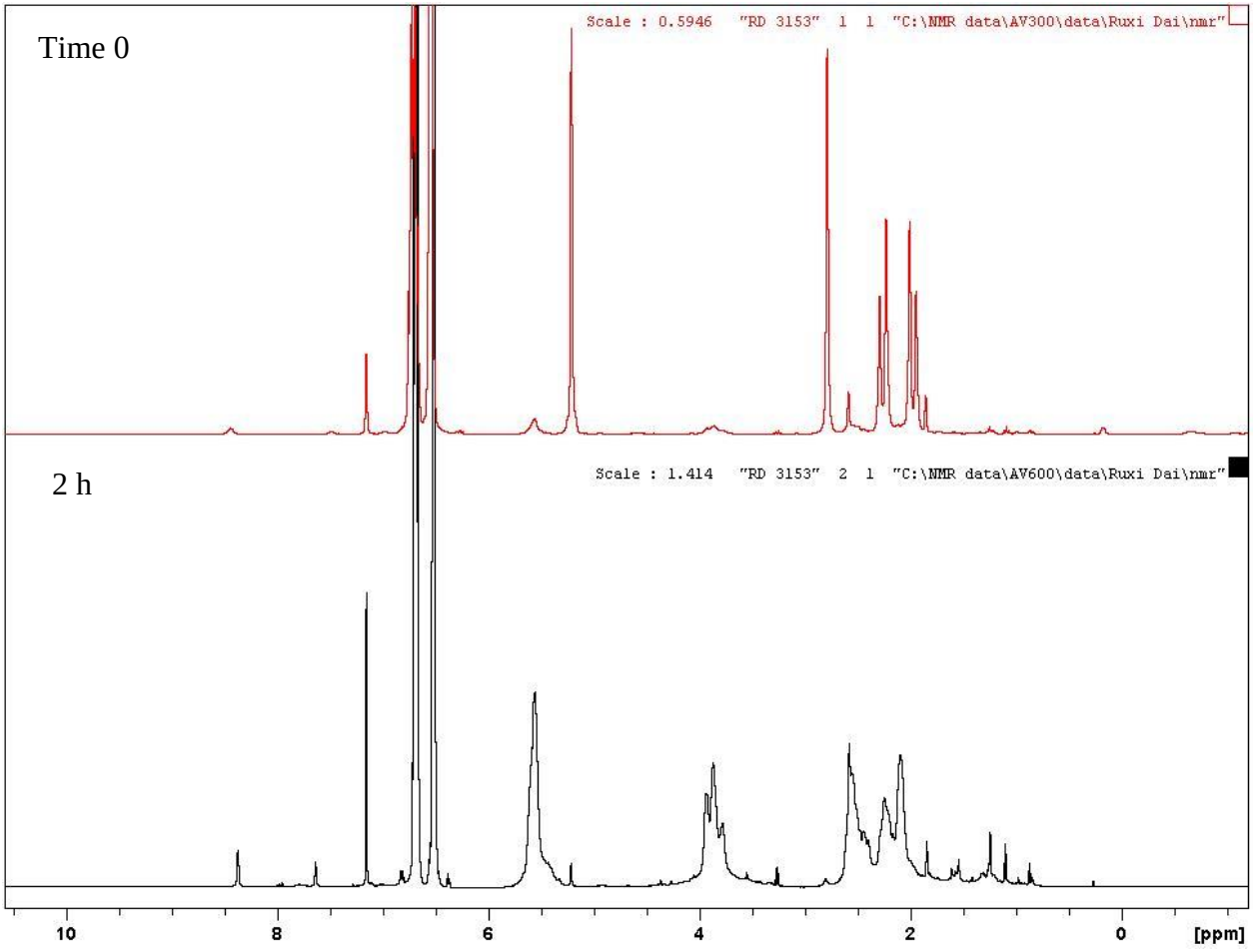

Figure 5.E2. CHDO homopolymerization by [(salfen)Zr(O^iPr)$_2$][BAr^F].

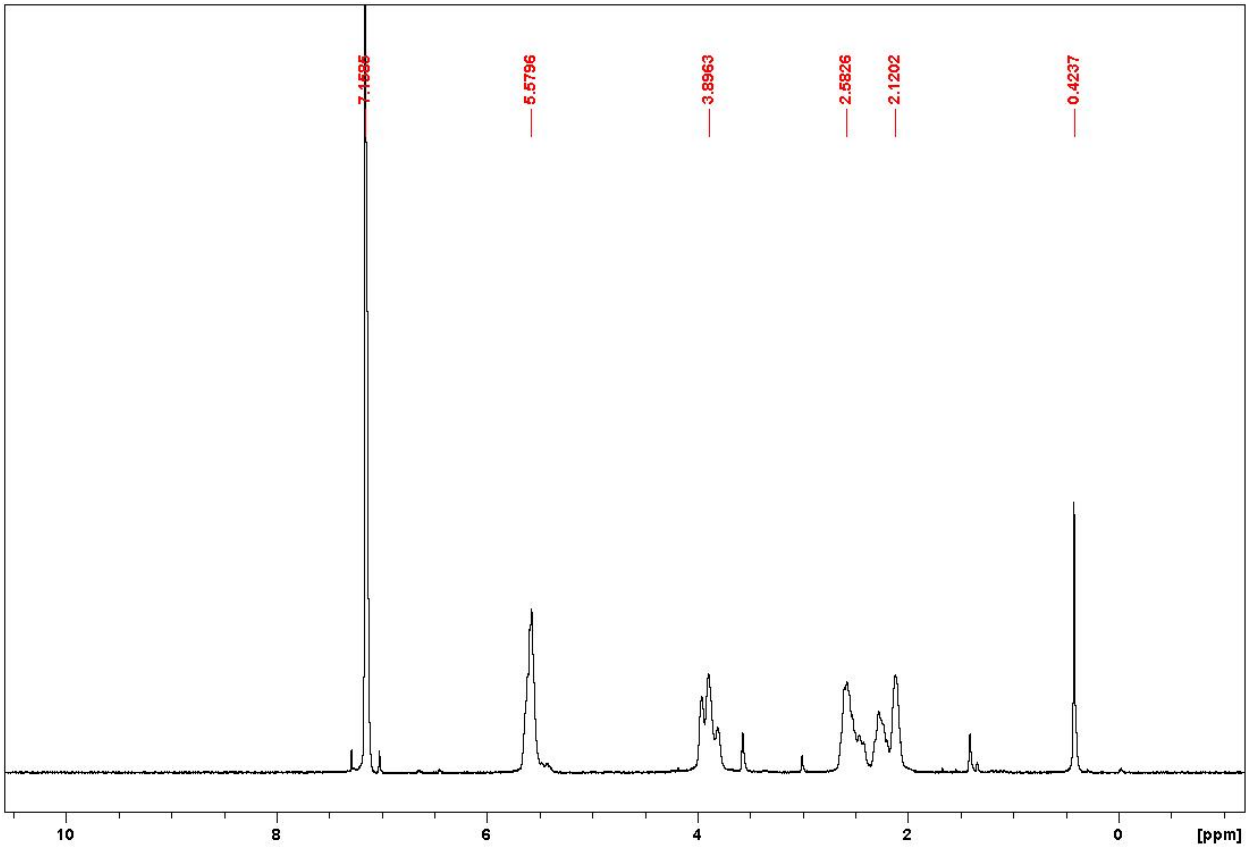

Figure 5.E3. The isolated CHDO homopolymer. ^{1}H NMR (600 MHz, C_6D_6, 25 ^{o}C) of isolated PCHDO homopolymer. δ, ppm: 7.16 (s, C_6D_6), 5.58 (br, PCHDO *H*C=C*H*), 3.90 (br, PCHDO C*H*$_2$), 2.58-2.12 (m, PCHDO ether region).

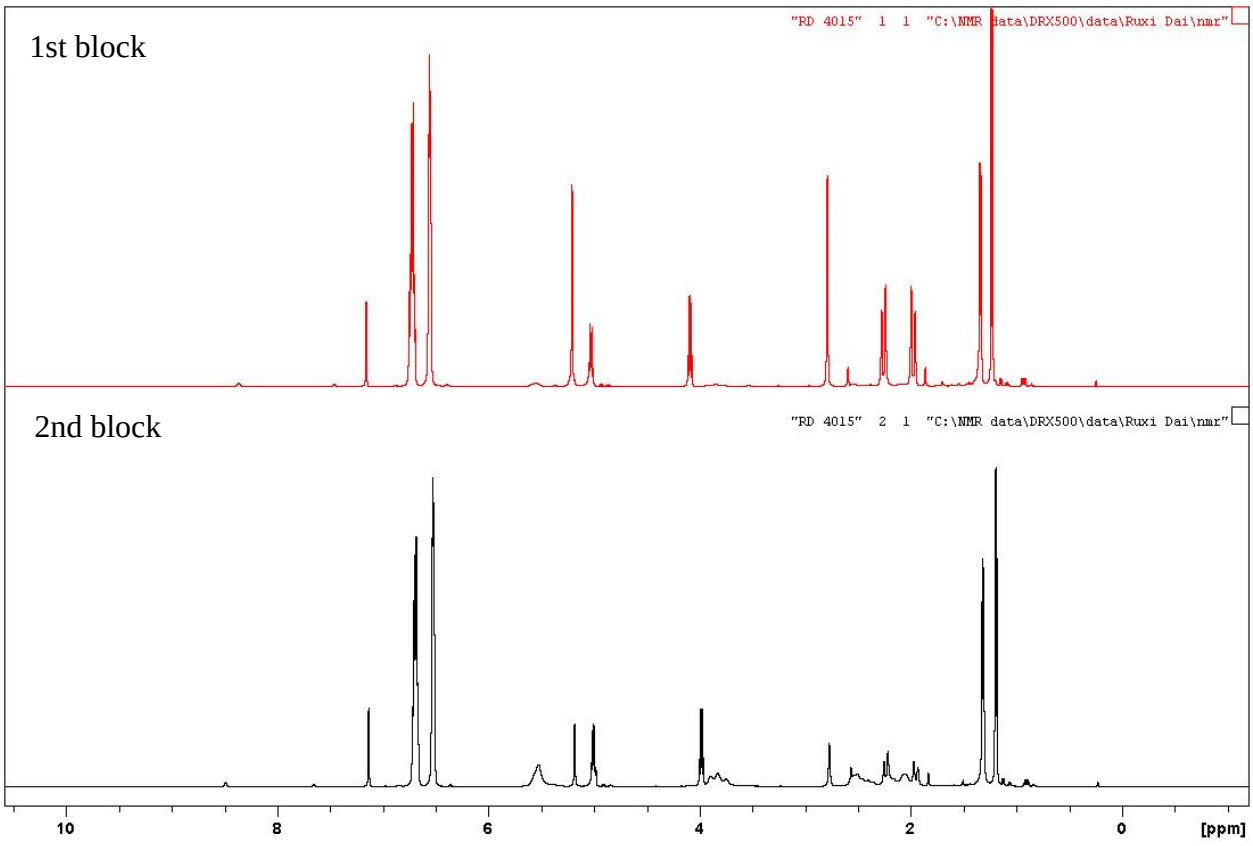

Figure 5.E4. The copolymerization of PLA-PCHDO diblock copolymer.

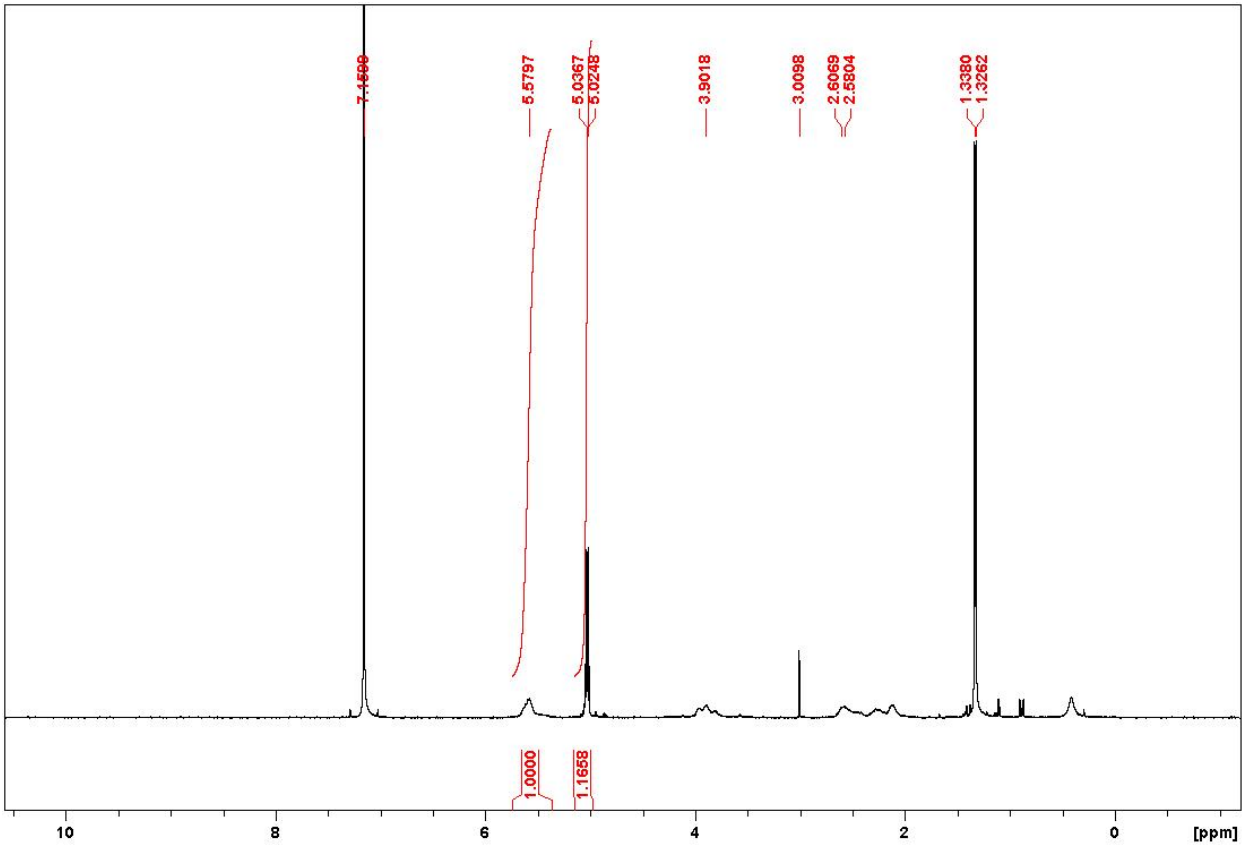

Figure 5.E5. The isolated PLA-PCHDO diblock copolymer. ^{1}H NMR (600 MHz, C_6D_6, 25 ^{o}C) of isolated PLA-PCHDO diblock copolymer. δ, ppm: 7.16 (s, C_6D_6), 5.58 (br, PCHDO *H*C=C*H*), 5.03 (d, PLA), 3.90 (br, PCHDO C*H*$_2$), 2.60 (m, PCHDO ether region), 1.52 (d, PLA).

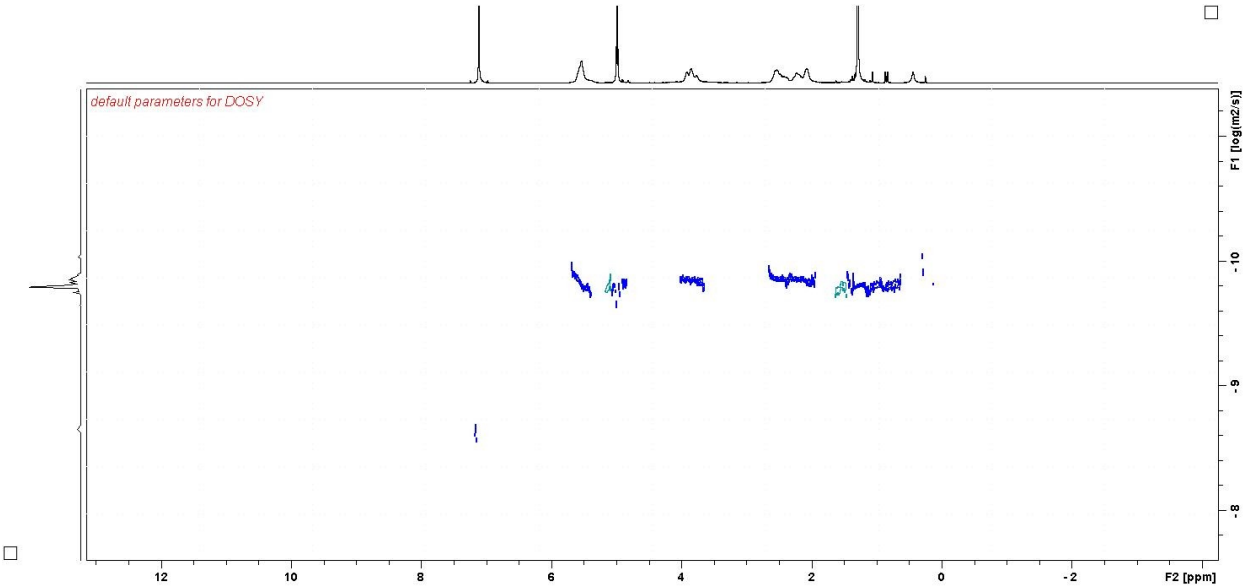

Figure 5.E6. The DOSY NMR of PLA-PCHDO diblock copolymer.

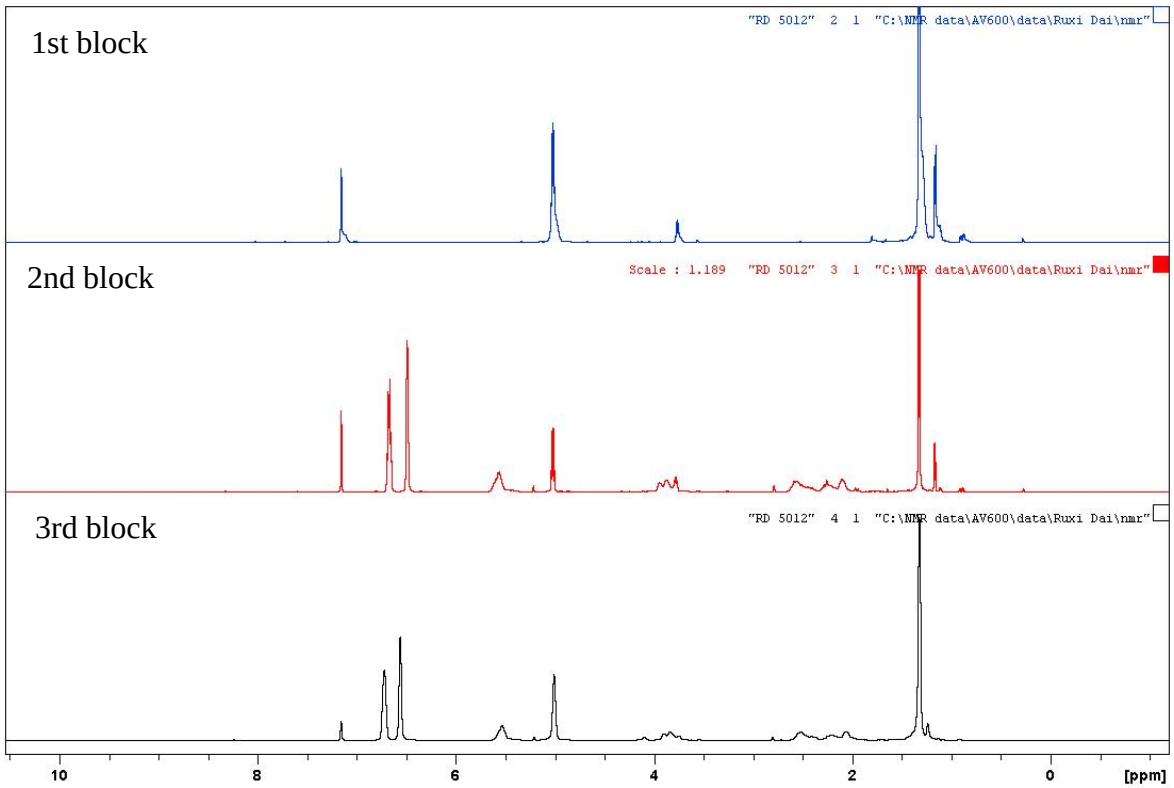

Figure 5.E7. The preparation of PLA-PCHDO-PLA triblock copolymer.

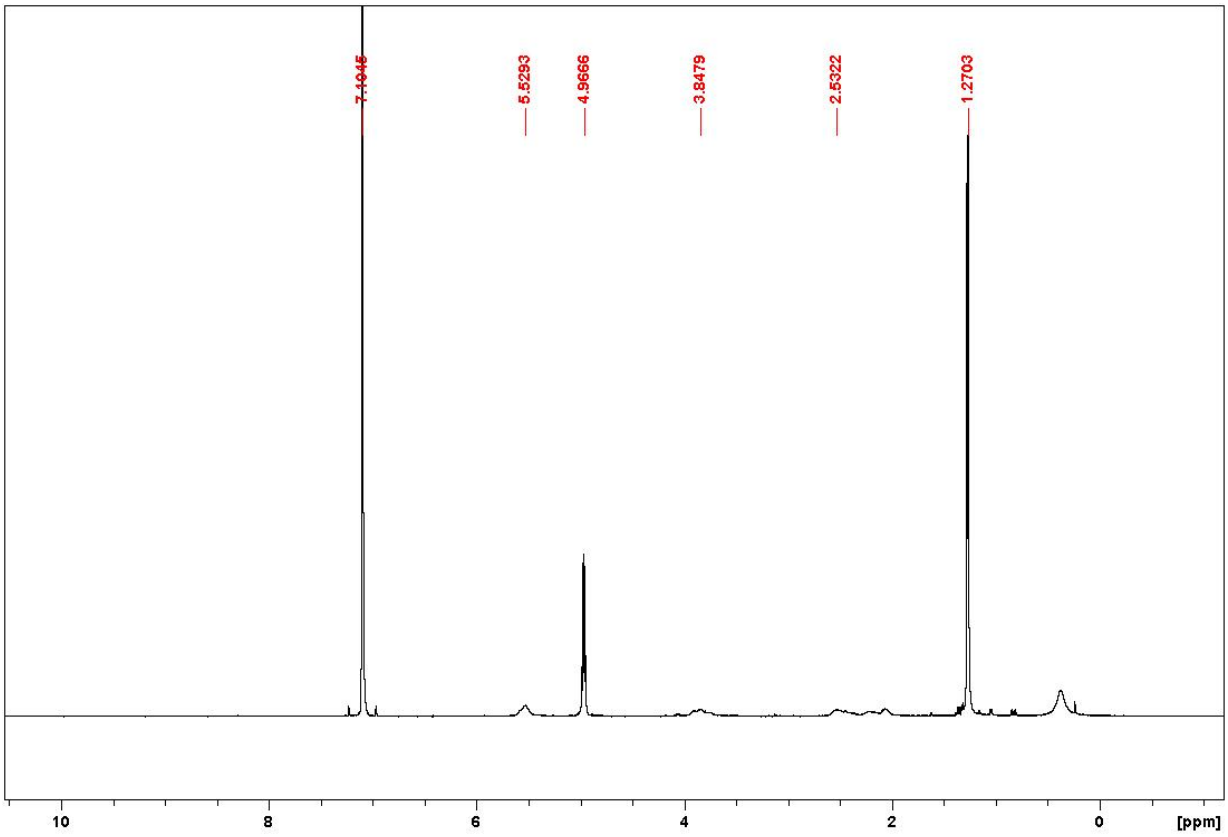

Figure 5.E8. The isolated PLA-PCHDO-PLA triblock copolymer. ^{1}H NMR (600 MHz, C_6D_6, 25 ^{o}C) of isolated PLA-PCHDO diblock copolymer. δ, ppm: 7.10 (s, C_6D_6), 5.53 (br, PCHDO *H*C=C*H*), 4.97 (d, PLA), 3.85 (br, PCHDO C*H*$_2$), 2.53 (m, PCHDO ether region), 1.27 (d, PLA).

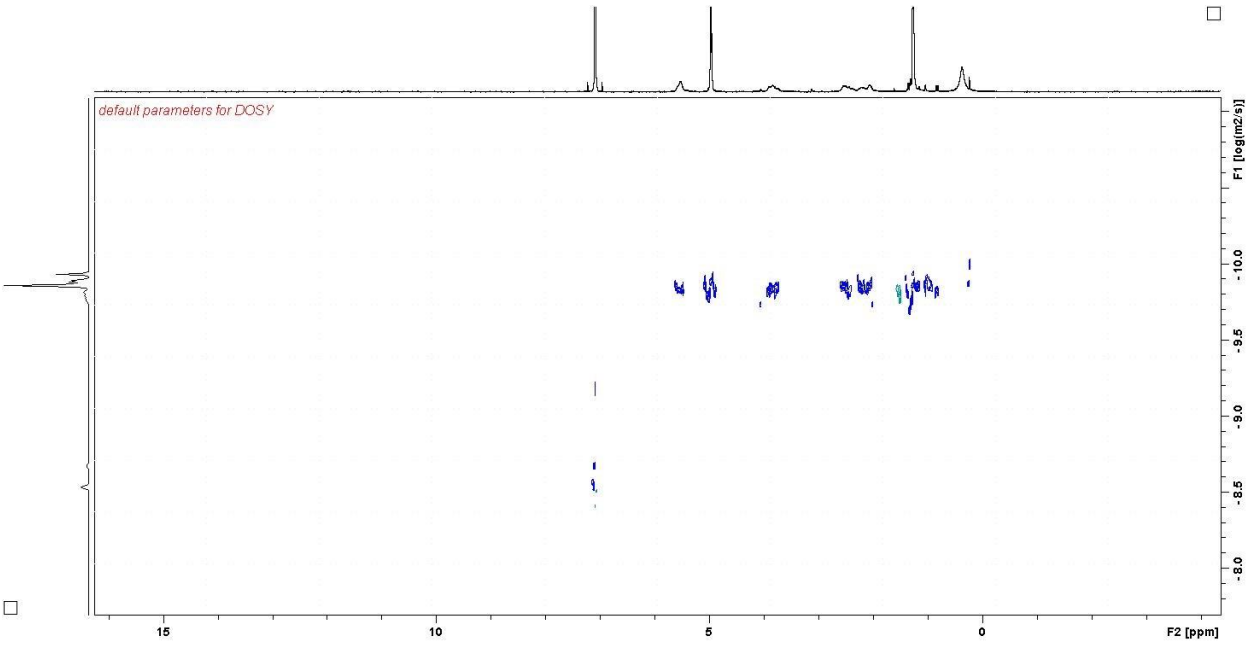

Figure 5.E9. The DOSY NMR of PLA-PCHDO-PLA triblock copolymer.

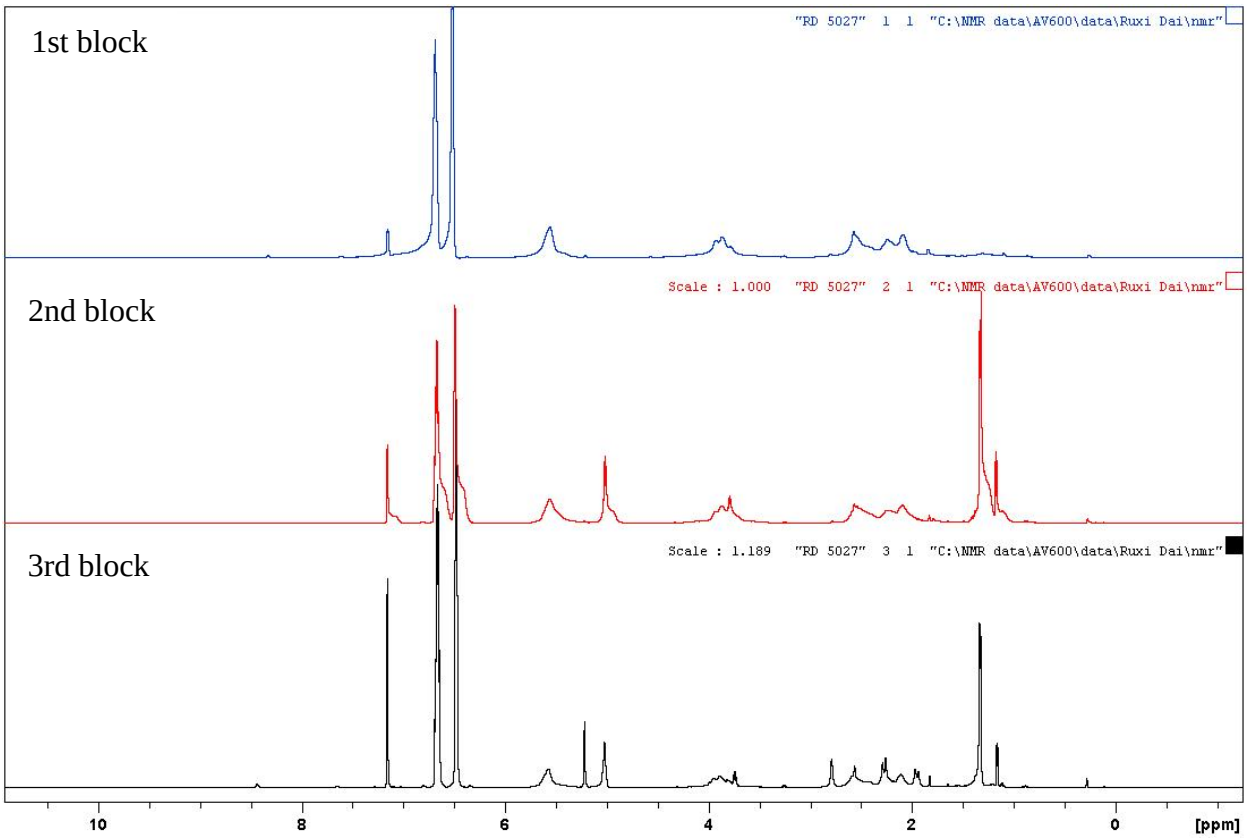

Figure 5.E10. The preparation of PCHDO-PLA-PCHDO triblock copolymer.

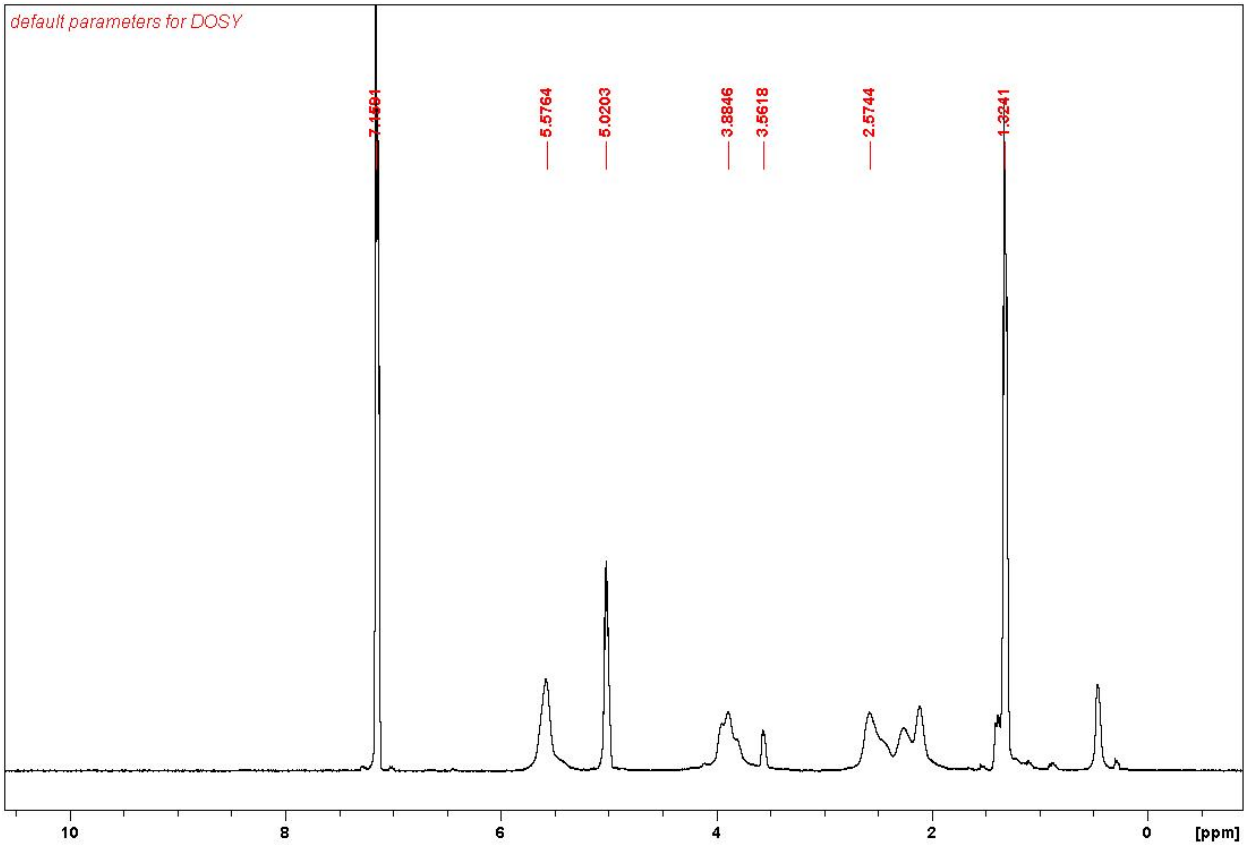

Figure 5.E11. The isolated PCHDO-PLA-PCHDO triblock copolymer. ^{1}H NMR (600 MHz, C_6D_6, 25 ^{o}C) of isolated PLA-PCHDO diblock copolymer. δ, ppm: 7.16 (s, C_6D_6), 5.58 (br, PCHDO *H*C=C*H*), 5.02 (d, PLA), 3.89 (br, PCHDO C*H*$_2$), 2.57 (m, PCHDO ether region), 1.32 (d, PLA).

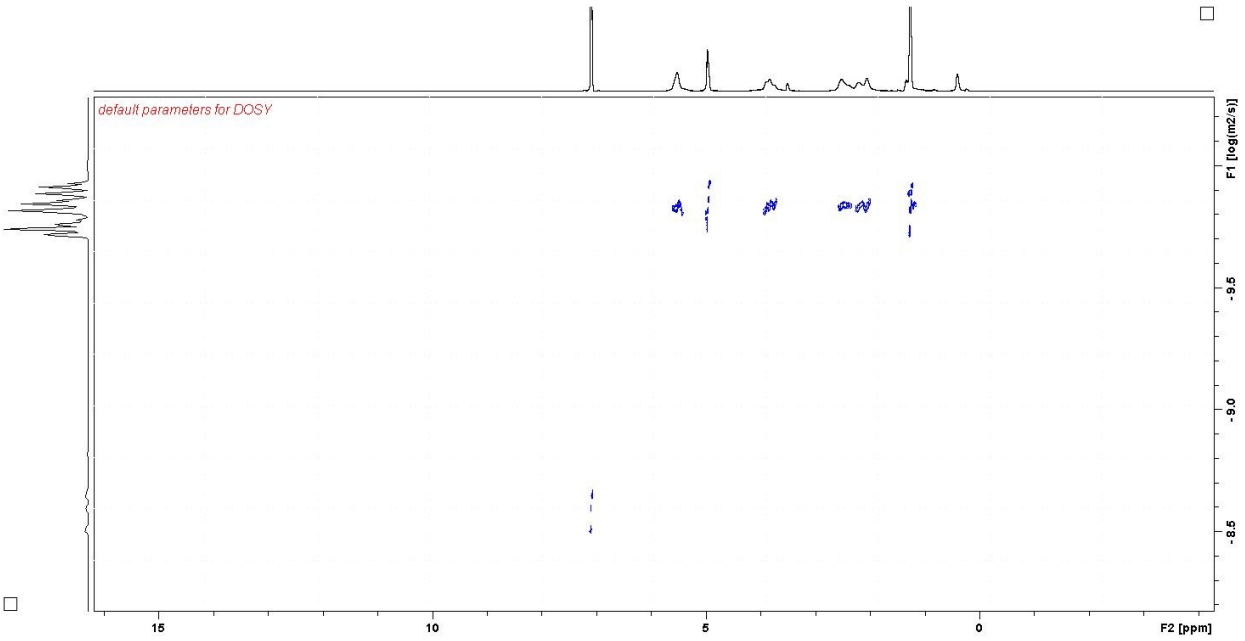

Figure 5.E12. The DOSY NMR of PCHDO-PLA-PCHDO triblock copolymer.

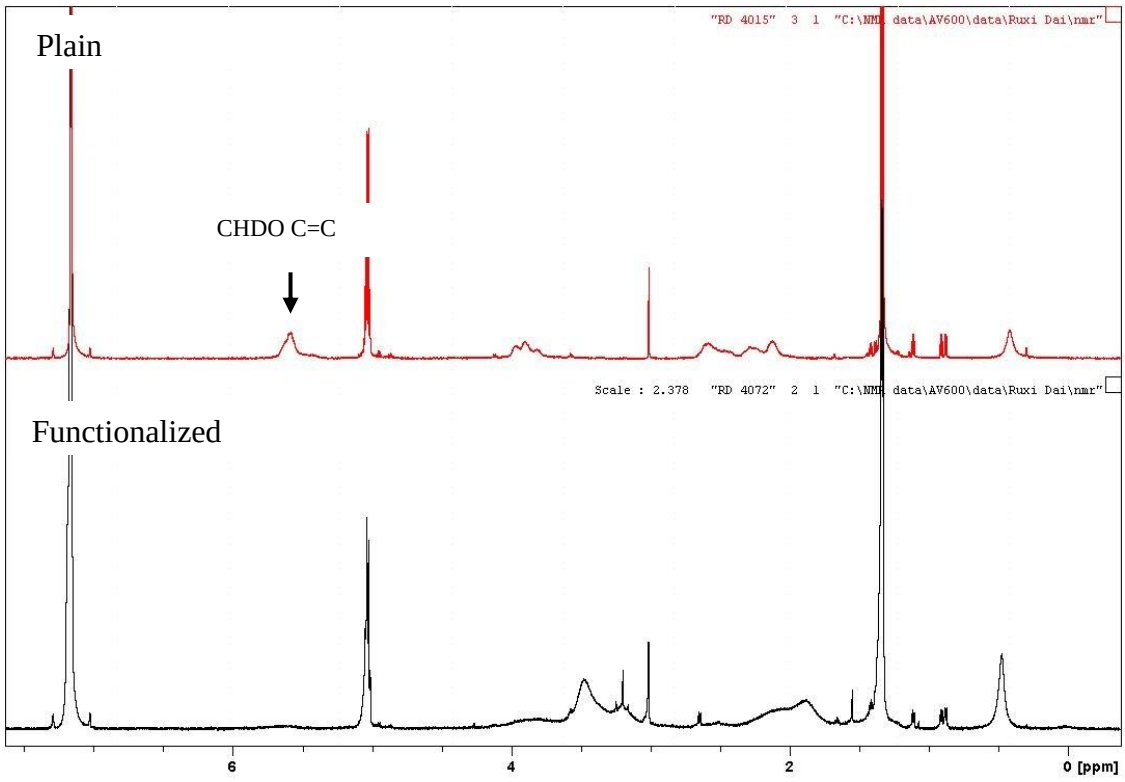

Figure 5.E13. Comparison between the plain copolymer and the functionalized copolymer.

SEC Measurements

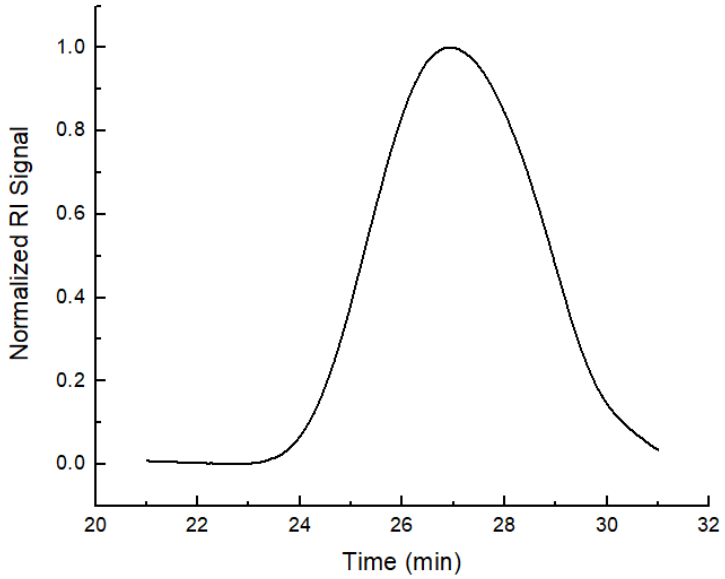

Figure 5.E14. SEC trace of PCHDO homopolymer.

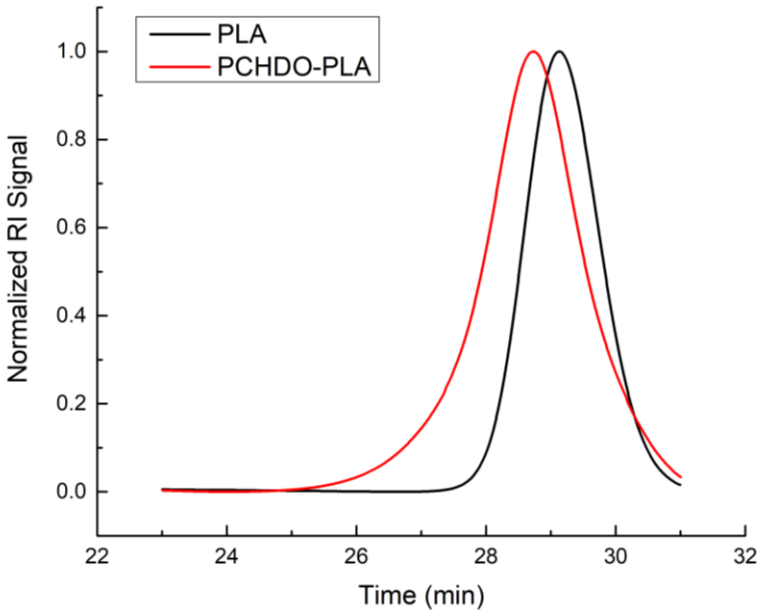

Figure 5.E15. Real-time monitor SEC traces of PCHDO-PLA copolymer preparation.

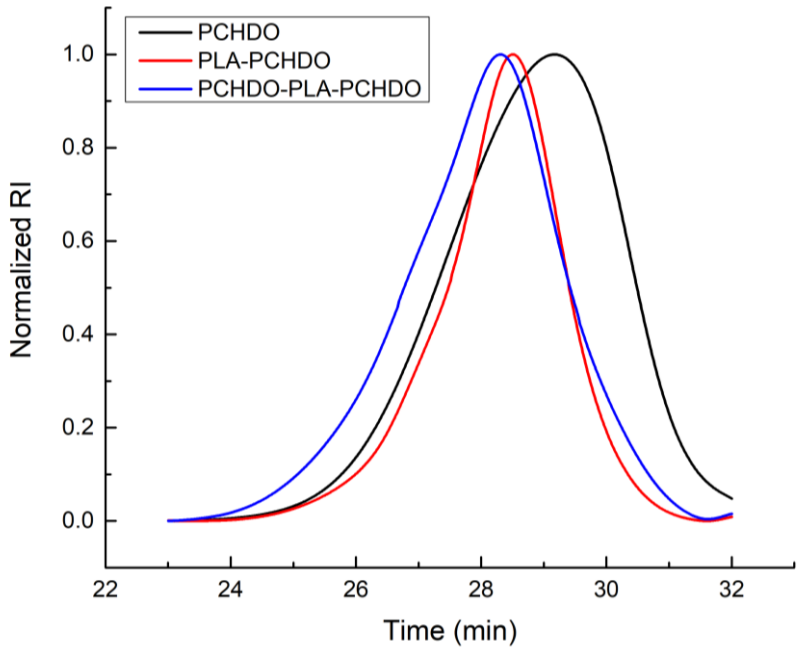

Figure 5.E16. Real-time monitor SEC traces of PCHDO-PLA-PCHDO copolymer preparation.

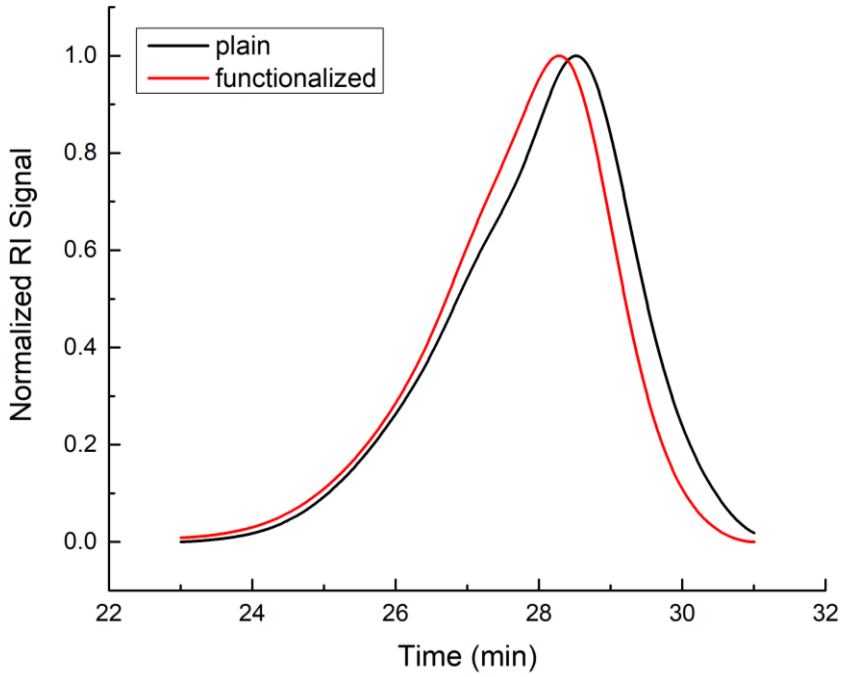

Figure 5.E17. SEC trace of functionalized PCHDO-PLA copolymer.

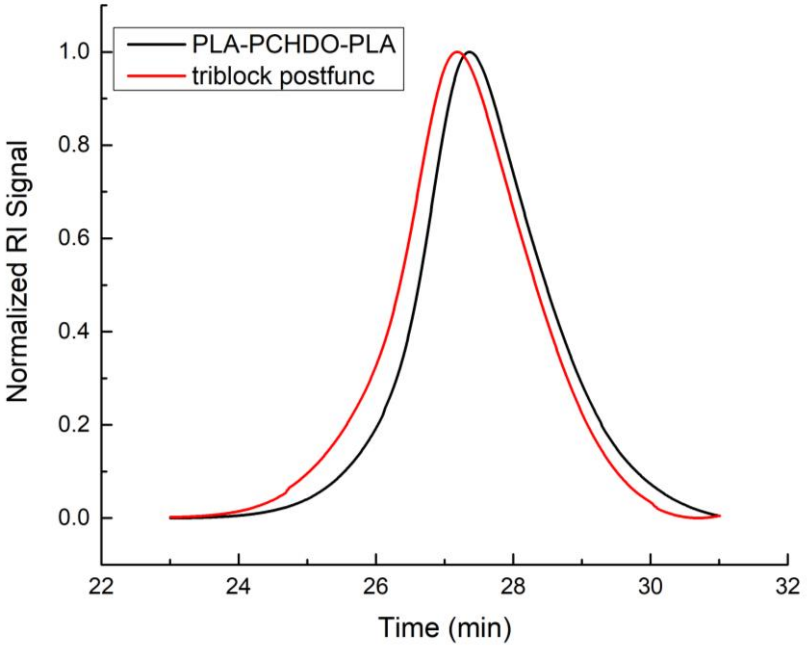

Figure 5.E18. SEC trace of functionalized PLA-PCHDO-PLA copolymer.

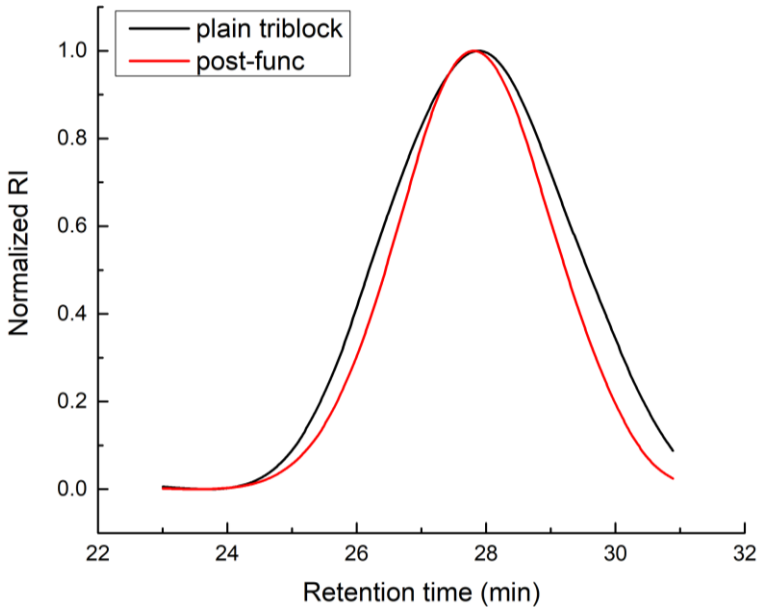

Figure 5.E19. SEC trace of functionalized PCHDO-PLA-PCHDO copolymer.

Stress strain curves (DMA)

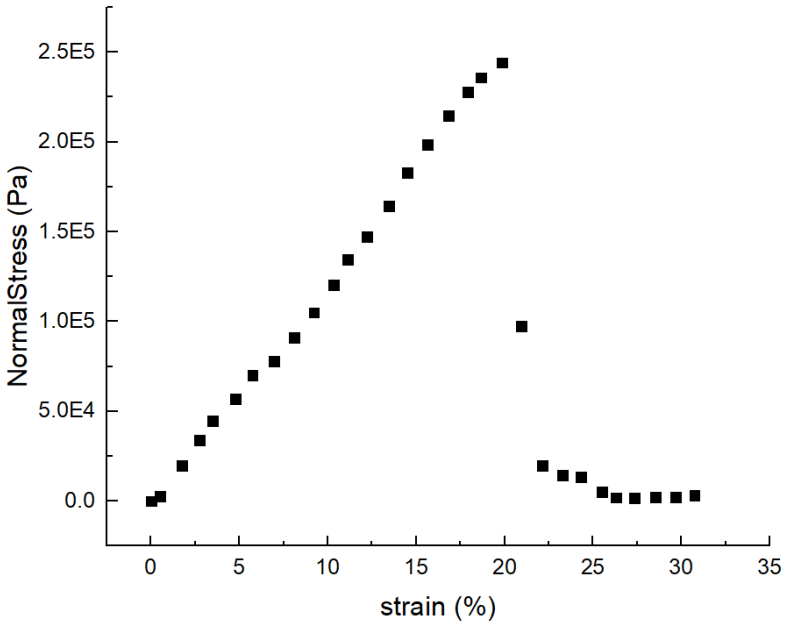

Figure 5.E20. Stress strain curve of PCHDO-PLA plain copolymer, 0.4 LA unit ratio.

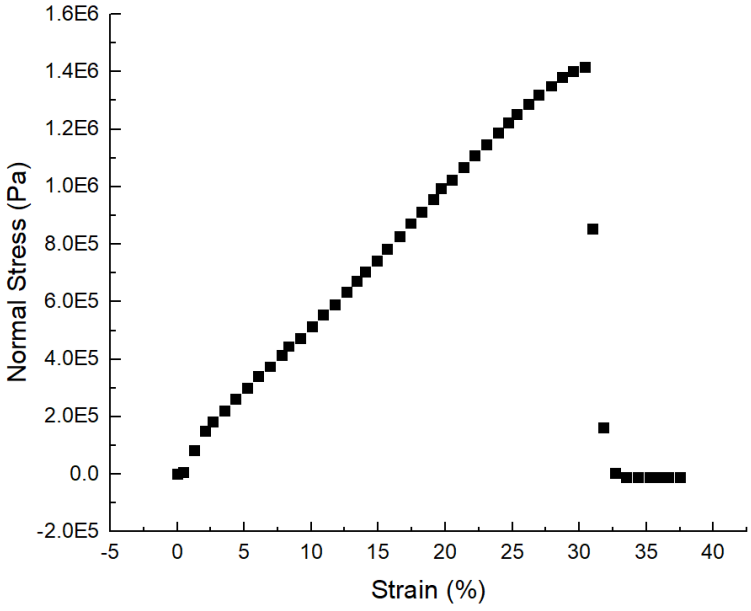

Figure 5.E21. Stress strain curve of PCHDO-PLA functionalized copolymer, 0.4 LA unit ratio.

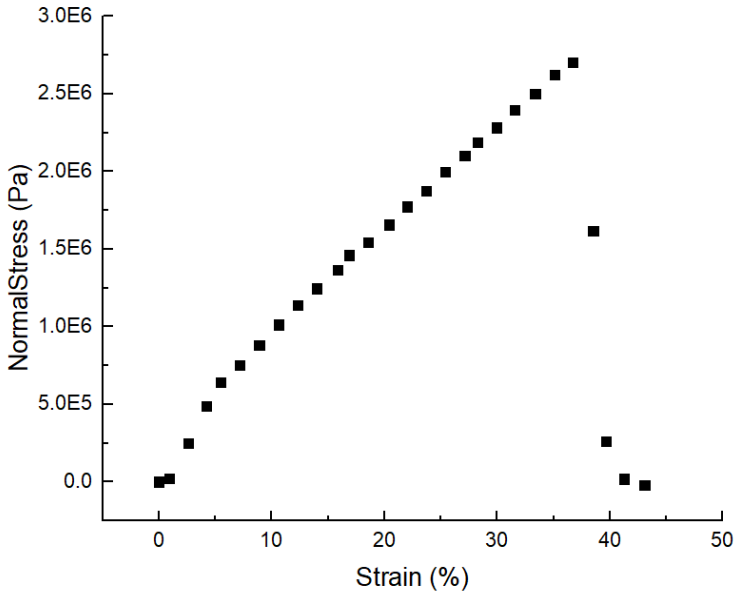

Figure 5.E22. Stress strain curve of PCHDO-PLA plain copolymer, 0.2 LA unit ratio.

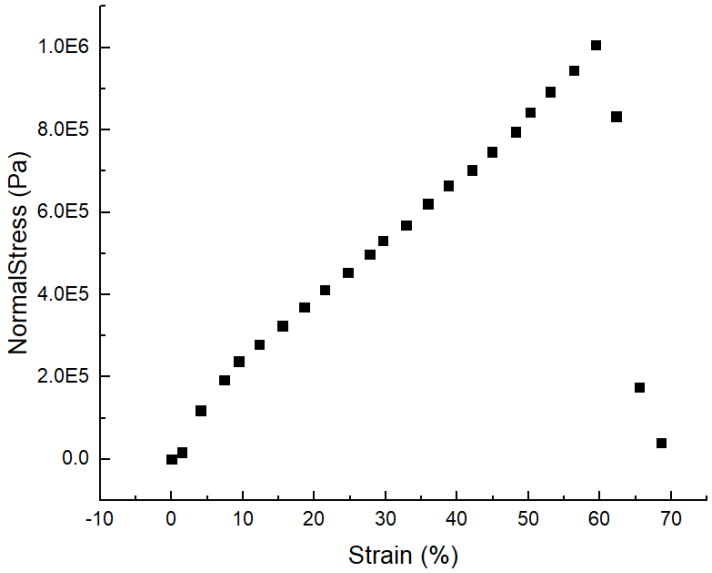

Figure 5.E23. Stress strain curve of PCHDO-PLA functionalized copolymer, 0.2 LA unit ratio.

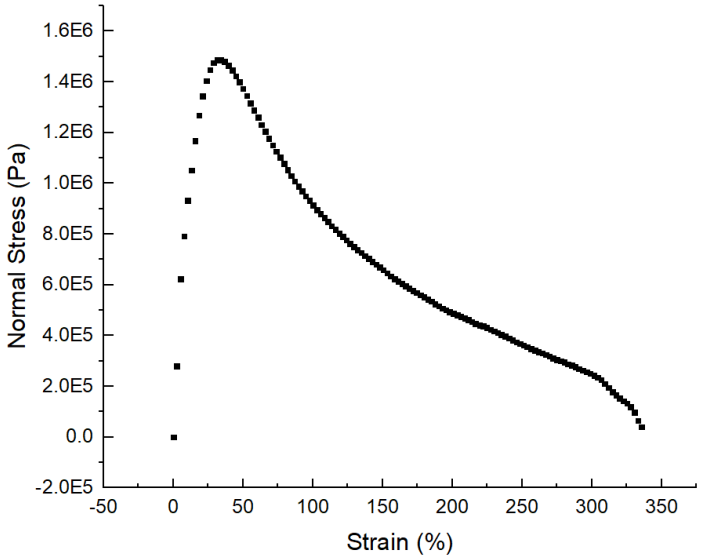

Figure 5.E24. Stress strain curve of PLA-PCHDO-PLA plain copolymer, 0.2 LA unit ratio.

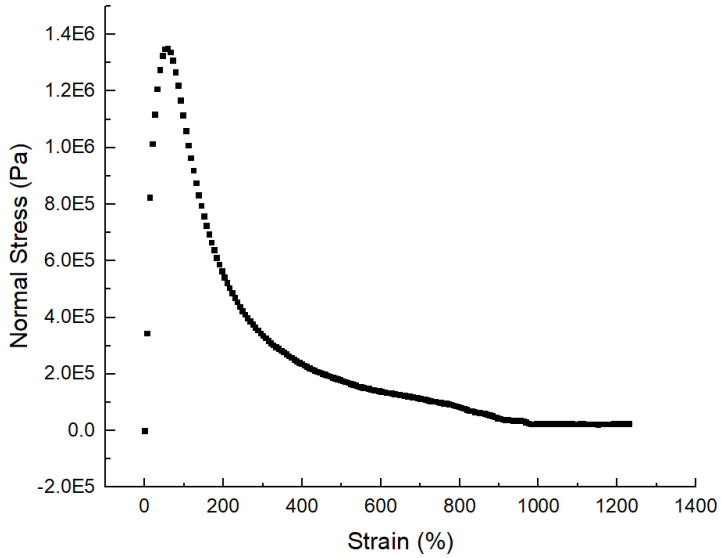

Figure 5.E25. Stress strain curve of PLA-PCHDO-PLA functionalized copolymer, 0.2 LA unit ratio.

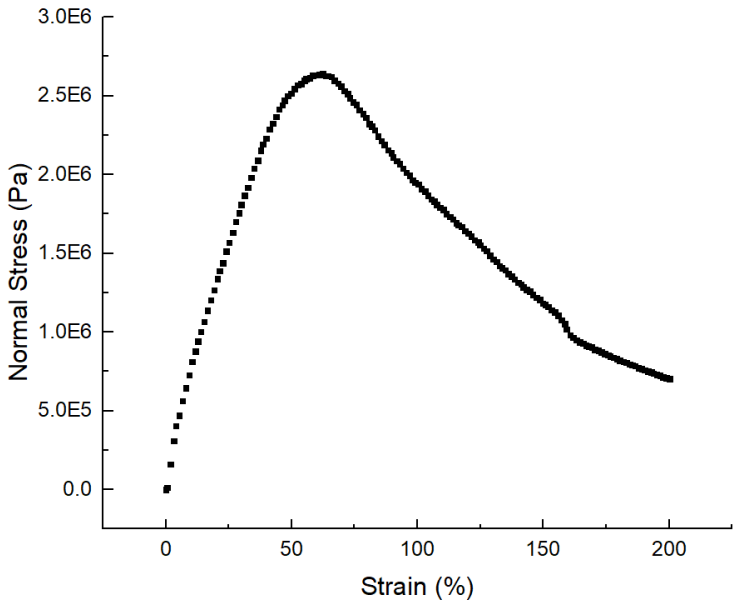

Figure 5.E26. Stress strain curve of PLA-PCHDO-PLA plain copolymer, 0.4 LA unit ratio.

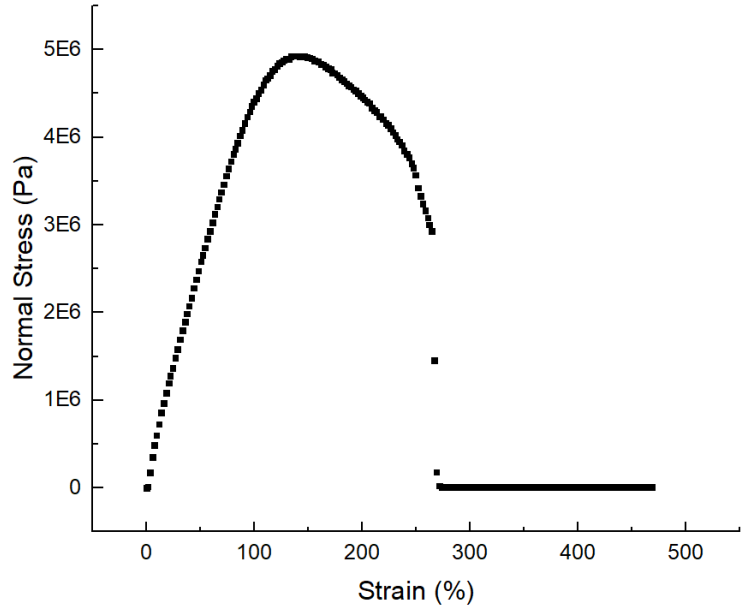

Figure 5.E27. Stress strain curve of PLA-PCHDO-PLA functionalized copolymer, 0.4 LA unit ratio.

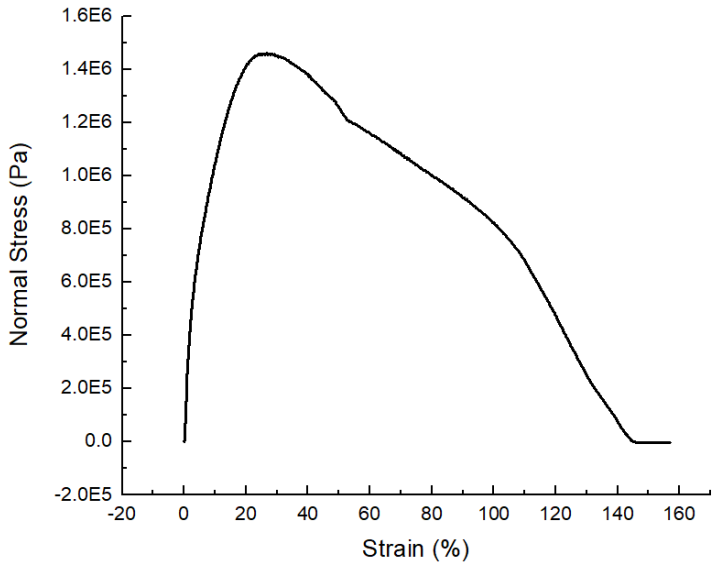

Figure 5.E28. Stress strain curve of PCHDO-PLA-PCHDO plain copolymer, 0.2 LA unit ratio.

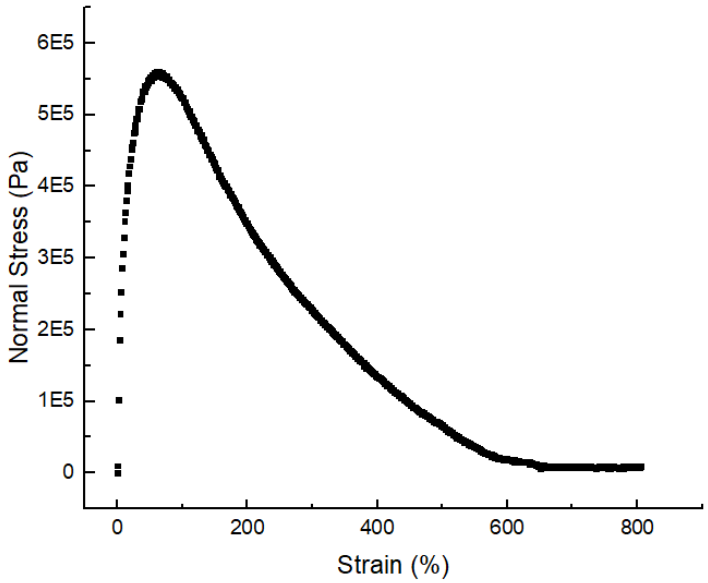

Figure 5.E29. Stress strain curve of PCHDO-PLA-PCHDO functionalized copolymer, 0.2 LA unit ratio.

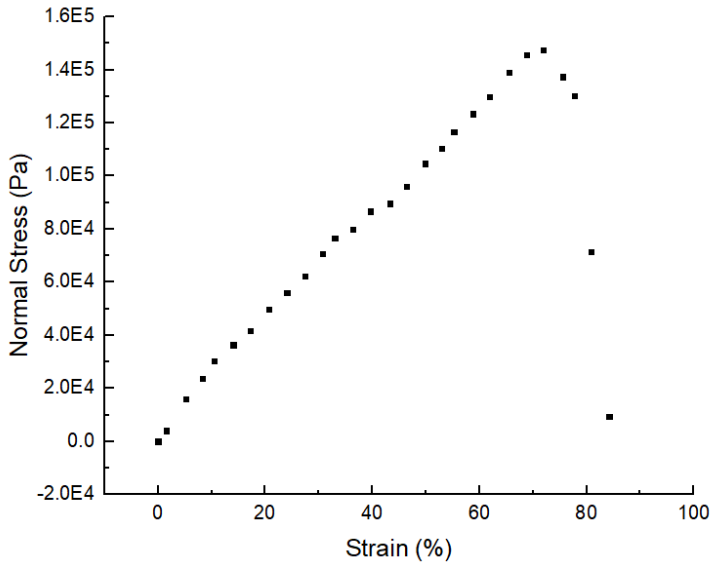

Figure 5.E30. Stress strain curve of PCHDO-PLA-PCHDO plain copolymer, 0.4 LA unit ratio.

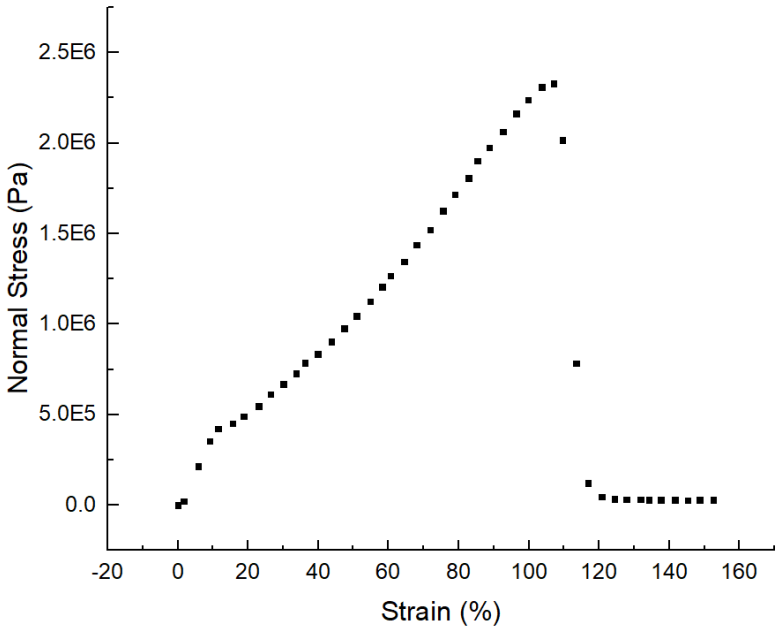

Figure 5.E31. Stress strain curve of PCHDO-PLA-PCHDO functionalized copolymer, 0.4 LA unit ratio.

DSC traces

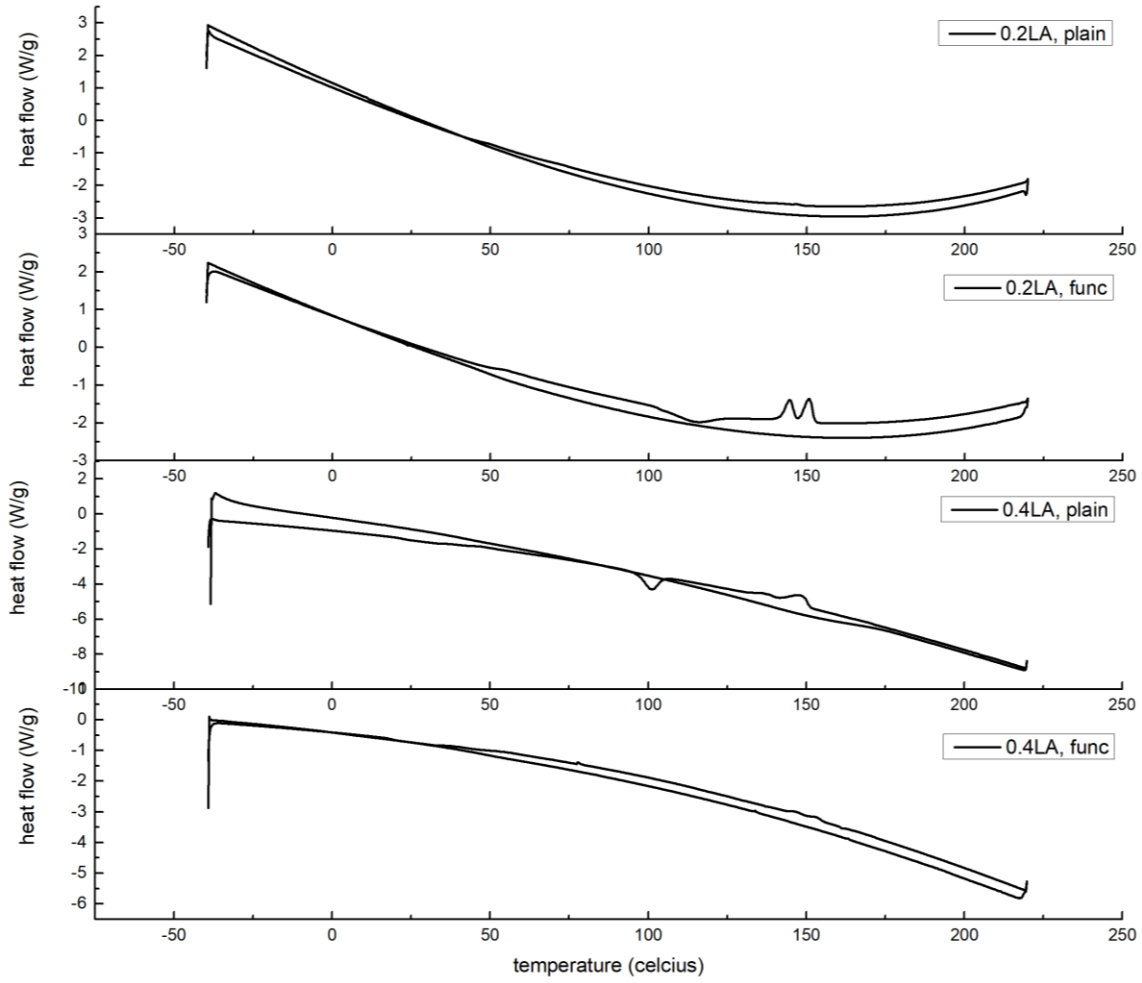

Figure 5.E32. DSC curves of PCHDO-PLA diblock copolymers. From top to bottom: 0.2 LA unit ratio plain copolymer, 0.2 LA unit ratio functionalized copolymer, 0.4 LA unit ratio plain copolymer, 0.4 LA unit ratio functionalized copolymer.

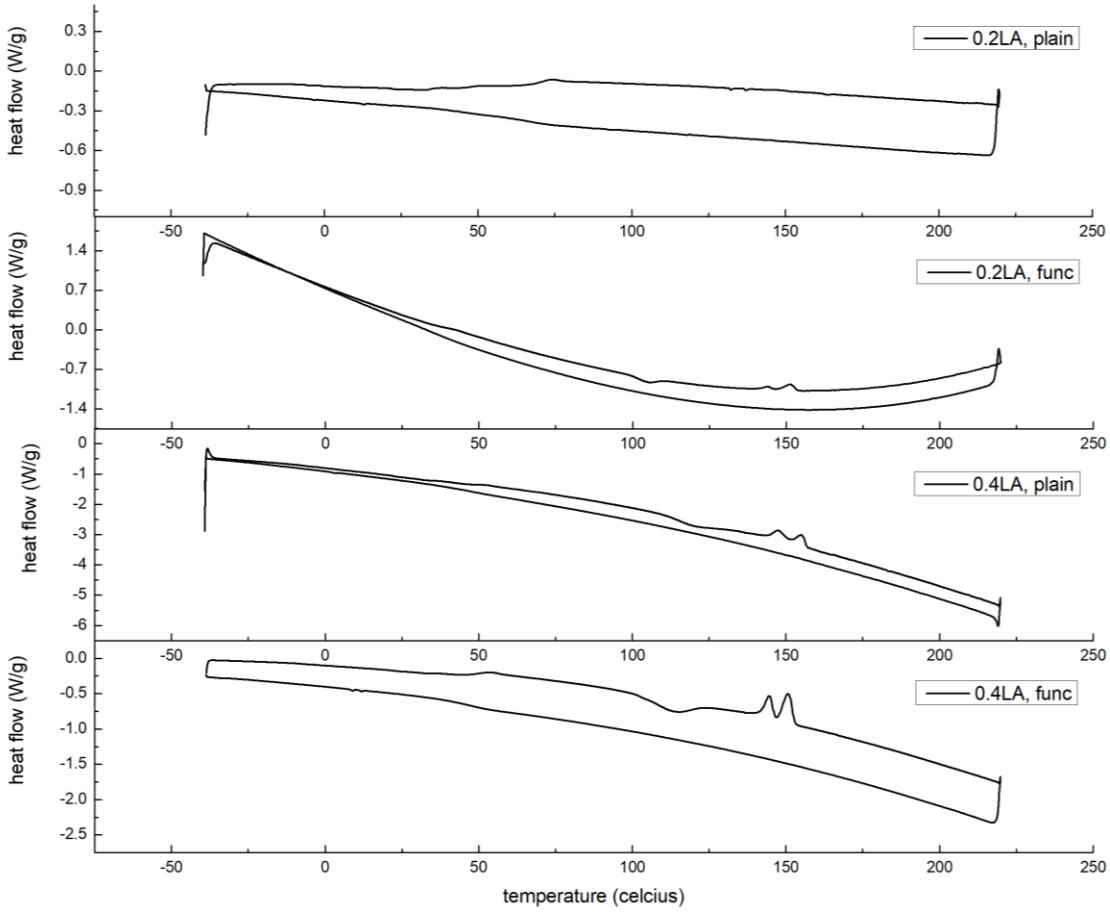

Figure 5.E33. DSC curves of PLA-PCHDO-PLA triblock copolymers. From top to bottom: 0.2 LA unit ratio plain copolymer, 0.2 LA unit ratio functionalized copolymer, 0.4 LA unit ratio plain copolymer, 0.4 LA unit ratio functionalized copolymer.

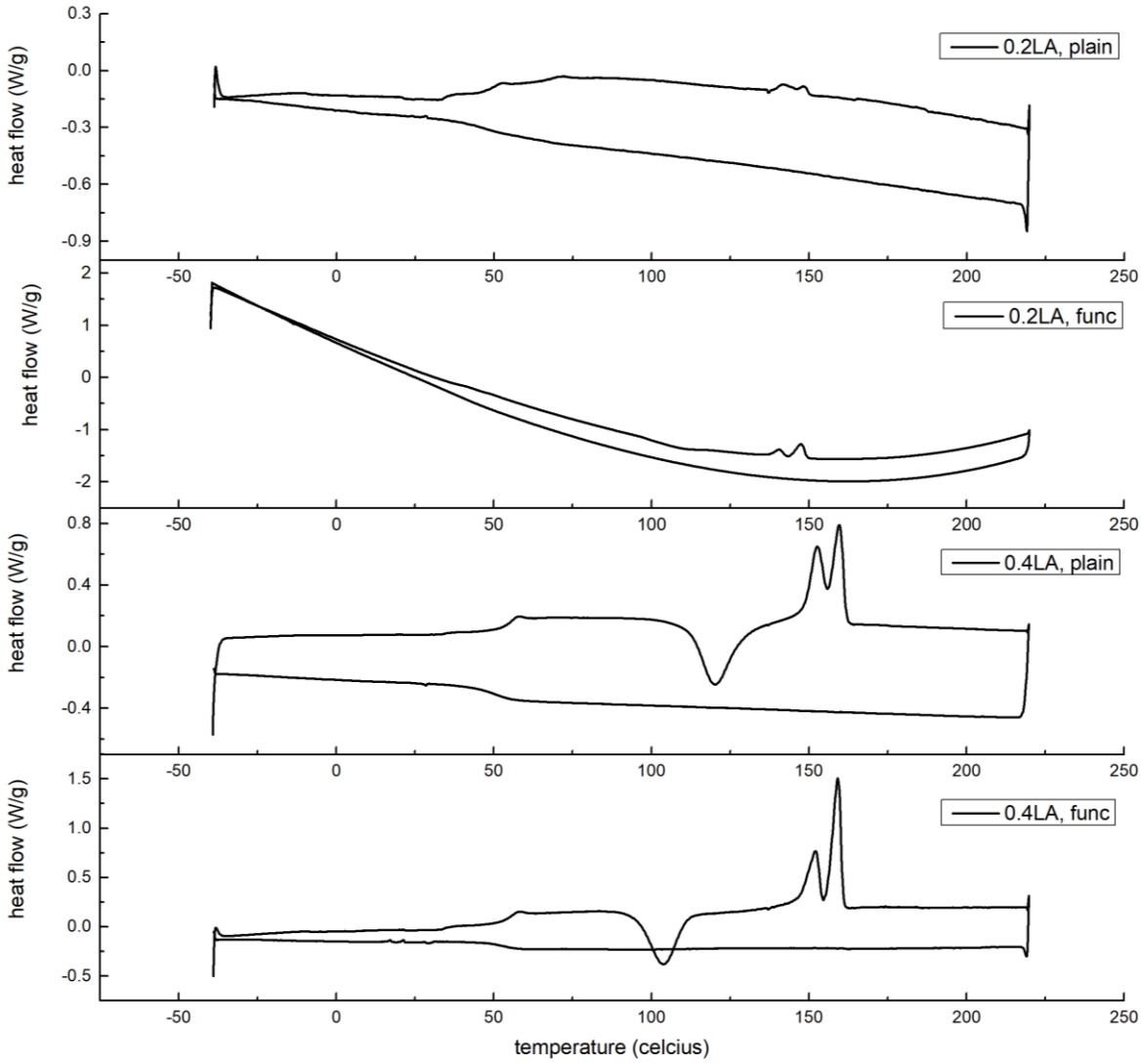

Figure 5.E34. DSC curves of PCHDO-PLA-PCHDO triblock copolymers. From top to bottom: 0.2 LA unit ratio plain copolymer, 0.2 LA unit ratio functionalized copolymer, 0.4 LA unit ratio plain copolymer, 0.4 LA unit ratio functionalized copolymer.

5.6. References

1. Pepic, D.; Zagar, E.; Zigon, M.; Krzan, A.; Kunaver, M.; Djonlagic, J., Synthesis and characterization of biodegradable aliphatic copolyesters with poly(ethylene oxide) soft segments. *European Polymer Journal* **2008,** *44*, 904-917.

2. Theiler, S.; Diamantouros, S. E.; Jockenhoevel, S.; Keul, H.; Moeller, M., Synthesis and characterization of biodegradable polyester/polyether resins via Michael-type addition. *Polymer Chemistry* **2011,** *2*, 2273-2283.

3. Detta, N.; El-Fattah, A. A.; Chiellini, E.; Walkenström, P.; Gatenholm, P., Biodegradable polymeric micro-nanofibers by electrospinning of polyester/polyether block copolymers. *Journal of Applied Polymer Science* **2008,** *110*, 253-261.

4. Martina, M.; Hutmacher, D. W., Biodegradable polymers applied in tissue engineering research: a review. *Polymer International* **2007,** *56*, 145-157.

5. Krieger, M. H., What's Wrong with Plastic Trees? *Science* **1973,** *179*, 446.

6. Galloway, T. S.; Cole, M.; Lewis, C., Interactions of microplastic debris throughout the marine ecosystem. *Nature Ecology & Evolution* **2017,** *1*, 0116.

7. N V Lakshmi Kavya, A.; Sundarrajan, S.; Ramakrishna, S., Identification and characterization of micro-plastics in the marine environment: A mini review. *Marine Pollution Bulletin* **2020,** *160*, 111704.

8. Groh, K. J.; Backhaus, T.; Carney-Almroth, B.; Geueke, B.; Inostroza, P. A.; Lennquist, A.; Leslie, H. A.; Maffini, M.; Slunge, D.; Trasande, L.; Warhurst, A. M.; Muncke, J., Overview of known plastic packaging-associated chemicals and their hazards. *Science of The Total Environment* **2019,** *651*, 3253-3268.

9. Alam, O.; Billah, M.; Yajie, D., Characteristics of plastic bags and their potential environmental hazards. *Resources, Conservation and Recycling* **2018,** *132*, 121-129.

10. Lebreton, L. C. M.; van der Zwet, J.; Damsteeg, J.-W.; Slat, B.; Andrady, A.; Reisser, J., River plastic emissions to the world's oceans. *Nature Communications* **2017,** *8*, 15611.

11. Baztan, J.; Carrasco, A.; Chouinard, O.; Cleaud, M.; Gabaldon, J. E.; Huck, T.; Jaffrès, L.; Jorgensen, B.; Miguelez, A.; Paillard, C.; Vanderlinden, J.-P., Protected areas in the Atlantic facing the hazards of micro-plastic pollution: First diagnosis of three islands in the Canary Current. *Marine Pollution Bulletin* **2014,** *80*, 302-311.

12. Johnson, W. H., Social Impact of Pollution Control Legislation. *Science* **1976,** *192*, 629.

13. Green, L., Energy Needs versus Environmental Pollution: A Reconciliation? *Science* **1967,** *156*, 1448.

14. Colleoni, C.; Guido, E.; Migani, V.; Rosace, G., Hydrophobic behaviour of non-fluorinated sol–gel based cotton and polyester fabric coatings. *Journal of Industrial Textiles* **2013,** *44*, 815-834.

15. Mishra, S.; Mohanty, A. K.; Drzal, L. T.; Misra, M.; Parija, S.; Nayak, S. K.; Tripathy, S. S., Studies on mechanical performance of biofibre/glass reinforced polyester hybrid composites. *Composites Science and Technology* **2003,** *63*, 1377-1385.

16. Pothan, L. A.; Oommen, Z.; Thomas, S., Dynamic mechanical analysis of banana fiber reinforced polyester composites. *Composites Science and Technology* **2003,** *63*, 283-293.

17. Bruce, T. F.; Slonecki, T. J.; Wang, L.; Huang, S.; Powell, R. R.; Marcus, R. K., Exosome isolation and purification via hydrophobic interaction chromatography using a polyester, capillary-channeled polymer fiber phase. *ELECTROPHORESIS* **2019,** *40*, 571-581.

18. Gao, Q.; Zhu, Q.; Guo, Y.; Yang, C. Q., Formation of Highly Hydrophobic Surfaces on Cotton and Polyester Fabrics Using Silica Sol Nanoparticles and Nonfluorinated Alkylsilane. *Industrial & Engineering Chemistry Research* **2009,** *48*, 9797-9803.

19. Garcia-Gonzalez, D.; Rusinek, A.; Jankowiak, T.; Arias, A., Mechanical impact behavior of polyether–ether–ketone (PEEK). *Composite Structures* **2015,** *124*, 88-99.

20. Lu, H.; Nguyen, B.; Powers, J. M., Mechanical properties of 3 hydrophilic addition silicone and polyether elastomeric impression materials. *The Journal of Prosthetic Dentistry* **2004,** *92*, 151-154.

21. Santos, C. C.; Delpech, M. C.; Coutinho, F. M. B., Thermal and mechanical profile of cast films from waterborne polyurethanes based on polyether block copolymers. *Journal of Materials Science* **2009,** *44*, 1317-1323.

22. Bistričić, L.; Baranović, G.; Leskovac, M.; Bajsić, E. G., Hydrogen bonding and mechanical properties of thin films of polyether-based polyurethane–silica nanocomposites. *European Polymer Journal* **2010,** *46*, 1975-1987.

23. Wilson, R.; Divakaran, A. V.; S, K.; Varyambath, A.; Kumaran, A.; Sivaram, S.; Ragupathy, L., Poly(glycerol sebacate)-Based Polyester–Polyether Copolymers and Their Semi-Interpenetrated Networks with Thermoplastic Poly(ester–ether) Elastomers: Preparation and Properties. *ACS Omega* **2018,** *3*, 18714-18723.

24. Guillaume, S. M., Recent advances in ring-opening polymerization strategies toward α,ω-hydroxy telechelic polyesters and resulting copolymers. *European Polymer Journal* **2013,** *49*, 768-779.

25. Wang, Y.; Hillmyer, M. A., Synthesis of Polybutadiene−Polylactide Diblock Copolymers Using Aluminum Alkoxide Macroinitiators. Kinetics and Mechanism. *Macromolecules* **2000,** *33,* 7395-7403.

26. Tamboli, V.; Mishra, G. P.; Mitra, A. K., Novel pentablock copolymer (PLA–PCL–PEG–PCL–PLA)-based nanoparticles for controlled drug delivery: effect of copolymer compositions on the crystallinity of copolymers and in vitro drug release profile from nanoparticles. *Colloid and Polymer Science* **2013,** *291*, 1235-1245.

27. Gregson, C. K. A.; Gibson, V. C.; Long, N. J.; Marshall, E. L.; Oxford, P. J.; White, A. J. P., Redox Control within Single-Site Polymerization Catalysts. *Journal of the American Chemical Society* **2006,** *128,* 7410-7411.

28. Lai, A.; Hern, Z. C.; Shen, Y.; Dai, R.; Diaconescu, P. L., Metal Complexes for Redox Switching and Control of Reactivity. In *Reference Module in Chemistry, Molecular Sciences and Chemical Engineering*, Elsevier: 2021.

29. Lai, A.; Clifton, J.; Diaconescu, P. L.; Fey, N., Computational mapping of redox-switchable metal complexes based on ferrocene derivatives. *Chem. Commun.* **2019,** *55,*, 7021-7024

30. Dai, R.; Diaconescu, P. L., Investigation of a Zirconium Compound for Redox Switchable Ring Opening Polymerization. *Dalton Trans.* **2019,** *48,* 2996-3002.

31. Broderick, E. M.; Thuy-Boun, P. S.; Guo, N.; Vogel, C. S.; Sutter, J.; Miller, J. T.; Meyer, K.; Diaconescu, P. L., Synthesis and Characterization of Cerium and Yttrium Alkoxide Complexes Supported by Ferrocene-Based Chelating Ligands. *Inorg. Chem.* **2011,** *50,* 2870-2877.

32. Abubekerov, M.; Khan, S. I.; Diaconescu, P. L., Ferrocene-bis(phosphinimine) Nickel(II) and Palladium(II) Alkyl Complexes: Influence of the Fe–M (M = Ni and Pd) Interaction on Redox Activity and Olefin Coordination. *Organometallics* **2017,** *36*, 4394-4402.

33. Abubekerov, M.; Vlcek, V.; Wei, J.; Miehlich, M. E.; Quan, S. M.; Meyer, K.; Neuhauser, D.; Diaconescu, P. L., Exploring Oxidation State-Dependent Selectivity in Polymerization of Cyclic Esters and Carbonates with Zinc(II) Complexes. *iScience* **2018,** *7*, 120-131.

34. Lai, A.; Hern, Z. C.; Diaconescu, P. L., Switchable Ring-Opening Polymerization by a Ferrocene Supported Aluminum Complex. *ChemCatChem* **2019,** *11*, 4210-4218.

35. Wei, J.; Riffel, M. N.; Diaconescu, P. L., Redox Control of Aluminum Ring-Opening Polymerization: A Combined Experimental and DFT Investigation. *Macromolecules* **2017,** *50*, 1847-1861.

36. Quan, S. M.; Wei, J.; Diaconescu, P. L., Mechanistic Studies of Redox-Switchable Copolymerization of Lactide and Cyclohexene Oxide by a Zirconium Complex. *Organometallics* **2017,** *36*, 4451-4457.

37. Quan, S. M.; Wang, X.; Zhang, R.; Diaconescu, P. L., Redox Switchable Copolymerization of Cyclic Esters and Epoxides by a Zirconium Complex. *Macromolecules* **2016,** *49*, 6768-6778.

38. Wang, X.; Thevenon, A.; Brosmer, J. L.; Yu, I.; Khan, S. I.; Mehrkhodavandi, P.; Diaconescu, P. L., Redox Control of Group 4 Metal Ring-Opening Polymerization Activity toward l-Lactide and ε-Caprolactone. *Journal of the American Chemical Society* **2014,** *136*, 11264-11267.

39. Wei, J.; Diaconescu, P. L., Redox-switchable Ring-opening Polymerization with Ferrocene Derivatives. *Acc. Chem. Res.* **2019**, in press.

40. Dai, R.; Lai, A.; Alexandrova, A. N.; Diaconescu, P. L., Geometry Change in a Series of Zirconium Compounds during Lactide Ring-Opening Polymerization. *Organometallics* **2018,** *37*, 4040-4047.

41. Madhavan Nampoothiri, K.; Nair, N. R.; John, R. P., An overview of the recent developments in polylactide (PLA) research. *Bioresource Technology* **2010,** *101*, 8493-8501.

42. Gupta, A. P.; Kumar, V., New emerging trends in synthetic biodegradable polymers – Polylactide: A critique. *European Polymer Journal* **2007,** *43*, 4053-4074.

43. Ates, B.; Koytepe, S.; Ulu, A.; Gurses, C.; Thakur, V. K., Chemistry, Structures, and Advanced Applications of Nanocomposites from Biorenewable Resources. *Chemical Reviews* **2020,** *120*, 9304-9362.

44. Graupner, N.; Ziegmann, G.; Müssig, J., Composite models for compression moulded long regenerated cellulose fibre-reinforced brittle polylactide (PLA). *Composites Science and Technology* **2017,** *149*, 55-63.

45. Becker, J. M.; Pounder, R. J.; Dove, A. P., Synthesis of Poly(lactide)s with Modified Thermal and Mechanical Properties. *Macromolecular Rapid Communications* **2010,** *31*, 1923-1937.

46. Abubekerov, M.; Wei, J.; Swartz, K. R.; Xie, Z.; Pei, Q.; Diaconescu, P. L., Preparation of multiblock copolymers via step-wise addition of l-lactide and trimethylene carbonate. *Chemical Science* **2018,** *9*, 2168-2178.

47. Stößer, T.; Li, C.; Unruangsri, J.; Saini, P. K.; Sablong, R. J.; Meier, M. A. R.; Williams, C. K.; Koning, C., Bio-derived polymers for coating applications: comparing poly(limonene carbonate) and poly(cyclohexadiene carbonate). *Polymer Chemistry* **2017,** *8*, 6099-6105.

48. Darensbourg, D. J.; Chung, W.-C.; Arp, C. J.; Tsai, F.-T.; Kyran, S. J., Copolymerization and Cycloaddition Products Derived from Coupling Reactions of 1,2-Epoxy-4-cyclohexene and Carbon Dioxide. Postpolymerization Functionalization via Thiol–Ene Click Reactions. *Macromolecules* **2014,** *47*, 7347-7353.

49. Hauenstein, O.; Agarwal, S.; Greiner, A., Bio-based polycarbonate as synthetic toolbox. *Nature Communications* **2016,** *7*, 11862.

50. Tan, Q.; Hayashi, M., Asymmetric Desymmetrization of 4,5-Epoxycyclohex-1-ene by Enantioselective Allylic Oxidation. *Organic Letters* **2009,** *11*, 3314-3317.

51. Dhar, D.; Yee, G. M.; Spaeth, A. D.; Boyce, D. W.; Zhang, H.; Dereli, B.; Cramer, C. J.; Tolman, W. B., Perturbing the Copper(III)–Hydroxide Unit through Ligand Structural Variation. *Journal of the American Chemical Society* **2016,** *138*, 356-368.